Development of biogenic thermoresponsive multilayers based on polysaccharides for tissue engineering applications

Dissertation

zur Erlangung des
Doktorgrades der Naturwissenschaften (Dr. rer. nat.)

der

Naturwissenschaftlichen Fakultät I – Biowissenschaften –

der Martin-Luther-Universität
Halle-Wittenberg,

vorgelegt

von Frau MSc. Yi-Tung Lu

geb. am 16.06.1992 in New Taipei City, Taiwan

Gutachter: Prof. Dr. rer. nat. habil. Thomas Groth
Prof. Dr. rer. nat. habil. Karsten Mäder
Prof. Dr. Dmitry Volodkin

Halle (Saale), 27.11.2023

To my family

Table of Contents

Abbreviations

ADSC	adipose-derived stem cell	**LMW***	PChi with DS 0.14 from 2 kDa of PNIPAM
AFM	atomic force microscopy	**MAPK**	mitogen-activated protein kinase
Alg	alginate	**MSC**	mesenchymal stem cell
ASC	adult stem cells	**NHS**	*N*-hydroxysuccinimide
BMP	bone morphogenetic protein	**NMR**	nuclear magnetic resonance
BSA	bovine serum albumin	**PAA**	propylacrylic acid
Cdc42	Cell division control protein 42 homolog	**PAH**	poly(allylamine hydrochloride)
Chi	chitosan	**PChi**	PNIPAM-*grafted*-chitosan
ChS	chondroitin sulfate	**PCS**	PNIPAM-*grafted*-cellulose sulfate
CLSM	confocal laser scanning microscopy	**PEL**	polyelectrolyte
CS	cellulose sulfate	**PEM**	polyelectrolyte multilayer
DLS	dynamic laser scattering	**PG**	proteoglycan
DS	degree of substitution	**pI**	isoelectric point
ECM	extracellular matrix	**PI3K**	phosphoinositide 3-kinase
EDC	1-ethyl-3-(3-dimethylaminopropyl)-carbodiimide	**PLL**	poly-L-lysin
EDTA	ethylenediaminetetraacetic acid	**PNIPAM**	Poly(*N*-isopropylacrylamide)
ERK	extracellular signal-regulated kinase	**PSC**	pluripotent stem cell
ESC	embryonic stem cell	**PSS**	poly(styrene sulfonate)
FAK	focal adhesion kinase	**QChi**	quaternized chitosan
FGF-2	fibroblast growth factor-2	**QCM-*D***	quartz crystal microbalance with dissipation monitoring
FGFR-2	FGF-2 receptor	**RGD**	arginine–glycine–aspartate
FN	fibronectin	**RhoA**	Ras homolog family member A
FTIR	Fourier-transform infrared spectroscopy	**ROCK**	Rho-associated protein kinase
GAG	glycosaminoglycan	**SEM**	scanning electron microscopy
GF	growth factor	**SPR**	surface plasmon resonance
HA	hyaluronic acid	**T_{CP}**	cloud point temperature
Hep	heparin	**TCPS**	tissue culture polystyrene
HMW	PChi with DS 0.03 from 10 kDa of PNIPAM	**TGF-β**	transforming growth factor beta
HSC	hematopoietic stem cell	**VEGF**	vascular endothelial growth factor
iPSC	induce pluripotent stem cell	**VN**	vitronectin
LbL	layer-by-layer	**WCA**	water contact angle
LCST	lower critical solution temperature		

Graphical abstract
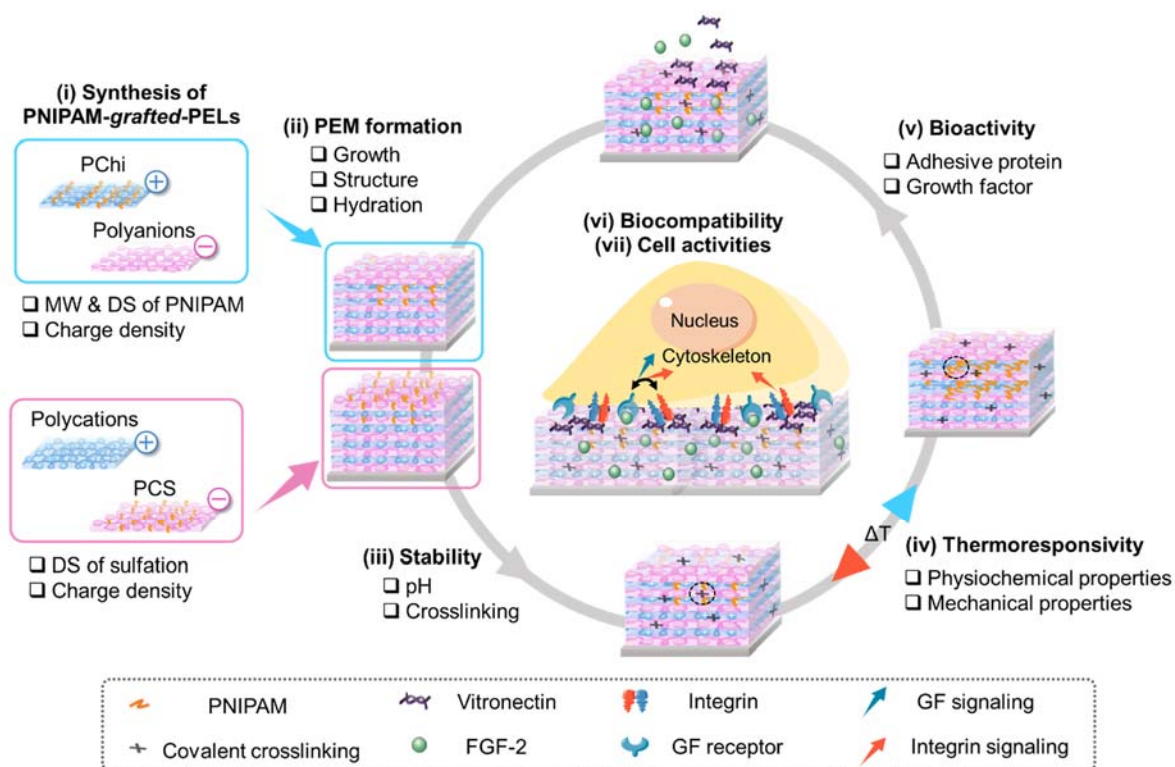
Schematic general overview on thesis chapters. To apply PNIPAM as a polyelectrolyte (PEL) for polyelectrolyte multilayer (PEM) formation, this work begins with (i) two approaches for the synthesis of PNIPAM-*grafted*-chitosan (PChi) as polycation and PNIPAM-*grafted*-cellulose sulfate (PCS) as polycation. While PChi-containing PEMs are prepared from PChi and polyanions using sulfated glycosaminoglycans (heparin, chondroitin sulfate), PCS-containing PEMs are combining PCS and polycations (poly-L-lysin, quaternized chitosan). The thesis focuses on the influence of molecular weight (MW), degree of substitution (DS) of PNIPAM and sulfate groups, and charge density on the PEM (ii) formation and structure, (iii) stability (ionic and/or covalent crosslinking) at different pH, (iv) thermoresponsivity (physiochemical and mechanical properties), (v) bioactivity with an immobilized adhesive protein (vitronectin) and a growth factor (FGF-2), and (vi) biocompatibility towards responses of mouse stem cells and fibroblasts. Finally, this work investigates the potential of PNIPAM-containing PEMs to control the release of the immobilized FGF-2, and to regulate cell activities in terms of cell adhesion, proliferation, and migration by the crosstalk between FGF-2 and vitronectin integrin receptor.

Abstract

Thermoresponsive Poly(N-isopropylacrylamide) (PNIPAM) is popularly applied in hydrogels and for surface modification allowing controlled release of drugs, cell sheet engineering, and tissue engineering. With the advantage of its lower critical solution temperature around 32 °C close to body temperature, PNIPAM is a promising material to modulate physiochemical properties of biomaterial surfaces. However, current methods for fabricating PNIPAM-modified surfaces are often ineffective or expensive, and lack bioactivity, which restrict their use as stimuli responsive cell culture substrata with the regulatory effect on cell or stem cell activities. By combining with native or semi-synthetic glycosaminoglycans (GAGs), a facile and cost-effective fabrication of bioactive PNIPAM-containing polyelectrolyte multilayers (PEMs) is established using a layer-by-layer (LbL) technique through the alternating adsorption of oppositely charged polyelectrolytes (PELs). Here, two approaches to apply PNIPAM as PELs for the PEM assembly are explored by conjugation of PNIPAM with the (i) polycation chitosan (Chi) or (ii) polyanion cellulose sulfate (CS).

The first part focuses on the use of PNIPAM-*grafted*-Chi (PChi) as polycation to form PEMs with native GAGs like heparin (Hep) or chondroitin sulfate (ChS) as polyanions. Molecular weight (MW) and degree of substitution (DS) of PNIPAM on PChi are found to affect charge density and cloud point of temperature where PChi undergoes a conformational change. Two PChi with high and low DS, LMW* (DS 0.14 from 2 kDa of PNIPAM) and HMW (DS 0.03 from 10 kDa of PNIPAM) are selected to form LMW*- or HMW-containing PEMs with polyanions at pH 4. The post covalent crosslinking using 1-ethyl-3-(3-dimethylaminopropyl) carbodiimide/*N*-hydroxysuccinimide is introduced to strengthen the stability of PEMs at physiological pH 7.4 by forming the amide bonds between Hep and Chi. The growth behavior, stability, physiochemical and mechanical properties of PEMs are systematically investigated. The results reveal that covalent crosslinking maintains the integrity of PEMs, while partial decomposition of uncrosslinked PEMs is found after exposure to physiological buffer at pH 7.4, particularly when formed from LMW*. Resulting surface wettability and mechanical properties confirm that the PEM containing HMW is responsive to temperature at 20 °C and 37 °C, while LMW* restricts the change in these properties. Moreover, using Hep as terminal layer in combination with HMW better retains the adhesive protein

vitronectin (VN) at 37 °C, which further corresponds to the sustained release of fibroblast growth factor-2 (FGF-2). This is the first study to explore the synergistic effect of VN and FGF-2 immobilized on PEM and its impact on cell activities. Not only specific interaction of Hep but also hydrophobic interaction of HMW contribute to the binding with VN and FGF-2, and in turn promote superior cell activities in terms of cell adhesion, spreading, proliferation and migration using multipotent mouse fibroblast cell line C3H10T1/2 and 3T3.

At the second part of this PhD study, a mimetic GAG, CS with exceptional bioactivity is used to seek for the possibility to replace native GAGs due to their batch-to-batch variation. Two novel synthetic routes for the preparation of PNIPAM-*grafted*-cellulose sulfate (PCS) as polyanion with distinct DS of PNIPAM and sulfate groups are developed to achieve thermoresponsive and bioactive PEM by LbL technique. Lower sulfated PCS 1 (DS 0.41) and higher sulfated PCS 2 (DS 0.93) are used to study their ability to form PEM with polycations (poly-L-lysin, PLL or quaternized chitosan, QChi). The resulting growth behavior, internal structure, stability, and surface properties are strongly dependent on the sulfation degree, type of polycation and the presence of PNIPAM. The higher sulfated PCS 2 overcomes the steric hindrance of PNIPAM allowing higher adsorption of both polycations and forms more stable PEM compared to the lower sulfated PCS 1 after exposure to pH 7.4. In addition, the smaller molecule PLL tends to form more intermingled PEM than the larger QCHI, resulting in a more pronounced effect on surface properties. The study on surface characterization is further related to the toxicity and biocompatibility of PEM towards cell behaviors. PEM combined with PLL leads to higher toxicity to 3T3 cells particularly in combination with PCS1, while the combination of QChi and PCS2 shows excellent biocompatibility and promotes cell adhesion and proliferation over 7 days.

Overall, this thesis presents the newly developed thermoresponsive coatings that elucidates the capability to modulate surface properties and improve the bioactivity by inclusion of PNIPAM combined with native or semi-synthetic GAGs. This coatings have an enormous potential as a cell culture substrate for growth factor delivery, production of (stem) cells and as a bioactive wound dressing for tissue regeneration.

ZUSAMMENFASSUNG

Thermoresponsives Poly(N-isopropylacrylamid) (PNIPAM) wird häufig in Hydrogelen und der Oberflächenmodifizierung zur kontrollierten Freisetzung von Arzneimitteln sowie im Zellblatt- und Tissue-Engineering eingesetzt. Mit dem Vorteil seiner niedrigeren kritischen Lösungstemperatur von etwa 32 °C nahe der Körpertemperatur ist PNIPAM ein vielversprechendes Material zur Modulation der physiochemischen Eigenschaften von Biomaterialoberflächen. Aktuelle Methoden zur Herstellung von PNIPAM-modifizierten Oberflächen sind jedoch oft ineffektiv oder teuer und weisen keine Bioaktivität auf, was ihre Verwendung als stimuliresponsive Zellkultursubstrate mit regulierender Wirkung auf Zell- oder Stammzellaktivitäten einschränkt. Durch die Kombination mit nativen oder halbsynthetischen Glykosaminoglykanen (GAGs) wird eine einfache und kostengünstige Herstellung bioaktiver PNIPAM-haltiger Polyelektrolyt-Mehrfachschichten (PEMs) mithilfe einer Schicht-für-Schicht-Technik (LbL) durch abwechselnde Adsorption entgegengesetzt geladener Polyelektrolyte (PELs) ermöglicht. Es werden zwei Ansätze zur Anwendung von PNIPAM als PELs für den PEM-Aufbau durch Konjugation von PNIPAM an (i) das Polykation Chitosan (Chi) oder (ii) das Polyanion Cellulosesulfat (CS) untersucht.

Der erste Teil konzentriert sich auf die Verwendung von PNIPAM-grafted-Chi (PCi) als Polykationen zur Bildung von PEMs, mit nativen GAGs wie Heparin (Hep) oder Chondroitinsulfat (ChS) als Polyanionen. Es wurde festgestellt, dass das Molekulargewicht (MW) und der Substitutionsgrad (DS) von PNIPAM auf PChi die Ladungsdichte und die Trübungspunkttemperatur beeinflussen, an welcher PChi eine Konformationsänderung erfährt. Zwei PChi mit hohem und niedrigem DS, LMW* (DS 0,14 von 2 kDa von PNIPAM) und HMW (DS 0,03 von 10 kDa von PNIPAM), werden ausgewählt, um LMW*- oder HMW-haltige PEMs mit Polyanionen bei pH 4 zu bilden. Nach der Multischichtbildung werden diese mit 1-Ethyl-3-(3-dimethylaminopropyl)carbodiimid/N-Hydroxysuccinimid kovalent vernetzt, um die Stabilität von PEMs bei physiologischem pH-Wert 7,4 durch Bildung der Amidbindungen zwischen Hep und Chi zu stärken. Das Wachstumsverhalten, die Stabilität, sowie die physiochemischen und mechanischen Eigenschaften von PEMs werden systematisch untersucht. Die Ergebnisse zeigen, dass die kovalente Vernetzung die Integrität von PEMs aufrechterhält, während eine teilweise Zersetzung

unvernetzter PEMs nach Einwirkung von physiologischem Puffer bei pH 7,4, insbesondere bei den aus LMW* gebildeten zu beobachten ist. Die sich ergebende Oberflächenbenetzbarkeit und die mechanischen Eigenschaften bestätigen, dass die PEM mit HMW auf Temperaturen bei 20 °C und 37 °C reagiert, während LMW* die Änderung dieser Eigenschaften einschränkt. Darüber hinaus hält die Verwendung von Hep als finale Schicht in Kombination mit HMW das adhäsive Protein Vitronektin (VN) bei 37 °C besser zurück, was außerdem mit der anhaltenden Freisetzung von Fibroblasten-Wachstumsfaktor-2 (FGF-2) korrespondiert. Dies ist die erste Studie, die den synergistischen Effekt von auf PEM immobilisiertem VN und FGF-2 und seinen Einfluss auf Zellaktivitäten untersucht. Nicht nur die spezifische Interaktion mit Hep, sondern auch die hydrophobe Interaktion mit HMW tragen zur Bindung von VN und FGF-2 bei und fördern wiederum überlegene Zellaktivitäten in Bezug auf Zelladhäsion, Ausbreitung, Proliferation und Migration unter Verwendung der multipotenten Maus-Fibroblasten-Zelllinie C3H10T1/2 und 3T3.

Im zweiten Teil dieser Doktorarbeit wird ein mimetisches GAG, CS mit außergewöhnlicher Bioaktivität, verwendet, um nach der Möglichkeit zu suchen, native GAGs aufgrund ihrer chemischen Variabilität in verschiedenen Chargen zu ersetzen. Es werden zwei neuartige Synthesewege zur Herstellung von PNIPAM-gepfropftem Cellulosesulfat (PCS) als Polyanion mit unterschiedlichen Substitutionsgraden von PNIPAM- und Sulfatgruppen entwickelt, um thermoresponsive und bioaktive PEM durch die LbL-Technik herzustellen. Niedrig sulfatiertes PCS 1 (DS 0,41) und höher sulfatiertes PCS 2 (DS 0,93) werden verwendet, um deren Fähigkeit zur Bildung von PEM mit Polykationen (Poly-L-Lysin (PLL) oder quaternisiertes Chitosan (QChi)) zu untersuchen. Das resultierende Wachstumsverhalten, die innere Struktur, die Stabilität und die Oberflächeneigenschaften hängen stark vom Sulfatierungsgrad, der Art des Polykations und der Anwesenheit von PNIPAM ab. Das höher sulfatierte PCS 2 überwindet die sterische Hinderung von PNIPAM, ermöglicht eine höhere Adsorption beider Polykationen und bildet nach Einwirkung von pH 7,4 ein stabileres PEM im Vergleich zum niedriger sulfatierten PCS 1. Darüber hinaus neigt das kleinere PLL-Molekül dazu, eine stärker vermischte PEM zu bilden als das größere QCHI, was zu einem stärkeren Effekt auf die Oberflächeneigenschaften führt. Die Studie zur Oberflächencharakterisierung steht außerdem im Zusammenhang mit der Toxizität und Biokompatibilität von PEM gegenüber dem Zellverhalten. PEM in Kombination mit

PLL führt insbesondere in Kombination mit PCS1 zu einer höheren Toxizität für 3T3-Zellen, während die Kombination von QChi und PCS2 eine ausgezeichnete Biokompatibilität aufweist und die Zelladhäsion und -proliferation über 7 Tage fördert.

Insgesamt stellt diese Arbeit die neu entwickelten thermoresponsiven Beschichtungen vor, die die Fähigkeit verdeutlichen, Oberflächeneigenschaften zu modulieren und die Bioaktivität durch Einbeziehung von PNIPAM in Kombination mit nativen oder halbsynthetischen GAGs zu verbessern. Diese Beschichtungen haben ein enormes Potenzial als Zellkultursubstrat für die Freisetzung von Wachstumsfaktoren und die Produktion von (Stamm-)Zellen sowie als bioaktive Wundauflage zur Geweberegeneration.

Chapter 1 – Introduction

This thesis consists of four publications. The first chapter is a general introduction for the research topics of this thesis. Three of four manuscripts have been published and assembled as chapter 2, 3, and 5 including a summary at the beginning of each chapter. The fourth manuscript has been submitted to Biomaterials Advances and represents chapter 4. Chapter 5 has been implemented partly in the introduction when discussing cellulose sulfates.

1   Basis of tissue engineering

Severe injuries but also infections and aging cause the failure of tissues and organs which represents a challenge for the body to repair completely. Although the development of organ transplantation has successfully treated many patients in the majority of cases, the clinical application is still limited due to critical shortage of donors, immune rejection by the recipient, and high mortality rate for aging people after surgery [1]. With the first concept by Langer and Vacanti in early 1990, tissue engineering has emerged as a different strategy with the main aim to maintain, restore and repair the function of tissues or organs and to overcome the drawbacks of organ transplantation [2].

Study on tissue engineering is highly interdisciplinary involving biology, chemistry, material science and engineering to create bioartificial substitutes that mimics the biological environment and functions for tissue regeneration [3]. Tissue engineering is classified into three main approaches: (i) cell therapy, treating injured tissues with the injection of cells grown in vitro; (ii) tissue inducing substance, delivering bioactive substances like growth factors to induce tissue regeneration in the local tissue; (iii) the bioartificial matrix combined with or without cells, transplanting cell adhered and fixed on the matrix (so called as 'scaffold') as a guiding template to induce local tissue regeneration in vivo [4]. However, most of cases are under clinical trials since cell transplantation requires a large number of cells, preservation of cell phenotype, and prevention of mutation during cell expansion [5]. Although stem cells have turned cell therapy into a new era, the lack of cell fixation in the local site of injury reduces the efficiency of new tissue regeneration [6]. Therefore, current strategy mostly focuses on the combination of cells, bioartificial matrix and growth factors/small molecules to promote cell responses including adhesion, growth, migration and differentiation that benefits rapid tissue regeneration at the desired injured site [4].

Progress in tissue engineering has evolved rapidly and helped to treat many patients, for instance, by commercially available skin substitutes, bone and cartilage replacements [5]. Also, engineered tissues like cornea and blood vessel are under clinical trials [7,8]. These engineered living constructs can also be used as reliable sources for in vitro models of healthy or pathological tissues or organs, applicable for disease modeling and drug screening. Despite the fast growing research in tissue engineering, challenges remain due to the complexity of native tissues or organs,

concerns regarding the compatibility of bioartificial constructs, and the difficulty of large-scale production of specific cells [1]. To design a biomimetic and functional tissue substitute, multiple factors must be considered including cell source, material properties and structures, and environment to mimic the native physiological conditions (**Figure 1**). Particularly, biocompatibility, biodegradability, and bioactivity of these constructs are critical characteristics to be integrated in the host tissues or organs to avoid toxicity and immune rejection. Thus, various components important for building the tissue-engineered constructs are discussed in the following section.
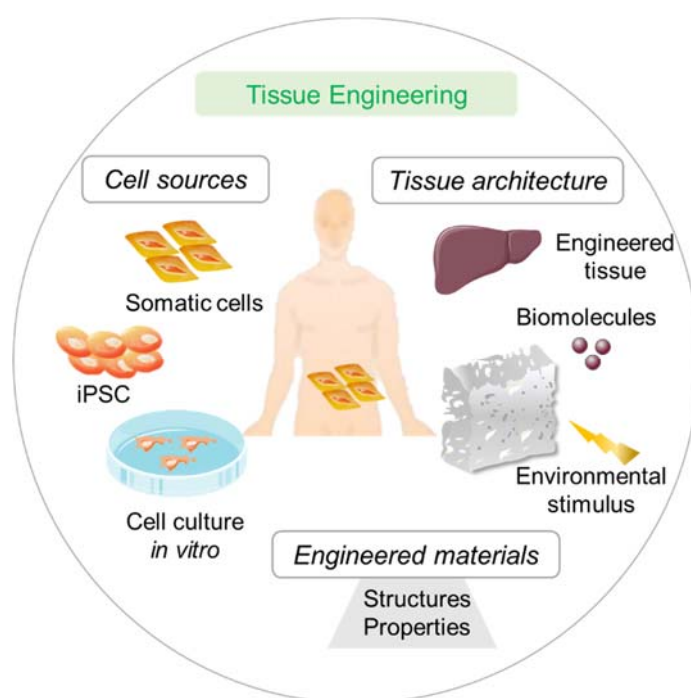

Figure 1. The development of tissue engineering focuses on derivation of cell sources, fabrication of tissue architecture and tailoring structures and properties of engineered materials to mimic native physiological condition of tissues and organs. Created by the Servier Medical Art Commons Attribution 3.0 Unported License.

1.1   *General introduction and application of (stem) cells in tissue engineering*

In general, cell types used for tissue engineering are derived from diverse sources including autologous cells, allogeneic cells, and xenogeneic cells of the same patient, genetically different donors, and different species, respectively [5]. Nevertheless, using allogeneic and xenogeneic cells are not preferred due to the issue of immune rejection. Although mature cells like fibroblasts, epithelial cells, and endothelial cells represent a

large population of specific cell type in the human body that are easily translational, they are still restricted in clinical application due to limited division in vitro and age-associated problem [9]. Stem cell research is popular as a promising cell source since they exist during embryonic development to differentiate into the whole organism of the fetus, and later contribute to the renewal and regeneration of tissues and organs in adult organism. Based on the ability of self-renewal and differentiation into multiple lineages, stem cells are classified into five types: totipotent, pluripotent, multipotent, oligopotent and unipotent (**Figure 2**) [5].
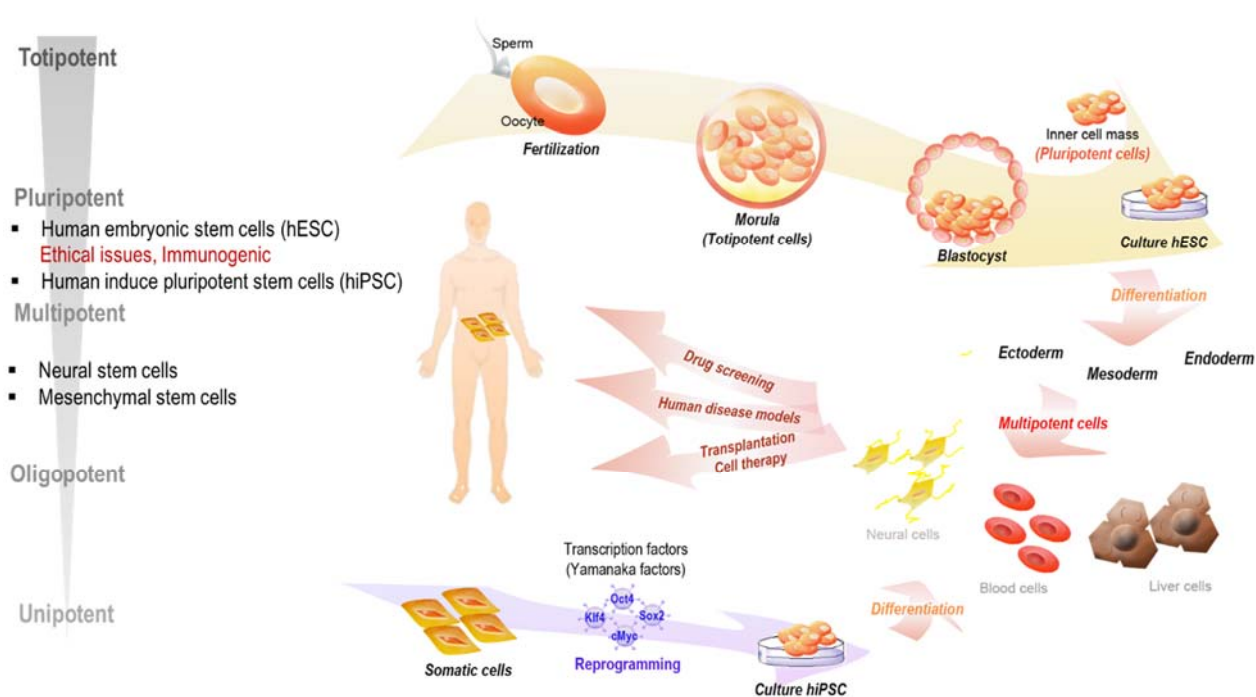

Figure 2. Classification of stem cells including totipotent, pluripotent, multipotent, oligopotent, and unipotent. Diagram of the development and differentiation of human pluripotent stem cells (embryonic stem cells, ESCs and induce pluripotent stem cells, iPSCs) into three germ layers (ectoderm, mesoderm, endoderm). Mature cells derived from pluripotent or multipotent stem cells can be applied for drug screening, human disease models and cell therapy to ultimately treat patients.

Totipotent stem cells are morula formed after fertilization of sperm and oocyte that have an ability to divide and differentiate into all types of the cells that form the whole organism [10]. They have the highest proliferative and differentiation ability to form the embryo and extra-embryonic structures. When an embryo undergoes preimplantation, the pluripotent embryonic stem cells (ESCs) can be derived from the inner cell mass of blastocysts (**Figure 2**). ECSs are capable of self-renewal and have the potential to

differentiate into three germ layers: ectoderm (epidermal tissues and nerves), mesoderm (bone, muscle and blood), endoderm (pancreas, liver and lungs) [5]. Under the control of transcription factors and a cascades of signal transduction pathways, ESCs can maintain their pluripotency at undifferentiated state, or generate multipotent and progenitor cells to differentiate into specific cell types. Since 1998, the first human ESCs (hESCs) was isolated by James Thomson's group [11], research on regenerative medicine, disease modeling and drug screening has been heavily relied on the therapeutic potential of hESCs. Several diseases using hESC-derived cells are under clinic trials such as Parkinson's disease, spinal cord injury, and type I diabetes [12]. However, there are two main concerns of using hESCs in the clinical trial, ethical issue regarding the damage of human embryo and immune rejection due to the allogenic cell source after transplantation [12]. Therefore, as a groundbreaking study conducted by Yamanaka's group in 2007, human induced pluripotent stem cells (human iPSCs) were successfully generated from patient's own somatic cells by reprogramming process with the pluripotent genes such as Oct3/4, Sox2, Klf4, and cMyc (**Figure 2**) [13]. With the similarity to ESCs in many aspects including expression of the same pluripotent genes and proteins, pluripotency, embryoid body formation and differentiation ability, iPSCs overcome the immunogenic and ethical issues of ESCs. Nevertheless, if there are some undifferentiated PSCs remain in the final derived cells, it will keep proliferation and may form tumor/teratoma [12].

While a complicated protocol is generally required to guide pluripotent ESCs and iPSCs differentiation into specific lineage and the following desired mature cells with low efficiency and purity, adult stem cells (ASCs) isolated from somatic cells of the adult human possess specific differentiation ability to the certain lineages. They can be derived from mature tissues, for example, multipotent stem cells like mesenchymal stem cells (MSCs) are isolated from bone marrow, amniotic fluid and fat [14], and hematopoietic stem cells (HSCs) are derived from umbilical cord blood [15]. Unlike pluripotent ESCs and iPSCs, no report shows these ASCs differentiate to tumors/teratoma. In addition, they can be used to reconstitute the damage tissues as an allogenic source for another patient, thereby mitigating the risk of immune rejection [16,17]. Therefore, ASCs are considered as more suitable and promising stem cell sources for the application in tissue engineering. The most widely used stem cells are MSCs with immunoregulatory functions and multilineage differentiation potentials ,

such as bone, muscle, and cartilage that have been approved to treat bone diseases [17]. They also play important roles in differentiation into cardiovascular cells to clinically improve and restore the cardiac function for the cardiovascular diseases such as heart attack or heart failure [16]. Although ASCs are more easily accessible in the clinical application, there are difficulties to isolate and purify them from tissues and maintain their phenotype during expansion. In addition, their proliferative capacity is limited depending on the kind of tissue and the age of patients [5]. The comparison of three main stem cells with benefits and limitations is listed in **Table 1**.

Table 1. Benefits and limitations using embryonic stem cells (ESC), induce pluripotent stem cells (iPSC) and adult stem cells (ASC).

	ESC (Embryonic stem cells)	iPSC (Induce pluripotent stem cells)	ASC (Adult stem cells)
Benefits	• Pluripotent • Indefinite self-renewal activity	• Pluripotent • Indefinite self-renewal activity • No ethical issues • Non- immunogenic (autologous)	• No ethical issues • Non- immunogenic (autologous, allogenic) • Low risk of teratoma formation
Limitations	• Ethical issues • Immunogenic • Potential risk of teratoma formation • Differentiation protocol: efficiency and purity initially slow to progress towards specific tissue cells	• Low programming efficiency • Potential risk of teratoma formation • Differentiation protocol: efficiency and purity initially slow to progress towards specific tissue cells	• Not pluripotent • Limited self-renewal activity • Difficult to isolate pure population

Compared to stem cells, fibroblasts are easily accessible by biopsies and has been widely used as a model cell in studies on tissue regeneration and wound healing. Fibroblast is the main cell type in connective tissue capable of synthesizing extracellular matrix (ECM) proteins like collagen and fibronectin (FN) to maintain structural integrity of tissues or organs [18]. In particular, fibroblasts play predominant roles in three phases of wound healing, namely inflammation, proliferation and remodeling after hemostasis [19]. During inflammation phase, fibroblasts are activated and recruited in a crosstalk with immune cells by producing proinflammatory cytokines and releasing chemokines [20,21]. They become more actively during proliferation phase, secreting proangiogenic molecules, including vascular endothelial growth factor (VEGF), fibroblast growth factors (FGFs) to promote angiogenesis and the formation

of granulation tissue [22,23]. Later of this stage, fibroblasts begin to differentiate into myofibroblasts for wound contraction and deposit the 'late provisional matrix' constituted of FN and collagen III that supports keratinocyte migration for re-epithelialization [24]. The final phase undergoes wound contraction, vascularization and cellularity decline regulated by myofibroblasts. Once the wound closes and repairs, myofibroblasts undergo apoptosis or turn into quiescent state.

When cultured under appropriate conditions such as stimulation by biological factors and mechanical force, fibroblasts have mesenchymal-like differentiation ability not only into adipogenic, osteoblastogenic, and chondrogenic lineages but also hepatocytes and neural cells [25–27]. In addition, fibroblasts were found to have a greater proliferative capacity with shorter doubling time than MSCs, making them an ideal model to efficiently promote cell growth and regeneration [27]. This provides the advantage of using fast-growing fibroblasts to shorten the time for reprogramming into patient-specific iPSC and differentiation into desired cell type [13].

1.2   The importance of microenvironment for (stem) cells

Stem cells are capable of self-renewal and giving rise to the differentiated daughter cells under a certain microenvironment. Like the somatic cells with important biological activities, cell adhesion, spreading, proliferation, migration, differentiation, and apoptosis are regulated by physical and chemical cues from the environment. These cues interact with specific ligands through transmembrane cell receptors leading to a cascade of molecular signal transduction events to determine structural change in cells [28].

Cell microenvironment, also called 'niche', is dynamic and composed of a complex combination of factors maintaining the balance between self-renewal and differentiation. Niches are specially recognized by each type of cells based on the key components including (i) communications between cells and the neighboring supportive cells, (ii) interaction between cells and surrounding ECM, (iii) soluble and secreted factors and (iv) additional sources like physical and environmental stimuli (**Figure 3**). The significance of niches maintains proper cell functions while protects them from damage by initiating the crosstalk of different factors for cell renewal and repair in tissues [29].
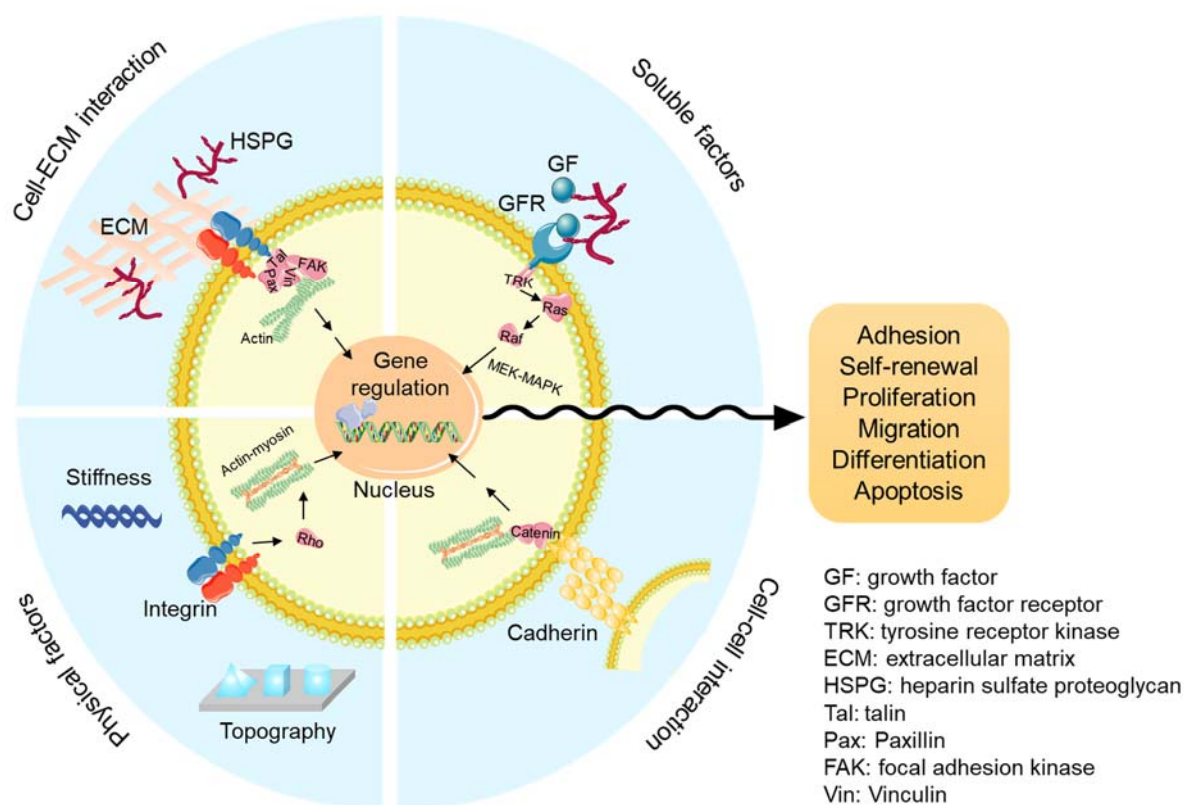
Figure 3. Cell responses are regulated by microenvironmental cues (niches) including cell−cell interaction, cell−ECM interaction, soluble factors, and physical factors that generate a cascade of molecular signal transductions through transmembrane cell receptors Created by the Servier Medical Art Commons Attribution 3.0 Unported License.

Communications between neighboring cells

The interaction between cells is mainly mediated by physical contact through cell−cell adhesion molecules and membrane receptors bound with ligands. The cell adhesion molecules dominantly associated with the cell−cell adhesion are selectins, members of immunoglobulin superfamily, and cadherins. While selectins and immunoglobulin superfamily on endothelial cells are involved in the heterophilic cell–cell interactions for trafficking and migration of lymphocytes to the site of inflammation or injury, cadherin is crucial for the homophilic adhesion between the neighboring epithelial cells [30]. Cadherins are a family of homophilic adhesion receptors that play a key role in anchoring the adjacent cells in the extracellular domain involving Ca^{2+}-dependent adhesion mechanism. Their association with α-, β- catenin, and p120 is essential to bind vinculin, actin or intermediate filaments for maintaining tissue stability and cell

mobilization [30]. In particular, E-cadherin is required to maintain self-renewal and pluripotency in PSCs regarding its role in embryonic development and early differentiation [31].

Role of the extracellular matrix in the cell niche

ECM plays a predominant role in cell niche in most of tissues while its composition and nature depends on the type and location of tissues. The interaction between ECM and cells involves various intracellular signaling pathways through a number of receptors not only for anchoring cells in the niches but also to determine cell fate. The major receptors mediating cell adhesion, anchorage and localization are integrins, a large family of transmembrane receptors including at least 24 heterodimers, which dimerize from an α subunit and a β subunit [30]. By specific binding of ECM components on cell surface as chemical signals, integrins activate the downstream signaling that is associated with the conformational change of integrin, a dozen of intracellular proteins forming cell attachment structure (named as 'focal adhesion'), and the stabilization of actin cytoskeleton. The affinity of integrins to different ECM proteins is especially distinct even to the same protein. For example, $\alpha_1\beta_1$ and $\alpha_2\beta_1$ integrin can bind to both the fibrillar collagen I in connective tissue and the non-fibrillar collagen IV in basement membrane. While the association of $\alpha_1\beta_1$ is stronger with collagen IV, $\alpha_2\beta_1$ has higher affinity to collagen I [32]. The integrin β_1 is particularly crucial for stem cell adhesion, self-renewal and proliferation that activates the downstream signaling pathway through focal adhesion kinase (FAK) and phosphoinositide 3-kinase (PI3K) [33]. In addition to integrin $\alpha_v\beta_1$ binding to FN and vitronectin (VN), the part of a region on both proteins containing the peptide sequence of arginine–glycine–aspartate (RGD) is important for stem cell adhesion and proliferation. Integrin $\alpha_v\beta_5$ interacting with VN has been demonstrated a key for adhesion and self-renewal of undifferentiated hPSCs essential for long-term culture [34]. Different to classical ECM proteins that support structural integrity of tissue, VN is a component of blood plasma and mostly synthesized by hepatocytes considered as matricellular protein and provisional ECM. Upon injury, VN interacts with fibrinogen and with PAI-1 as complexes to prevent unintended coagulation and fibrinolysis. It undergoes a conformational change and self-assembly into fibrils forming an interconnected network with other proteins (e.g. fibrin, FN, factor XIII) to support cell survival and tissue repair [35].

On the other hand, proteoglycans (PGs) and GAGs are also major ECM components existing in basal lamina and connective tissues, contributing to the formation of network structures within ECM and to the stabilization of the interactions between different ECM components like collagen, FN, laminin, and glycoproteins [30]. PGs act importantly not only as a structure support for the formation of ECM scaffold but also as an integrator to govern cell behaviors through the main signaling cascades. PGs are generally characterized by a protein core with specific protein sequences containing serine that serve as links to longer linear chains of GAGs. Regarding abundant negatively charged sulfate, carboxylic, and hydroxyl groups, these GAGs are highly hydrated important for mechanical properties of tissues, such as the compression stability, and contribution to homeostasis of electrolytes. GAGs also have high affinity to numerous proteins that possesses GAG-binding domains, including ECM proteins, cell surface receptors, growth factors, chemokines, and cytokines to mediate cell functions [36]. For instance, syndecans are the typical cell surface PGs carrying the GAG chains including heparin sulfate and chondroitin sulfate. They function as co-receptors for the binding of growth factors or adhesive proteins to the corresponding receptors and involved in several signal transduction cascades [37]. Among GAGs, heparin with the highest sulfation degree (2.3−2.8 sulfates/disaccharide) has been reported to enhance activity of FGF-2 signaling to maintain the stemness of human PSCs [38,39].

Soluble factors

The soluble factors including growth factors (GFs) and other cytokines are secreted by cells and act locally during tissue development, homeostasis and repair. They not only mediate indirect communication between cells and niches through paracrine or autocrine actions but also trigger intracellular signal transductions via surface cell receptors (e.g., FGFs act through tyrosine receptor kinases) to regulate cell functions such as stimulation or inhibition of cell proliferation, migration, and differentiation. Many GFs have pleiotropic effects playing pivotal roles in maintaining self-renewal and pluripotency in stem cells. FGF-2 alone or in concomitance with Activin/Nodal/transforming growth factor beta (TGF-β) are well-known for maintaining hPSC undifferentiated and alive by binding to corresponding receptors to stimulate FGF and Activin/Nodal/TGFβ signaling pathways [40]. The following activation of downstream signaling cascades including mitogen-activated protein kinases (MAPKs), PI3K, and Smad2/3 promotes the expression of pluripotent genes and blocks the bone

morphogenetic protein (BMP) signaling from differentiation. On the other hand, FGF-2 also induces angiogenesis and bone regeneration, which has been reported to enhance the differentiation potentials of MSCs to osteoblasts and chondrocytes by upregulating the respective signaling molecules [41,42]. Another key feature of these secreted factors is their capability to bind to ECM components like adhesive proteins (e.g. VN, FN) and PGs, increasing the local concentration of these agonists to induces signal transductions and regulate cell functions [28]. Owing to the GAG-binding domain on GFs, GAGs also acts as a storage depot protecting GFs from proteolytic degradation to prolong their half-life as it is found for PG of the ECM [36,43]. In addition, integrin and GF receptor can either independently or cooperatively activate the same signal pathways in a concomitant way. The crosstalk between integrin and GF receptor can activate the important downstream signaling that regulate cell activities and stemness of stem cells, such as PI3K and MAPK signaling [33,44].

Biophysical properties of microenvironment

In addition to biological cues such as ECM components and secreted factors, biophysical cues like topography and mechanical properties of microenvironment are considerably important for determination of cell fate. Throughout the human body, tissues exhibit different levels of stiffness from soft neural tissue to rigid bone. Cells can sense external forces generated from the elasticity of ECMs and the compression of neighboring cells primarily through local cell−integrin anchoring sites. Integrins are responsible for mechanosensing to transmit the extracellular mechanical signal from ECMs to cells and regulate intracellular cytoskeleton [45]. The multiprotein complexes, focal adhesion, plays a central role in linking the contractile actomyosin cytoskeleton and integrins that induces mechanotransduction involving Rho family GTPases to regulates cell phenotype, such as cell geometry, and cytoskeleton organization [45]. In addition, recent evidence has found that cell morphology can be affected by a direct transmission of the mechanical signal to nucleus through the cytoskeleton. This signal causes the deformation of nucleus and conformational change of nuclear lamina to induce chromatin stretching and expression of a reporter transgene [46]. Integrin-induced mechanosensing alone or involving GFs could determine cell phenotype, especially associated with differentiation of stem cell to specific lineage by the crosstalk between integrin, mechanotransduction and GF signaling pathway [44]. For example, the combination of matrix stiffness and TGF-β has been demonstrated to promote the

expression of chondrocyte differentiation, as cells integrate the signaling from both biophysical and biochemical cues [47]. Therefore, elasticity of ECM is important for specific lineage differentiation of stem cells regarding the structural regulation of focal adhesion and cytoskeleton manipulated by the mechanosensing.

Engineered tissue-like scaffolds

Understanding the interactions between cells and microenvironments is crucial for designing biomaterials used in tissue-engineered constructs that mimic the niches of real tissues. Currently, the abovementioned factors are intensely employed in biomimetic biomaterials to render the bioactivity of the constructs, aiming to restore the functions of the damaged site, or controlling cellular behaviors into desired cell types. Biomaterials used in tissue engineering are generally categorized into two subtypes: naturally occurring and synthetic materials. Naturally occurring materials are based on components derived from ECM such as proteins (e.g. collagen, FN) and GAGs or from other organism like polysaccharides (e.g. chitosan, cellulose, alginate) [48]. These natural polymers are usually biodegradable and biocompatible, possessing exceptional advantages such as similar physical and inherent biological properties to native tissue environment. In particular, using ECM proteins in biomaterials can improve the bioactivity toward cell responses due to the recognition of receptor−ligand interactions. However, purification, batch-to-batch quality, cost, and control over the mechanical properties of natural polymers are the main concerns to be used [5]. By contrast, synthetic materials provide a wide range of selections from metals, ceramics to synthetic polymers that can be precisely and consistently produced with readily controlled mechanical strength depending on the damaged site. One of the issues is that the majority of the synthetic materials are not biodegradable and biocompatible, causing the pro-inflammatory response in the host tissue resulted in cell death and impairment of tissue function [49]. Thus, the most beneficial strategy for engineering tissue-like biomaterials is combining both advantages from properties of natural and synthetic materials to control biodegradability, biocompatibility, bioactivity, and mechanical strength.

2 Isolation and production of cells for tissue engineering applications

Cell adhesion plays an important role in cell communication and regulation for maintenance and development of tissues and organs [48]. In vivo, cell fate is

predominately controlled by cell adhesion between cell−cell or cell−ECM matrix that stimulates intracellular signals through cell receptors to regulate cell phenotype, cycle, migration and survival. The tight cell−cell interaction at epithelia is mediated by cadherin forming impermeable layers outside and inside of the organisms. These cells interact with the underlying thin layer of ECM through integrins called lamina containing key components such as collagen IV and laminin. Connective tissue is a combination of cells, abundant fibrous ECM proteins and GAGs providing structural integrity of tissues [30]. Remodeling of ECM by resident cells through synthesis, enzymatic degradation and release of biomolecules is necessary for embryonic and tissue development, regeneration and homeostasis [50,51]. Cell adhesion is also related to pathological diseases including cancer, arthritis, and osteoporosis resulting from lower adhesion and destruction of tissue structure that can be observed by the morphological change [52]. Therefore, engineering an appropriate adhesive surface of biomaterials is prerequisite for cell adhesion and the progressive processes such as cell movement, proliferation and differentiation in tissue regeneration. Interaction between cells and an engineered substrate is not only dependent on surface properties of the substrate, but also associated with adsorption of ECM proteins on the substrate that is from tissue fluids, the serum in the culture medium, or secreted from cells [30]. Primary adhesion of suspended cells on surfaces in vitro is mediated by non-specific interaction, such as Coulomb, van der Waals forces, hydrogen bonds, and hydrophobic interaction [30]. Physiochemical properties of substrata like charge density, wettability and chemical functionality affect protein adsorption and subsequent cell adhesion [53,54]. For example, cell adhesion is inhibited by highly hydrophilic and hydrophobic surfaces due to suppression of protein binding to hydrated surfaces and the conformational change of proteins driven by hydrophobic interaction. Denatured proteins on the hydrophobic surface hinder specific cell binding site for cell adhesion [55]. When cells bind to the adsorbed ECM proteins, specific interaction between cells and these proteins through integrin occurs to activate the intracellular responses including the formation of focal adhesions and cytoskeleton. The following event is accompanied by the formation and organization of stress fiber and generation of contractile force to promote cell spreading and migration. After cell adhesion, cells can undergo growth and expansion to reach a maximum confluent cell monolayer which has strong connections between cells through cadherin and cell−substrate [56].

The most common approaches for cell transplantation in tissue regeneration therapies including intravenous/intraarterial infusion or direct intratissue injection require cell harvest process from the substrata (**Figure 4B**) [57]. Cell detachment is typically achieved by potentially harmful proteolytic enzymes, chelating agents, or mechanical forces **(Figure 4A)**. Enzymes like trypsin digest cell adhesion molecules and deposited ECM on the interfaces between cell−substrate and cell−cell, while chelating treatment using ethylenediaminetetraacetic acid (EDTA) depletes divalent cations (e.g. calcium ion, magnesium ion) from cells [58,59]. Consequently, damages on ECM/cell receptors and breaks between cell−cell junctions disrupt cell integrity resulted in the suspension of individual cells. Physical detachment by scraping a cell sheet from the surface could impair cell integrity leading to low cell viability due to the destruction of the cell membrane and membrane proteins [60]. In addition to these processes for cell harvest, poor cell localization, persistence and survival at the injury site are also the main reasons for low efficiency of cell transplantation [57]. On the other hand, scaffold-embedded cells for tissue engineering may overcome the limitations of direct cell injections as it provides bioartificial tissue analogues that is promising for cell delivery in preclinical and clinical trials **(Figure 4B)** [61,62]. However, complicated technology, poor understanding of the mechanism, and critical balance between the rate of tissue formation and scaffold degradation limit its clinical application and large-scale reproduction.

Therefore, scaffold-free cell constructs consisting of layers of cell sheets from the same or different cell types surrounded by secreted and tissue-specific ECMs that allow retention of cell−cell and cell−ECM interaction exploit the tissue analogues by engineering macrotissues (**Figure 4B**). Through certain environmental stimuli like temperature, pH or electricity, a change in physicochemical properties of substrata and protein desorption can be induced, and thereby detachment of a cell monolayer 'sheet' from the culture substrate is achieved [63–65]. Since the generated cell sheets preserve cell junctions and deposited ECMs adhesive to biological entities, they can be directly transplanted to injured tissue without any additional fixation like sutures at the target site. It has shown a superior cell survival at the transplanted site to recover heart function after four weeks transplantation of cardiac cell sheets in comparison to cell injection [66]. Over the years, cell sheet engineering has shown successful

outcomes to treat the damaged tissues such as bone defect, heart failure, and corneal injury [67–70].
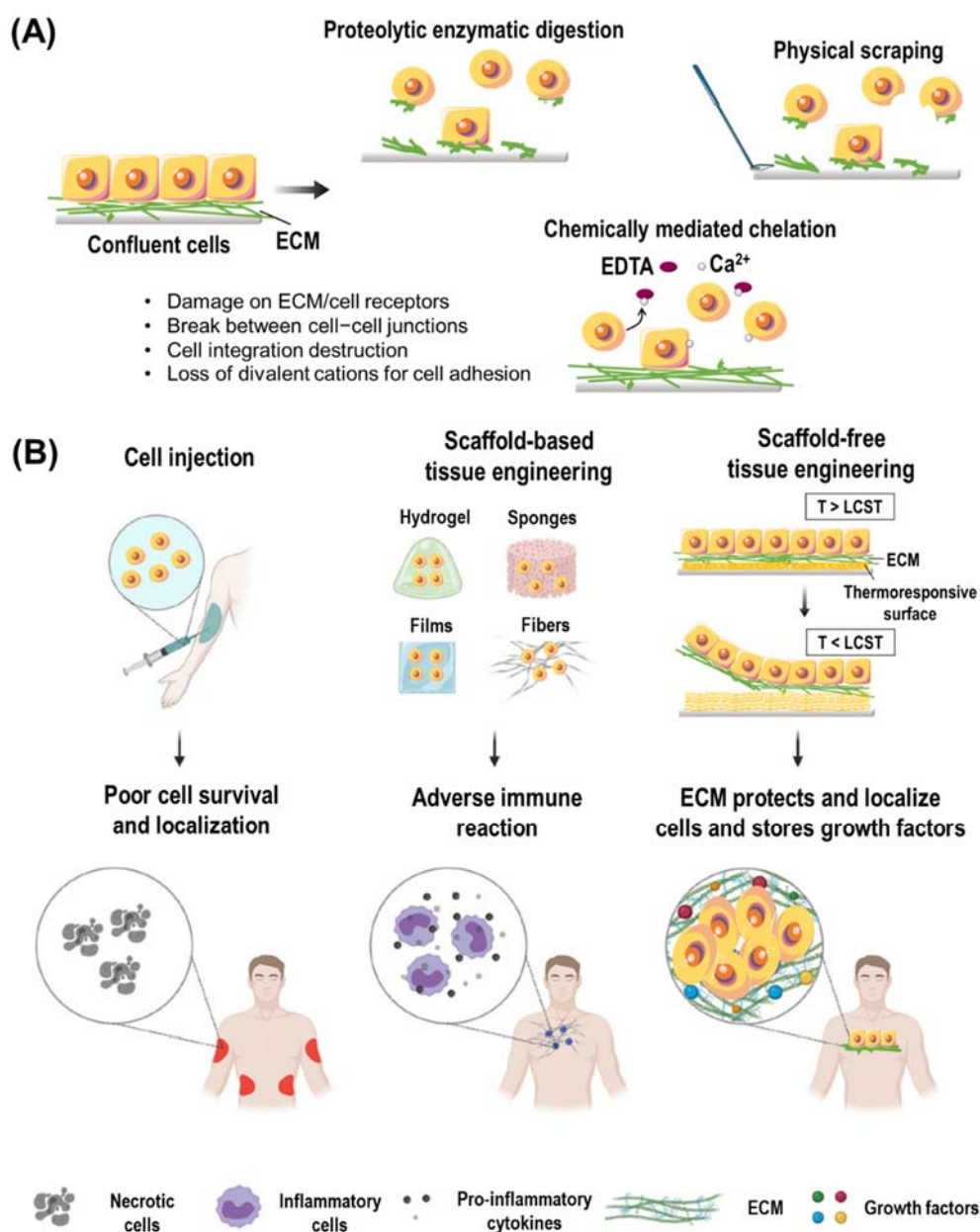

Figure 4. (A) Conventional cell harvesting methods: proteolytic enzymatic digestion, chemically mediated chelation, and physical scrapping. (B) Cell-based tissue engineering therapies through transplantation of cell suspension, scaffold-embedded cells, or scaffold-free cell sheets. Adapted from [57] using the Servier Medical Art Commons Attribution 3.0 Unported License.

2.1 Thermoresponsive poly(N-isopropylacrylamide) for cell sheet engineering

The concept of cell sheet engineering is pioneered by Okano's group during 1990s, controlling the interaction between a thermoresponsive cell culture substratum and proteins/cells by simply reducing the temperature [71]. A thermoresponsive polymer, poly(*N*-isopropylacrylamide) (PNIPAM) was the first and most intensively studied material for cell sheet engineering. In 1967, Heskins and Guillet reported the unique phase transition behavior of PNIPAM in an aqueous solution across 32 °C, known as lower critical solution temperature (LCST) [72]. The conformation, solubility, and wettability of PNIPAM can be reversibly altered when passing through LCST ascribed to hydrophilic amide groups and hydrophobic isopropyl groups of PNIPAM. Below LCST, the structure of PNIPAM is extended and hydrated surrounded by the water molecules through hydrogen bonds with hydrophilic groups (**Figure 5A**). When heating across LCST, an immense amount of water is released from hydrophilic groups and hydrophobic groups are exposed leading to the conformational change that undergoes a coil-to-globule transition. Consequently, PNIPAM becomes insoluble in the aqueous solution resulting from dehydration of the collapsed chains and hydrophobic interaction between the hydrophobic groups. The popularity of PNIPAM used for cell sheet engineering is because of the non-toxic feature, excellent biocompatibility, and its LCST close to human body temperature (37 °C) that is independent of molecular weight and concentration [73,74]. To generate a cell sheet, cells are initially seeded on PNIPAM-grafted surface and cultured at 37 °C above LCST, at which PNIPAM chains are collapsed resulting in a dehydrated surface facilitating protein adsorption, and consequently promoting cell adhesion through integrin binding to the adsorbed proteins. In general, adherent cells generate traction and contraction forces by the formation of stress fibers on the surface [75]. These pulling forces of cytoskeleton and tensile stress of the ECMs reach equilibrium on the surface. When cells reach confluency, reducing environmental temperature to below LCST (e.g., 4 °C or 20 °C) weakens the binding of proteins to the surface due to the hydration force caused by exposure of the hydrophilic groups on PNIPAM. As a result, tensile stress generated by cytoskeleton is remained from the loss of equilibrium force leading to rolling and contraction of a cell layer to generate a cell sheet (**Figure 5B**) [74].
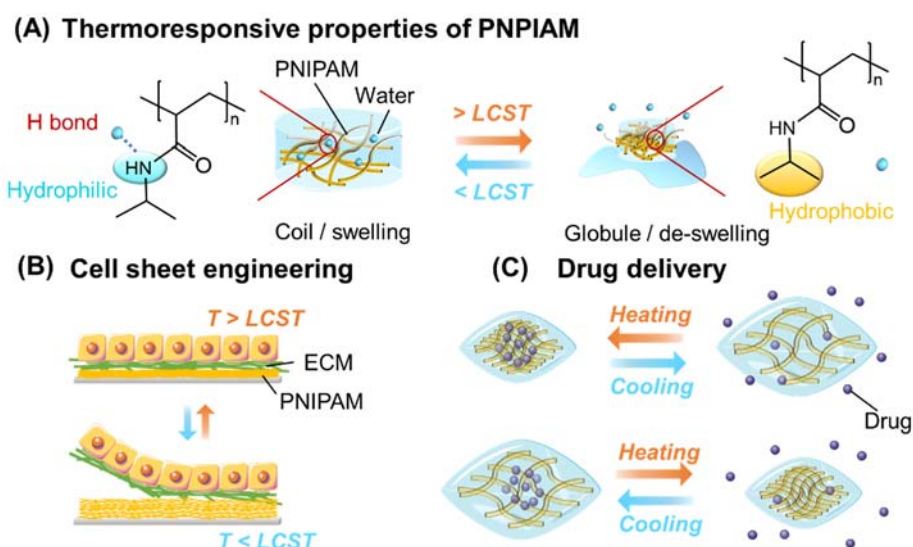
Figure 5. Illustration of (A) PNIPAM conformation below and above LCST. Application of PNIPAM hydrogels (B) as cell culture substrata for cell sheet engineering and (C) as drug reservoirs to control drug delivery. Created by the Servier Medical Art Commons Attribution 3.0 Unported License.

The first commercially available thermoresponsive culture substrate was established by Yamada et al. in 1990, introducing a PNIPAM layer on the substrate by electron-beam (EB) irradiation [71]. This PNIPAM-grafted surface exhibits thermoresponsive behaviors, allowing modulation of wettability to successfully harvest cell sheets by the temperature control. To fabricate PNIPAM-grafted surface for cell sheet engineering, a balance between hydrophobicity for cell adhesion and hydrophilicity for cell detachment must be taken into consideration [76,77]. Thickness and type of substrate are the direct factors to be adjusted for the surface wettability. The PNIPAM layer with a thickness of 15−20 nm on tissue culture polystyrene (TCPS) is optimal for cell adhesion and detachment. In comparison, a PNIPAM layer with only 3.5−5 nm on the glass is ideal for controlling cell adhesion and detachment, which is linked to the wettability of the substrate. Other methods to fabricate PNIPAM-grafted surfaces were also developed to better control thickness, grafting density, chain length and polydispersity of layers and surface wettability such as plasma polymerization [78], UV and visible light irradiation [79,80], living radical polymerization such as atom transfer radical polymerization (ATRP) and reversible addition fragmentation chain transfer (RAFT) [81–83].

Physical deposition of the polymer PNIPAM provides a rather easier procedure and economic process of surface modification such as using spin coating [84]. This approach enables the introduction of various blocks, such as hydrophilic, hydrophobic, ionic or functional polymer to PNIPAM. It facilitates the physical binding of functionalized PNIPAM to the surface and modulation of the properties including transition temperature, surface wettability, mechanical properties, biodegradability and biocompatibility [85].

2.2 *Thermoresponsive poly(N-isopropylacrylamide) for controlled release including growth factor delivery*

Regarding the sol-gel transition of PNIPAM changing from a soluble fluid to an insoluble hydrogel above LCST, another important application of PNIPAM has been explored as drug carriers for control release of drugs or biomolecules such as proteins, GFs, and antibodies (**Figure 5C**) [86–88]. In addition, PNIPAM can be incorporated with other polymers to form hydrogels based on physical and chemical crosslinking to better control release the drugs [89,90]. In general, small drugs can freely diffuse in and adsorb to the swollen PNIPAM-based hydrogel below LCST, while the release of the drugs is driven by slow physical diffusion [91,92]. Above LCST, the hydrogel becomes shrunk suddenly and pushes the dugs outwards to be rapidly released. However, some studies reported that cooling-mediated release liberates the drugs from the swollen hydrogel below LCST by passive diffusion when the drugs can be entrapped in the shrunken and collapsed hydrogel above LCST [93,94]. The mechanism of biomolecule delivery is very complicated mainly govern by interaction between these molecules and PNIPAM-based hydrogels, which depends on the nature of molecules such as hydrophobicity and isoelectric point (pI), medium pH, and ionic strength [89,95,96]. Aside from the common physical diffusion, Wu et al. thoroughly investigated other driving forces including electrostatic interaction, seizing action, and hydrophobic interaction that control biomolecule delivery in response to pH and temperature strongly related to the biomolecule−PNIPAM hydrogel interaction [88]. They studied the mechanism of the adsorption and controlled release of bovine serum albumin (BSA) as an example in the PNIPAM-based nanogel (**Figure 6**). The electrostatic interaction comes from the positive charges of BSA and negative charges of the nanogel when pH is below the pI of BSA. When temperature is heated to 37 °C, hydrophobic interaction and seizing action contributed to the controlled delivery as

phase transition occurs breaking hydrogen bonds leading to shrinkage of the nanogel and enhanced interaction between BSA and nanogel.
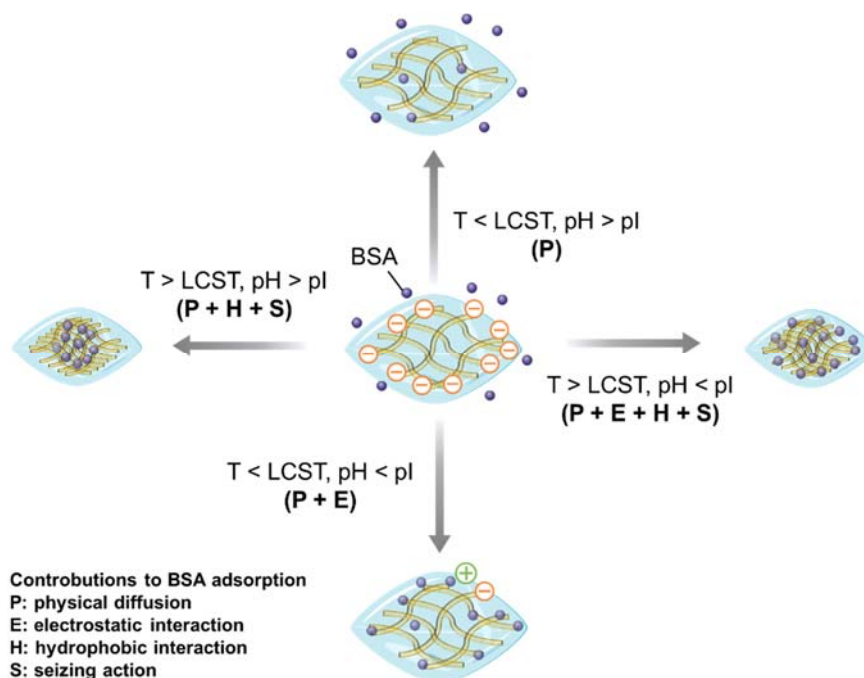

Figure 6. The driving forces including physical diffusion, electrostatic interaction, hydrophobic interaction and seizing action contributing to bovine serum albumin (BSA) adsorption in the PNIPAM nanogel are dependent on environmental temperature and pH. Adapted from [88] using the Servier Medical Art Commons Attribution 3.0 Unported License.

Therefore, PNIPAM-based hydrogel can be employed for the sustained release of proteins including GFs to avoid their rapid degradation in physiological environments and burst release that causes serious side effects such as abnormal tissue formation and inflammation [97]. It has been studied to couple PNIPAM-based hydrogels with GFs in skin wound healing and induction of bone, nerve and retinal regeneration [87,89,98,99]. **Table 2** summarizes delivery systems of GFs based on various PNIPAM-based hydrogels. Mostly, GFs were initially uploaded at low temperature below LCST and encapsulated in the hydrogels by elevating the temperature above LCST. As mentioned earlier, incorporation of PNIPAM with other polymers can modulate its properties like LCST and hydrophobicity to enhance the interaction with GFs. For example, hydrophobic ethyl methacrylate (EMA) and *N*-tert-butylacrylamide (NtBAAm) were used to reduce the LCST of PNIPAM-based hydrogels that not only increased the stability of the hydrogels but also increased the interaction with GFs like

EGF and BMP-2 through hydrophobic interaction above LCST [89,94]. Based on the pI of GFs, the charge density of GFs is dependent on the environmental pH. FGF-2 and EGF are positively charged at pH 7.4 regarding their pI ≈ 9.5 and 8.5, respectively [90,96]. By integrating pH sensitive polymers like propylacrylic acid (PAA) with PNIPAM with a pKa ≈ 6, the gel formation could be controlled and the bioactivity of FGF-2 could be maintained by appropriate pH and temperature [96]. Moreover, association of PNIPAM with bioactive molecules such as polydopamine, collagen, GAGs can improve the interaction between hydrogel and GFs and cell adhesion [98,99]. For example, heparin was immobilized on the PNIPAM-modified surface to bind FGF-2 and promote rapid proliferations of fibroblasts and hepatocytes [100,101].

Table 2. PNIPAM-based hydrogels for GF delivery.

GF/protein delivery	PNIPAM scaffold	Driving force for controlled release	Application	Remarks	Ref.
BMP-2	NIPAM/NASI gel NIPAM/EMA gel	Hydrophobic interaction/ Chemical bond (amide formation)	Rat bone induction	• Loading BMP-2 in the polymer solution at 4 °C Implantation with a collagen sponge • Injection directly without collogen sponge	[89]
VEGF/Alb umin	NIPAM-*co*-NtBAAm film	Slow diffusion/ Hydrophobic interaction	Culture and promote proliferation of human aortic endothelial cells	• Loading EGF/albumin on the film for 7 days at 4 °C and transferred the dish to 37 °C for 1 h • Higher adsorption and slower release of albumin above LCST than below LCST	[94]
FGF-2	PNIPAM-*b*-sulfated PMAGlcC$_5$ film	Hydrophobic interaction/ Specific electrostatic interaction	Promote adhesion and proliferation of human umbilical vein endothelial cells	• Sulfation of glyco-polymers enhanced binding of FGF-2 together with PNIPAM at 37 °C than at RT	[102]
EGF	SPSHU-PNIPAM gel	Slow diffusion/ Specific electrostatic interaction	Promote blood vessel formation and protect cardiac function	• Sulfonation groups helped retain EGF and reduced burst release	[103]
EGF	PDA-NPs-coated PDA-NPs/PNIPAM hydrogels		Promote fibroblast adhesion in vitro and skin wound healing in vivo	• Loading EGF for 3 days at 20 °C and releasing at 37 °C • PDA-NPs-coated PDA-NPs/PNIPAM hydrogels showed better retention of EGF and performance on fibroblast adhesion and wound healing	[99]
NGF	Collagen-PNIPAM	Seizing action/ Hydrophobic interaction	Promote neuronal differentiation of rat pheochromocytoma	• Loading NGF at 4 °C and release at RT or 37 °C • Higher release of NGF at 4 °C than 37 °C • Pre-loaded NGF scaffolds were incubated at 4 °C or 37 °C for 2 h before seeding rat pheochromocytoma for neural study	[98]

Insulin	PNIPAM-*grafted* dish	Slow diffusion	Promoting proliferation of retinal pigmented epithelial cells; Cell sheet engineering	• Loading insulin on the dish for 3 days at 4 °C and transferred the dish to 37 °C for 30 min	[87]
FGF-2 EGF	[P(IPAM-*co*-CIPAM)]-*grafted* surface immobilized with heparin		Enhance adhesion and proliferation of fibroblast; Maintain hepatic function of hepatocytes Cell sheet engineering	• Loading FGF-2 at 20 °C • Stable binding of FGF-2 on heparinized surfaces	[100, 101]
FGF-2/VEGF	P(NIPAM-*co*-PAA) hydrogel	Electrostatic interaction	Storage of FGF-2 Controlled release of VEGF	• Maintaining bioactivity of FGF-2 • Release of EGF depending on pH, temperature for gel formation and electrostatic interaction	[96]
FGF-2/DS	SA/bFGF@pNIPAM/DS@p(NIPAM-co-AA) hydrogel	Slow diffusion/ Electrostatic interaction/ Hydrophobic interaction/ Seizing action	Increase the wound contraction percentage, reduced the inflammation and promoted the angiogenesis	• FGF-2 solution mixed with PNIPAM nanogel at RT and incubated at 37 °C for 2 h • Hydrophobic interaction between PNIPAM and FGF-2 at 37 °C facilitate FGF-2 loading and sustained release	[90]

NASI: nacryloxysuccinimide; EMA: ethyl methacrylate; NtBAAm: *N*-tert-butylacrylamide; MAGlcC5: a,b-*D*-glucofuranosyl-6-methacrylamido hexanoate; SPSHU: salfonated poly(serinol hexamethylene urea); PDA: polydopamine; NP: nanoparticle; CIPAM: 2-carboxyisopropylacrylamide; PAA: propylacrylic acid; DS: diclofenac sodium; SA: sodium alginate

3   Surface modification by layer-by-layer technique

Although several techniques modifying surfaces with PNIPAM have been found versatile for cell sheet engineering and controlled release, some difficulties limit their application including the use of expensive machinery, transition metal ions, toxic initiators, chain transfer agents and chemicals, complicated fabrication processes, and the need of introducing cell-adhesive molecules like RGD to improve cell adhesion [104]. During the last two decades, a facile, flexible, and inexpensive technique, layer-by-layer (LbL) assembly became popular to fabricate a controllable architecture with a thin coating from nano to micrometer scale [105]. The first concept of LbL technique can be traced back to 1966 when Iller generated a film on a solid surface by alternating deposition of a positively and a negatively charged colloidal particle based on inorganic materials (e.g. silica, alumina) [106]. In 1990, Decher et al. further explored this concept and provided the possibility of employing LbL technique to form polyelectrolyte multilayers (PEMs) for biomedical application with organic and biological materials [107,108]. The formation of PEM is initially based on alternating adsorption of the oppositely charged polyelectrolytes (PELs) from aqueous solution via electrostatic interaction followed by washing steps in between to remove the weakly bound PEL

(**Figure 7A**). This deposition process is repeated to reach the desired number of layers representing a multilayer assembly. Since intrinsic ion paring between the oppositely charged PELs is more favorable than extrinsic charge compensation between PEL and small counterions, the main driving force of PEM formation is attributed to thermodynamically entropy gain from the release of counterions and water [109,110]. When the charges within the PEM cannot be neutralized by the oppositely charged PEL due to steric hindrance, the extrinsic compensation by small counterions can occur to neutralize the charges. In addition to the majority of LbL assembly fabricated via electrostatic interaction, other non-electrostatic interactions have attracted attention such as hydrogen bonding, hydrophobic interactions, covalent bonding and specifically biological interactions [111].

3.1 Factors and strategies for multilayer formation via LbL technique

The most effective force to mediate LbL assembly is electrostatic interaction and the following ion paring mainly relying on the long ranged attractive or repulsive force but may also involve other shorted range interactions such as van der Waals force or hydrogen bonding [111]. Using LbL technique to construct multilayer architectures allows precise control of film thickness and properties depending on the type, charge density, and molecular weight of PEL, adsorption and rinsing time, and environment such as ionic strength, pH and temperature [105]. These factors play predominant roles in modulating the growth and internal structure of the PEMs, given with tunable physiochemical, mechanical, topographical, and biological properties. Since the construction process of PEM is important for its internal structure, a thorough screening is required with diverse techniques such as surface plasmon resonance (SPR), quartz crystal microbalance (QCM), ellipsometry, atomic force microscopy (AFM), scanning electron microscopy (SEM) and confocal laser scanning microscopy (CLSM) [111]. In addition, without the prerequisite of active functional groups for the underlying substrate, there are a variety of choices of substrates for PEM deposition.

As LbL assembly represents a constitution of multiple materials, a wide range of building blocks can be served as PELs to construct a PEM including synthetic and biogenic PELs. Synthetic PELs, such as poly(styrene sulfonate) (PSS), poly(allylamine hydrochloride) (PAH), and PAA, with controllable molecular weight, charge density, and structure are generally easier to tailor the internal structure and properties of PEM in a wide range of environments (e.g. pH and ionic strength) [112]. However, they are

often non-biodegradable causing potentially harmful effects and not bioactive that limits their use in biomedical application. On the other hand, biogenic PELs with special structures are usually biodegradable, biocompatible, and often bioactive that presents similar properties to tissues and more suitable ingredients for constructing PEMs under biological environment [105]. These naturally occurring polymers are mainly divided into polysaccharides, polypeptides, and polynucleotides that comprise ECM, cell membrane components and can be directly or indirectly influence signaling pathways of cells. The main drawbacks of PEM built from biogenic PELs are the difficulty for quality control associated with limited availability of origins with poor-defined properties due to heterogeneity from batch-to-batch purification process. They also exhibit high hydration, and low mechanical properties due to the abundance of hydrophilic groups like hydroxyl and carboxylic groups on the backbone of PELs [113,114].
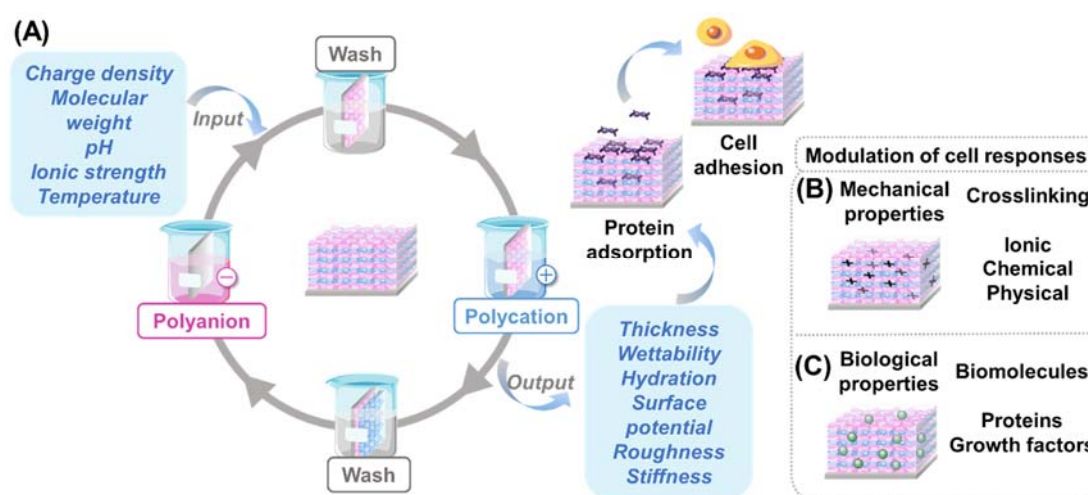

Figure 7. (A) Schematics of layer-by-layer (LbL) adsorption of oppositely charged polyelectrolytes (PELs) based on electrostatic interaction and ion pairing. PEM formation is achieved by alternating deposition of the solutions of polycation and polyanion on the substrate. Each deposition is followed by a washing step to remove unbound PEL. The physiochemical and mechanical properties of PEM are dependent on the charge density and molecular weight of PEL and environmental conditions (e.g., pH, ionic strength, temperature). These properties (e.g., wettability, surface charge density) are associated with protein adsorption and subsequent interaction with cells. Cell responses towards PEMs can be regulated (B) by modulation of mechanical properties using different crosslinking methods (ionic, chemical and physical crosslinking) or (C) by introduction of biomolecules like proteins and GFs. Created by the Servier Medical Art Commons Attribution 3.0 Unported License.

The overall properties including growth behavior, internal structure, hydration, and thickness of PEM depends on the structure of the building blocks and the buildup parameters (**Figure 7A**). Strong PELs persist constant structure and charge density in media with a wide range of pH or ionic strength while the charge density, structure and swelling ability of weak PELs are strongly dependent on their pKa and media condition. The working range of pH for biogenic PELs is 3−10 regarding pKa of carboxylic group (3−5), sulfate group (0.5−1.5) and amino group (6.5−10) [105]. For example, the sulfate groups in Hep are always negatively charged within the working range (pH 3−10) when carboxylic groups become fully charged above pH 5. Chitosan (Chi) with a pKa ≈ 6.5 as a typical weak polycation for PEM formation is considered fully positively charged at pH 4 but not available to serve as polycation at pH above 5.5. pH effect has thoroughly investigated on the PEM built from Chi and alginate (Alg) at pH 5.5. PEM de-swelled after exposure to solution with a pH of 4 leading to a decrease in thickness attributed to increased charge density in Chi. The PEM is swelling when pH was elevated to 8 resulting in increased thickness related to deprotonation and loopy structure of Chi and electrostatic repulsion between negative charges in Alg [115].

The growth behavior and internal structure of PEM is based on the capability of interdiffusion of PELs linked to the charge density, structure and molecular weight. For [PSS/PAH] PEMs composed of both strong PELs, interdiffusion only occurs to the neighboring layer because they are fully charged in the media and mostly compensated intrinsically with almost equal stoichiometry [116,117]. As a result, the LbL process exhibits linear growth behavior to form denser and less hydrated PEMs. Moreover, different charge densities on Hep, chondroitin sulfate (ChS) and hyaluronic acid (HA) as polyanions showed different patterns on PEL diffusion and PEM thickness in combination with PLL [118]. Highly charged Hep formed denser, thinner, less hydrated PEMs with almost linear growth attributed to its extended conformation and stronger electrostatic interaction, compared to exponentially grown, thicker and highly hydrated PEM built from weakly charged and coiled HA. The molecular weight comes into the effect on the growth behavior. Chi or PLL with a low molecular weight was more diffusible to the outer region to interact with HA while the diffusion was almost inhibited by high molecular weights of both polycations [119]. Of note, to achieve the desired properties for further application, the growth behavior and structure of PEM can be controlled by the choice of PEL and environmental conditions.

3.2 *Application of LbL technique in tissue engineering*

The straightforward and facile LbL technique brings enormous potential for modification of biomaterials using either synthetic or biogenic polymers for biomedical applications such as drug delivery, engineering of tissue analogs and implant coatings. It is already known that terminal layer, topography, wettability, surface charge and mechanical properties of PEMs affect protein adsorption and subsequent cell behaviors in terms of cell adhesion, proliferation, and differentiation. Although several reports have claimed PEMs made of synthetic PELs permit better control over the aforementioned parameters, biogenic PELs are preferred in the construction of PEM to mimic biological environments with excellent biocompatibility and biodegradability [105]. In particular, ECM components including polysaccharides and adhesive proteins can mimic the properties and structures of native matrix regulating in this way cell responses with their inherent bioactivity. GAGs with abundant sulfate and carboxylic groups are widely used as polyanions owing to their specific interaction with protein ligands, such as GFs and cell receptors [36]. Chi as one of the most used polycations is often studied with GAGs to form bioactive PEM because of its anti-bacterial and anti-inflammatory properties [120,121]. However, the PEMs formed from these biogenic PELs are sensitive to changes of environmental conditions (e.g., pH, ionic strength and temperature) usually causing PEM partial disassembly or structural rearrangement at physiological pH. In addition, the rather soft and hydrated features of these biogenic PEMs reduce protein adsorption leading to poor cell attachment [113,120]. Considerable efforts have been made to tailor the properties of PEMs, from chemical modification of PELs, modulation of surface physicochemical and mechanical properties to render PEMs with bioactivity. For instance, the solubility and protonation of Chi are poor when pH is above its pKa ≈ 6.5 affecting electrostatic interaction with polyanions to form PEM. Quaternization of Chi makes it more soluble in aqueous solution and appropriately protonated in a wider range of pH, which has been found to improve fidelity of LbL assembly at neutral pH [122].

Since cells can sense mechanical stimuli from the surrounding environment that induces mechanical and biochemical signals, strengthening the interaction between layers with an additional non-electrostatic crosslinking is one of common approaches to avoid partial loss or rearrangement of layers and enhance stiffness of PEMs (**Figure 7B**). Different crosslinking methods has been explored to modulate stiffness and

improve cell behaviors including chemical crosslinkers such as 1-ethyl-3-(3-dimethylaminopropyl)-carbodiimide/*N*-hydroxysuccinimide (EDC/NHS), glutaraldehyde, and genipin [123,124]. EDC/NHS crosslinking of PEMs has been extensively studied in a range of concentrations corresponding to a stiffness range of 200 kPa–600 kPa. Better adhesion and spreading of pre-osteoblasts and myocytes were found on stiffer [PLL/HA] PEMs [125]. Niepel et al. also investigated increasing concentrations of EDC ranging from 2 to 50 mg mL^{-1} resulted in increasing stiffness of [PLL/HA] PEMs [113]. The stiffer PEM not only supported better adhesion and spreading of human adipose-derived stem cells (ADSCs) but also promoted their osteogenic differentiation. Apart from carbodiimide crosslinking based on amide bond formation via the activation of carboxyl groups for direct reaction with primary amino groups, a nature crosslinker, genepin is popularly used for the crosslinking of amino groups of amine-containing polymers. Mano et al. has systematically studied the continuous gradients of stiffness by genipin crosslinking in the PEMs comprised of Chi and Alg [126]. The results showed that density of fibroblasts was promoted on stiffer region of the PEMs. An alternative approach introduced by Zhao et al. is the functionalization of GAGs (e.g. HA, ChS) with aldehyde groups to intrinsically crosslink with amino groups of collagen I, rendering PEMs with better stability and superior cell behaviors using multipotent embryonic fibroblasts [127].

On the other hand, LbL assembly allows the presentation of biochemical signals to activate specific cellular pathways by embedding bioactive molecules inside or on the PEMs during the buildup process or after the assembly (**Figure 7C**). ECM proteins like FN, collagen and VN are advantageous to form bioactive PEMs that regulate cell adhesion and further cell behavior, particularly in combination with GAGs. Collagen I has been used as polycation for PEM assembly with GAGs (e.g. HA, ChS) to support adhesion and induce osteogenic differentiation of hADSCs [127]. In particular, fibril-like reorganization occurred when combined with ChS, which mimicked the ECM structure of the native tissue [128]. Pre-coating FN on Hep-based PEMs has been found to support adhesion and proliferation of MSCs [129].

High concentration of soluble GFs is generally added to the growth or differentiation culture medium to promote cell proliferation and differentiation. However, rapid deactivation and consumption of GFs can lead to inconsistent cell performance like slow rate in cell proliferation [129]. One of the most appealing strategies for LbL

assembly is to act as a reservoir for GFs storage, protecting them from proteases and rapid degradation and controlling their delivery in a matrix-bound manner. There are two major approaches to simply employ GFs in the PEM, as a regular PEL layer or post-loading in the as-prepared PEM without exposure to harsh condition. Incorporation of FGF-2 into PEMs has been widely studied regarding its promoting effect on cell proliferation, migration, and differentiation. As a polycation, FGF-2 was used to prepare PEMs with Hep or ChS, which was found to enhance proliferation of preosteoblast cells over 7 days compared to negligible effect of FGF-2 supplemented in culture medium [130]. Furthermore, synergistic effect of bioactive molecules used in PEM has been explored. Simultaneous embedding TGF-β1 and BMP-2 on succinylated PLL-based PEM was found to induce differentiation of embryonic bodies to cartilage and bone [131]. Such synergistic effect was also observed in [Hep/Chi] PEM by cooperation of GFs (e.g. FGF-2, TGF-β1) with ECM protein like FN to promote MSC proliferation or enhance the function of primary human hepatocytes [129,132].

The concept of GFs in a matrix-bound manner in PEM was introduced by Crouzier et al., which is closer to the native ECM environment, where GFs are bound to ECM proteins and GAGs [133]. By investigating the presentation of BMP-2 on [PLL/HA] PEM, they demonstrated that diffusion of BMP-2 was restricted due to spatial confinement of BMP-2 ligand and receptor complexes of myoblasts. The matrix-bound GFs enabled the crosstalk between GF receptors and integrin, which induced cytoskeleton remodeling (**Figure 8**). In comparison, such effects cannot be achieved by presentation of GFs in solution since they can freely diffuse and limit their availability to receptors. The release profile of GFs from PEM can be tuned by various factors such as the environment during PEM preparation, composition, structure, thickness, and crosslinking degree of PEM. Different crosslinking methods have impacts on GF uptake and release. Anouz et al. has found the presentation of BMP-2 in matrix-bound manner was sustained in the intrinsically crosslinked PEMs composed of collagen I/oxidized CS over 14 days, showing ability to promote osteogenic differentiation of myoblasts, which surpassed the effect of uncrosslinked PEM and BMP-2 released in solution [134]. Hautmann et al. reported a thick free-standing PEM film of Chi/Alg with 200 layers took up more FGF-2 and sustained release of FGF-2 when crosslinked by genipin, showing promoting effects on fibroblast migration and *in vivo* wound closure compared to crosslinking by EDC/NHS [135]. In this regards, LbL assembly presents

a reservoir to mimic ECM in a role that binds with GFs and deliver them to cells for consequent cell activities.
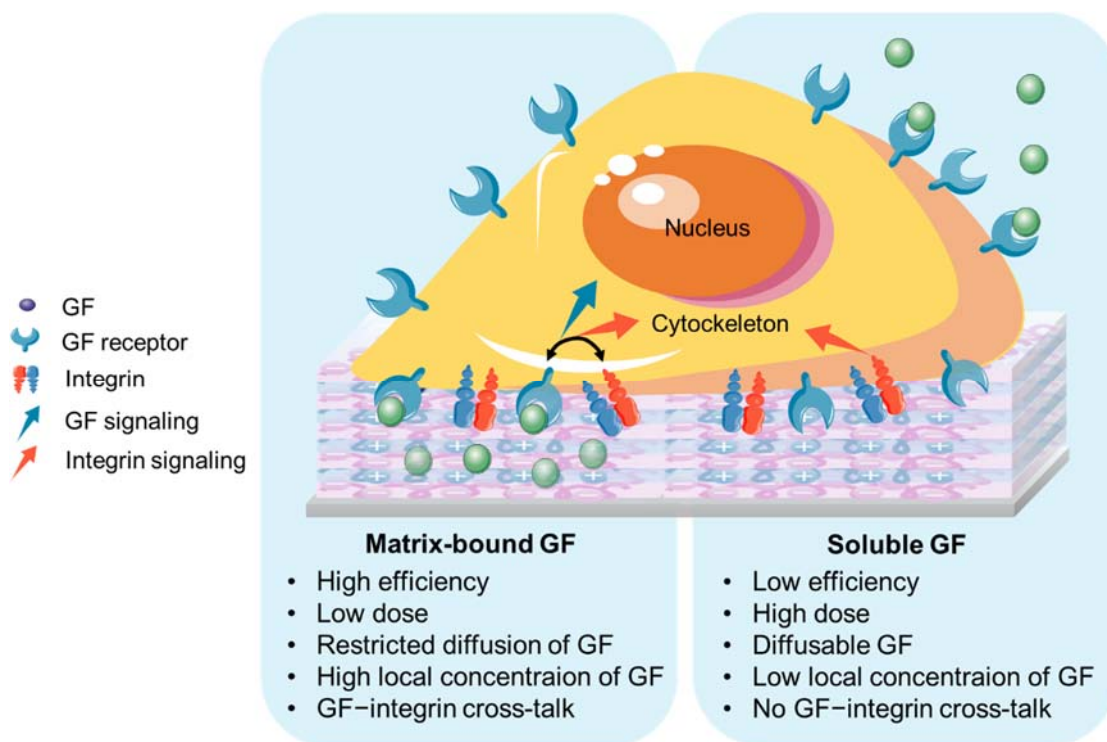

Figure 8. Scheme summarizes the differences of GF presentation from PEM in matrix-bound manner and soluble form. Diffusion of matrix-bound GF is restricted due to spatial confinement of GF and its receptor complexes. Due to the proximity of GF receptor and integrin, the matrix-bound GF enables the crosstalk between GF receptors and integrin, which induces signal transduction, cytoskeleton remodeling, etc. In comparison, such effects cannot be achieved by presentation of GFs in solution since they can freely diffuse which limits their stability and availability to receptors. Adapted from [133] using the Servier Medical Art Commons Attribution 3.0 Unported License.

3.3 Examples of biogenic polyelectrolytes used for LbL technique
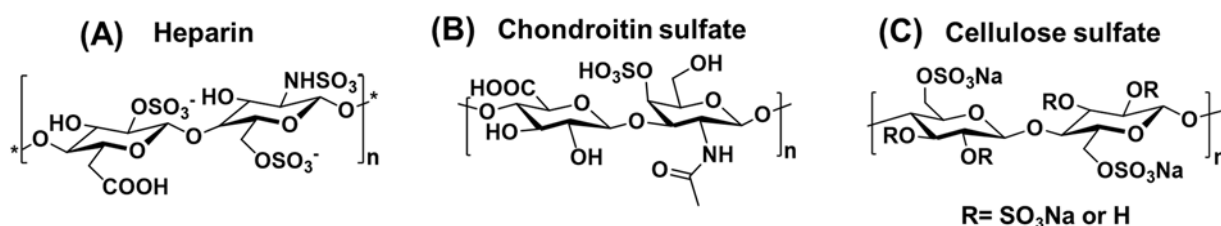
3.3.1 Polyanions

Figure 9. Structures of polyanions including (A) heparin, (B) chondroitin sulfate and (C) cellulose sulfate.

(a) Heparin (Hep, H)

Heparin (Hep) is known as GAG with the highest negative charge related to the presence of a large numbers of sulfate and carboxylic groups. It consists of repeating saccharide units of N-acetylated or N-sulfated D-glucosamine that are α(1-4)- or β(1-4)-linked to uronic acids (L-iduronic or D-glucuronic acid). Specially, the major disaccharide units are iduronic acid with 2-O-sulfation and glucosamine with N- and 6-O-sulfation [136]. Hep is only produced in connective-tissue-type mast cells or basophils where it is synthesized on a specific core protein (serglycin, MW: 750–1000 kDa) with a MW of 60–100 kDa. During degranulation of mast cells or basophils, Hep chains are cleaved with a MW of 5–25 kDa and stored in cytoplasmic secretory granules of mast cells from where they can be secreted into ECM [137]. The presence of sulfate groups at carbon 2 and glucosamine with N- and 6-O-sulfation and carboxylic groups generates strong negative charges along its chains, playing important roles in association with a plethora of proteins. The interaction between Hep and proteins is based on the Hep-binding domains via ionic interaction or hydrogen bonding [138]. One of the important therapeutic applications of Hep is the anticoagulant properties by binding to antithrombin III that inactivates clotting factors [137]. Due to the well-known affinity to adhesive proteins (e.g. FN, VN) and GFs (e.g. FGF-2) forming the complexes with corresponding cell receptors, Hep is often incorporated into biomaterials to mediate integrin- or GF-related signal transduction for cell adhesion, proliferation and differentiation [36].

(b) Chondroitin sulfate (ChS)

Chondroitin sulfate (ChS) as the other sulfated GAG with similar structure to Hep, is composed of alternating β(1-4) glucuronic acid (GlcA) and β(1-3) N-acetylgalactosamine that can be sulfated at the carbon 4 or 6 of the galactosamine (named as ChS-A or ChS-C, respectively), and additionally at C2 and/or C3 of the GlcA (named as ChS-B) [136]. ChS exists abundantly in the cell surfaces and within extra/pericellular matrices of connective tissues in the form of proteoglycans (ChSPGs) with varying molecular weights from 5-70 kDa. ChS is the major component in central nervous systems where ChSPGs are found to interact with neurons and neural cell adhesion molecules for the development and pathophysiology of the brain and spinal cord [139]. ChS with strong negative charges has specific interaction with ECM proteins and GFs, making them important regulator for biological functions including anti-inflammation, interaction with collagen in the regulation of fibrillogenesis, acceleration of mineralization process and repair in bone. In particular, treatment of osteoarthritis with ChS has been reported widely to reduce pain and swelling of the joint [140].

(c) Cellulose sulfate (CS)

The purification of GAGs from animal sources requires several critical processes that limit their availability, and heterogeneous GAGs from batch to batch are usually obtained, sometimes even with the risk of contamination [39]. Cellulose draws a plenty of attention due to the presence of hydroxyl groups that permit versatile chemical modifications to mimic anionic GAGs or other glycans, which can provide superior tunable functionality of such GAGs mimicking biopolymers [36]. Cellulose, as the most abundant polysaccharide in nature, is a linear-chain polysaccharide composed of β-1,4-linked d-anhydroglucopyranose units (AGUs). Each AGU contains hydroxyl groups at C2, C3, and C6 position, which can undergo the typical sulfation reactions of primary and secondary alcohols to synthesize cellulose sulfate (CS). CS with GAGs-analogue sulfation patterns can be synthesized using diverse sulfating reagents [141,142]. A particular sulfating route could affect the intrinsic characteristics of obtained CS, which include the molecular weight, total degree of substitution (DS) ascribed to sulfate groups (DS$_S$), the distribution and the position of sulfate groups [143]. Based on the knowledge about sulfation pattern of natural GAGs, the binding affinity of CS toward GFs was investigated by Peschel et al. and Zhang et al., especially regarding the

substantial effects of regioselectivity and overall DS$_S$ between 0.58 and 1.94 on GF binding and cellular activities [141,144,145]. Studies showed that CS with overall DS$_S$ more than 1.57 in addition to a gradual increase of sulfation at both the 2-O- and the 6-O-position exhibited a stronger binding ability toward FGF-2, while a higher affinity to BMP-2 was found for CS with intermediate DS$_S$ and more sulfation at the 6-O-position, but lower sulfation at the 2-O-position. Mitogenic and osteogenic activities of CS promoted cell proliferation and differentiation, which was comparative or even surpassing that of heparin. CS also acts to protect GFs from proteolytic cleavage that prolonged their half-life resulted in a sustained stability and bioactivity with increasing DS$_S$ and concentration [43].
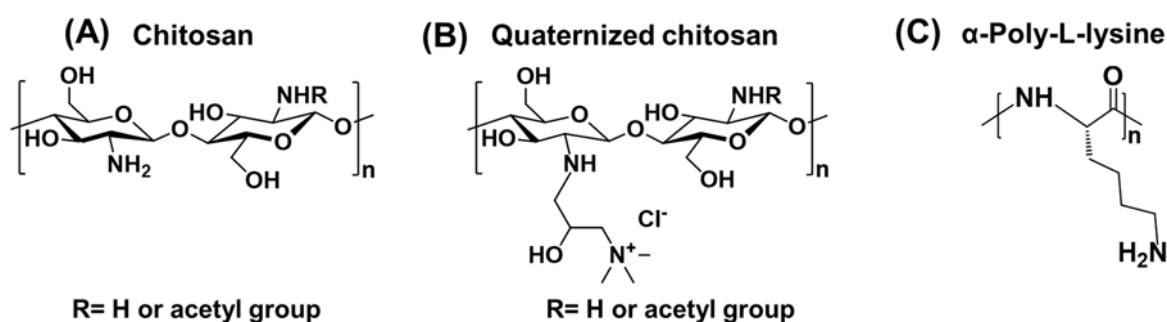
3.3.2 Polycations

Figure 10. Structures of polycations including (A) chitosan, (B) quaternized chitosan and (C) α-Poly-L-lysine.

   (a) Chitosan (Chi)

Chitosan (Chi) is obtained by the deacetylation of chitin, a naturally occurring polysaccharide as the second most abundant natural polymer on earth after cellulose which exists in shells of crustaceans such as crabs, but also insects, spiders and funghi [146]. Chi is a cationic linear polysaccharide consisting repeating units of N-acetyl-D-glucosamine and D-glucosamine. It is available in a wide range of MW and degrees of deacetylation (DD) linked to physiochemical properties like viscosity, wettability, colloidal stability and sensitivity to pH [147]. Some studies point out that a DD of 50% is considered as Chi [148]. Based on the protonation of primary amino groups at C-2 position of the D-glucosamine unit, Chi with a pKa of ≈ 6.5 is soluble and positively charged in an acidic solution but becomes insoluble and uncharged at neutral and

basic pH. It is hydrophilic and shows great biocompatibility and biodegradability with lysozyme in living human tissues, making it attractive for biomedical application [149]. Regarding the positive charges, Chi has an antibacterial activity by electrostatically interacting with anionic groups at the bacterial cell wall and the polycation leading to an increase in membrane permeability resulted in cell death [150]. The protonated amino groups also endow Chi with an ability to interact with anionic polymers or functionalize with multiple functional groups such as carboxylic groups and hydroxyl groups [146]. These beneficial properties of Chi are particularly highlighted by its application as one of the most popular polycations for LbL assembly in tissue engineering and would healing [151,152].

(b) Quaternized chitosan (QChi)

Since solubility and protonation of Chi depends on DD and pH, the physiochemical (solubility, absorption, bioavailability) and biological properties (antibacterial property, antioxidant, bioadhesion, mucoadhesive property) can be improved by quaternization of Chi. The insertion of a hydrophilic group is involved in the process of quaternization including three general approaches: direct quaternary ammonium substitution, epoxy derivative open loop and N-alkylation [153]. N,N,N-trimethyl chitosan chloride (TMC) is the most intensely explored QChi derivative that mainly relies on the methylation of the amino group at the C-2 site of Chi backbone [154]. N-[(2-hydroxyl-3-trimethyl ammonium) propyl] chitosan (HTCC) is another most explored QChi via alkylation process by grafting quaternary ammonium groups using the reagent 'glycidyltrimethylammonium chloride' at the site of C-2 attached amino groups [155]. These QChi derivatives exhibit enhanced aqueous solubility, superior antibacterial properties and biocompatibility attributed to the increased positive charges [156]. The physiochemical and biological properties are highly linked to the degree of quaternization (DQ) and preparation methods, as the reports have shown increased DQ, resulting in amplified viscosity, solubility, antibacterial property, bioadhesive and mucoadhesive property in HTCC while opposite trends of these properties were observed in TMC due to steric hindrance during the quaternization process [157–159]. QChi has shown inhibitory effect *on E. coli* and *S. aureus* while excellent cytocompatibility was found with *in vivo* test by subcutaneous implantation on rat [160]. QChi also has promoting effect on wound healing and tissue engineering, which is evident by the skin regeneration treated with a nanofiber containing QChi [161].

(c) α-Poly-L-lysine (PLL)

α-Poly-L-lysine (PLL) is a synthetic polypeptide and composed of repeating monomeric α-L-lysine that is one of the naturally occurring amino acids involved in biological processes such as injury recovery and protein functions. PLL exhibits cationic properties in a wide range of pH owing to the amino side chains with a pKa of around 9−10, making it applicable under physiological condition. [162] Regarding positive charges of the primary amino groups, it has been extensively explored in biomedical application as nanocarriers, coating biomaterials, and antibacterial biofilms interacting with negatively charged components via electrostatic interaction [163]. PLL is highly soluble in aqueous solution, however, depending on the environment (e.g. pH, temperature, solvent variations, and surfactants), it can fold into secondary structures with varying solubility and hydrophobicity related to intramolecular hydrogen bonding between their backbones and side chains [164,165]. PLL is commonly used as antibacterial agents because it is positively charged at physiological conditions that could cause physical disruption of the anionic membrane of bacterial cells [166]. Although the cationic amino groups and secondary structure of PLL has been demonstrated to improve cell adhesion, proliferation and induce stem cell differentiation, it was also reported to disrupt membrane of human epithelial cells through permeabilization particularly using high HW [167,168]. The toxicity of PLL can be alleviated by balance of its positive charges with negatively charged materials, or chemical modification of the primary amino groups. Therefore, the construction of hybrid biomaterials such as hydrogel or PEM is one of the most strategic method to apply PLL in tissue engineering [163].

4   State-of-the art of PNIPAM-containing PEM for biomedical applications

Since PNIPAM is uncharged, some strategies for incorporation of PNIPAM into PEM have been developed for deposition of PNIPAM element on the substrate (**Table 3**). One of the earliest studies on the fabrication of thermoresponsive PEM is through hydrogen bonding between PNIPAM and PAA at pH 3, which has shown the ability to reversibly load and unload with dye (Rhodamine B) in response to temperature [169]. In contrast to form PNIPAM-containing PEMs via hydrogen bond with only few reports, more studies focused on the conjugation of PNIPAM with ionic polymers to facilitate LbL deposition process via electrostatic interaction and ion paring. Jaber and Schlenoff

constructed a PNIPAM-containing PEM by modification PNIPAM with PAH as polycation and PSS as polyanion at pH 6.5 [170]. They demonstrated reversible thermoresponsivity of the PEM in the cyclic temperature range of 10−50 °C under thorough investigation. Another example is forming an anionic microgel combining PNIPAM and PAA to construct PEMs with PAH [171]. In this study, a chemotherapeutic drug agent, doxorubicin, was loaded into the PEMs and found the release of the drug could be thermally controlled by a cycle modulation of the temperature between 50 and 20 °C. Regarding the nature of ionic polymers dependent on the environmental stimulus, Osypova et al. included both temperature and pH effects of a PEM composed of PAH and PAA-b-PNIPAM to study the protein (ovalbumin) adsorption [172,173]. Higher adsorption of ovalbumin was found at higher temperature and acidic pH related to the hydrophobic interaction, conformation and charge repulsion between the PEM and protein. Study on PNIPAM-containing PEMs for biomedical application mostly focuses on controlling drug release, such as delivery of the lung cancer drug, osimertinib and recent anti-COVID-19 drug favipiravir. However, none of these studies are proceeded to preclinical trial [174,175]. The application of PNIPAM-containing PEMs in tissue regeneration and cell sheet engineering is scarcely found with only a report with comprehensive study by Liao et al., thermally controlling adhesion/detachment of hMSCs on PNIPAM-containing PEMs [176]. They prepared PNIPAM-containing PEM by assembling PNIPAM copolymers that modified with cationic allylamine hydrochloride segment and with anionic styrene sulfonic acid segment. They claimed that the cationic moiety on the outermost surface retained cell-secreted proteins like FN on the positively charged surface, which promoted cell adhesion and proliferation. The aforementioned PNIPAM-containing PEMs were only comprised of synthetic PELs lacking specific interaction with biological molecules to regulate cell responses, which might be the reason why no study was conducted for GF delivery and tissue engineering.

Table 3. PEMs containing PNIPAM and their biomedical application.

Category	PNIPAM-contained PEM	Driving force for PEM formation	Application	Remarks	Ref.
Small molecule	[PNIPAM/PAA]$_{10}$	pH3 Hydrogen bond	Reversibly loaded and unloaded with dye (Rhodamine B) at pH3	• Higher loading and release amount of dye at high temperature. • PEM prepared at a higher temperature tended to be slower both in the impregnation and in the release of dye.	2004 [169]
Small molecule	[PAH-co-PNIPAM/PSS-co-PNIPAM]$_{18}$	pH6.5 Ion paring	Reversibly loaded and unloaded with potassium ferricyanide at pH6.5	• PEM exhibited reversible thermoresponsivity. • PEM built at pH9 provided extrinsic site for more loading capacity at pH6.5 (where more positive charges of PAH were interated with anionic ferricyanide) .	2005 [170]
Drug	PNIPAM-AA microgels/PAH	pH 6.5 Ion paring	Loading chemotherapeutic drug agent doxorubicin at pH7 and release at pH3	• Loading and release of doxorubicin at cycling temperatue of 50 and 20 °C for 1 h each is more efficient than release at constant 20 °C	2005 [171]
Drug	[PNIPAM-b-PHEMA/HA]$_6$	pH 2.2, 55°C Hydrogen bond	Release of lung cancer drug osimertinib at pH 2.2	• PEM exhibited reversible thermoresponsivity. • Binding of osimertinib to the hydrophobic cores resulted in slower release at higher temperature, particularly when increasing ionic strength that facilitates collapse of PNIPAM.	2020 [174]
Drug	[silica nanocapsules-g-PNIPAM-b-quaternized PDMAEMA/PMAA]$_3$	pH 4.5 Ion paring	Release of anti-COVID-19 drug favipiravir	• PEM exhibited reversible thermoresponsivity. The nanocapsule-embedded • PEMs were able to encapsulate a large amount of favipiravir, possessing a long-term drug release curve at higher temperature.	2021 [175]
Protein	[PAH/PAA-b-PNIPAM]$_4$	pH5.7 Ion paring	Adsorption of ovalbumin at pH 5.7 and at 20 or 37 °C	• PEM exhibited thermoresponsivity. • Higher adsorption of ovalbumin at higher temperature and acidic pH related to the less repulsive charge with thicker PEM.	2015 , 2017 [172, 173]
Tissue engineering	[PSS-co-PNIPAM/PAH-co-PNIPAM]$_4$-PAH [PSS-co-PNIPAM/PAH-co-PNIPAM]$_4$-PSS	Ion paring	Culture and detachment of hMSCs	• PEM could thermally control cell adhesion/detachment (at 4 °C) but also retain cell-secreted proteins like FN on the positively charged surface, which promoted the proliferation.	2010 [176]
Tissue engineering	[Chitosan-*grafted*-PNIPAM/Alg]$_5$-Chitosan-*grafted*-PNIPAM	Ion paring	Culture and detachment of human osteoblast-like cell	• PEM could thermally control cell adhesion/detachment.	2011 [177]

PAA: poly(acrylic acid); PAH: poly-(allylamine hydrochloride); PSS: poly(styrene sulfonate); PHEMA: 2-hydroxyethyl methacrylate; Alg: alginate.

5   Aim of this study

LbL technique provides a facile approach to modify surfaces with PNIPAM without requiring a prior chemical activation of the surface. Such technique may allow a precise control of thickness and physiochemical properties of the PNIPAM surface. PNIPAM-containing PEMs may represent an attractive system for drug delivery and cell sheet engineering. Since cell activities are regulated by signal transduction activated by cell receptors binding to corresponding biological ligands such as GFs and adhesive proteins, combining biopolymers or bioactive molecules like polysaccharide-based Hep, ChS, CS, and Chi with PNIPAM-containing PEM may enhance biocompatibility and mimic the native tissue environment. The superior bioactivity of sulfated Hep, ChS and CS towards adhesive proteins and GFs can control cell activities in terms of cell adhesion, proliferation, and differentiation. The aim of this study is to investigate if thermoresponsive surface coatings can be prepared via LbL technique from the PELs based on the derivatives of either polycation Chi or polyanion CS modified with PNIPAM. The molecular weight and grafting density of PNIPAM on these derivatives may affect the structure and charge density in response to the temperature that are further associated with the growth behavior, internal structure, and physicochemical properties of PEMs. It is essential to study thermoresponsive properties related to swelling/de-swelling ability, wettability, roughness, and stiffness of the PNIPAM-containing PEMs which is important for the association with biomolecules (e.g., proteins, GFs) and controlling cell adhesion and detachment. As cells are sensible to the mechanical signal of the microenvironment, surface properties and stiffness of the PEMs can be modulated by additional covalent crosslinking of PEL.

These PEMs may act as storage depot to bind GFs and protect and prolong their activity under physiological environment. The mitogenic and migratory activities of FGF-2 are well-known to induce angiogenesis and tissue regeneration and the key for maintaining self-renewal and differentiation ability of stem cells. It is known that FGF-2 receptor (FGFR-2) and VN integrin can cooperatively regulate cell behaviors via MAPK pathway. Therefore, evaluation of VN adsorption/desorption and release kinetic of FGF-2 on these PEMs over a period of time is important to gain a comprehensive understanding on how it regulates cell adhesion, proliferation and migration using multipotent mouse fibroblast cell line C3H10T1/2 and 3T3. Such PEM systems combining bioactive polysaccharides and PNIPAM with tunable physiochemical and

biological properties may provide a great potential for not only GF delivery but also effective expansion and generation of cell sheets.

6   References

[1]   A. Shafiee, A. Atala, Tissue Engineering: Toward a New Era of Medicine, Annu. Rev. Med. 68 (2017) 29–40.

[2]   R. Langer, J.P. Vacanti, Tissue engineering, Science 260 (1993) 920–926.

[3]   R. Langer, Tissue engineering: perspectives, challenges, and future directions, Tissue Eng. 13 (2007) 1–2.

[4]   J. Lott, P.H. de Carvalho, D. Assis, A.M. de Goes, Innovative Strategies for Tissue Engineering, in: R. Pignatello (Ed.), Advances in Biomaterials Science and Biomedical Applications, InTech, 2013.

[5]   S.M. van Belleghem, B. Mahadik, K.L. Snodderly, J.P. Fisher, Overview of Tissue Engineering Concepts and Applications, in: William R. Wagner, Shelly E. Sakiyama-Elbert, Guigen Zhang, Michael J. Yaszemski (Ed.), 2.6.2 - Overview of Tissue Engineering Concepts and Applications, Biomaterials Science (Fourth Edition), Elsevier, 2020, pp. 1289–1316.

[6]   C.M. Madl, S.C. Heilshorn, H.M. Blau, Bioengineering strategies to accelerate stem cell therapeutics, Nature 557 (2018) 335–342.

[7]   P. Català, G. Thuret, H. Skottman, J.S. Mehta, M. Parekh, S. Ní Dhubhghaill, R.W.J. Collin, R.M.M.A. Nuijts, S. Ferrari, V.L.S. LaPointe, M.M. Dickman, Approaches for corneal endothelium regenerative medicine, Prog. Retin. Eye Res. 87 (2022) 100987.

[8]   K.M. Naegeli, M.H. Kural, Y. Li, J. Wang, E.A. Hugentobler, L.E. Niklason, Bioengineering Human Tissues and the Future of Vascular Replacement, Circ. Res. 131 (2022) 109–126.

[9]   M. Khorraminejad-Shirazi, M. Dorvash, A. Estedlal, A.H. Hoveidaei, M. Mazloomrezaei, P. Mosaddeghi, Aging: A cell source limiting factor in tissue engineering, World J. Stem Cells 11 (2019) 787–802.

[10] W. Zakrzewski, M. Dobrzyński, M. Szymonowicz, Z. Rybak, Stem cells: past, present, and future, Stem Cell Res. Ther. 10 (2019) 68.

[11] J.A. Thomson, J. Itskovitz-Eldor, S.S. Shapiro, M.A. Waknitz, J.J. Swiergiel, V.S. Marshall, J.M. Jones, Embryonic stem cell lines derived from human blastocysts, Science 282 (1998) 1145–1147.

[12] S. Yamanaka, Pluripotent Stem Cell-Based Cell Therapy-Promise and Challenges, Cell Stem Cell 27 (2020) 523–531.

[13] K. Takahashi, K. Tanabe, M. Ohnuki, M. Narita, T. Ichisaka, K. Tomoda, S. Yamanaka, Induction of pluripotent stem cells from adult human fibroblasts by defined factors, Cell 131 (2007) 861–872.

[14] B.R. Sousa, R.C. Parreira, E.A. Fonseca, M.J. Amaya, F.M.P. Tonelli, S.M.S.N. Lacerda, P. Lalwani, A.K. Santos, K.N. Gomes, H. Ulrich, A.H. Kihara, R.R. Resende, Human adult stem cells from diverse origins: an overview from multiparametric immunophenotyping to clinical applications, Cytometry A 85 (2014) 43–77.

[15] V. Rocha, E. Gluckman, Clinical use of umbilical cord blood hematopoietic stem cells, Biol. Blood Marrow Transplant. 12 (2006) 34–41.

[16] Y. Guo, Y. Yu, S. Hu, Y. Chen, Z. Shen, The therapeutic potential of mesenchymal stem cells for cardiovascular diseases, Cell Death Dis. 11 (2020) 349.

[17] D.E. Rodríguez-Fuentes, L.E. Fernández-Garza, J.A. Samia-Meza, S.A. Barrera-Barrera, A.I. Caplan, H.A. Barrera-Saldaña, Mesenchymal Stem Cells Current Clinical Applications: A Systematic Review, Arch. Med. Res. 52 (2021) 93–101.

[18] C.B. Croft, D. Tarin, Ultrastructural studies of wound healing in mouse skin. I. Epithelial behaviour, J. Anat. 106 (1970) 63–77.

[19] F. Cialdai, C. Risaliti, M. Monici, Role of fibroblasts in wound healing and tissue remodeling on Earth and in space, Front. Bioeng. Biotechnol. 10 (2022) 958381.

[20] L.A. Bautista-Hernández, J.L. Gómez-Olivares, B. Buentello-Volante, V.M. Bautista-de Lucio, Fibroblasts: The Unknown Sentinels Eliciting Immune Responses Against Microorganisms, Eur. J. Microbiol. Immunol. (Bp) 7 (2017) 151–157.

[21] D. Correa-Gallegos, D. Jiang, S. Christ, P. Ramesh, H. Ye, J. Wannemacher, S. Kalgudde Gopal, Q. Yu, M. Aichler, A. Walch, U. Mirastschijski, T. Volz, Y. Rinkevich, Patch repair of deep wounds by mobilized fascia, Nature 576 (2019) 287–292.

[22] J. Li, Y.-P. Zhang, R.S. Kirsner, Angiogenesis in wound repair: angiogenic growth factors and the extracellular matrix, Microsc. Res. Tech. 60 (2003) 107–114.

[23] M.G. Tonnesen, X. Feng, R.A. Clark, Angiogenesis in wound healing, J. Investig. Dermatol. Symp. Proc. 5 (2000) 40–46.

[24] I.A. Darby, B. Laverdet, F. Bonté, A. Desmoulière, Fibroblasts and myofibroblasts in wound healing, Clin. Cosmet. Investig. Dermatol. 7 (2014) 301–311.

[25] A. Blasi, C. Martino, L. Balducci, M. Saldarelli, A. Soleti, S.E. Navone, L. Canzi, S. Cristini, G. Invernici, E.A. Parati, G. Alessandri, Dermal fibroblasts display similar phenotypic and differentiation capacity to fat-derived mesenchymal stem cells, but differ in anti-inflammatory and angiogenic potential, Vasc. Cell 3 (2011) 5.

[26] F.G. Chen, W.J. Zhang, D. Bi, W. Liu, X. Wei, F.F. Chen, L. Zhu, L. Cui, Y. Cao, Clonal analysis of nestin(-) vimentin(+) multipotent fibroblasts isolated from human dermis, J. Cell Sci. 120 (2007) 2875–2883.

[27] P.A. Lysy, F. Smets, C. Sibille, M. Najimi, E.M. Sokal, Human skin fibroblasts: From mesodermal to hepatocyte-like differentiation, Hepatology 46 (2007) 1574–1585.

[28] F. Gattazzo, A. Urciuolo, P. Bonaldo, Extracellular matrix: a dynamic microenvironment for stem cell niche, Biochim. Biophys. Acta 1840 (2014) 2506–2519.

[29] S.W. Lane, D.A. Williams, F.M. Watt, Modulating the stem cell niche for tissue regeneration, Nat. Biotechnol. 32 (2014) 795–803.

[30] O. Guillame-Gentil, O. Semenov, A.S. Roca, T. Groth, R. Zahn, J. Vörös, M. Zenobi-Wong, Engineering the Extracellular Environment: Strategies for Building 2D and 3D Cellular Structures, Adv. Mater. 22 (2010) 5443–5462.

[31] F. Soncin, C.M. Ward, The function of e-cadherin in stem cell pluripotency and self-renewal, Genes (Basel) 2 (2011) 229–259.

[32] J. Khoshnoodi, V. Pedchenko, B.G. Hudson, Mammalian collagen IV, Microsc. Res. Tech. 71 (2008) 357–370.

[33] L. Vitillo, S.J. Kimber, Integrin and FAK Regulation of Human Pluripotent Stem Cells, Curr. Stem Cell Rep. 3 (2017) 358–365.

[34] T.J. Rowland, L.M. Miller, A.J. Blaschke, E.L. Doss, A.J. Bonham, S.T. Hikita, L.V. Johnson, D.O. Clegg, Roles of integrins in human induced pluripotent stem cell growth on Matrigel and vitronectin, Stem Cells Dev. 19 (2010) 1231–1240.

[35] D.I. Leavesley, A.S. Kashyap, T. Croll, M. Sivaramakrishnan, A. Shokoohmand, B.G. Hollier, Z. Upton, Vitronectin--master controller or micromanager?, IUBMB Life 65 (2013) 807–818.

[36] Y. Yang, Y.-T. Lu, K. Zeng, T. Heinze, T. Groth, K. Zhang, Recent Progress on Cellulose-Based Ionic Compounds for Biomaterials, Adv. Mater. (2020) e2000717.

[37] N.A. Afratis, D. Nikitovic, H.A.B. Multhaupt, A.D. Theocharis, J.R. Couchman, N.K. Karamanos, Syndecans - key regulators of cell signaling and biological functions, FEBS J. 284 (2017) 27–41.

[38] M.K. Furue, J. Na, J.P. Jackson, T. Okamoto, M. Jones, D. Baker, R.-I. Hata, H.D. Moore, J.D. Sato, P.W. Andrews, Heparin promotes the growth of human embryonic stem cells in a defined serum-free medium, PNAS 105 (2008) 13409–13414.

[39] H. Liu, Z. Zhang, R.J. Linhardt, Lessons learned from the contamination of heparin, Nat. Prod. Rep. 26 (2009) 313–321.

[40] B. Greber, H. Lehrach, J. Adjaye, Fibroblast growth factor 2 modulates transforming growth factor beta signaling in mouse embryonic fibroblasts and human ESCs (hESCs) to support hESC self-renewal, Stem Cells 25 (2007) 455–464.

[41] S. Gromolak, A. Krawczenko, A. Antończyk, K. Buczak, Z. Kiełbowicz, A. Klimczak, Biological Characteristics and Osteogenic Differentiation of Ovine Bone Marrow Derived Mesenchymal Stem Cells Stimulated with FGF-2 and BMP-2, Int. J. Mol. Sci. 21 (2020).

[42] T. Ito, R. Sawada, Y. Fujiwara, T. Tsuchiya, FGF-2 increases osteogenic and chondrogenic differentiation potentials of human mesenchymal stem cells by inactivation of TGF-beta signaling, Cytotechnology 56 (2008) 1–7.

[43] A. Weltrowski, M.-L. Da Silva Almeida, D. Peschel, K. Zhang, S. Fischer, T. Groth, Mitogenic activity of sulfated chitosan and cellulose derivatives is related to protection of FGF-2 from proteolytic cleavage, Macromol. Biosci. 12 (2012) 740–750.

[44] M.F. Brizzi, G. Tarone, P. Defilippi, Extracellular matrix, integrins, and growth factors as tailors of the stem cell niche, Curr. Opin. Cell Biol. 24 (2012) 645–651.

[45] R.G. Wells, The Role of Matrix Stiffness in Regulating Cell Behavior, Hepatology 47 (2008) 1394–1400.

[46] T.J. Kirby, J. Lammerding, Emerging views of the nucleus as a cellular mechanosensor, Nat. Cell Biol. 20 (2018) 373–381.

[47] J.L. Allen, M.E. Cooke, T. Alliston, ECM stiffness primes the TGFβ pathway to promote chondrocyte differentiation, Mol. Biol. Cell 23 (2012) 3731–3742.

[48] G.S. Hussey, J.L. Dziki, S.F. Badylak, Extracellular matrix-based materials for regenerative medicine, Nat Rev Mater 3 (2018) 159–173.

[49] M. Rahmati, E.A. Silva, J.E. Reseland, C. A Heyward, H.J. Haugen, Biological Responses to Physicochemical Properties of Biomaterial Surface, Chem. Soc. Rev. 49 (2020) 5178–5224.

[50] J.P. Medema, L. Vermeulen, Microenvironmental regulation of stem cells in intestinal homeostasis and cancer, Nature 474 (2011) 318–326.

[51] C. Bonnans, J. Chou, Z. Werb, Remodelling the extracellular matrix in development and disease, Nat. Rev. Mol. Cell Biol. 15 (2014) 786–801.

[52] W.H. Goldmann, Role of vinculin in cellular mechanotransduction, Cell Biol. Int. 40 (2016) 241–256.

[53] N. Faucheux, R. Tzoneva, M.-D. Nagel, T. Groth, The dependence of fibrillar adhesions in human fibroblasts on substratum chemistry, Biomaterials 27 (2006) 234–245.

[54] S. Guo, X. Zhu, M. Li, L. Shi, J.L.T. Ong, D. Jańczewski, K.G. Neoh, Parallel Control over Surface Charge and Wettability Using Polyelectrolyte Architecture: Effect on Protein Adsorption and Cell Adhesion, ACS Appl. Mater. Interfaces 8 (2016) 30552–30563.

[55] N. Faucheux, R. Schweiss, K. Lützow, C. Werner, T. Groth, Self-Assembled Monolayers with Different Terminating Groups as Model Substrates for Cell Adhesion Studies, Biomaterials 25 (2004) 2721–2730.

[56] A.A. Khalili, M.R. Ahmad, A Review of Cell Adhesion Studies for Biomedical and Biological Applications, Int. J. Mol. Sci. 16 (2015) 18149–18184.

[57] A. de Pieri, Y. Rochev, D.I. Zeugolis, Scaffold-free cell-based tissue engineering therapies: advances, shortfalls and forecast, NPJ Regen. Med. 6 (2021) 18.

[58] T. Okano, N. Yamada, H. Sakai, Y. Sakurai, A novel recovery system for cultured cells using plasma-treated polystyrene dishes grafted with poly(N-isopropylacrylamide), J. Biomed. Mater. Res. 27 (1993) 1243–1251.

[59] K. Zhang, J. Chen, The regulation of integrin function by divalent cations, Cell Adh. Migr. 6 (2012) 20–29.

[60] M. Mutin, F. George, G. Lesaule, J. Sampol, Reevaluation of Trypsin-EDTA for Endothelial Cell Detachment before Flow Cytometry Analysis, Endothelium 4 (1996) 289–295.

[61] M.M. Hasani-Sadrabadi, P. Sarrion, S. Pouraghaei, Y. Chau, S. Ansari, S. Li, T. Aghaloo, A. Moshaverinia, An engineered cell-laden adhesive hydrogel promotes craniofacial bone tissue regeneration in rats, Sci. Transl. Med. 12 (2020).

[62] K. Kobayashi, Y. Ichihara, N. Sato, N. Umeda, L. Fields, M. Fukumitsu, Y. Tago, T. Ito, S. Kainuma, M. Podaru, F. Lewis-McDougall, K. Yamahara, R. Uppal, K. Suzuki, On-site fabrication of Bi-layered adhesive mesenchymal stromal cell-dressings for the treatment of heart failure, Biomaterials 209 (2019) 41–53.

[63] K. Nagase, M. Yamato, H. Kanazawa, T. Okano, Poly(N-isopropylacrylamide)-Based Thermoresponsive Surfaces Provide New Types of Biomedical Applications, Biomaterials 153 (2018) 27–48.

[64] O. Guillaume-Gentil, O.V. Semenov, A.H. Zisch, R. Zimmermann, J. Vörös, M. Ehrbar, pH-controlled recovery of placenta-derived mesenchymal stem cell sheets, Biomaterials 32 (2011) 4376–4384.

[65] Y. Kobayashi, C.E.J. Cordonier, Y. Noda, F. Nagase, J. Enomoto, T. Kageyama, H. Honma, S. Maruo, J. Fukuda, Tailored cell sheet engineering using microstereolithography and electrochemical cell transfer, Sci. Rep. 9 (2019) 10415.

[66] H. Sekine, T. Shimizu, I. Dobashi, K. Matsuura, N. Hagiwara, M. Takahashi, E. Kobayashi, M. Yamato, T. Okano, Cardiac cell sheet transplantation improves damaged heart function via superior cell survival in comparison with dissociated cell injection, Tissue Eng. Part A 17 (2011) 2973–2980.

[67] K. Nishida, M. Yamato, Y. Hayashida, K. Watanabe, K. Yamamoto, E. Adachi, S. Nagai, A. Kikuchi, N. Maeda, H. Watanabe, T. Okano, Y. Tano, Corneal reconstruction with tissue-engineered cell sheets composed of autologous oral mucosal epithelium, N. Engl. J. Med. 351 (2004) 1187–1196.

[68] M. Sato, M. Yamato, K. Hamahashi, T. Okano, J. Mochida, Articular cartilage regeneration using cell sheet technology, Anat. Rec. (Hoboken) 297 (2014) 36–43.

[69] Y. Sawa, Y. Yoshikawa, K. Toda, S. Fukushima, K. Yamazaki, M. Ono, Y. Sakata, N. Hagiwara, K. Kinugawa, S. Miyagawa, Safety and Efficacy of Autologous Skeletal Myoblast Sheets (TCD-51073) for the Treatment of Severe Chronic Heart Failure Due to Ischemic Heart Disease, Circ. J. 79 (2015) 991–999.

[70] J. Kobayashi, A. Kikuchi, T. Aoyagi, T. Okano, Cell sheet tissue engineering: Cell sheet preparation, harvesting/manipulation, and transplantation, J. Biomed. Mater. Res. 107 (2019) 955–967.

[71] N. Yamada, T. Okano, H. Sakai, F. Karikusa, Y. Sawasaki, Y. Sakurai, Thermo-responsive polymeric surfaces; control of attachment and detachment of cultured cells, Makromol. Chem., Rapid Commun. 11 (1990) 571–576.

[72] M. Heskins, J.E. Guillet, Solution Properties of Poly(N-isopropylacrylamide), Journal of Macromolecular Science: Part A - Chemistry 2 (1968) 1441–1455.

[73] S. Fujishige, K. Kubota, I. Ando, Phase transition of aqueous solutions of poly(N-isopropylacrylamide) and poly(N-isopropylmethacrylamide), J. Phys. Chem. 93 (1989) 3311–3313.

[74] F. Doberenz, K. Zeng, C. Willems, K. Zhang, T. Groth, Thermoresponsive Polymers and their Biomedical Application in Tissue engineering - A Review, J. Mater. Chem. B 8 (2020) 607–628.

[75] M. Yamato, M. Okuhara, F. Karikusa, A. Kikuchi, Y. Sakurai, T. Okano, Signal transduction and cytoskeletal reorganization are required for cell detachment from cell culture surfaces grafted with a temperature-responsive polymer, J. Biomed. Mater. Res. 44 (1999) 44–52.

[76] Y. Akiyama, A. Kikuchi, M. Yamato, T. Okano, Ultrathin poly(N-isopropylacrylamide) grafted layer on polystyrene surfaces for cell adhesion/detachment control, Langmuir 20 (2004) 5506–5511.

[77] K. Fukumori, Y. Akiyama, M. Yamato, J. Kobayashi, K. Sakai, T. Okano, Temperature-responsive glass coverslips with an ultrathin poly(N-isopropylacrylamide) layer, Acta. Biomater. 5 (2009) 470–476.

[78] H.E. Canavan, X. Cheng, D.J. Graham, B.D. Ratner, D.G. Castner, Surface characterization of the extracellular matrix remaining after cell detachment from a thermoresponsive polymer, Langmuir 21 (2005) 1949–1955.

[79] K. Fukumori, Y. Akiyama, M. Yamato, T. Okano, A Facile Method for Preparing Temperature-Responsive Cell Culture Surfaces by Using a Thioxanthone Photoinitiator Immobilized on a Polystyrene Surface, ChemNanoMat 2 (2016) 454–460.

[80] J. DENG, L. WANG, L. LIU, W. YANG, Developments and new applications of UV-induced surface graft polymerizations, Progress in Polymer Science 34 (2009) 156–193.

[81] G. Conzatti, S. Cavalie, C. Combes, J. Torrisani, N. Carrere, A. Tourrette, PNIPAM grafted surfaces through ATRP and RAFT polymerization: Chemistry and bioadhesion, Colloids Surf. B Biointerfaces 151 (2017) 143–155.

[82] H. Takahashi, M. Nakayama, M. Yamato, T. Okano, Controlled Chain Length and Graft Density of Thermoresponsive Polymer Brushes for Optimizing Cell Sheet Harvest, Biomacromolecules 11 (2010) 1991–1999.

[83] N. Matsuzaka, H. Takahashi, M. Nakayama, A. Kikuchi, T. Okano, Effect of the hydrophobic basal layer of thermoresponsive block co-polymer brushes on thermally-induced cell sheet harvest, J. Biomater. Sci. Polym. Ed. 23 (2012) 1301–1314.

[84] N.G. Patel, J.P. Cavicchia, G. Zhang, B. Zhang Newby, Rapid cell sheet detachment using spin-coated pNIPAAm films retained on surfaces by an aminopropyltriethoxysilane network, Acta. Biomater. 8 (2012) 2559–2567.

[85] L. Yang, X. Fan, J. Zhang, J. Ju, Preparation and Characterization of Thermoresponsive Poly(N-Isopropylacrylamide) for Cell Culture Applications, Polymers 12 (2020).

[86] S. Inal, J.D. Kölsch, F. Sellrie, J.A. Schenk, E. Wischerhoff, A. Laschewsky, D. Neher, A water soluble fluorescent polymer as a dual colour sensor for temperature and a specific protein, J. Mater. Chem. B 1 (2013) 6373–6381.

[87] H. von Recum, T. Okano, S. Wan Kim, Growth factor release from thermally reversible tissue culture substrates, J. Control. Release 55 (1998) 121–130.

[88] Y. Wu, H. Li, Z. Rao, H. Li, Y. Wu, J. Zhao, J. Rong, Controlled protein adsorption and delivery of thermosensitive poly(N-isopropylacrylamide) nanogels, J. Mater. Chem. B 5 (2017) 7974–7984.

[89] T. Gao, N. Kousinioris, S.R. Winn, J.M. Wozney, H. Uludag, Enhanced Retention of rhBMP-2In Vivo by Thermoreversible Polymers, Mat.-wiss. u. Werkstofftech. 32 (2001) 953–961.

[90] X. Lin, X. Guan, Y. Wu, S. Zhuang, Y. Wu, L. Du, J. Zhao, J. Rong, J. Zhao, M. Tu, An alginate/poly(N-isopropylacrylamide)-based composite hydrogel dressing with stepwise delivery of drug and growth factor for wound repair, Mater. Sci. Eng. C Mater. Biol. Appl. 115 (2020) 111123.

[91] N. Lu, J. Liu, J. Li, Z. Zhang, Y. Weng, B. Yuan, K. Yang, Y. Ma, Tunable dual-stimuli response of a microgel composite consisting of reduced graphene oxide nanoparticles and poly(N-isopropylacrylamide) hydrogel microspheres, J. Mater. Chem. B 2 (2014) 3791–3798.

[92] Y. Wang, M. Yan, L. Xu, W. Zhao, X. Wang, S. Dong, J. Hao, Aptamer-functionalized DNA microgels: a strategy towards selective anticancer therapeutic systems, J. Mater. Chem. B 4 (2016) 5446–5454.

[93] A.S. Vikulina, N.A. Feoktistova, N.G. Balabushevich, R. von Klitzing, D. Volodkin, Cooling-Triggered Release from Mesoporous Poly(N-isopropylacrylamide) Microgels at Physiological Conditions, ACS Appl. Mater. Interfaces (2020).

[94] C.A. Kavanagh, T.A. Gorelova, I.I. Selezneva, Y.A. Rochev, K.A. Dawson, W.M. Gallagher, A.V. Gorelov, A.K. Keenan, Poly(N-isopropylacrylamide) copolymer films as vehicles for the sustained delivery of proteins to vascular endothelial cells, J. Biomed. Mater. Res. A 72 (2005) 25–35.

[95] J.C. Garbern, E. Minami, P.S. Stayton, C.E. Murry, Delivery of basic fibroblast growth factor with a pH-responsive, injectable hydrogel to improve angiogenesis in infarcted myocardium, Biomaterials 32 (2011) 2407–2416.

[96] J.C. Garbern, A.S. Hoffman, P.S. Stayton, Injectable pH- and temperature-responsive poly(N-isopropylacrylamide-co-propylacrylic acid) copolymers for delivery of angiogenic growth factors, Biomacromolecules 11 (2010) 1833–1839.

[97] M. Qu, X. Jiang, X. Zhou, C. Wang, Q. Wu, L. Ren, J. Zhu, S. Zhu, P. Tebon, W. Sun, A. Khademhosseini, Stimuli-Responsive Delivery of Growth Factors for Tissue Engineering, Adv. Healthc. Mater. 9 (2020) e1901714.

[98] S. Doleski, L. Yao, A. Pandit, C. Elvira, NGF release from thermo-responsive collagen-polyNIPAam polymer networks supports neuronal cell growth and differentiation, J. Biomed. Mater. Res. A 94 (2010) 457–465.

[99] L. Han, Y. Zhang, X. Lu, K. Wang, Z. Wang, H. Zhang, Polydopamine Nanoparticles Modulating Stimuli-Responsive PNIPAM Hydrogels with Cell/Tissue Adhesiveness, ACS Appl. Mater. Interfaces 8 (2016) 29088–29100.

[100] Y. Arisaka, J. Kobayashi, M. Yamato, Y. Akiyama, T. Okano, Switching of Cell Growth/Detachment on Heparin-functionalized Thermoresponsive Surface for Rapid Cell Sheet Fabrication and Manipulation, Biomaterials 34 (2013) 4214–4222.

[101] Y. Arisaka, J. Kobayashi, K. Ohashi, K. Tatsumi, K. Kim, Y. Akiyama, M. Yamato, T. Okano, A heparin-modified thermoresponsive surface with heparin-binding epidermal growth factor-like growth factor for maintaining hepatic functions in vitro and harvesting hepatocyte sheets, Regen. Ther. 3 (2016) 97–106.

[102] Z. Oezyuerek, K. Franke, M. Nitschke, R. Schulze, F. Simon, K.-J. Eichhorn, T. Pompe, C. Werner, B. Voit, Sulfated glyco-block copolymers with specific receptor and growth factor binding to support cell adhesion and proliferation, Biomaterials 30 (2009) 1026–1035.

[103] D.J. Lee, M.A. Cavasin, A.J. Rocker, D.E. Soranno, X. Meng, R. Shandas, D. Park, An injectable sulfonated reversible thermal gel for therapeutic angiogenesis to protect cardiac function after a myocardial infarction, J. Biol. Eng. 13 (2019) 6.

[104] M. Ebara, M. Yamato, T. Aoyagi, A. Kikuchi, K. Sakai, T. Okano, Temperature-responsive cell culture surfaces enable "on-off" affinity control between cell integrins and RGDS ligands, Biomacromolecules 5 (2004) 505–510.

[105] J.M. Silva, R.L. Reis, J.F. Mano, Biomimetic Extracellular Environment Based on Natural Origin Polyelectrolyte Multilayers, Small 12 (2016) 4308–4342.

[106] R.K. Iler, Multilayers of colloidal particles, J. Colloid Interface Sci. 21 (1966) 569–594.

[107] G. Decher, J.D. Hong, J. Schmitt, Buildup of ultrathin multilayer films by a self-assembly process: III. Consecutively alternating adsorption of anionic and cationic polyelectrolytes on charged surfaces, Thin Solid Films 210-211 (1992) 831–835.

[108] G. Decher, B. Lehr, K. Lowack, Y. Lvov, J. Schmitt, New nanocomposite films for biosensors: layer-by-layer adsorbed films of polyelectrolytes, proteins or DNA, Biosensors and Bioelectronics 9 (1994) 677–684.

[109] Joseph B. Schlenoff, Hiep Ly, Ming Li, Charge and Mass Balance in Polyelectrolyte Multilayers, J. Am. Chem. Soc. 120 (1998) 7626–7634.

[110] S.T. Dubas, J.B. Schlenoff, Factors Controlling the Growth of Polyelectrolyte Multilayers, Macromolecules 32 (1999) 8153–8160.

[111] J. Borges, J.F. Mano, Molecular Interactions Driving the Layer-by-Layer Assembly of Multilayers, Chem. Rev. 114 (2014) 8883–8942.

[112] T. Boudou, T. Crouzier, K. Ren, G. Blin, C. Picart, Multiple functionalities of polyelectrolyte multilayer films: new biomedical applications, Adv. Mater. 22 (2010) 441–467.

[113] M.S. Niepel, F. Almouhanna, B.K. Ekambaram, M. Menzel, A. Heilmann, T. Groth, Cross-linking Multilayers of Poly-l-lysine and Hyaluronic Acid: Effect on Mesenchymal Stem Cell Behavior, Int. J. Artif. Organs 41 (2018) 223–235.

[114] L. Richert, F. Boulmedais, P. Lavalle, J. Mutterer, E. Ferreux, G. Decher, P. Schaaf, J.-C. Voegel, C. Picart, Improvement of Stability and Cell Adhesion Properties of Polyelectrolyte Multilayer Films by Chemical Cross-linkin, Biomacromolecules 5 (2004) 284–294.

[115] J.M. Silva, S.G. Caridade, R.R. Costa, N.M. Alves, T. Groth, C. Picart, R.L. Reis, J.F. Mano, pH Responsiveness of Multilayered Films and Membranes Made of Polysaccharides, Langmuir 31 (2015) 11318–11328.

[116] H. Riegler, F. Essler, Polyelectrolytes. 2. Intrinsic or Extrinsic Charge Compensation? Quantitative Charge Analysis of PAH/PSS Multilayers, Langmuir 18 (2002) 6694–6698.

[117] J.M.C. Lourenço, P.A. Ribeiro, A.M. Botelho do Rego, F.M. Braz Fernandes, A.M.C. Moutinho, M. Raposo, Counterions in poly(allylamine hydrochloride) and poly(styrene sulfonate) layer-by-layer films, Langmuir 20 (2004) 8103–8109.

[118] T. Crouzier, C. Picart, Ion Pairing and Hydration in Polyelectrolyte Multilayer Films Containing Polysaccharides, Biomacromolecules 10 (2009) 433–442.

[119] C. Porcel, P. Lavalle, G. Decher, B. Senger, J.-C. Voegel, P. Schaaf, Influence of the polyelectrolyte molecular weight on exponentially growing multilayer films in the linear regime, Langmuir 23 (2007) 1898–1904.

[120] N. Aggarwal, N. Altgärde, S. Svedhem, G. Michanetzis, Y. Missirlis, T. Groth, Tuning Cell Adhesion and Growth on Biomimetic Polyelectrolyte Multilayers by Variation of pH During Layer-by-Layer Assembly, Macromol. Biosci. 13 (2013) 1327–1338.

[121] N. Aggarwal, Modulating cell behaviour through biomimetic multilayers of natural and semi-synthetic glycosaminoglycans, Universitäts- und Landesbibliothek Sachsen-Anhalt, 2014.

[122] K.B. Rufato, P.R. Souza, A.C. de Oliveira, S.B.R. Berton, R.M. Sabino, E.C. Muniz, K.C. Popat, E. Radovanovic, M.J. Kipper, A.F. Martins, Antimicrobial and cytocompatible chitosan, N,N,N-trimethyl chitosan, and tanfloc-based polyelectrolyte multilayers on gellan gum films, Int. J. Biol. Macromol. 183 (2021) 727–742.

[123] S. Ida, R. Kimura, S. Tanimoto, Y. Hirokawa, End-Crosslinking of Controlled Telechelic Poly(N-isopropylacrylamide) Toward a Homogeneous Gel Network with Photo-Induced Self-Healing, Polym. J. 49 (2017) 237–243.

[124] G. Apte, A. Repanas, C. Willems, A. Mujtaba, C.E.H. Schmelzer, A. Raichur, F. Syrowatka, T. Groth, Effect of Different Crosslinking Strategies on Physical Properties and Biocompatibility of Freestanding Multilayer Films Made of Alginate and Chitosan, Macromol. Biosci. 19 (2019) e1900181.

[125] J. Almodóvar, T. Crouzier, Š. Selimović, T. Boudou, A. Khademhosseini, C. Picart, Gradients of physical and biochemical cues on polyelectrolyte multilayer films generated via microfluidics, Lab Chip 13 (2013) 1562–1570.

[126] J.M. Silva, S.G. Caridade, N.M. Oliveira, R.L. Reis, J.F. Mano, Chitosan-Alginate Multilayered Films with Gradients of Physicochemical Cues, J. Mater. Chem. B 3 (2015) 4555–4568.

[127] M. Zhao, L. Li, C. Zhou, F. Heyroth, B. Fuhrmann, K. Maeder, T. Groth, Improved stability and cell response by intrinsic cross-linking of multilayers from collagen I and oxidized glycosaminoglycans, Biomacromolecules 15 (2014) 4272–4280.

[128] M. Zhao, G. Altankov, U. Grabiec, M. Bennett, M. Salmeron-Sanchez, F. Dehghani, T. Groth, Molecular Composition of GAG-collagen I Multilayers Affects Remodeling of

Terminal Layers and Osteogenic Differentiation of Adipose-Derived Stem Cells, Acta. Biomater. 41 (2016) 86–99.

[129]   J. Almodóvar, S. Bacon, J. Gogolski, J.D. Kisiday, M.J. Kipper, Polysaccharide-Based Polyelectrolyte Multilayer Surface Coatings Can Enhance Mesenchymal Stem Cell Response to Adsorbed Growth Factors, Biomacromolecules 11 (2010) 2629–2639.

[130]   M.L. Macdonald, N.M. Rodriguez, N.J. Shah, P.T. Hammond, Characterization of tunable FGF-2 releasing polyelectrolyte multilayers, Biomacromolecules 11 (2010) 2053–2059.

[131]   A. Dierich, E. Le Guen, N. Messaddeq, J.-F. Stoltz, P. Netter, P. Schaaf, J.-C. Voegel, N. Benkirane-Jessel, Bone Formation Mediated by Synergy-Acting Growth Factors Embedded in a Polyelectrolyte Multilayer Film, Adv. Mater. 19 (2007) 693–697.

[132]   C. Lin, R. Romero, L.V. Sorokina, K.R. Ballinger, L.W. Place, M.J. Kipper, S.R. Khetani, A Polyelectrolyte Multilayer Platform for Investigating Growth Factor Delivery Modes in Human Liver Cultures, J. Biomed. Mater. Res. A 106 (2018) 971–984.

[133]   T. Crouzier, L. Fourel, T. Boudou, C. Albigès-Rizo, C. Picart, Presentation of BMP-2 from a soft biopolymeric film unveils its activity on cell adhesion and migration, Adv. Mater. 23 (2011) H111-8.

[134]   R. Anouz, A. Repanas, E. Schwarz, T. Groth, Novel Surface Coatings Using Oxidized Glycosaminoglycans as Delivery Systems of Bone Morphogenetic Protein 2 (BMP-2) for Bone Regeneration, Macromol. Biosci. 18 (2018) e1800283.

[135]   A. Hautmann, D. Kedilaya, S. Stojanović, M. Radenković, C.K. Marx, S. Najman, M. Pietzsch, J.F. Mano, T. Groth, Free-standing multilayer films as growth factor reservoirs for future wound dressing applications, Biomater. Adv. 142 (2022) 213166.

[136]   A. Köwitsch, G. Zhou, T. Groth, Medical Application of Glycosaminoglycans: A Review, J. Tissue Eng. Regen. Med. 12 (2018) e23-e41.

[137]   D.L. Rabenstein, Heparin and heparan sulfate: structure and function, Nat. Prod. Rep. 19 (2002) 312–331.

[138]   R.E. Hileman, J.R. Fromm, J.M. Weiler, R.J. Linhardt, Glycosaminoglycan-protein interactions: definition of consensus sites in glycosaminoglycan binding proteins, Bioessays 20 (1998) 156–167.

[139]   J. Martel-Pelletier, A. Farran, E. Montell, J. Vergés, J.-P. Pelletier, Discrepancies in composition and biological effects of different formulations of chondroitin sulfate, Molecules 20 (2015) 4277–4289.

[140]   N. Volpi, Chondroitin Sulfate Safety and Quality, Molecules 24 (2019).

[141]   K. Zhang, D. Peschel, E. Brendler, T. Groth, S. Fischer, Synthesis and Bioactivity of Cellulose Derivatives, Macromol. Symp. 280 (2009) 28–35.

[142]   L. Zhu, J. Qin, X. Yin, L. Ji, Q. Lin, Z. Qin, Direct sulfation of bacterial cellulose with a ClSO 3 H/DMF complex and structure characterization of the sulfates, Polym. Adv. Technol. 25 (2014) 168–172.

[143]   K. Zeng, T. Groth, K. Zhang, Recent Advances in Artificially Sulfated Polysaccharides for Applications in Cell Growth and Differentiation, Drug Delivery, and Tissue Engineering, Chembiochem 20 (2019) 737–746.

[144]   D. Peschel, K. Zhang, S. Fischer, T. Groth, Modulation of osteogenic activity of BMP-2 by cellulose and chitosan derivatives, Acta. Biomater. 8 (2012) 183–193.

[145]   D. Peschel, K. Zhang, N. Aggarwal, E. Brendler, S. Fischer, T. Groth, Synthesis of Novel Celluloses Derivatives and Investigation of Their Mitogenic Activity in the Presence and Absence of FGF2, Acta. Biomater. 6 (2010) 2116–2125.

[146]   G. Cavallaro, S. Micciulla, L. Chiappisi, G. Lazzara, Chitosan-based smart hybrid materials: a physico-chemical perspective, J. Mater. Chem. B 9 (2021) 594–611.

[147]   Q.Z. Wang, X.G. Chen, N. Liu, S.X. Wang, C.S. Liu, X.H. Meng, C.G. Liu, Protonation Constants of Chitosan with Different Molecular Weight and Degree of Deacetylation, Carbohydr. Polym. 65 (2006) 194–201.

[148]   D.I. Sánchez-Machado, J. López-Cervantes, M.A. Correa-Murrieta, R.G. Sánchez-Duarte, P. Cruz-Flores, G.S. de La Mora-López, Chitosan, in: Sánchez-Machado, D.I., et al. (Ed.), Nonvitamin and Nonmineral Nutritional Supplements, Elsevier, 2019, pp. 485–493.

[149]   N. Kahya, Water Soluble Chitosan Derivatives and their Biological Activities: A Review, Polym Sci 05 (2019).

[150]   D.R. Perinelli, L. Fagioli, R. Campana, J.K.W. Lam, W. Baffone, G.F. Palmieri, L. Casettari, G. Bonacucina, Chitosan-based nanosystems and their exploited antimicrobial activity, Eur. J. Pharm. Sci. 117 (2018) 8–20.

[151]   M.P. Sousa, F. Cleymand, J.F. Mano, Elastic Chitosan/Chondroitin Sulfate Multilayer Membranes, Biomed. Mater. 11 (2016) 35008.

[152]   J.M. Silva, J.R. García, R.L. Reis, A.J. García, J.F. Mano, Tuning Cell Adhesive Properties via Layer-by-Layer Assembly of Chitosan and Alginate, Acta. Biomater. 51 (2017) 279–293.

[153]   K. Pathak, S.K. Misra, A. Sehgal, S. Singh, S. Bungau, A. Najda, R. Gruszecki, T. Behl, Biomedical Applications of Quaternized Chitosan, Polymers 13 (2021).

[154]   W. Sajomsang, S. Tantayanon, V. Tangpasuthadol, W.H. Daly, Quaternization of N-aryl chitosan derivatives: synthesis, characterization, and antibacterial activity, Carbohydr. Res. 344 (2009) 2502–2511.

[155]   X. Mi, K.S. Vijayaragavan, C.L. Heldt, Virus adsorption of water-stable quaternized chitosan nanofibers, Carbohydr. Res. 387 (2014) 24–29.

[156]   K. Chen, B. Guo, J. Luo, Quaternized carboxymethyl chitosan/organic montmorillonite nanocomposite as a novel cosmetic ingredient against skin aging, Carbohydr. Polym. 173 (2017) 100–106.

[157]   B. Shagdarova, A. Lunkov, A. Il'ina, V. Varlamov, Investigation of the properties of N-(2-hydroxy-3-trimethylammonium) propyl chloride chitosan derivatives, Int. J. Biol. Macromol. 124 (2019) 994–1001.

[158]   B. Wang, X. Yang, C. Qiao, Y. Li, T. Li, C. Xu, Effects of chitosan quaternary ammonium salt on the physicochemical properties of sodium carboxymethyl cellulose-based films, Carbohydr. Polym. 184 (2018) 37–46.

[159]   D. Snyman, J.H. Hamman, A.F. Kotze, Evaluation of the mucoadhesive properties of N-trimethyl chitosan chloride, Drug Dev. Ind. Pharm. 29 (2003) 61–69.

[160]   B.-I. Andreica, A. Anisiei, I. Rosca, A.-I. Sandu, A.S. Pasca, L.M. Tartau, L. Marin, Quaternized chitosan/chitosan nanofibrous mats: An approach toward bioactive materials for tissue engineering and regenerative medicine, Carbohydr. Polym. 302 (2023) 120431.

[161]   K. Zhang, X. Jiao, L. Zhou, J. Wang, C. Wang, Y. Qin, Y. Wen, Nanofibrous composite aerogel with multi-bioactive and fluid gating characteristics for promoting diabetic wound healing, Biomaterials 276 (2021) 121040.

[162]   A. Mirtič, J. Grdadolnik, The structure of poly-L-lysine in different solvents, Biophys. Chem. 175-176 (2013) 47–53.

[163]   M. Zheng, M. Pan, W. Zhang, H. Lin, S. Wu, C. Lu, S. Tang, D. Liu, J. Cai, Poly(α-l-lysine)-based nanomaterials for versatile biomedical applications: Current advances and perspectives, Bioact. Mater. 6 (2021) 1878–1909.

[164]   R. Semenyshyn, M. Hentschel, C. Stanglmair, T. Teutsch, C. Tarin, C. Pacholski, H. Giessen, F. Neubrech, In Vitro Monitoring Conformational Changes of Polypeptide Monolayers Using Infrared Plasmonic Nanoantennas, Nano Lett. 19 (2019) 1–7.

[165]   A. Rahikkala, S. Junnila, V. Vartiainen, J. Ruokolainen, O. Ikkala, E. Kauppinen, J. Raula, Polypeptide-based aerosol nanoparticles: self-assembly and control of

conformation by solvent and thermal annealing, Biomacromolecules 15 (2014) 2607–2615.

[166] Y. Xi, T. Song, S. Tang, N. Wang, J. Du, Preparation and Antibacterial Mechanism Insight of Polypeptide-Based Micelles with Excellent Antibacterial Activities, Biomacromolecules 17 (2016) 3922–3930.

[167] A. Hall, L.-P. Wu, L. Parhamifar, S.M. Moghimi, Differential Modulation of Cellular Bioenergetics by Poly(L-lysine)s of Different Molecular Weights, Biomacromolecules 16 (2015) 2119–2126.

[168] J.S. Heo, H.O. Kim, S.Y. Song, D.H. Lew, Y. Choi, S. Kim, Poly-L-lysine Prevents Senescence and Augments Growth in Culturing Mesenchymal Stem Cells Ex Vivo, Biomed Res. Int. 2016 (2016) 8196078.

[169] J.F. Quinn, F. Caruso, Facile Tailoring of Film Morphology and Release Properties Using Layer-by-Layer Assembly of Thermoresponsive Materials, Langmuir 20 (2004) 20–22.

[170] J.A. Jaber, J.B. Schlenoff, Polyelectrolyte Multilayers with Reversible Thermal Responsivity, Macromolecules 38 (2005) 1300–1306.

[171] M.J. Serpe, K.A. Yarmey, C.M. Nolan, L.A. Lyon, Doxorubicin uptake and release from microgel thin films, Biomacromolecules 6 (2005) 408–413.

[172] A. Osypova, D. Magnin, P. Sibret, A. Aqil, C. Jérôme, C. Dupont-Gillain, C.-M. Pradier, S. Demoustier-Champagne, J. Landoulsi, Dual Stimuli-Responsive Coating Designed Through Layer-by-Layer Assembly of PAA-b-PNIPAM Block Copolymers for the Control of Protein Adsorption, Soft Matter 11 (2015) 8154–8164.

[173] A. Osypova, C.-A. Fustin, C.-M. Pradier, J. Landoulsi, S. Demoustier-Champagne, Factors impacting protein adsorption on layer-by-layer assembled stimuli-responsive thin films, Eur. Polym. J. 95 (2017) 195–206.

[174] Li Xu, H. Wang, Z. Chu, L. Cai, H. Shi, C. Zhu, D. Pan, J. Pan, X. Fei, Y. Lei, Temperature-Responsive Multilayer Films of Micelle-Based Composites for Controlled Release of a Third-Generation EGFR Inhibitor, ACS Appl. Polym. Mater. 2 (2020) 741–750.

[175] L. Xu, X. Zhang, Z. Chu, H. Wang, Y. Li, X. Shen, L. Cai, H. Shi, C. Zhu, J. Pan, D. Pan, Temperature-Responsive Multilayer Films Based on Block Copolymer-Coated Silica Nanoparticles for Long-Term Release of Favipiravir, ACS Appl. Nano Mater. 4 (2021) 14014–14025.

[176] T. Liao, M.D. Moussallem, J. Kim, J.B. Schlenoff, T. Ma, N-isopropylacrylamide-Based Thermoresponsive Polyelectrolyte Multilayer Films for Human Mesenchymal Stem Cell Expansion, Biotechnol. Prog. 26 (2010) 1705–1713.

[177] G.V. Martins, J.F. Mano, N.M. Alves, Dual Responsive Nanostructured Surfaces for Biomedical Applications, Langmuir 27 (2011) 8415–8423.

[178] Z. Wang, Z. Wang, W.W. Lu, W. Zhen, D. Yang, S. Peng, Novel biomaterial strategies for controlled growth factor delivery for biomedical applications, NPG Asia Mater 9 (2017) e435-e435.

[179] B. Boilly, A.S. Vercoutter-Edouart, H. Hondermarck, V. Nurcombe, X. Le Bourhis, FGF signals for cell proliferation and migration through different pathways, Cytokine Growth Factor Rev. 11 (2000) 295–302.

[180] A.N. Sohi, H. Naderi-Manesh, M. Soleimani, E.R. Yasaghi, H.K. Manjili, S. Tavaddod, S. Nojehdehi, Synergistic effect of co-immobilized FGF-2 and vitronectin-derived peptide on feeder-free expansion of induced pluripotent stem cells, Mater. Sci. Eng. C Mater. Biol. Appl. 93 (2018) 157–169.

[181] A. Novais, E. Chatzopoulou, C. Chaussain, C. Gorin, The Potential of FGF-2 in Craniofacial Bone Tissue Engineering: A Review, Cells 10 (2021).

[182]   M. Rusnati, E. Tanghetti, P. Dell'Era, A. Gualandris, M. Presta, alphavbeta3 integrin mediates the cell-adhesive capacity and biological activity of basic fibroblast growth factor (FGF-2) in cultured endothelial cells, Mol. Biol. Cell 8 (1997) 2449–2461.

[183]   S. Mori, Y. Takada, Crosstalk between Fibroblast Growth Factor (FGF) Receptor and Integrin through Direct Integrin Binding to FGF and Resulting Integrin-FGF-FGFR Ternary Complex Formation, Medical Sciences 1 (2013) 20–36.

[184]   I. Ding, A.M. Peterson, Half-life modeling of basic fibroblast growth factor released from growth factor-eluting polyelectrolyte multilayers, Sci. Rep. 11 (2021) 9808.

[185]   M. Garcia-Maya, A.A. Anderson, C.E. Kendal, A.V. Kenny, L.C. Edwards-Ingram, A. Holladay, J.L. Saffell, Ligand concentration is a driver of divergent signaling and pleiotropic cellular responses to FGF, J. Cell. Physiol. 206 (2006) 386–393.

[186]   Á. Apáti, T. Berecz, B. Sarkadi, Calcium signaling in human pluripotent stem cells, Cell Calcium 59 (2016) 117–123.

[187]   R. Mhanna, J. Becher, M. Schnabelrauch, R.L. Reis, I. Pashkuleva, Sulfated Alginate as a Mimic of Sulfated Glycosaminoglycans: Binding of Growth Factors and Effect on Stem Cell Behavior, Adv. Biosyst. 1 (2017) e1700043.

[188]   M. Prawatborisut, S. Jiang, J. Oberländer, V. Mailänder, D. Crespy, K. Landfester, Modulating Protein Corona and Materials–Cell Interactions with Temperature-Responsive Materials, Adv. Funct. Mater. 32 (2022) 2106353.

[189]   J. Kobayashi, Y. Arisaka, N. Yui, Y. Akiyama, M. Yamato, T. Okano, Effect of Temperature Changes on Serum Protein Adsorption on Thermoresponsive Cell-Culture Surfaces Monitored by A Quartz Crystal Microbalance with Dissipation, Int. J. Mol. Sci. 19 (2018).

[190]   M. Cao, Y. Wang, X. Hu, H. Gong, R. Li, H. Cox, J. Zhang, T.A. Waigh, H. Xu, J.R. Lu, Reversible Thermoresponsive Peptide-PNIPAM Hydrogels for Controlled Drug Delivery, Biomacromolecules 20 (2019) 3601–3610.

[191]   E. Smith, J. Yang, L. McGann, W. Sebald, H. Uludag, RGD-grafted thermoreversible polymers to facilitate attachment of BMP-2 responsive C2C12 cells, Biomaterials 26 (2005) 7329–7338.

[192]   Y.-T. Lu, P.-T. Hung, K. Zeng, C. Woelk, B. Fuhrmann, K. Zhang, T. Groth, Surface properties and bioactivity of PNIPAM-grafted-chitosan/chondroitin multilayers, Smart Materials in Medicine 4 (2023) 356–367.

[193]   K. Zeng, F. Doberenz, Y.-T. Lu, J.P. Nong, S. Fischer, T. Groth, K. Zhang, Synthesis of Thermoresponsive PNIPAM-Grafted Cellulose Sulfates for Bioactive Multilayers via Layer-by-Layer Technique, ACS Appl. Mater. Interfaces 14 (2022) 48384–48396.

[194]   Y.-T. Lu, K. Zeng, B. Fuhrmann, C. Woelk, K. Zhang, T. Groth, Engineering of Stable Cross-Linked Multilayers Based on Thermo-Responsive PNIPAM-Grafted-Chitosan/Heparin to Tailor Their Physiochemical Properties and Biocompatibility, ACS Appl. Mater. Interfaces 14 (2022) 29550–29562.

[195]   R. Tsou, F.F. Isik, Integrin activation is required for VEGF and FGF receptor protein presence on human microvascular endothelial cells, Mol. Cell. Biochem. 224 (2001) 81–89.

[196]   S. Preibisch, S. Saalfeld, P. Tomancak, Globally optimal stitching of tiled 3D microscopic image acquisitions, Bioinformatics 25 (2009) 1463–1465.

[197]   M. Lundin, F. Solaqa, E. Thormann, L. Macakova, E. Blomberg, Layer-by-Layer Assemblies of Chitosan and Heparin: Effect of Solution Ionic Strength and pH, Langmuir 27 (2011) 7537–7548.

[198]   P. Nazaran, V. Bosio, W. Jaeger, D.F. Anghel, R.V. Klitzing, Lateral mobility of polyelectrolyte chains in multilayers, J. Phys. Chem. B 111 (2007) 8572–8581.

[199]   T. Fujie, J.Y. Park, A. Murata, N.C. Estillore, M.C.R. Tria, S. Takeoka, R.C. Advincula, Hydrodynamic transformation of a freestanding polymer nanosheet induced by a thermoresponsive surface, ACS Appl. Mater. Interfaces 1 (2009) 1404–1413.

[200]   G. Liu, G. Zhang, Collapse and swelling of thermally sensitive poly(N-isopropylacrylamide) brushes monitored with a quartz crystal microbalance, J. Phys. Chem. B 109 (2005) 743–747.

[201]   E. Maza, C. von Bilderling, M.L. Cortez, G. Díaz, M. Bianchi, L.I. Pietrasanta, J.M. Giussi, O. Azzaroni, Layer-by-Layer Assembled Microgels Can Combine Conflicting Properties: Switchable Stiffness and Wettability without Affecting Permeability, Langmuir 34 (2018) 3711–3719.

[202]   A.S. Vikulina, Y.G. Anissimov, P. Singh, V.Z. Prokopović, K. Uhlig, M.S. Jaeger, R. von Klitzing, C. Duschl, D. Volodkin, Temperature effect on the build-up of exponentially growing polyelectrolyte multilayers. An exponential-to-linear transition point, Phys. Chem. Chem. Phys. 18 (2016) 7866–7874.

[203]   K. Köhler, H. Möhwald, G.B. Sukhorukov, Thermal behavior of polyelectrolyte multilayer microcapsules: 2. Insight into molecular mechanisms for the PDADMAC/PSS system, J. Phys. Chem. B 110 (2006) 24002–24010.

[204]   R. Mueller, K. Köhler, R. Weinkamer, G. Sukhorukov, A. Fery, Melting of PDADMAC/PSS Capsules Investigated with AFM Force Spectroscopy, Macromolecules 38 (2005) 9766–9771.

[205]   M.H. Futscher, M. Philipp, P. Müller-Buschbaum, A. Schulte, The Role of Backbone Hydration of Poly(N-isopropyl acrylamide) Across the Volume Phase Transition Compared to its Monomer, Sci. Rep. 7 (2017) 17012.

[206]   T. Groth, G. Altankov, A. Kostadinova, N. Krasteva, W. Albrecht, D. Paul, Altered Vitronectin Receptor (αv Integrin) Function in Fibroblasts Adhering on Hydrophobic Glass, J. Biomed. Mater. Res. 44 (1999) 341–351.

[207]   I. Kiesel, M. Paulus, J. Nase, S. Tiemeyer, C. Sternemann, K. Rüster, F.J. Wirkert, K. Mende, T. Büning, M. Tolan, Temperature-driven adsorption and desorption of proteins at solid-liquid interfaces, Langmuir 30 (2014) 2077–2083.

[208]   G. Jackler, C. Czeslik, R. Steitz, C.A. Royer, Spatial distribution of protein molecules adsorbed at a polyelectrolyte multilayer, Phys. Rev. E Stat. Nonlin. Soft Matter Phys. 71 (2005) 41912.

[209]   G. Toromanov, D. Gugutkov, J. Gustavsson, J. Planell, M. Salmerón-Sánchez, G. Altankov, Dynamic Behavior of Vitronectin at the Cell-Material Interface, ACS Biomater. Sci. Eng. 1 (2015) 927–934.

[210]   I. Capila, R.J. Linhardt, Heparin-Protein Interactions, Angewandte Chemie International Edition 41 (2002) 390–412.

[211]   J.L. Bohnert, T.A. Horbett, Changes in adsorbed fibrinogen and albumin interactions with polymers indicated by decreases in detergent elutability, J. Colloid Interface Sci. 111 (1986) 363–377.

[212]   L.Y.W. Yap, J. Li, I.Y. Phang, L.T. Ong, J.Z.-E. Ow, J.C.H. Goh, V. Nurcombe, J. Hobley, A.B.H. Choo, S.K.W. Oh, S.M. Cool, W.R. Birch, Defining a threshold surface density of vitronectin for the stable expansion of human embryonic stem cells, Tissue Eng. Part C Methods 17 (2011) 193–207.

[213]   M. Kumorek, O. Janoušková, A. Höcherl, M. Houska, E. Mázl-Chánová, N. Kasoju, L. Cuchalová, R. Matějka, D. Kubies, Effect of Crosslinking Chemistry of Albumin/Heparin Multilayers on FGF-2 Adsorption and Endothelial Cell Behavior, Appl. Surf. Sci. 411 (2017) 240–250.

[214]   G.E. Plopper, H.P. McNamee, L.E. Dike, K. Bojanowski, D.E. Ingber, Convergence of integrin and growth factor receptor signaling pathways within the focal adhesion complex, Mol. Biol. Cell 6 (1995) 1349–1365.

[215]   J. Blacklock, A. Vetter, A. Lankenau, D. Oupický, H. Möhwald, Tuning the mechanical properties of bioreducible multilayer films for improved cell adhesion and transfection activity, Biomaterials 31 (2010) 7167–7174.

[216]   S. Tojkander, G. Gateva, P. Lappalainen, Actin stress fibers--assembly, dynamics and biological roles, J. Cell Sci. 125 (2012) 1855–1864.

[217]   J.G. Lee, E.P. Kay, Cross-talk among Rho GTPases acting downstream of PI 3-kinase induces mesenchymal transformation of corneal endothelial cells mediated by FGF-2, Invest. Ophthalmol. Vis. Sci. 47 (2006) 2358–2368.

[218]   S. Klein, F.G. Giancotti, M. Presta, S.M. Albelda, C.A. Buck, D.B. Rifkin, Basic fibroblast growth factor modulates integrin expression in microvascular endothelial cells, Mol. Biol. Cell 4 (1993) 973–982.

[219]   Y.-J. Jin, I. Park, I.-K. Hong, H.-J. Byun, J. Choi, Y.-M. Kim, H. Lee, Fibronectin and vitronectin induce AP-1-mediated matrix metalloproteinase-9 expression through integrin $\alpha(5)\beta(1)/\alpha(v)\beta(3)$-dependent Akt, ERK and JNK signaling pathways in human umbilical vein endothelial cells, Cell. Signal. 23 (2011) 125–134.

[220]   J.L. Bays, K.A. DeMali, Vinculin in cell-cell and cell-matrix adhesions, Cell. Mol. Life Sci. 74 (2017) 2999–3009.

[221]   J. Lehtimäki, M. Hakala, P. Lappalainen, Actin Filament Structures in Migrating Cells, Handb. Exp. Pharmacol. 235 (2017) 123–152.

[222]   S. Schmidt, M. Zeiser, T. Hellweg, C. Duschl, A. Fery, H. Möhwald, Adhesion and Mechanical Properties of PNIPAM Microgel Films and Their Potential Use as Switchable Cell Culture Substrates, Adv. Funct. Mater. 20 (2010) 3235–3243.

[223]   R.M.P. Da Silva, J.F. Mano, R.L. Reis, Smart thermoresponsive coatings and surfaces for tissue engineering: switching cell-material boundaries, Trends Biotechnol. 25 (2007) 577–583.

[224]   T. Okano, N. Yamada, M. Okuhara, H. Sakai, Y. Sakurai, Mechanism of cell detachment from temperature-modulated, hydrophilic-hydrophobic polymer surfaces, Biomaterials 16 (1995) 297–303.

Chapter 2

Summary – Engineering of stable cross-linked multilayers based on thermo-responsive PNIPAM-*grafted*-chitosan/heparin to tailor their physiochemical properties and biocompatibility

It is known that PNIPAM lack of specific bioactive interaction with cells restricts its application in drug delivery and tissue engineering. The first paper explored the possibility to develop thermoresponsive multilayers containing poly(N-isopropylacrylamide) (PNIPAM) with the aim to tailor their physiochemical properties and improve biocompatibility in combination with bioactive glycosaminoglycans (GAGs). In this study, PNIPAM was integrated with chitosan (Chi) into PNIPAM-*grafted*-chitosan (PNIPAM-Chi or PChi) to be employed as a polycation for assembly of PChi-containing polyelectrolyte multilayers (PEM) with a polyanion heparin (Hep) via layer-by-layer technique. Grafting carboxylic terminated− PNIPAM chains on the primary amino groups of Chi backbone was carried out by carbodiimide chemistry using 1-ethyl-3-(3- dimethylaminopropyl) carbodiimide/N-hydroxysuccinimide (EDC/NHS). Different degree of substitutions (DS) of PNIPAM on PChi were derived by changing the molecular weight (MW) of PNIPAM with either 2 or 10 kDa or by changing the weight ratio of PNIPAM and Chi. The structure, DS, cloud point temperature (T$_{CP}$) and hydrodynamic diameter were subsequently analyzed by NMR (nuclear magnetic resonance), FTIR (Fourier-transform infrared spectroscopy) and DLS (dynamic laser scattering). The results showed T$_{CP}$ of the PChi mainly depends on the MW in the range from 31 to 33 °C. Two PChi, from 10 kDa but lower DS, and 2 kDa but higher DS of PNIPAM (referred as HMW and LMW*) exhibited more pronounced thermoresponsive behavior regarding the significant increase in diameter when heating above T$_{CP}$. Therefore, both were further investigated to form PEMs with Hep at pH 4. Chi-containing PEMs composed of Chi and H was compared as control systems. A series of studies were conducted to evaluate the effect of MW and DS of PNIPAM, components and environment (e.g., pH, temperature) on the internal structure, swelling ability, thickness and wettability of PEMs by surface plasmon

resonance (SPR), quartz crystal microbalance with dissipation monitoring (QCM-*D*), ellipsometry, and water contact angle (WCA) measurement.

The first observation was the interdiffusion of Hep into the layers making the structure more compacted, stiffer, and dehydrated because of its smaller MW. Compared to PEM containing HMW showing striking swelling ability and layer growth, LMW* rather restricted these effects. In addition, decrease in thickness of all PEMs was found particularly more obvious for LMW*-containing PEMs after exposure to physiological buffer, pH 7.4, indicating partial disassembly due to deprotonation of Chi. Hence, covalent crosslinking using carbodiimide chemistry was introduced to form amide bonds between H and Chi, which was demonstrated to strengthen the integrity of multilayers. The surface wettability confirmed certain thermoresponsive behaviors for PChi-containing PEMs attributed to the conformational change of PNIPAM chains. Biocompatibility of PEMs was studied using C3H10T1/2 multipotent embryonic mouse fibroblasts as the model cells that have differentiation ability to adipogenic, osteoblastogenic and chondrogenic lineages. The results showed that covalent crosslinking and the presence of dehydrated PNIPAM displayed no toxic effect of on cells, instead, they enhanced cell adhesion particularly on PEMs with Hep terminal layers.

Overall, such PEM combining PNIPAM and bioactive GAG represents a temperature stimuli cell culture system that provides a potential for controlled release of growth factors that may further promote tissue regeneration.

Engineering of Stable Cross-Linked Multilayers Based on Thermo-Responsive PNIPAM-*Grafted*-Chitosan/Heparin to Tailor Their Physiochemical Properties and Biocompatibility

Yi-Tung Lu, Kui Zeng, Bodo Fuhrmann, Christian Woelk, Kai Zhang, and Thomas Groth*

Cite This: *ACS Appl. Mater. Interfaces* 2022, 14, 29550−29562 | Read Online

ACCESS | Metrics & More | Article Recommendations | SI Supporting Information

ABSTRACT: The thermo-responsive poly(*N*-isopropylacrylamide) (PNIPAM) is ubiquitously applied in controlled drug release and tissue engineering. However, the lack of bioactivity of PNIPAM restricts its use in cell-containing systems being a thermo-responsive adhesive substratum with no regulating effect on cell growth and differentiation. In this study, integrating PNIPAM with chitosan into PNIPAM-*grafted*-chitosan (PNIPAM−Chi) allows a layer-by-layer assembly with bioactive heparin to fabricate PNIPAM-modified polyelectrolyte multilayers (PNIPAM−PEMs). Grafting PNIPAM chains of either 2 (LMW) or 10 kDa (HMW) on the chitosan backbone influences the cloud point (CP) temperature in the range from 31 to 33 °C. PNIPAM−Chi with either a higher molecular weight or a higher degree of substitution of PNIPAM chains exhibiting a significant increase in diameter above CP as ensured by dynamic light scattering is selected to fabricate PEM with heparin as a polyanion at pH 4. Little difference of layer growth is detected between the chosen PNIPAM−Chi used as polycations by surface plasmon resonance, while multilayers formed with HMW-0.02 are more hydrated and show striking swelling-and-shrinking abilities when studied with quartz crystal microbalance with dissipation monitoring. Subsequently, the multilayers are covalently cross-linked using 1-ethyl-3-(3-dimethylaminopropyl) carbodiimide/*N*-hydroxysuccinimide to strengthen the stability of the systems under physiological conditions. Ellipsometry results confirm the layer integrity after exposure to the physiological buffer at pH 7.4 compared to those without cross-linking. Moreover, significantly higher adhesion and more spreading of C3H10T1/2 multipotent embryonic mouse fibroblasts on cross-linked PEMs, particularly with heparin terminal layers, are observed owing to the bioactivity of heparin. The slightly more hydrophobic surfaces of cross-linked PNIPAM−PEMs at 37 °C also increase cell attachment and growth. Thus, layer-by-layer constructed PNIPAM−PEM with cross-linking represents an interesting cell culture system that can be potentially employed for thermally uploading and controlled release of growth factors that further promotes tissue regeneration.

KEYWORDS: poly(*N*-isopropylacrylamide), layer-by-layer technique, multilayer growth, covalent cross-linking surface properties, multipotent stem cell adhesion
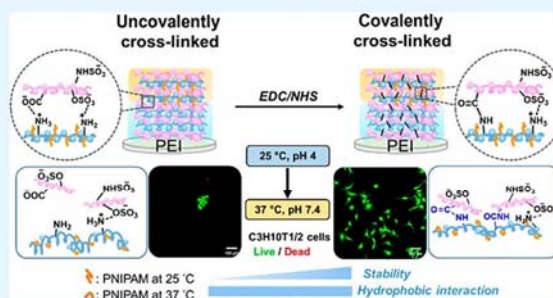
1. INTRODUCTION

Chemical design and physical design of biomaterials and interfaces utterly govern the responses of biological entities for further important applications in biomedical sciences.[1] Considerable efforts have been made to improve the physiochemical and mechanical properties of the biomaterial surfaces in terms of surface charge, wettability, topography, and stiffness.[2] A facile layer-by-layer (LbL) assembly technique has been introduced by Decher and co-workers based on electrostatic interactions and ion paring.[3] The compositions, internal structure, and physiochemical properties of polyelectrolyte multilayers (PEMs) are strongly dependent on the choice of polyelectrolytes and the complexation conditions (e.g., time, temperature, pH, ionic strength).[4]

Recent progress has grown great interest in using stimuli-responsive polymers in multilayer systems for controlling uptake/release of drugs and biomolecules like proteins including growth factors to regulate cell behavior.[5,6] Poly(*N*-isopropylacrylamide) (PNIPAM) as one of the mostly used thermo-responsive polymers exhibits a lower critical solution temperature (LCST) at 32 °C ascribed to the presence of hydrophobic (isopropyl group) and hydrophilic (amide group) side chains. The formation of hydrogen bonds to the amide side chains from surrounding water allows its dissolution in

aqueous solutions below LCST, while it becomes insoluble and dehydrated at a temperature above LCST due to the exposure of hydrophobic isopropyl groups.[7] Specially, the LCST close to physiological temperature and high biocompatibility of PNIPAM are favorable for biomedical applications.[8,9] While most approaches to immobilize PNIPAM on biomaterial surfaces require covalent grafting and a certain thickness to develop thermoresponsive properties,[5,10,11] LbL assembly may permit the fabrication of PEM with PNIPAM associated with ionic polymers that can be tailored regarding their thickness, wetting properties, mechanical properties, and topography and used as a reservoir for uploading of bioactive molecules.[12–14]

For instance, Liao et al. fabricated PNIPAM-containing multilayers by electrostatic interactions of oppositely charged poly (allylamine hydrochloride)-*co*-PNIPAM and poly (styrene sulfonate)-*co*-PNIPAM. They demonstrated that such a surface could not only be used to thermally control cell adhesion/detachment but also retain cell-secreted proteins like fibronectin on the positively charged surface, which promoted the proliferation of human mesenchymal stem cells.[15] In other studies, PNIPAM-modified multilayer coatings on nano/microcapsules were investigated to control uptake and release of enzymes, drugs, and other proteins with the aid of swelling/shrinking behavior of PNIPAM.[16–19] However, investigations on the effect of PNIPAM grafting to polyelectrolytes on the structure and physicochemical properties of PEM are rarely found. The most thorough study was conducted by Jaber and Schlenoff using synthetic copolymers of NIPAM with allylamine and styrenesulfonate.[20] Although they observed that the ionic cross-linking in the multilayer suppressed the effectiveness of coil-to-globular transition of PNIPAM, the film still showed thermoresponsive behavior.

So far, no studies can be found that demonstrate the regulation of cell growth and differentiation on PNIPAM-containing PEM due to their lack of bioactivity. Heparin with high affinity to extracellular matrix proteins (e.g., fibronectin) and growth factors like FGF 2 represents an interesting bioactive polyanion.[21,22] On the other hand, PNIPAM-*graft*-chitosan (PNIPAM−Chi) possesses thermoresponsivity and excellent biocompatibility,[23,24] which make it useful as a polycation for the formation of bioactive PEM in combination with heparin. One of the challenges to apply PNIPAM−Chi as a polycation for PEM is its sensitivity to pH changes because chitosan with a pK_a of about 6.5 deprotonates at physiological pH 7.4, leading to a certain instability of PEM.[25] The integrity of PEM may be stabilized by using chemical cross-linkers with the formation of chemical bonds.[13,25,26]

The combination of bioactive heparin and thermoresponsive PNIPAM−Chi for the formation of PANIPAM-modified PEM was explored here for first time. Since physical properties of PNIPAM coatings depend on its grafting density and molecular weight,[27] it was interesting to see whether the presence of grafting bulky PNIPAM onto Chi as a weak polycation reduces PEM growth behavior and stability. Hence, studies were done to investigate the stability of PEM with and without chemical cross-linking. Furthermore, it was expected that the use of heparin as a terminal layer may increase the biocompatibility of PNIPAM−PEM, which was studied regarding adhesion and growth of multipotent murine embryo fibroblast C3H10T1/2. Understanding the properties of these biogenic PNIPAM-modified PEMs can pave the way for applications as stimuli-responsive coatings controlling adsorption and release of ECM proteins and growth factors to regulate growth and differentiation of stem and other cells on cell culture supports but also implants and tissue engineering scaffolds.

2. EXPERIMENTAL SECTION

2.1. Materials. Chitosan (Chi) with ≥92.6% deacetylation (40−150 kDa) was obtained from HMC Heppe Medical Chitosan GmbH (Halle, Germany). Heparin sodium salt (H, sulfation degree = 1.06, 8−25 kDa) and 1-ethyl-3-(3-dimethylaminopropyl) carbodiimide (EDC) were obtained from Thermo Fisher (Kandel) GmbH (Karlsruhe, Germany). Carboxylic acid-terminated PNIPAM (PNIPAM−COOH, 2 and 10 kDa represented as LMW and HMW, respectively), *N*-hydroxysuccinimide (NHS), and polyethylenimine (PEI) (750 kDa) were purchased from Sigma-Aldrich Chemie GmbH (Steinheim, Germany). Tetrahydrofuran (THF) and *n*-hexane were provided by Th. Geyer GmbH & Co. KG (Renningen, Germany).

2.2. Synthesis and Characterization of Thermoresponsive PNIPAM−Chi. PNIPAM−Chi was prepared with the previous carbodiimide chemistry protocol.[28,29] The amino groups at the C2-position of chitosan were modified with the carboxyl groups of PNIPAM−COOH by their activation to form amide bonds by adding EDC and NHS at room temperature shown in Figure S1. Briefly, Chi and LMW or HMW were separately dissolved in 2% acetic acid solution. EDC and NHS were added to the PNIPAM−COOH solutions to react for 1 h at 25 °C. Subsequently, the PNIPAM solution was mixed with Chi solution, and the mixture was continuously stirred at 25 °C overnight. Different degrees of substitution (DSs) ascribed to PNIPAM grafted to Chi were achieved by changing the weight ratio of Chi/PNIPAM = 1:1 and 1:3 and the molar ratio of Chi (based on the repeating unit)/EDC/NHS = 1:1:0.5 and 1:3:1.5, respectively. The amount of Chi used in all the reactions was fixed to 0.2 g. After the reaction, the product was precipitated in a THF/*n*-hexane (4:1) solution and purified with a dialysis membrane (MWCO: 12,000−14,000) against micropure water. Finally, the pure PNIPAM−Chi was obtained after lyophilization with a freeze dryer (ALPHA 1−2 LDplus, Christ, Osterode am Harz, Germany). The structure and composition of PNIPAM−Chi were characterized by Fourier transform infrared spectroscopy and ^{1}H NMR (Supporting Information).

The dynamic light scattering (DLS) measurements were performed on a Zetasizer Nano ZS ZEN3600 (Zetasizer Nano ZS, Malvern Instruments Ltd., UK) using 5 mW laser with the incident beam of 633 nm (He−Ne laser). In order to mimic the concentration of NaCl under physiological conditions, the conformational change regarding the hydrodynamic diameter and polydispersity index (PDI) (calculated using Zetasizer software 7.12) of PNIPAM−Chi derivatives at a concentration of 1 mg mL^{-1} in 0.15 M NaCl buffer at pH 4 were determined in the temperature range of 20−38 °C. Each measurement with 15 runs was done three times, and the average was calculated for plotting the results.

Zeta potential measurements were performed as described previously.[30] To avoid the corrosion of electrodes and inaccurate measurements due to heating, H, Chi, and PNIPAM−Chi derivatives were prepared at a lower concentration of 0.5 mg mL^{-1} in 0.02 M NaCl solution at pH 4 for zeta potential measurements which were performed with the laser Doppler electrophoresis technique using a Zetasizer Nano ZS ZEN3600 (Zetasizer Nano ZS, Malvern Instruments Ltd., UK) with folded capillary measuring cells.

2.3. Cleaning of Substrates. Glass cover slips (Ø 12 mm, Menzel, Braunschweig, Germany) and silicon wafers (Silicon materials, Kaufering, Germany) were cleaned with 25% NH$_4$OH and 35% H$_2$O$_2$ and rinsed with Milli-Q water (1:1:5, v/v/v) at 80 °C for 15 min. Afterward, the samples were washed with Milli-Q water for 6 × 5 min and dried with nitrogen stream. The gold-coated glass sensors (10 × 10 mm^2) for surface plasmon resonance (SPR, IBIS Technologies B.V., Enschede, The Netherlands) and quartz chips (Au/Ti, 10 MHz) for quartz crystal microbalance with dissipation monitoring (QCM-D, qCell T, 3t Analytik, Tuttlingen, Germany)
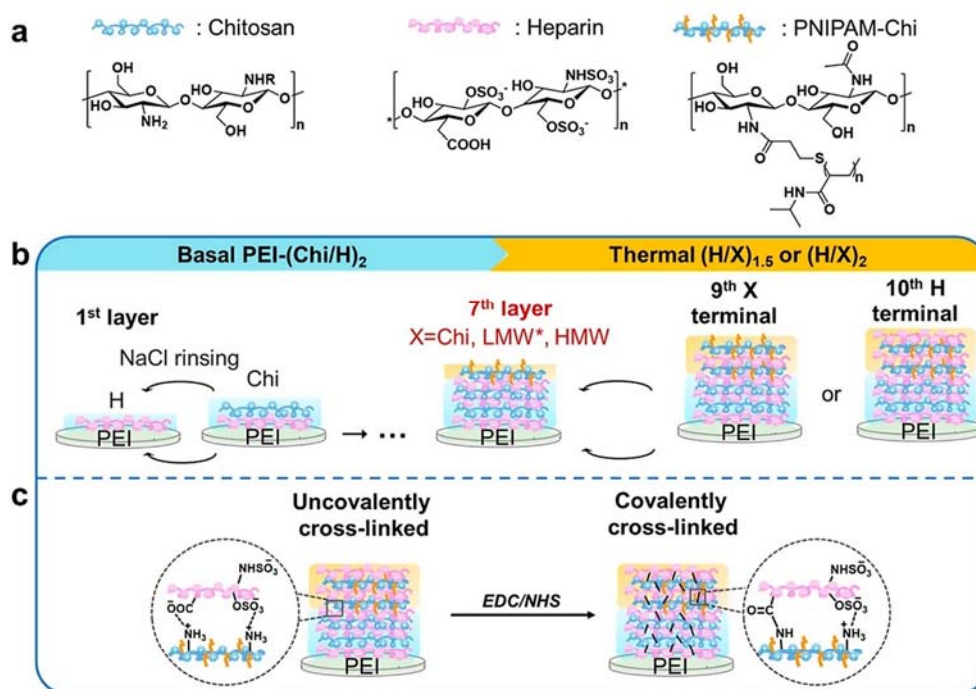
Figure 1. Schematic illustration of the preparation of PNIPAM−PEM. (a) Chemical structures of heparin (H) as a polyanion, chitosan (Chi), and PNIPAM−Chi as polycations. (b) Positively charged polyethylene coating on the substrate as the anchoring layer for subsequent H and Chi adsorption using the LbL technique. Chi was replaced by PNIPAM−Chi from the seventh layer. (c) Amide bond formation between Chi and H by cross-linking PEM using EDC/NHS after multilayer formation.

were cleaned with 99% ethanol, followed by rinsing with Milli-Q water and drying under nitrogen stream.

2.4. PNIPAM−PEM Formation by the LbL Technique. The used polyelectrolytes and assembly of PEM are illustrated in Figure 1a,b on gold-coated sensors, cleaned silicon, and glass cover slips used as substrates for SPR, QCM measurements, ellipsometry, and cell culture studies. PEI was prepared as the first anchoring layer for generation of positive charges on the surface, followed by two double layers of heparin (H) as polyanion and Chi as a polycation. After assembling the basal multilayer without the thermoresponsive element, Chi was replaced by PNIPAM-Chi from the 7th layer for additional 2 cycles of deposition to achieve 9 or 10 layers, where the final layer of PNIPAM−PEM was either PNIPAM−Chi- or H-terminated, respectively. Each layer was prepared by incubation of substrata in the polyelectrolyte solution for 15 min, followed by three times rinsing with 0.15 M NaCl buffer for 4 min. The concentrations of all polyelectrolytes at 1 mg mL^{-1} were prepared in 0.15 M NaCl buffer. Considering that Chi is fully protonated at pH 4, the pH of all solutions was adjusted to 4 for effective ion pairing with heparin. Chi solution containing 0.05 mol L^{-1} acetic acid was solubilized at 50 °C for 3 h and stirred overnight. Chi−PEM composed of Chi and H was used for comparison. Different PEMs were defined as B-$[X/H]_{1.5}$ with X-terminated and B-$[X/H]_2$ with H-terminated layers, where the term "B" refers to basal layers composed of 1−6 layers and "X" represents LMW*, HMW, or Chi.

2.5. Cross-Linking of PNIPAM−Chi PEM Using EDC/NHS. The cross-linking process shown in Figure 1c was carried out using EDC and NHS according to a protocol established earlier in our group.[25,31] The concentration of EDC is 50 mg mL^{-1} and NHS is 11 mg mL^{-1} in 0.15 M NaCl buffer. Concerning the multilayer stability and cross-linking efficiency during the reaction, the pH value was adjusted to 5. The cross-linking solution was added to the PNIPAM−PEMs and Chi−PEMs and incubated at 4 °C for 18 h. After the amide bonds were formed between layers increasing their stability,[26]

the solution was aspirated and the samples were rinsed three times with 0.15 M NaCl buffer at pH 8 for 1 h to remove unreacted NHS ester.

2.6. Characterization of Physical Properties of Multilayers. *2.6.1. Measurement of Layer Adsorption and Multilayer Growth.* The layer growth and multilayer formation were investigated by IBIS-iSPR (SPR) (IBIS Technologies B.V., Enschede, The Netherlands) and QCM-D (qCell T, 3t Analytik, Tuttlingen, Germany).

SPR allows for the determination of optical (dry) mass. The incidence of the polarized light is reflected through a hemispheric prism with a refractive index of $n = 1.518$ on a gold coating sensor (IBIS Technologies B.V., Enschede, The Netherlands). When molecules are adsorbed on the gold sensor, the shift of resonance angle (m°) from refracted light can be monitored in real time by IBIS SPR software 2.1.21. Before measurements, the cleaned gold sensor was fixed on the prism and mounted in the flow chambers to be placed in the SPR device. At the beginning of the measurement of PEM formation, PEI was initially injected into the flow cell, followed by alternating injection of Chi, H, and PNIPAM-Chi for 15 min. Interval rinsing steps (3 × 4 min) with 0.15 M NaCl solution at pH 4 were employed after each deposition of the polyelectrolyte to remove unbound molecules. After 10 layers were achieved, the PEMs were rinsed successively with phosphate-buffered saline (PBS) under pH 7.4 for 15 min and Dulbecco's modified Eagle's medium (DMEM, HiMedia Laboratories Pvt. Ltd., Germany) for another 15 min to study the stability of PEM. The adsorption of each polyelectrolyte was calculated through the average of 10 angle shift values (m°) and used for plotting the graphs.

On the other hand, QCM-D provides complementary information about adsorbed mass of macromolecules including their hydration state as total absorbed mass (acoustic mass). The frequency F related to the mass of the crystal generated by the oscillation is monitored as a function of time. Any material adsorbed and desorbed induces a frequency shift ΔF related to the change in sensed mass Δm. For a

thin, rigid, and evenly distributed film, the relationship between ΔF and Δm is proportional and can be calculated by the Sauerbrey equation

$$\Delta F_n = \frac{-C \bullet \Delta m}{n} \tag{1}$$

where n is the overtone number and C is 0.23 Hz·cm²/ng.

For non-rigid films, the damping of oscillation occurs and is measured as an increase in the energy dissipation D that provides information about the viscoelastic and mechanical properties of the adsorbed layers. Since polysaccharide-based multilayers may have a soft nature due to their higher water content and swelling, further calculations were based on the Kevin−Voigt viscoelastic model related to the change in ΔF and ΔD of the quartz sensor.[32] The bulk liquid viscosity and density were assumed to be equal to those of water and set to 0.89 Pa s and 0.997 g cm⁻³, respectively. The value of film density was set to 1050 kg m⁻³ taken from other QCM multilayer studies using Chi and H with 10 layers.[32] The thicknesses of PEM adsorption on the sensor were automatically calculated by the qGraph Viewer 1.8 software.

All the measurements of PEL adsorption were performed at 25 °C. The cleaned quartz gold sensor was mounted in the device. The same adsorption procedure like in SPR measurements was applied. Each PEL at a concentration of 1 mg mL⁻¹ was alternatingly pumped into the device at a constant flow rate of 60 μL min⁻¹ for 15 min to reach the equilibrium state with interval rinsing steps with NaCl solution at pH 4 for another 12 min.

2.6.2. Determination of Cross-Linking Degrees. Degrees of cross-linking of PEM by EDC and NHS prepared on the glass slides placed in multiwell plates were determined by the treatment with trypan blue that can bind to free amino groups on Chi.[14] The uncross-linked and cross-linked PEMs were immersed in 0.4% trypan blue diluted 50× in 0.15 M, pH 4 NaCl buffer at 37 °C overnight. Afterward, the supernatant of trypan blue solution was discarded, and PEMs were subsequently rinsed with NaCl buffer twice to remove excess trypan blue solution. The absorbances were detected at 595 nm by a microplate reader (BMGLABTECH, Fluostar OPTIMA, Offenburg, Germany) using the matrix scanning mode, which performed line-by-line scanning 10 × 10 times. The average intensity was calculated by Fluostar OPTIMA software from a total of 80 values obtained in each well of a 24-well plate. The cross-linking degree was calculated

$$\text{cross-linking (\%)}$$
$$= \frac{\text{absorbance of ((uncross-linked)} - \text{(cross-linked))}}{\text{absorbane of (uncross-linked)}} \tag{2}$$

2.6.3. Multilayer Thickness and Surface Potential Measurements. The dry thickness of PNIPAM−PEMs was measured by spectroscopic ellipsometry (M−2000 V, J.A. Woollam Company, Lincoln, NE, USA) within a wavelength range of λ = 375−1000 nm under ambient conditions as previously described.[33] The spot size of the linear polarized light on the samples was around 1−2 mm² at the incident angles of 55, 60, and 65°. Cleaned Si wafers were used as a PEM reference with SiO₂ layers. Likewise, the layer thickness was also measured after layer formation, rinsing with PBS and DMEM to assure the stability of uncross-linked and cross-linked systems. The data acquisition was analyzed using a Cauchy model with the WVase32 software. The hydration degrees of all PEMs were calculated in eq 3 from the dry and wet thicknesses obtained by ellipsometry and the Voigt model, respectively

$$\text{Hydration \%} = \frac{\text{thickness (Voigt} - \text{Ellipsometry)}}{\text{thickness (Voigt)}} \tag{3}$$

The zeta potential of the multilayers was determined by streaming potential measurements using a SurPASS Electrokinetic Analyzer (Anton Paar, Austria). Uncross-linked and cross-linked PEMs were prepared on special sized glass cover slides (10 × 20 mm²). Two glass samples were mounted oppositely in the flow chamber. A flow rate of 100−150 mL min⁻¹ was adjusted with a maximum pressure of 300

mbar, and 1 mM potassium chloride was used as the electrolyte solution. 0.1 N hydrochloric acid and 0.1 N potassium chloride were used for pH titration, and the measurements were from acidic to basic pH. The zeta potential was calculated through the software of the device.

2.6.4. Surface Wettability and Temperature Effect of PNIPAM− PEMs. The static water contact angle (WCA) measurement for surface wettability of terminal layers was carried out on an OCA15 + device (DataPhysics, Filderstadt, Germany) equipped with a heating chamber allowing temperature change. The sessile drop method was applied and recorded by the built-in software under 20 and 37 °C. A water droplet of 1 μL was dispensed on the samples at a flow rate of 0.5 μL s⁻¹. The measurements were first performed at 20 °C, and thereafter, the temperature was elevated to 37 °C and WCAs were measured again. The WCA was calculated through the ellipse-fitting method. At least 10 measurements were done for each sample to obtain the average value and standard deviations (SDs).

2.7. Biological Investigation. *2.7.1. Cell Culture.* The multipotent murine embryonic fibroblast C3H10T1/2 cell line was used for the cell studies. The cryopreserved C3H10T1/2 cells were thawed and cultured in DMEM supplemented with 10% v/v heat-inactivated fetal bovine serum (FBS, Biochrom AG, Berlin, Germany) and 1% pen/strep at 37 °C in a humidified 5% CO₂/95% air atmosphere using a NuAire DH Autoflow incubator (NuAire Corp., Plymouth, Minnesota, USA). When cells reached 70% confluence, they were harvested from the flask using 0.25% trypsin/0.02% ethylenediaminetetraacetic acid (Biochrom AG, Berlin, Germany) solution for 5 min at 37 °C, followed by centrifugation at 500g for 5 min. The supernatant was aspirated, and the cell pellet was resuspended in DMEM with 10% FBS. The cell number was manually counted using a Neubauer chamber.

2.7.2. Study on Cell Viability, Adhesion, and Growth. Cell studies were conducted seeding cells on the uncross-linked and cross-linked PEMs with the Chi/PNIPAM−Chi terminal or H terminal layer prepared on 24-well tissue culture polystyrene plates (TCPS). After deposition of PEMs on TCPS, the plate was sterilized by ultraviolet (UV) light at 254 nm for 30 min, followed by washing with sterile PBS. Afterward, all the substrates were pre-treated with DMEM containing 1% pen/strep at 37 °C for 1 h to deactivate any unreacted EDC/NHS ester. Then, C3H10T1/2 cells suspended in DMEM with 10% FBS and 1% pen/strep were seeded at a concentration of 20,000 cells mL⁻¹ on the PEMs and incubated at 37 °C/5% CO₂/95% air atmosphere.

Cell viability was determined after 24 and 72 h cultivation by a fluorescent live/dead assay using Calcein AM to stain living cells (green fluorescence) and EthD-III to stain dead cells (red fluorescence) (Viability/Cytotoxicity Assay Kit, Biotium, Hayward, USA). Adherent cells on PEMs in the 24-well plate were washed once with Dulbecco's PBS (DPBS, Lonza Group Ltd, Belgium) added with 1 g L⁻¹ glucose. Each well was added with the staining solution containing 2 μM calcein AM and 4 μM EthD-III and incubated in the dark at 37 °C in a 5% CO₂/95% air atmosphere. After 30 min incubation, the stained cells were rinsed once with DPBS and studied with a confocal laser scanning microscope by a set of Ar 488 nm laser and He−Ne 543 nm laser [confocal laser scanning microscopy (CLSM) 701, Carl Zeiss Micro-Imaging GmbH, Jena, Germany]. The cell images were taken with 10×, 20× objectives and processed through ZEN2012 software (Carl Zeiss). The quantification of cell count and the calculation of cell area and cell coverage were performed by Image J.

2.8. Statistical Analysis. All data processing for the calculation of mean value ± SD and statistical analysis were carried out by Origin 8 software. The statistics were calculated through one-way ANOVA, followed by post hoc Tukey's test. The asterisk in the respective figures indicates a significant difference as p value ≤0.05. On the other hand, the box-whisker plots illustrate 25th and 75th percentiles, the median (dash) and mean value (empty circle), respectively.

Table 1. Properties of PNIPAM−Chi Derivatives with Different DSs Obtained by Adjusting the Weight Ratio of Chi/PNIPAM[a]

sample	MW_{PNIPAM} (kDa)[b]	chitosan/PNIPAM[c]	yield (wt %) (%)	DS_{PNIPAM}	CP (°C)[d]	zeta potential (mV)[e]
LMW-0.04	2	1:1	50.00	0.04	33	
LMW-0.14	2	1:3	43.38	0.14	33	23.2 ± 0.87
HMW-0.007	10	1:1	45.75	0.007		
HMW-0.03	10	1:3	42.00	0.03	31	30.7 ± 0.53
chitosan						33.8 ± 0.56
heparin						−18.67 ± 1.18

[a]PNIPAM−Chi from PNIPAM of 2 and 10 kDa with different DSs (Y) were referred to as LMW-Y and HMW-Y, respectively. [b]Molecular weight. [c]Weight ratio of chitosan and PNIPAM. [d]Prepared at 1 mg mL^{-1}, pH 4 in 0.15 M NaCl. [e]Prepared at 0.5 mg mL^{-1}, pH 4 in 0.02 M NaCl.

3. RESULTS AND DISCUSSION

3.1. PNIPAM−Chi and The Thermoresponsive Properties.

The different molecular weights of PNIPAM−COOH grafted onto the chitosan backbone via EDC/NHS-catalyzed reaction have a direct impact on the DS and charge density of derivatives for further PEM formation. In this study, PNIPAM−Chi with various DSs were obtained by adjusting the weight ratio of Chi/PNIPAM as listed in Table 1. The structures and DS of PNIPAM−Chi were determined and are shown in the Supporting Information (Figures S1 and S2, respectively). PNIPAM−Chi from LMW or HMW of PNIPAM with calculated DS (Y) is denominated as LMW-Y or HMW-Y, respectively. While a higher DS of LMW-0.04 and 0.14 was easily achieved, the maximum DS of HMW was only 0.03 when using the same ratio of Chi/PNIPAM. The yields represent the efficiency of the grafting process using varying parameters. Lower amounts or LMW of PNIPAM yielded 50% derivatives with a low DS in contrast to around 5−10% reduction of the yields with a high DS from higher amounts or HMW. It can be concluded that steric hindrance between PNIPAM and chitosan is more pronounced when using a higher molecular weight of PNIPAM and therefore obstructs the efficiency on yield and DS during the reaction.

The coil-to-globular transition of PNIPAM−Chi dissolved at a concentration of 1 mg mL^{-1}, pH 4 in NaCl solution regarding hydrodynamic diameter (D_h) and PDI was examined by DLS in the temperature range from 20 to 38 °C. Recent reports clarified that the cloud point (CP) is the phase-transition temperature at a certain concentration, while LCST refers to the minimum temperature value of the phase diagram with a function of the polymer/solvent volume (or weight) fraction in the full composition range.[34] Here, the CPs of PNIPAM−Chi at a specific concentration can be determined at the reflection point of the transition range in the particle size measurement as shown in Figure 2a.[35] Lower CPs were found in HMW-0.03 at 31 °C in comparison to higher in LMW-0.04, 0.14 at around 33 °C. Although CP can be affected by environmental conditions like the existence of salt and pH, the measurements were done under the same concentration of NaCl and pH for comparison between different derivatives.[36] Previous studies using the same conjugation methods also showed no significant difference in CP independent of the amount of PNIPAM grafting on chitosan.[28] Instead, the CP of PNIPAM associated with the hydrophilic component is inversely dependent on the molecular weight.[37] Due to more hydrophilic effect from the Chi end group, the CP increases with a decreased molecular weight. Below CP, HMW has an approximate hydrodynamic diameter around 40 nm, which is twice larger than that of LMW regardless of DS. Larger particle sizes of all PNIPAM-Chi were observed above CP; notably,
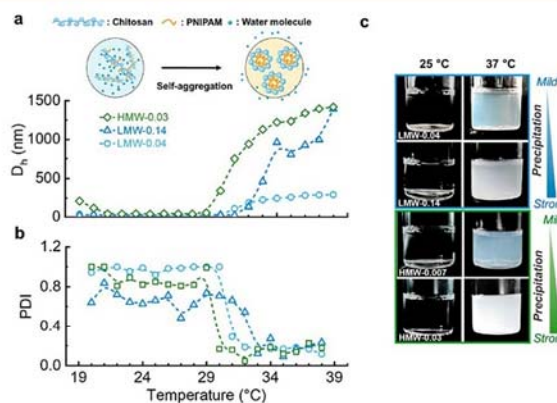

Figure 2. Conformational change of PNIPAM−Chi at the concentration of 1 mg ml^{-1}, pH 4 in 0.15 M NaCl. (a) Hydrodynamic diameter (D_h) and (b) PDI of the derivatives were monitored by DLS in the range of 20−38 °C. (c) Solution state and conformation at 25 and 37 °C. PNIPAM−Chi from PNIPAM of 2 and 10 kDa with different DSs (Y) were referred to as LMW-Y and HMW-Y, respectively.

LMW-0.14 and HMW-0.03 showed a remarkably sharper rise in size to 1000 nm in contrast to only approximately 300 nm increase in LMW-0.04. At a lower temperature, PNIPAM-Chi extended the structures because the hydrophilic moieties of PNIPAM molecules are surrounded by water molecules in addition to the charge repulsion from highly protonated Chi under acidic conditions. When the temperature is elevated above CP, PNIPAM chains collapse and aggregate due to hydrophobic interactions. As a result, core−shell structured micelles with a larger size are formed with the PNIPAM core and protonated Chi shell.[36] Since HMW-0.03 has a longer chain of PNIPAM, the size is much larger than the shorter chain, even though the maximum DS of HMW is apparently lower than those of LMW. In addition, according to the investigation from Bao et al.,[36] the existence of Cl$^-$ and the increasing ionic strength favor dehydration of PNIPAM that is evident by the larger size of aggregates (from 20 to 40 nm below CP to 1000−1500 nm above CP) than other studies in the absence of salt.[23] PDI in DLS means the intensity distribution of the light scattered from the various size segments. In other words, a polymer with a low PDI has a narrow size distribution.[38] The PDI values presented in Figure 2b are larger than 0.2 at a lower temperature below CP and decreased to less than 0.2 at higher temperatures, indicating that the structure changed from random coils to more organized core−shell micelles of PNIPAM−Chi.[36] Figure 2c depicts that these samples were well dissolved in the solution

at room temperature, while precipitation occurred as the temperature was elevated to 37 °C. In particular, the phase separation was more obvious in the solution containing LMW-0.14 or HMW-0.03. Taking size and DS together, the temperature effect on conformational changes is heavily reliant on the grafting density and molecular weight of PNIPAM.

Since the charge density of PELs not only affects the deposition of charged entities during multilayer formation but also determines the subsequent structure and physiochemical properties of PEMs, zeta potentials of LMW-0.14 and HMW-0.03 were measured by the laser Doppler electrophoresis technique (Table 1). The average zeta potential of Chi was 33.8 ± 0.56 mV. After PNIPAM grafting on Chi, LMW-0.14 and HMW-0.03 have lower values of 23.2 ± 0.87 and 30.7 ± 0.53 mV, respectively. The reduction of potential is attributed to the occupation of amino groups by PNIPAM on Chi, and therefore, the zeta potential is particularly lower with a higher DS of LMW-0.14. Although there are secondary amines on PNIPAM that can also contribute to positive charges, it is not enough to compensate the reduction of primary amines in both LMW-0.14 and HMW-0.03 due to the lower value of pK_a.[39] On the other hand, the zeta potential of the strong polyanion H was -18.67 ± 1.18 mV. Although reduced zeta potentials were obtained in PNIPAM−Chi, it has enough positive charges and can potentially serve as a polycation to form PEM with H.

3.2. Growth Behavior and Viscoelastic Properties of Multilayers. Considering their significant conformational changes with temperature, two PNIPAM−Chi of LMW-0.14 (referred to as LMW*) and HMW-0.03 (referred to as HMW) were selected as polycations to form PEM with the polyanion H. The growth behavior of PNIPAM−PEMs from B-[LMW*/H]$_2$ and B-[HMW/H]$_2$ and Chi−PEMs from B-[Chi/H]$_2$ as a reference was studied by the optical SPR technique. SPR provides the information about the adsorbed mass of each polyelectrolyte on the sensor excluding water mass, corresponding to the increase in angle shift.[40] Figure 3a shows an initially linear growth from the first to fourth layers and then exponential growth during the following depositions for all PEMs. This kind of growth is related to the results of other studies when polysaccharides were used for multilayer formation.[41,42] Even though the presence of uncharged and bulky PNIPAM, both LMW* and HMW as polycations have the ability to form PEMs with the polyanion H. Figure S3 in the Supporting Information demonstrates the differences between PNIPAM−PEMs and Chi−PEMs when the value of angle shift was normalized and set as 0 at layer 6. In comparison to Chi−PEMs, the replacement of Chi by PNIPAM−Chi from the seventh layer on caused a significant increase in angle shift of more than 50° until multilayer formation was completed. This indicates that grafting PNIPAM on Chi increased the layer mass in PNIPAM−PEMs owing to the larger molecular weight of PNIPAM−Chi.[43,44] pH 4 was kept to maintain positive charges of the protonated Chi and PNIPAM−Chi because pK_a of primary amino groups of Chi is ~6.5. If the system is exposed to physiological conditions for cell culture, amino groups might be deprotonated above their pK_a.[25] It was observed that the values of angle shift in all PEMs returned to the level of the eighth layer after PBS rinsing and to the level of the seventh layer after rinsing with the cell culture medium (DMEM). Notably, a threefold decrease in B-[LMW*/H]$_2$ to that of B-[Chi/H]$_2$ occurred with only PBS rinsing under pH 7.4 after
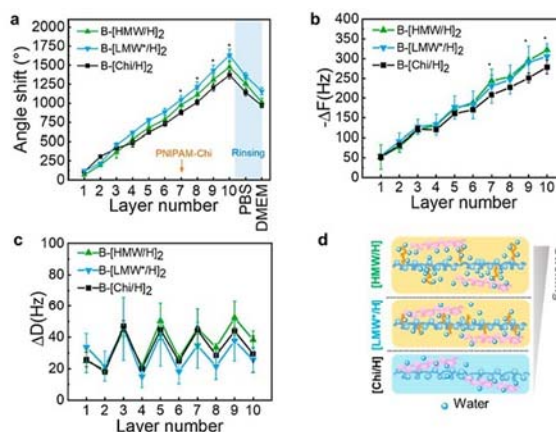

Figure 3. Layer growth of PNIPAM−PEMs of B-[LMW*/H]$_2$ and B-[HMW/H]$_2$ from H and PNIPAM-Chi (LMW* and HMW) monitored by (a) SPR ($n = 10$, means $\pm$ SD, $*p < 0.05$) and quartz crystal microbalance with (b) frequency change ΔF and (c) dissipation change ΔD numbered from layer 1 to 10. Chi−PEM of B-[Chi/H]$_2$ composed of H and Chi as a reference. The first layer is PEI. Odd layer numbers represent polycations Chi for third and fifth layers and Chi, LMW*, or HMW for seventh and ninth layers; even layer numbers correspond to polyanion H; $n = 20$, means $\pm$ SD. (d) Scheme illustrating swelling ability of layers between polyanions and polycations.

the complete layer formation. The loss of layer mass is attributed to the higher DS of LMW* with less primary amino groups of Chi. As a result, weaker interactions between layers may cause decomposition more easily in B-[LMW*/H]$_2$ than in B-[HMW/H]$_2$ and reference B-[Chi/H]$_2$.

Apart from the PEM assemblies in SPR, the results of QCM-D measurements provide additional details not only about the mass of the adsorbed layer including the solvent but also the viscoelastic properties of the entire multilayer. As shown in Figure 3b, the increase of $-\Delta F$ means the increment of mass adsorbed on the sensor surface regarding the Sauerbrey equation in eq 1. In all PEMs, $-\Delta F$ increased more upon deposition of Chi and PNIPAM−Chi, while the increment declined in addition of H. $-\Delta F$ normalized in the Supporting Information (Figure S3b) illustrates a steeper and 1.5 times more increase upon deposition of HMW and LMW* than that of Chi, which was similar to angle shifts during SPR measurements. The QCM mass (Δm_{QCM}) in the Supporting Information (Figure S4a) was calculated from the Voigt model using the Voigt thickness and the layer density (1050 kg m^{-3}) taken from a previous study.[32] The accumulated mass fitting shows a proportional relationship indicating the linear growth of all PEMs (Supporting Information, Figure S4b). Since multilayers composed of hydrophilic biopolymers typically have viscoelastic properties, an increasing dissipation ΔD can be seen in Figure 3c and Figure S3c of the Supporting Information.[45] ΔD increased after addition of Chi, followed by a marked decrease after addition of H. This phenomenon was also observed after inclusion of LMW* or HMW from the seventh layer. The growth behaviors in QCM-D pointed out the discrepancy to the results in SPR that showed a consistent layer increase. As mentioned earlier, solvent content also accounts for layer growth measured by QCM-D. The decrease in frequency and dissipation after addition of H was mainly

---

attributed to the interpenetration of H that electrostatically cross-links with Chi or PNIPAM−Chi and formed the complexes of the polyanion and polycation.[46] The hydrogen bonds between water molecules and PELs were disrupted to release the prior coupled water from these complexes, making the PEM structures de-swelling, more compact, and stiffer.[46,47] Therefore, the diffusion of H causes the dehydration and resulted in approximately linear growth for 10 layers measured by QCM that is different from SPR results.[41] When Chi again adsorbed and took up the solvent, multilayers are swelling and become soft again.[40,48] Nevertheless, the noticeable differences from both the frequency and dissipation shift in these three PEMs were detected after using LMW* or HMW. The de-swelling/swelling effect was more pronounced during the subsequent adsorption of [LMW*/H] and [HMW/H] illustrated in Figure 3d. Since the temperature was fixed at 25 °C throughout the process, the extended conformation of PNIPAM chains not only facilitates PEM formation but also couples more water, leading to a more hydrated and softer layer as −ΔF and ΔD increase. PNIPAM−Chi in aqueous solution has loss moduli larger than storage moduli at 25 °C.[58] Jaber and Schlenoff have explained that the strong polymer−solvent interaction of the monomeric NIPAM segment induces more hydrated multilayers.[20] In addition, the slight decrease in −ΔF upon addition of H could be linked to the grafting density of PNIPAM. LMW* with a higher DS and less charge density of Chi may reduce H adsorption compared to HMW with a lower DS.

3.3. Effect of PNIPAM−Chi on Cross-Linking Degree.

It was assumed that covalent cross-linking between carboxyl groups of H and amino groups of Chi by EDC−NHS will improve their stability. The cross-linking degree was determined by trypan blue assay comparing uncross-linked and cross-linked PEMs. The absorbance from all PEMs prepared in multiwell plates is shown in Figure 4a. An increase of intensity indicates more free amines. Before cross-linking, B-[Chi/H]₂ had the strongest intensity. The intensity became slightly weaker in B-[LMW*/H]₂ and B-[HMW/H]₂ because of less free primary amino groups. The intensities decreased when amino groups were covalently connected to carboxyl groups after cross-linking; particularly, the weakest was found with B-[Chi/H]₂. The cross-linking degrees calculated by eq 2 show the dependence on the presence of PNIPAM. Almost 60% cross-linking occurred in B-[Chi/H]₂, whereas less cross-linking was found in B-[LMW*/H]₂ and B-[HMW/H]₂ with a degree of 54 and 39%, respectively. The reduced cross-linking degree was due to the lower quantity of amino groups on Chi replaced by PNIPAM. Theoretically, the cross-linking degree should decrease proportionally with a higher grafting density of PNIPAM. Nevertheless, a lower DS of HMW had an even lesser cross-linking degree in B-[HMW/H]₂ than the higher DS of LMW in B-[LMW*/H]₂. Since the entire cross-linking process was done at 4 °C, PNIPAM exhibited an extended structure. As stated earlier in the diameter detected by DLS, HMW was twice larger than LMW* at low temperature. Therefore, steric hindrance in B-[HMW/H]₂ was assumed by using larger molecules of HMW that inhibited the cross-linking between amines and carboxyl groups.[49,50]

3.4. Stability of Multilayers.

As far as the stability under the physiological conditions at pH 7.4 was concerned, the thickness of PEMs in Figure 4b,c was evaluated. In uncross-linked PEMs, the thickness was found overall between 9.6 and 12.0 nm after layer formation, while the thickness was around
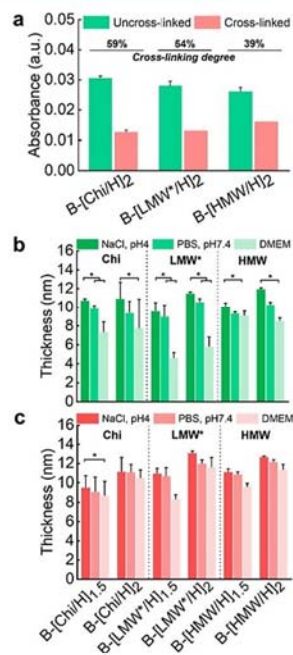

Figure 4. (a) Absorbance of uncross-linked (green bar) and cross-linked (red bar) B-[X/H]₂ PEM performed by trypan blue assay. The cross-linking degrees were calculated by eq 2, means ± SD. Dry thickness of (b) uncross-linked and (c) cross-linked PEMs measured by ellipsometry after layer formation, rinsing with PBS and with DMEM. B-[X/H]₁,₅ represented PEM with terminal layer X = Chi, LMW*, or HMW, while B-[X/H]₂ referred to PEM with terminal layer H. Data represented means ± SD with a significance level of *$p \leq 0.05$, $n = 4$.

9.6–13.1 nm in cross-linked PEMs. Cross-linking of PEM has been implemented by Picart et al. to improve the mechanical stability of multilayers.[12] Indeed, the chemical cross-linking forms covalent amide bonds from amines of Chi and carboxyl groups of H, resulting in denser layers in cross-linked B-[Chi/H] PEMs with a decreased thickness that is well in line with observations on other multilayer systems made of biopolymers such as hyaluronic acid/poly-L-lysine and alginate/Chi PEMs.[25,43] On the contrary, the thickness of cross-linked B-[LMW*/H] and B-[HMW/H] PEMs after cross-linking was slightly higher, which corresponds to the reduced cross-linking degree and also implies an inhibition of shrinkage when PNIPAM is involved.[31] After sequential application of PBS and DMEM to the PEMs, uncross-linked PEMs showed a substantial decrease in thickness that was in accordance with SPR results. To be more specific, the greatest effect was seen with B-[LMW*/H] PEMs of about 5 nm loss. This is in agreement with SPR results due to a higher grafting density of LMW*, leading to easier removal of adsorbed polyelectrolytes. On the other hand, compared to uncross-linked PEMs, negligible changes were observed in all cross-linked PEMs with less than 2 nm decrease, even though B-[HMW/H] PEMs have a lower cross-linking degree. It suggests that the stability was improved through intrinsic cross-linking by the formation of amide bonds.

Table 2 provides a comparison between the dry and hydrodynamic thicknesses of either uncross-linked CHI/LMW*/HMW or H-terminated PEMs measured by ellipsom-

Table 2. Comparison of Dry Thickness (from Ellipsometry) and Hydrodynamic Thickness (from the Sauerbrey or Voigt Model) of Uncross-Linked PEMs and Hydration Degrees Calculated from eq 3

thickness (nm)	Chi/LMW*/HMW-terminated				H-terminated			
	Sauerbrey	Voigt	ellipsometry	hydration (%)	Sauerbrey	Voigt	ellipsometry	hydration (%)
B-[Chi/H]	10.9 ± 0.1	12.6 ± 1.4	10.8 ± 0.1	15.0	12.0 ± 0.2	13.3 ± 1.8	11.0 ± 1.7	18.2
B-[LMW*/H]	12.0 ± 1.7	14.4 ± 2.4	9.6 ± 0.9	35.0	12.7 ± 1.3	14.0 ± 1.2	11.5 ± 0.1	18.8
B-[HMW/H]	12.2 ± 0.3	15.1 ± 1.0	10.1 ± 0.4	34.8	13.3 ± 0.2	15.7 ± 0.7	12.0 ± 0.1	24.7
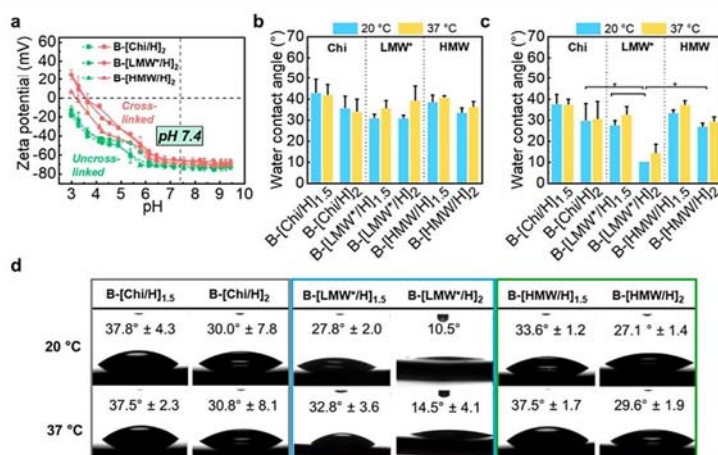
Figure 5. (a) Zeta potential of uncross-linked (green dash) and cross-linked (red line) PEMs in the pH range of 3 to 9.5; data represent means ± SD. Static WCA measurements of (b) uncross-linked and (c) cross-linked PEMs with Chi/LMW*/HMW or the H terminal layer at 20 °C (blue bar) and 37 °C (yellow bar); values indicate mean ± SD with a significance level of *$p \leq 0.05$, $n = 10$. (d) Water drops on cross-linked PEMs at 20 and 37 °C.

etry and QCM-D, respectively. Taking viscoelastic properties of our PEMs into account, the thickness might be underestimated using the Sauerbrey model that makes a better estimation for rigid layers. Thus, the Voigt model was also applied to calculate the viscoelastic thickness for all PEMs.[32] It should be noted that diffusion of H can cause more dense and less hydrated films. Hence, the thickness calculated by the Sauerbrey model is only 2 nm lesser than that calculated by the Voigt model. The results from both measurements are comparable since PEMs were hydrated when studied with QCM-D and have a relatively low thickness. In addition, the hydration degree calculated in Table 2 based on the difference of dry thickness and wet thickness obtained from ellipsometry and Voigt thickness shows that the hydration degrees are smaller than 30% in all PEMs, indicating that PEMs are very condensed. Several reports have mentioned that polysaccharides or GAGs with hydrophilic functional groups like hydroxyl, amino, and sulfate groups coupling water lead to swelling of PEM.[40,51] Most importantly, our study shows that hydration significantly depends on the grafted PNIPAM as approximately 2 nm more swelling and a higher hydration degree were observed in B-[LMW*/H] and B-[HMW/H] PEMs than in B-[Chi/H] PEMs. Moreover, the PEM swelled about 5 nm in LMW*/HMW-terminated compared to 3 nm in H-terminated layers, again indicating that the multilayers shrank and were less hydrated upon addition of H due to increased ion pairing and replacement of small counterions and water.[40] Conversely, the hydration degrees are similar in both the terminal layers of B-[Chi/H], which can be linked to more ionic cross-linking compared to the PEMs containing PNIPAM.

3.5. Characterization of Surface Properties.
Surface properties, which can be modulated by the composition of PEMs, play critical roles in biological effects. One of the essential characters to be considered is the surface charge that has shown previously to determine cell adhesion and cell fate, particularly in those made of biopolymers.[2,52] Zeta potential referring to surface charge density not only reflects the charge distribution of the outmost polyelectrolyte layer but also reflects that of the intrinsically swollen and permeable layers beneath.[53] Figure 5a shows the zeta potential of the terminal H layers in uncross-linked and cross-linked PEMs with titration from pH 3 to 9.5. The zeta potentials in uncross-linked PEMs were negative throughout the investigated pH range. Chi as a weak polycation with a deacetylation degree about 95% has the corresponding pK_a at 6.1, which should be considered fully charged at pH 4.[54] However, H possesses the highest negative charges among biological polyanions owing to its high contents of sulfate and carboxyl groups with pK_a 0.5−3.13 and 1.4−1.9, respectively.[55,56] This makes H highly charged over the measured pH range. When the environment became nearly neutral above pH 6.5 and basic, the values utterly turned to very negative potential of about −75 mV, confirming complete deprotonation of Chi. Our results are corroborated by our previous study about [Chi/H] PEMs that demonstrates that H is the dominant molecule in the multilayer systems.[40,57] In contrast, the values were elevated upon cross-linking under acidic conditions below pH 4. When the cross-linking forms amide bonds between the functional groups of Chi, LMW*, or HMW and H, negative charges from free carboxylic groups are reduced. Hence, the potential becomes more positive at acidic pH and also points out that the inner layers that are composed
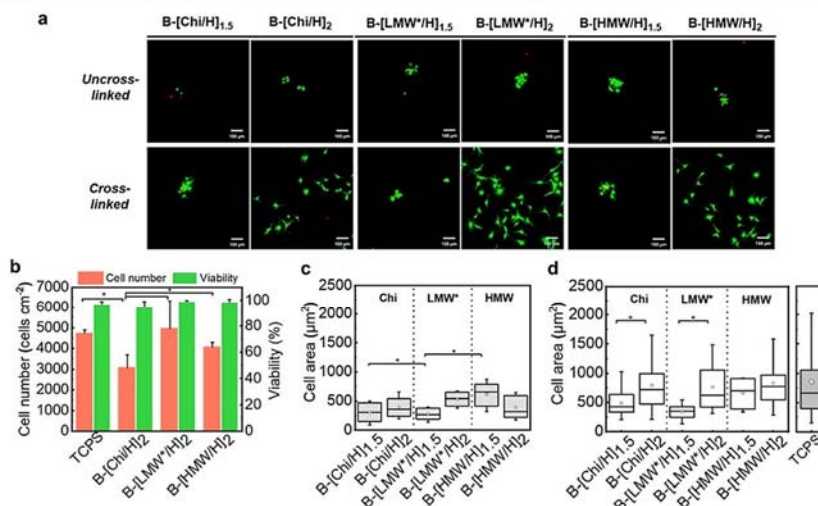
Figure 6. Viability test and quantification of C3H10T1/2 cells after 24 h cultivation on different multilayers in the medium with 10% FBS. (a) CLSM images of live (green) and dead (red) cells on uncross-linked (upper row) and cross-linked (lower row) PEMs. Scale bars: 100 μm. Measurement of (b) cell number and viability on cross-linked PEMs; cell area on (c) uncross-linked and (d) cross-linked PEMs using ImageJ software. Cell seeded on TCPS as a control. Box plot with whiskers show the first and third quartiles, medians and means; mean value ± SD with a significance level of *$p \leq 0.05$.

of Chi contribute to the zeta potential in these PEMs.[40] The point of zero charges (PZCs) of all non-CL PEMs are close to pK_a of H below pH 3, but they are shifted to pH 3.5−4 upon cross-linking. While CL B-[Chi/H]$_2$ and B-[LMW*/H]$_2$ showed similar profiles of zeta potential and PZCs close to pH 4, the value in B-[HMW/H]$_2$ was less positive with a lower PZC at around 3.5. The trends are echoed with the cross-linking degree, highlighting more free carboxylic groups existing in less cross-linked B-[HMW/H]$_2$. Regardless of cross-linking, the overall zeta potentials are all negative under physiological conditions under pH 7.4, which may not favor cell adhesion due to electrostatic repulsion with negatively charged cell surfaces but contingent on the functional groups.[52,58,59]

On the other hand, surface wettability is another dominant factor that governs protein adsorption and cell adhesion, typically dependent on the outermost composition of the interface.[2,52,60] To study the wettability of PEMs at pH 7.4, which is the relevant pH value for cell adhesion studies, all the surfaces had been already exposed to PBS and DMEM, washed with Milli-Q water, and dried prior to the measurement. Static WCAs are depicted in Figure 5b,c of uncross-linked and cross-linked systems, respectively. In both cases, different values of WCA are observed based on the terminal species, even if all surfaces are quite hydrophilic (WCA < 60°). Lower values of WCA are always found in H-terminated PEMs in comparison to higher in Chi-, LMW*-, and HMW-terminated PEMs. The reason is because H leads to high wettability of surfaces, while the existence of primary amines in Chi, LMW*, and HMW makes the surfaces less wettable.[55,61] The different WCA values display the composition of the terminal layer and dominance of H or Chi, LMW*, and HMW. Moreover, when integrating PNIPAM in PEMs, the wettability increased with the following order: B-[LMW*/H] > B-[HMW/H] > B-[Chi/H] without any effect of cross-linking on this sequence. Notwithstanding the similar tendency between uncross-linked and cross-linked PEMs, special attention is paid to the cross-linked B-[LMW*/

H]$_2$ with notably high wettability (WCA < 20°), leading to complete spreading of the water droplet, as shown in Figure 5d. We attribute this superior wettability to the lower molecular weight, the higher grafting density of PNIPAM, and the association with the very hydrophilic compound used as a polyanion (i.e., heparin).[10,11,62] In addition, cross-linked PEMs exhibited reduced values in WCA. This finding is consistent with other reports using carbodiimide chemistry for PEMs presenting an increasing hydrophilicity upon cross-linking.[63] More hydrophilic surfaces after cross-linking have been previously explained by the formation of new cross-linker conjugates and denser structures between the polyelectrolytes as well as an enhanced roughness.[63−65]

With respect to the change in wettability of the PNIPAM interface by switching the temperature across CP, the temperature effect on WCA of PEMs was investigated at 20 °C (below CP) and 37 °C (above CP). The results show 3−8° higher WCA in uncross-linked and cross-linked B-[LMW*/H] and B-[HMW/H] at 37 °C compared to WCA at 20 °C, indicating the presence of PNIPAM in the surface region of PEM with its effect on changing surface wettability in response to temperature. On the contrary, a different WCA in dependence on temperature was barely observed for B-[Chi/H] PEMs as the unchanged shape of water droplets can be evidently seen in Figure 5d and the Supporting Information (Figure S4). Lower wettability at a higher temperature above CP is probably a result of collapsed PNIPAM chains making the surface slightly less hydrophilic and the smoother surface that was found previously.[66] In addition, the change in WCA could be restricted due to PNIPAM surrounded by the very hydrophilic sulfate groups from H, leading to delay of PNIPAM chain dehydration.[36]

3.6. Biocompatibility Studies. The initial interaction between substrates and cells in terms of cell adhesion and spreading plays a crucial role in regulating cell fate like proliferation and differentiation.[67] To better understand the biocompatibility and cell behavior on PEM surfaces regarding
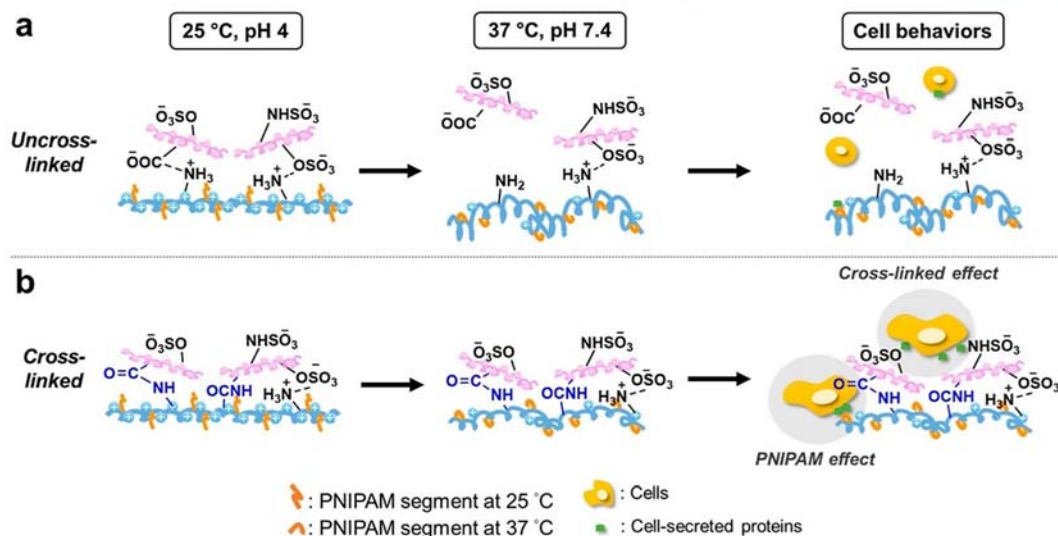
Figure 7. Schematic representation of structure evolution of PNIPAM−PEMs with (a) uncross-linking and (b) cross-linking under 25 °C, pH 4 and 37 °C, pH 7.4 and the effects on biological behaviors.

the effect of PNIPAM grafting and cross-linking, multipotent murine embryo fibroblast C3H10T1/2 were used for the study. A cell viability study was carried out to quantify live (green) and dead (red) cells. Figure 6a shows a substantial difference on cell distribution between uncross-linked and cross-linked PEMs after 24 h incubation visualized by CLSM. More dead cells were observed, and viable cells tended to form aggregates on the surfaces of uncross-linked PEMs. In contrast, more cells densely populated on cross-linked PEMs but only with H terminal layers. Furthermore, nearly 100% cells were alive with higher cell numbers on B-[LMW*/H]$_2$, B-[HMW/H]$_2$, and TCPS than on B-[Chi/H]$_2$ in cross-linked PEMs, as shown in Figure 6b. The quantification of cell area in Figure 6c,d manifests twice larger areas of cells spreading on cross-linked PEMs compared to uncross-linked PEM. Further observation on cell proliferation in the Supporting Information (Figure S5) also shows more cell expansion on cross-linked B-[LMW*/H]$_2$ and B-[HMW/H]$_2$ than on B-[Chi/H]$_2$ after 72 h incubation.

There are multiple factors regulating cell behavior on foreign material surfaces. One of the reasons behind poor biocompatibility and cell adhesion in uncross-linking systems is the soft and hydrated nature of PEMs composed of polysaccharides, particularly softer substrates of PNIPAM−PEMs regarding their exceptional viscoelastic properties. In addition, these native PEMs based on ion pairing are relatively unstable and can partly decompose upon exposure to physiological environments, which changes the ionization state of weak PELs like chitosan.[4] Consequently, H acting as a ligand for adhesive proteins adsorbed from serum or secreted by cells may get lost during the decomposition of PEM.[68] This further leads to the loss of specific cell ligands with reduced attachment, therefore promoting detachment of cells (Figure 7a). It has been suggested that cell behaviors can be improved by chemical cross-linking that changes the mechanical and wetting properties of PEMs, particularly their stability to retain H on the surfaces. Hence, it might promote adsorption of proteins secreted by cells and from serum.[12,31] In addition, our results

show that all the H terminal layers are negatively charged, attributed to sulfate and carboxylic groups, which are biofunctional sides to interact with proteins and cells.[21] On the other hand, PEM with Chi and PNIPAM−Chi terminal layers can hinder H to contact with cells diminishing cell adhesion on the surfaces.

Furthermore, the superior cell number and growth on cross-linked B-[LMW*/H]$_2$ and B-[HMW/H]$_2$ could also be contributed by the positive effect of PNIPAM. At 37 °C (above CP) used during culture of cells, the decreased wettability of PNIPAM can promote more protein adsorption from serum and cells on the surface, allowing more cell adhesion on PNIPAM-PEMs due to hydrophobic interactions.[62,69,70] Biomolecule adsorption and cell adhesion can be regulated by grafting the density and molecular weight of PNIPAM. A lower density or lower molecular weight of PNIPAM immobilized on the surface supports more cell adhesion.[7,27] However, no such perceptible difference was observed between B-[LMW*/H]$_2$ and B-[HMW/H]$_2$. We postulate that LMW* and HMW present similar behaviors of hydrodynamic diameters across the CPs, consequently giving rise to a minor difference on cell numbers. Therefore, taking all the factors into consideration, biocompatibility and cell behaviors can be controlled by our cross-linked PEMs modified with PNIPAM (Figure 7b).

4. CONCLUSIONS

Here, we demonstrate for the first time the use of PNIPAM−Chi with different molecular weights and grafting densities to generate thermoresponsive multilayers as culture substrata for cells. Despite the extended conformation of PNIPAM at 25 °C, multilayer formation between heparin and PNIPAM−Chi can be achieved at pH 4. However, both multilayer growth and stability are restricted when using LMW*, probably due to the higher grafting degree of PNIPAM, reducing the charge density and increasing steric hindrance. Hence, the use of HMW* even at a lower grafting degree is desirable to enable the formation of more swollen and thicker multilayers which may also serve

as a reservoir for bioactive substances like growth factors. An increase in multilayer stability at pH values above the pK_a value of Chi can be achieved by covalent cross-linking between amino groups of Chi and carboxylic groups of H, strengthening the integrity of multilayers without any toxicity to cells. Cross-linking of multilayers is also useful to enhance cell adhesion on these multilayers as a prerequisite for their subsequent growth and differentiation. Overall, the grafting of PNIPAM to polysaccharides like Chi in combination with polyanions like heparin is a promising approach to develop bioactive multilayer systems as stimuli-responsive surface coatings on implant materials for control of protein adsorption and cell behavior.

■ ASSOCIATED CONTENT

ⓈI Supporting Information

The Supporting Information is available free of charge at https://pubs.acs.org/doi/10.1021/acsami.2c05297.

> FTIR and ^{1}H NMR spectra for all compounds including experimental details; additional results for growth and characterizations of multilayers; and fluorescence images of cells (PDF)

■ AUTHOR INFORMATION

Corresponding Author

Thomas Groth − *Department of Biomedical Materials, Institute of Pharmacy, Martin Luther University Halle-Wittenberg, 06120 Halle (Saale), Germany; Interdisciplinary Center of Material Science, Martin Luther University Halle-Wittenberg, 06099 Halle (Saale), Germany;* ⓞ orcid.org/0000-0001-6647-9657; Email: thomas.groth@pharmazie.uni-halle.de

Authors

Yi-Tung Lu − *Department of Biomedical Materials, Institute of Pharmacy, Martin Luther University Halle-Wittenberg, 06120 Halle (Saale), Germany*

Kui Zeng − *Department of Wood Technology and Wood-based Composites, Georg-August-University of Göttingen, 37077 Göttingen, Germany*

Bodo Fuhrmann − *Interdisciplinary Center of Material Science, Martin Luther University Halle-Wittenberg, 06099 Halle (Saale), Germany*

Christian Woelk − *Pharmaceutical Technology, Institute of Pharmacy, Faculty of Medicine, Leipzig University, 04317 Leipzig, Germany*

Kai Zhang − *Department of Wood Technology and Wood-based Composites, Georg-August-University of Göttingen, 37077 Göttingen, Germany;* ⓞ orcid.org/0000-0002-5783-946X

Complete contact information is available at:
https://pubs.acs.org/10.1021/acsami.2c05297

Author Contributions

Y.-T.L. performed most of the experiments and writing of the manuscript. K.Z. performed the synthesis and characterization of polymers and writing of the manuscript. B.F. and C.W. were involved in the ellipsometry and zeta potential measurements. K.Z. was involved in the conceptualization, synthesis, and characterization and writing of the manuscript. T.G. was responsible for supervision and involved in conceptualization, validation, and writing of the manuscript. All authors have given approval to the final version of the manuscript.

Notes

The authors declare no competing financial interest.

■ ACKNOWLEDGMENTS

■ ABBREVIATIONS

Chi, chitosan
CP, cloud point
D, dissipation
DLS, dynamic light scattering
DS, degree of substitution
DMEM, Dulbecco's modified Eagle's medium
EDC, 1-ethyl-3-(3-dimethylaminopropyl)-carbodiimide
F, frequency
GAG, glycosaminoglycan
H, heparin
HMW, high molecular weight
LbL, layer-by-layer
LCST, lower critical solution temperature
LMW, low molecular weight
NHS, *N*-hydroxysuccinimide
PBS, phosphate-buffered saline
PDI, polydispersity index
PEM, polyelectrolyte multilayer
PEI, polyethylenimine
PNIPAM, poly(*N*-isopropylacrylamide)
PNIPAM−Chi, PNIPAM-*graft*-chitosan
PZC, point of zero charge
QCM-D, quartz crystal microbalance with dissipation monitoring
SPR, surface plasmon resonance
TCPS, tissue culture polystyrene plate
WCA, water contact angle

■ REFERENCES

(1) Rahmati, M.; Silva, E. A.; Reseland, J. E.; Heyward, C.; Haugen, H. J. Biological Responses to Physicochemical Properties of Biomaterial Surface. *Chem. Soc. Rev.* **2020**, 49, 5178−5224.

(2) Bauer, S.; Schmuki, P.; von der Mark, K.; Park, J. Engineering Biocompatible Implant Surfaces. *Prog. Mater. Sci.* **2013**, 58, 261−326.

(3) Decher, G. Fuzzy Nanoassemblies: Toward Layered Polymeric Multicomposites. *Science* **1997**, 277, 1232−1237.

(4) Silva, J. M.; Reis, R. L.; Mano, J. F. Biomimetic Extracellular Environment Based on Natural Origin Polyelectrolyte Multilayers. *Small* **2016**, 12, 4308−4342.

(5) Doberenz, F.; Zeng, K.; Willems, C.; Zhang, K.; Groth, T. Thermoresponsive Polymers and their Biomedical Application in Tissue engineering - A Review. *J. Mater. Chem. B* **2020**, 8, 607−628.

(6) El-Husseiny, H. M.; Mady, E. A.; Hamabe, L.; Abugomaa, A.; Shimada, K.; Yoshida, T.; Tanaka, T.; Yokoi, A.; Elbadawy, M.; Tanaka, R. Smart/stimuli-Responsive Hydrogels: Cutting-Edge Platforms for Tissue Engineering and Other Biomedical Applications. *Mater. Today Bio* **2022**, 13, 100186.

(7) Nagase, K.; Yamato, M.; Kanazawa, H.; Okano, T. Poly(N-isopropylacrylamide)-Based Thermoresponsive Surfaces Provide New Types of Biomedical Applications. *Biomaterials* **2018**, 153, 27−48.

(8) Vikulina, A. S.; Feoktistova, N. A.; Balabushevich, N. G.; von Klitzing, R.; Volodkin, D. Cooling-Triggered Release from Mesoporous Poly(N-isopropylacrylamide) Microgels at Physiological Conditions. *ACS Appl. Mater. Interfaces* **2020**, *12*, 57401.

(9) Xu, X.; Liu, Y.; Fu, W.; Yao, M.; Ding, Z.; Xuan, J.; Li, D.; Wang, S.; Xia, Y.; Cao, M. Poly(N-isopropylacrylamide)-Based Thermoresponsive Composite Hydrogels for Biomedical Applications. *Polymers* **2020**, *12*, 580.

(10) Ebara, M.; Yamato, M.; Hirose, M.; Aoyagi, T.; Kikuchi, A.; Sakai, K.; Okano, T. Copolymerization of 2-carboxyisopropylacrylamide with N-isopropylacrylamide accelerates Cell Detachment from Grafted Surfaces by Reducing Temperature. *Biomacromolecules* **2003**, *4*, 344−349.

(11) Nakayama, M.; Yamada, N.; Kumashiro, Y.; Kanazawa, H.; Yamato, M.; Okano, T. Thermoresponsive Poly(N-isopropylacrylamide)-Based Block Copolymer Coating for Optimizing Cell Sheet Fabrication. *Macromol. Biosci.* **2012**, *12*, 751−760.

(12) Richert, L.; Boulmedais, F.; Lavalle, P.; Mutterer, J.; Ferreux, E.; Decher, G.; Schaaf, P.; Voegel, J.-C.; Picart, C. Improvement of Stability and Cell Adhesion Properties of Polyelectrolyte Multilayer Films by Chemical Cross-linkin. *Biomacromolecules* **2004**, *5*, 284−294.

(13) Anouz, R.; Repanas, A.; Schwarz, E.; Groth, T. Novel Surface Coatings Using Oxidized Glycosaminoglycans as Delivery Systems of Bone Morphogenetic Protein 2 (BMP-2) for Bone Regeneration. *Macromol. Biosci.* **2018**, *18*, No. e1800283.

(14) Silva, J. M.; Duarte, A. R. C.; Caridade, S. G.; Picart, C.; Reis, R. L.; Mano, J. F. Tailored Freestanding Multilayered Membranes Based on Chitosan and Alginate. *Biomacromolecules* **2014**, *15*, 3817−3826.

(15) Liao, T.; Moussallem, M. D.; Kim, J.; Schlenoff, J. B.; Ma, T. N-isopropylacrylamide-Based Thermoresponsive Polyelectrolyte Multilayer Films for Human Mesenchymal Stem Cell Expansion. *Biotechnol. Prog.* **2010**, *26*, 1705−1713.

(16) Xu, L.; Wang, H.; Chu, Z.; Cai, L.; Shi, H.; Zhu, C.; Pan, D.; Pan, J.; Fei, X.; Lei, Y. Temperature-Responsive Multilayer Films of Micelle-Based Composites for Controlled Release of a Third-Generation EGFR Inhibitor. *ACS Appl. Polym. Mater.* **2020**, *2*, 741−750.

(17) Osypova, A.; Magnin, D.; Sibret, P.; Aqil, A.; Jérôme, C.; Dupont-Gillain, C.; Pradier, C.-M.; Demoustier-Champagne, S.; Landoulsi, J. Dual Stimuli-Responsive Coating Designed Through Layer-by-Layer Assembly of PAA-b-PNIPAM Block Copolymers for the Control of Protein Adsorption. *Soft Matter* **2015**, *11*, 8154−8164.

(18) Vikulina, A. S.; Aleed, S. T.; Paulraj, T.; Vladimirov, Y. A.; Duschl, C.; von Klitzing, R.; Volodkin, D. Temperature-Induced Molecular Transport through Polymer Multilayers Coated with PNIPAM Microgels. *Phys. Chem. Chem. Phys.* **2015**, *17*, 12771−12777.

(19) Liu, X.; Wang, X.; Voit, B.; Appelhans, D. Control of Nanoparticle Release by Membrane Composition for Dual-Responsive Nanocapsules. *Chemistry* **2019**, *25*, 13694−13700.

(20) Jaber, J. A.; Schlenoff, J. B. Polyelectrolyte Multilayers with Reversible Thermal Responsivity. *Macromolecules* **2005**, *38*, 1300−1306.

(21) Yang, Y.; Lu, Y. T.; Zeng, K.; Heinze, T.; Groth, T.; Zhang, K. Recent Progress on Cellulose-Based Ionic Compounds for Biomaterials. *Adv. Mater.* **2021**, *33*, No. e2000717.

(22) Peschel, D.; Zhang, K.; Aggarwal, N.; Brendler, E.; Fischer, S.; Groth, T. Synthesis of Novel Celluloses Derivatives and Investigation of Their Mitogenic Activity in the Presence and Absence of FGF2. *Acta Biomater.* **2010**, *6*, 2116−2125.

(23) Mellati, A.; Fan, C.-M.; Tamayol, A.; Annabi, N.; Dai, S.; Bi, J.; Jin, B.; Xian, C.; Khademhosseini, A.; Zhang, H. Microengineered 3D Cell-Laden Thermoresponsive Hydrogels for Mimicking Cell Morphology and Orientation in Cartilage Tissue Engineering. *Biotechnol. Bioeng.* **2017**, *114*, 217−231.

(24) Pitakchatwong, C.; Chirachanchai, S. Thermo-Magneto-responsive Dual Function Nanoparticles: An Approach for Magnetic Entrapable-Releasable Chitosan. *ACS Appl. Mater. Interfaces* **2017**, *9*, 10398−10407.

(25) Apte, G.; Repanas, A.; Willems, C.; Mujtaba, A.; Schmelzer, C. E. H.; Raichur, A.; Syrowatka, F.; Groth, T. Effect of Different Crosslinking Strategies on Physical Properties and Biocompatibility of Freestanding Multilayer Films Made of Alginate and Chitosan. *Macromol. Biosci.* **2019**, *19*, No. e1900181.

(26) Richert, L.; Schneider, A.; Vautier, D.; Vodouhe, C.; Jessel, N.; Payan, E.; Schaaf, P.; Voegel, J.-C.; Picart, C. Imaging Cell Interactions With Native and Crosslinked Polyelectrolyte Multilayers. *Cell Biochem. Biophys.* **2006**, *44*, 273−286.

(27) Takahashi, H.; Nakayama, M.; Yamato, M.; Okano, T. Controlled Chain Length and Graft Density of Thermoresponsive Polymer Brushes for Optimizing Cell Sheet Harvest. *Biomacromolecules* **2010**, *11*, 1991−1999.

(28) Chen, J.-P.; Cheng, T.-H. Thermo-Responsive Chitosan-Graft-Poly(N-isopropylacrylamide) Injectable Hydrogel for Cultivation of Chondrocytes and Meniscus Cells. *Macromol. Biosci.* **2006**, *6*, 1026−1039.

(29) Lee, S. B.; Ha, D. I.; Cho, S. K.; Kim, S. J.; Lee, Y. M. Temperature/pH-Sensitive Comb-Type Graft Hydrogels Composed of Chitosan and Poly(N-isopropylacrylamide). *J. Appl. Polym. Sci.* **2004**, *92*, 2612−2620.

(30) Giselbrecht, J.; Janich, C.; Pinnapireddy, S. R.; Hause, G.; Bakowsky, U.; Wölk, C.; Langner, A. Overcoming the Polycation Dilemma - Explorative Studies to Characterise the Efficiency and Biocompatibility of Newly Designed Lipofection Reagents. *Int. J. Pharm.* **2018**, *541*, 81−92.

(31) Niepel, M. S.; Almouhanna, F.; Ekambaram, B. K.; Menzel, M.; Heilmann, A.; Groth, T. Cross-linking Multilayers of Poly-l-lysine and Hyaluronic Acid: Effect on Mesenchymal Stem Cell Behavior. *Int. J. Artif. Organs* **2018**, *41*, 223−235.

(32) Lundin, M.; Solaqa, F.; Thormann, E.; Macakova, L.; Blomberg, E. Layer-by-Layer Assemblies of Chitosan and Heparin: Effect of Solution Ionic Strength and pH. *Langmuir* **2011**, *27*, 7537−7548.

(33) Barrera, Y. A. B.; Menzel, M.; Schmelzer, C. E. H.; Lehner, E.; Mäder, K.; Wölk, C.; Groth, T.; Groth, T. Engineering Osteogenic Microenvironments by Combination of Multilayers from Collagen Type I and Chondroitin Sulfate with Novel Cationic Liposomes. *Mater. Today Bio* **2020**, *7*, 100071.

(34) Zhang, Q.; Weber, C.; Schubert, U. S.; Hoogenboom, R. Thermoresponsive Polymers with Lower Critical Solution Temperature: from Fundamental Aspects and Measuring Techniques to Recommended Turbidimetry Conditions. *Mater. Horiz.* **2017**, *4*, 109−116.

(35) Osváth, Z.; Iván, B. The Dependence of the Cloud Point, Clearing Point, and Hysteresis of Poly(N -isopropylacrylamide) on Experimental Conditions: The Need for Standardization of Thermoresponsive Transition Determinations. *Macromol. Chem. Phys.* **2017**, *218*, 1600470.

(36) Bao, H.; Li, L.; Leong, W. C.; Gan, L. H. Thermo-Responsive Association of Chitosan-Graft-Poly(N-isopropylacrylamide) in Aqueous Solutions. *J. Phys. Chem. B* **2010**, *114*, 10666−10673.

(37) Xia, Y.; Burke, N. A. D.; Stöver, H. D. H. End Group Effect on the Thermal Response of Narrow-Disperse Poly(N -isopropylacrylamide) Prepared by Atom Transfer Radical Polymerization. *Macromolecules* **2006**, *39*, 2275−2283.

(38) Danaei, M.; Dehghankhold, M.; Ataei, S.; Davarani, F. H.; Javanmard, R.; Dokhani, A.; Khorasani, M.; Mozafari, M. R. Impact of Particle Size and Polydispersity Index on the Clinical Applications of Lipidic Nanocarrier Systems. *Pharmaceutics* **2018**, *10*, 57.

(39) Brotzel, F.; Chu, Y. C.; Mayr, H. Nucleophilicities of Primary and Secondary Amines in Water. *J. Org. Chem.* **2007**, *72*, 3679−3688.

(40) Aggarwal, N.; Altgärde, N.; Svedhem, S.; Michanetzis, G.; Missirlis, Y.; Groth, T. Tuning Cell Adhesion and Growth on Biomimetic Polyelectrolyte Multilayers by Variation of pH During Layer-by-Layer Assembly. *Macromol. Biosci.* **2013**, *13*, 1327−1338.

(41) Ruan, Q.; Zhu, Y.; Li, F.; Xiao, J.; Zeng, Y.; Xu, F. Investigation of Layer-by-Layer Assembled Heparin and Chitosan Multilayer Films via Electrochemical Spectroscopy. *J. Colloid Interface Sci.* **2009**, *333*, 725−733.

(42) Crouzier, T.; Picart, C. Ion Pairing and Hydration in Polyelectrolyte Multilayer Films Containing Polysaccharides. *Biomacromolecules* **2009**, *10*, 433−442.

(43) Amorim, S.; Pashkuleva, I.; Reis, C. A.; Reis, R. L.; Pires, R. A. Tunable Layer-by-Layer films Containing Hyaluronic Acid and their Interactions with CD44. *J. Mater. Chem. B* **2020**, *8*, 3880−3885.

(44) Martins, G. V.; Mano, J. F.; Alves, N. M. Dual Responsive Nanostructured Surfaces for Biomedical Applications. *Langmuir* **2011**, *27*, 8415−8423.

(45) Borges, J.; Mano, J. F. Molecular Interactions Driving the Layer-by-Layer Assembly of Multilayers. *Chem. Rev.* **2014**, *114*, 8883−8942.

(46) Almodóvar, J.; Place, L. W.; Gogolski, J.; Erickson, K.; Kipper, M. J. Layer-by-Layer Assembly of Polysaccharide-Based Polyelectrolyte Multilayers: A Spectroscopic Study of Hydrophilicity, Composition, and Ion pairing. *Biomacromolecules* **2011**, *12*, 2755.

(47) Crouzier, T.; Boudou, T.; Picart, C. Polysaccharide-Based Polyelectrolyte Multilayers. *Curr. Opin. Colloid Interface Sci.* **2010**, *15*, 417−426.

(48) Porcel, C.; Lavalle, P.; Ball, V.; Decher, G.; Senger, B.; Voegel, J.-C.; Schaaf, P. From Exponential to Linear Growth in Polyelectrolyte Multilayers. *Langmuir* **2006**, *22*, 4376−4383.

(49) Decher, G.; Schlenoff, J. B. *Multilayer Thin Films:Sequential Assembly of Nanocomposite Materials*, 2nd ed.; Decher, G., Schlenoff, J., Eds.; Wiley-VCH, 2012.

(50) Ida, S.; Kimura, R.; Tanimoto, S.; Hirokawa, Y. End-Crosslinking of Controlled Telechelic Poly(N-isopropylacrylamide) Toward a Homogeneous Gel Network with Photo-Induced Self-Healing. *Polym. J.* **2017**, *49*, 237−243.

(51) Sousa, M. P.; Cleymand, F.; Mano, J. F. Elastic Chitosan/Chondroitin Sulfate Multilayer Membranes. *Biomed. Mater.* **2016**, *11*, 35008.

(52) Altankov, G.; Richau, K.; Groth, T. The Role of Surface Zeta Potential and Substratum Chemistry for Regulation of Dermal Fibroblasts Interaction. *Materialwiss. Werkstofftech.* **2003**, *34*, 1120−1128.

(53) Zimmermann, R.; Birkert, O.; Gauglitz, G.; Werner, C. Electrosurface Phenomena at Polymer Films for Biosensor Applications. *Chemphyschem* **2003**, *4*, 509−514.

(54) Wang, Q. Z.; Chen, X. G.; Liu, N.; Wang, S. X.; Liu, C. S.; Meng, X. H.; Liu, C. G. Protonation Constants of Chitosan with Different Molecular Weight and Degree of Deacetylation. *Carbohydr. Polym.* **2006**, *65*, 194−201.

(55) Wang, H. M.; Loganathan, D.; Linhardt, R. J. Determination of the pKa of Glucuronic Acid and the CarboxyGgroups of Heparin by 13C-Nuclear-Magnetic-Resonance Spectroscopy. *Biochem. J.* **1991**, *278*, 689.

(56) Remko, M.; Broer, R.; van Duijnen, P. T. How Acidic are Monomeric Structural Units of Heparin? *Chem. Phys. Lett.* **2013**, *590*, 187−191.

(57) Zhou, G.; Niepel, M. S.; Saretia, S.; Groth, T. Reducing the Inflammatory Responses of Biomaterials by Surface Modification with Glycosaminoglycan Multilayers. *J. Biomed. Mater. Res.* **2016**, *104*, 493−502.

(58) Wilson, J. T.; Cui, W.; Kozlovskaya, V.; Kharlampieva, E.; Pan, D.; Qu, Z.; Krishnamurthy, V. R.; Mets, J.; Kumar, V.; Wen, J.; Song, Y.; Tsukruk, V. V.; Chaikof, E. L. Cell Surface Engineering with Polyelectrolyte Multilayer Thin Films. *J. Am. Chem. Soc.* **2011**, *133*, 7054−7064.

(59) Almeida, A. C.; Vale, A. C.; Reis, R. L.; Alves, N. M. Bioactive and Adhesive Properties of Multilayered Coatings Based on Catechol-Functionalized Chitosan/Hyaluronic Acid and Bioactive Glass Nanoparticles. *Int. J. Biol. Macromol.* **2020**, *157*, 119−134.

(60) Altankov, G.; Grinnell, F.; Groth, T. Studies on the Biocompatibility of Materials: Fibroblast Reorganization of Substratum-Bound Fibronectin on Surfaces Varying in Wettability. *J. Biomed. Mater. Res.* **1996**, *30*, 385−391.

(61) Faucheux, N.; Schweiss, R.; Lützow, K.; Werner, C.; Groth, T. Self-Assembled Monolayers with Different Terminating Groups as Model Substrates for Cell Adhesion Studies. *Biomaterials* **2004**, *25*, 2721−2730.

(62) Psarra, E.; König, U.; Ueda, Y.; Bellmann, C.; Janke, A.; Bittrich, E.; Eichhorn, K.-J.; Uhlmann, P. Nanostructured Biointerfaces: Nanoarchitectonics of Thermoresponsive Polymer Brushes Impact Protein Adsorption and Cell Adhesion. *ACS Appl. Mater. Interfaces* **2015**, *7*, 12516−12529.

(63) Ren, K.; Crouzier, T.; Roy, C.; Picart, C. Polyelectrolyte Multilayer Films of Controlled Stiffness Modulate Myoblast Cells Differentiation. *Adv. Funct. Mater.* **2008**, *18*, 1378−1389.

(64) Imbir, G.; Mzyk, A.; Trembecka-Wójciga, K.; Jasek-Gajda, E.; Plutecka, H.; Schirhagl, R.; Major, R. Polyelectrolyte Multilayer Films Modification with Ag and rGO Influences Platelets Activation and Aggregate Formation under In Vitro Blood Flow. *Nanomaterials* **2020**, *10*, 859.

(65) Silva, J. M.; Caridade, S. G.; Oliveira, N. M.; Reis, R. L.; Mano, J. F. Chitosan-Alginate Multilayered Films with Gradients of Physicochemical Cues. *J. Mater. Chem. B* **2015**, *3*, 4555−4568.

(66) Quinn, J. F.; Caruso, F. Facile Tailoring of Film Morphology and Release Properties Using Layer-by-Layer Assembly of Thermoresponsive Materials. *Langmuir* **2004**, *20*, 20−22.

(67) Guillame-Gentil, O.; Semenov, O.; Roca, A. S.; Groth, T.; Zahn, R.; Vörös, J.; Zenobi-Wong, M. Engineering the Extracellular Environment: Strategies for Building 2D and 3D Cellular Structures. *Adv. Mater.* **2010**, *22*, 5443−5462.

(68) Köwitsch, A.; Zhou, G.; Groth, T. Medical Application of Glycosaminoglycans: A Review. *J. Regen. Med. Tissue Eng.* **2018**, *12*, e23−e41.

(69) Kobayashi, J.; Arisaka, Y.; Yui, N.; Akiyama, Y.; Yamato, M.; Okano, T. Effect of Temperature Changes on Serum Protein Adsorption on Thermoresponsive Cell-Culture Surfaces Monitored by A Quartz Crystal Microbalance with Dissipation. *Int. J. Mol. Sci.* **2018**, *19*, 1516.

(70) Schmidt, S.; Zeiser, M.; Hellweg, T.; Duschl, C.; Fery, A.; Möhwald, H. Adhesion and Mechanical Properties of PNIPAM Microgel Films and Their Potential Use as Switchable Cell Culture Substrates. *Adv. Funct. Mater.* **2010**, *20*, 3235−3243.

Chapter 3

Summary – Surface properties and bioactivity of PNIPAM-*grafted*-chitosan/chondroitin sulfate multilayers

Glycosaminoglycans (GAGs) play a crucial role in binding to adhesive proteins and growth factors (GFs) to regulate cell activities. The study in chapter 2 provided a possibility to fabricate PNIPAM-containing PEMs in combination with a GAG that improved biocompatibility and cell adhesion. In this paper, the capability of another member of GAGs, chondroitin sulfate (ChS), as polyanion to form PEMs with PNIPAM-Chi (PChi) at pH 4 was investigated. HMW was used as the only thermoresponsive polycation throughout this study based on its ability to promote growth and retain assembly of PEM in chapter 2. Not only the growth and internal structure during PEM formation, but also more insight into surface properties and swelling ability of PEMs in responsive to temperature were investigated by a comprehensive screening using SPR, QCM-*D*, ellipsometry and WCA measurements. PEM comprised of ChS and Chi was compared as a control. A total of 10 layers by alternating deposition of Chi and PChi was achieved that showed remarkable exponential growth and swelling ability because PNIPAM chains extended at 25 °C coupling more water molecules. ChS as smaller molecule diffused into the layers, resulting in a denser and more rigid PEM. Moreover, the thermoresponsive behavior of PEMs was studied by QCM-*D* with NaCl solution at physiological pH 7.4 in a temperature swap of 20–40 °C. Compared to the control PEM, PChi-containing PEM exhibited noticeable swelling and deswelling effect in response to temperature. However, thermoresponsive behaviors was not observed by the surface wettability, possibly attributed to the rearrangement and partial disassembly of PEM after rinsing with physiological buffer, pH 7.4. After covalent crosslinking by EDC/NHS, the integrity of PChi-containing PEMs was maintained and able to thermally change wettability.

Temperature and wettability are important factors for protein adsorption. The association of PEMs with protein was studied by adsorption and desorption of vitronectin (VN), which is a major cell adhesive protein that has specific binding site to

cell integrin to promote cell adhesion and spreading. Higher amount of VN adsorption/desorption were promoted at 37 °C in comparison to at 20 °C linked to the hydrophobic interaction between PChi-containing PEMs and VN adsorption. Importantly, PEMs with ChS terminal layers retained more VN on the surface owing to the specific interaction between ChS and VN, which was further corroborated with the behaviors of C3H10T1/2 multipotent embryonic mouse fibroblasts. Both ChS and PChi provides the advantage of binding more adhesive proteins secreted by cells (e.g., FN) and from serum (e.g., VN) on the surface, resulted in the enhanced adhesion and spreading of cells through integrin ligation. In addition, the used materials ChS and PChi and crosslinking process were confirmed again showing no toxicity to cells.

Therefore, this study suggested PEMs combined with PNIPAM and GAGs like ChS with greater bioactivity, nontoxicity, and stimuli-responsivity may be useful as culture substrata for in vitro culture of stem and other cells.

Surface properties and bioactivity of PNIPAM-*grafted*-chitosan/chondroitin multilayers

Yi-Tung Lu [a,1], Pei-Tzu Hung [a,1], Kui Zeng [b], Christian Woelk [c], Bodo Fuhrmann [d], Kai Zhang [b], Thomas Groth [a,d,*]

[a] *Department of Biomedical Materials, Institute of Pharmacy, Martin Luther University Halle-Wittenberg, Heinrich-Damerow-Strasse 4, 06120, Halle (Saale), Germany*
[b] *Department of Wood Technology and Wood-based Composites, Georg-August-University of Göttingen, Büsgenweg 4, D-37077, Göttingen, Germany*
[c] *Pharmaceutical Technology, Institute of Pharmacy, Faculty of Medicine, Leipzig University, 04317, Leipzig, Germany*
[d] *Interdisciplinary Center of Material Science, Martin Luther University Halle-Wittenberg, D-06099, Halle (Saale), Germany*

ARTICLE INFO

ABSTRACT

The thermoresponsive poly(*N*-isopropylacrylamide) (PNIPAM) is widely applied in the biomedical field particularly as thermoresponsive substrate for culture of cells. To be used as a stimuli-responsive coating for cell culture, combining PNIPAM with glycosaminoglycans might be an effective approach to improve its bioactivity. In this study, chitosan is grafted with PNIPAM moieties (PCHI) possessing a cloud point at 31 °C and used as a polycation to fabricate thermoresponsive polyelectrolyte multilayers (PEM) with the bioactive polyanion chondroitin sulfate (CS) at pH 4 by layer-by-layer technique. The *in-situ* investigation by surface plasmon resonance and quartz crystal microbalance with dissipation monitoring confirms that the formation of PEMs with CS can be achieved despite the bulky structure of PCHI at 25 °C. The stability of the PEMs is further improved at physiological pH 7.4 by chemical crosslinking using 1-ethyl-3-(3-dimethylaminopropyl) carbodiimide/*N*-hydroxysuccinimide. Moreover, these PEMs exhibit de-swelling and swelling ability with different surface wettability in response to temperature, which triggers the adsorption and desorption of adhesive protein vitronectin on the PEMs. At 37 °C, the PEMs containing PNIPAM particularly associated with CS terminal layer supports protein adsorption and consequently enhances cell adhesion using multipotent murine stem cells. Overall, due to improved stability, crosslinked PNIPAM-modified biogenic multilayers are cytocompatible and hold great potential as culture substrate for different tissue cells and application in tissue engineering.

1. Introduction

The interaction between biomaterial surfaces and biomolecules like proteins is considered a key factor for subsequent regulation of cell adhesion, proliferation and differentiation and thus relevant for biomedical applications [1]. Surface properties of biomaterials including wettability, charge density, topography, and mechanical properties play profound roles for these biological responses [2–6]. In recent years, functionalization of biomaterials with smart polymers has become an attractive strategy to modulate the surface properties in response to environmental cues such as pH, temperature, light, and others [7]. Among them, poly(-*N*-isopropylacrylamide) (PNIPAM) with a lower critical solution temperature (LCST) around 32 °C close to physiological temperature has been applied as a thermoresponsive and biocompatible surface coating used for the application in tissue engineering, drug delivery and protein separation [8,9]. Below LCST, the hydrated feature is attributed to the dominance of hydrophilic amide groups of PNIPAM which are protein repellent and thus anti-cell adhesive. Above LCST, PNIPAM undergoes coil-to-globular transition dominated by its hydrophobic isopropyl groups leading to dehydration of the polymer that favors protein adsorption and promotes cell adhesion [10]. With this advantage, cell sheet engineering has become a major application to detach complete cell sheets below LCST without using harmful enzymatic digestion that destroy cell-cell and cell-matrix adhesions [9]. Therefore, PNIPAM coated substrata have been used for culture and temperature-based harvesting of stem cells maintaining their differentiation ability for tissue regeneration [11–13].

However, immobilization of PNIPAM on surface requires a certain thickness to permit cell adhesion at temperatures above LCST (e.g. during cell culture in incubators) [8]. Functionalization of surfaces with PNIPAM can be done by *grafting-to* or direct synthesis on the surfaces among other techniques, which requires costly equipment, sophisticated chemical processes to activate surfaces and use of cytotoxic chemicals (e.g. photo initiators) [8,9]. In the last decades, layer-by-layer (LbL) technique has been established for surface modification based on physical adsorption of polyelectrolytes (PEL) and other macromolecular entities as a straightforward approach to precisely control the thickness of surface coatings. Mostly film formation is driven by the electrostatic interaction between oppositely charged PEL [14]. The physiochemical properties of such polyelectrolyte multilayers (PEMs) can be tuned by the nature of selected polymers and environmental conditions such as temperature, pH and ionic strength [15].

The use of polysaccharides as PEL is typically more preferable for biomedical application because of their high biocompatibility, biodegradability, and can represent or mimic components of human tissue [15]. For example, glycosaminoglycans (GAGs) with numerous negatively charged groups are polysaccharide-based components of extracellular matrix (ECM) and cells. They are perfect candidates for natural and biocompatible PELs [15]. Specially, they are highly bioactive, interacting with ECM proteins and growth factors that play important roles in cell adhesion, and regulation of cell growth and differentiation [16]. Among them, chondroitin sulfate (CS) is frequently used as polyanion for PEM formation to make biomimetic surfaces promoting several cell functions. For instance, the expression of adhesive proteins (e.g. fibronectin) secreted from cells was enhanced during culture on CS containing PEM, along with an enhanced osteogenic and chondrogenic differentiation by controlled release of different morphogens from CS-based PEM [17–19]. Chitosan (CHI) as further example, which is derived from the polysaccharide chitin, is one of the mostly chosen polycations for PEM formation due to its abundancy, biocompatibility and antibacterial properties [20]. However, the highly hydrated characteristics and fact that its charge density depends on pH is related to lower cell adhesion when CHI as weak PEL is used for PEM formation [21,22]. Improvement of cell adhesion and bioactivity of such PEM can be achieved by chemical crosslinking processes [17,22].

Since PNIPAM is uncharged, a conjugation of PNIPAM with PELs is required for deposition on the surface through LbL processes. The inherent thermoresponsive property of PNIPAM-modified PEMs has been used for stimuli-responsive controlled release of drugs such as EGF receptor inhibitor or anti COVID-19 drug Favipiravir [23,24]. On the other hand, studies on the use of PNIPAM-modified PEM for tissue engineering are rarely found. A first study on PNIPAM-modified PEM to control cell adhesion/detachment was reported by Liao et al. [25]. They prepared PNIPAM film by assembling PNIPAM copolymers with cationic allylamine hydrochloride segment and with anionic styrene sulfonic acid segment. The cationic moiety on the outermost surface seemed to promote FN adsorption that was secreted from cells and further cell adhesion. Although there are a few studies about protein adsorption on PNIPAM-based PEMs using ovalbumin, structure and properties of PNIPAM-modified PEM related to protein adsorption and cell behavior remain still to be further elucidated [26,27].

In this study, we establish a protocol to modify CHI covalently with PNIPAM (referred as PCHI) studying its thermoresponsive properties and applicability to serve as polycation for making thermoresponsive PEM with CS as bioactive polyanion. The effect of the presence of bulky PNIPAM on growth behavior, thickness, viscoelastic and surface properties of PEM are investigated with physical methods. An attempt to increase stability and cell-adhesive properties of PEM under physiological conditions is done by covalent crosslinking. In particular, crosslinking and terminal layer composition like CHI and PCHI versus CS are supposed to affect adsorption of adhesive (extracellular matrix) proteins and adhesion of cells. Thus, these factors are analyzed towards adsorption of the cell-adhesive protein vitronectin, as well as cytocompatibility,

including the study of adhesion and growth of the multipotent mouse fibroblast cell line C3H10T1/2 as a general model for culture of stem cells that is interesting for applications in regenerative medicine.

2. Materials and methods

2.1. Materials

Chitosan (CHI, deacetylation ≥92.6%, Mw = 40–150 kDa) was purchased from HMC Heppe Medical Chitosan GmbH (Halle, Germany). Chondroitin sulfate A (CS) from the bovine trachea (Mw ~ 25 kDa) was provided by Sigma-Aldrich (Steinheim, Germany). Carboxylic acid−terminated PNIPAM (PNIPAM-COOH, Mw = 10 kDa), N-hydroxysuccinimide (NHS), polyethylene imine (PEI, Mw ~ 750 kDa) and fluorescein isothiocyanate (FITC) were purchased from Sigma-Aldrich (Steinheim, Germany). Tetrahydrofuran (THF) and *n*-hexane were provided by Th. Geyer GmbH & Co. KG (Renningen, Germany). 1-ethyl-3-(3-dimethylaminopropyl) carbodiimide (EDC) were obtained from Thermo Fisher (Kandel) GmbH (Karlsruhe, Germany). Recombinant human vitronectin (VN) was from PeproTech, Inc. (Hamburg, Germany).

2.2. Synthesis of thermoresponsive PNIPAM-grafted-CHI

PNIPAM-*grafted*-CHI (PCHI) synthesis has been described in more detail elsewhere [28–30]. Briefly, a weight ratio of 1:3 of chitosan and PNIPAM-COOH were separately dissolved in 2% acetic acid. The PNIPAM-COOH aqueous solution was activated by EDC and NHS for 1 h at 25 °C and mixed with the chitosan solution afterwards. The molar ratio based on the repeating unit of chitosan/EDC/NHS molar was 1: 3: 1.5. The mixture was left to react and stirred overnight at 25 °C. After the reaction, precipitation of the product was obtained in a THF/hexane solution (4:1) for 2 times. Finally, the precipitant was purified by dialysis using a membrane with molecular weight cut off (MWCO): 12–14 kDa against Milli-Q water followed by lyophilization with a freeze dryer (ALPHA 1–2 LDplus, Christ, Osterode am Harz, Germany).

The zeta potential measurements were done by laser Doppler velocimetry using a Zetasizer Nano ZS ZEN3600 (Malvern Instruments Ltd., UK) and a clear disposable folded capillary cell (DTS1060, Malvern Instruments). Since high concentration of salt can cause degradation of the electrodes and inaccurate measurement, CS, CHI, and PNIPAM-CHI were prepared at low concentration of 0.5 mg mL^{-1} in 20 mM NaCl solution at pH 4. Three measurements of 20 cycles were performed under the Smoluchowski approximation with a voltage of 50 V at 25 °C (Zetasizer software 7.12) [31]. The viscosity of 0.8872 mPa s, dielectric constant of 78.5 F/m and refractive index of 1.33 were assumed.

Dynamic light scattering (DLS) was performed with a Zetasizer Nano ZS ZEN3600 (Zetasizer Nano ZS, Malvern Instruments Ltd., UK) using a 5 mW laser with the incident beam of 633 nm (He−Ne laser). To align the conditions of further multilayer process, PCHI was prepared at a concentration of 1 mg mL^{-1} in 150 mM NaCl solution, pH 4. The hydrodynamic diameter and polydispersity index (PDI) of PCHI were determined in the temperature range of 20–38 °C. Each measurement with 15 runs was done in triplicate and the average was calculated for plotting the results.

2.3. Cleaning of substrates

Silicon wafers (Silicon materials, Kaufering, Germany) and round glass cover slips (Ø 12 mm, Menzel, Braunschweig, Germany) were cleaned using a solution of 35% H_2O_2, 25% NH_4OH, and Milli-Q water (1:1:5, v/v/v) at 80 °C for 15 min. Thereafter, the samples were rinsed repetitively with Milli-Q water (6 × 5 min) and dried with a nitrogen stream. The gold-coated glass sensors (10 × 10 mm^2) for surface plasmon resonance (SPR) (IBIS Technologies B.V., Enschede, The Netherlands) and quartz chips (Au/Ti, 10 MHz) for quartz crystal microbalance with dissipation monitoring (QCM-D) (qCell T, 3t Analytik, Tuttlingen,
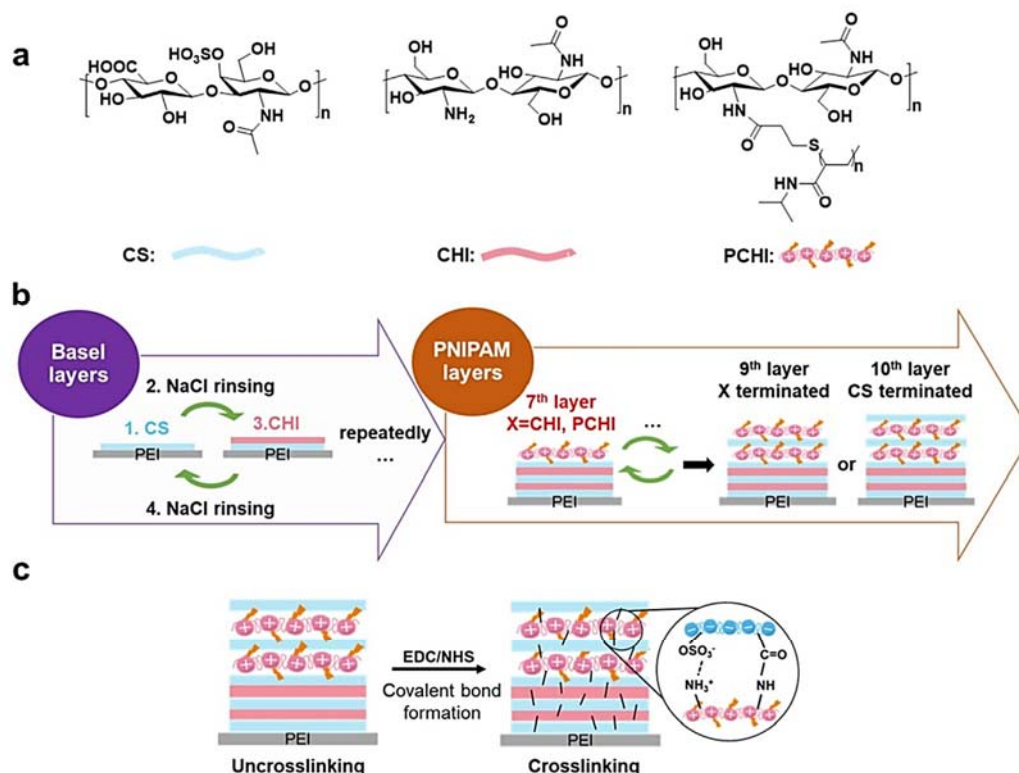
Fig. 1. (a) Molecular units of polymers used in the polyelectrolyte multilayer (PEM) buildup: chondroitin sulfate (CS) as polyanion, chitosan (CHI) and PNIPAM-*grafted*-chitosan (PCHI) as polycations. (b) Schematic representation for preparation of PCHI−PEM using the layer-by-layer (LbL) technique. The substrate was coated with positively charged polyethylene imine (PEI) as an anchoring layer followed by subsequent CS and CHI adsorption. CHI was replaced by PCHI from 7th layer. (c) Crosslinking of the PEM using EDC/NHS to form amide bonds between CHI or PCHI and CS.

Germany) were gently cleaned with 99% ethanol and Milli-Q water followed by drying with nitrogen.

2.4. Preparation of multilayers with layer-by-layer technique

The PEMs were fabricated on silicon wafers, gold-coated glass sensors, polystyrene well plates, or glass cover slips for SPR, QCM, ellipsometry, water contact angle and biological experiments. The used PELs and assembly procedure of PEM are illustrated in Fig. 1a and b. All PELs were dissolved in 150 mM NaCl solution at a concentration of 1 mg mL^{-1}. CHI was solubilized in 150 mM NaCl solution containing 0.05 M acetic acid at 50 °C for 3 h and stirred overnight. The pH of all polyelectrolyte solutions was set at pH 4. All solutions were filtered through a 0.2 μm pore size membrane (Whatman). Considering mobility of PNIPAM chain is restricted inside PEM in response to temperature [32,33], here PCHI was only deposited at the outermost region of the entire PEM. An initial anchoring layer of PEI was deposited on the substrate to obtain a positively charged surface which enables strong bonding of PEM to the different substrates. By alternating adsorption of CS as polyanion and CHI as polycation, the basal PEM were built up to 6 total layers. For the PCHI−PEMs, CHI was replaced by PCHI from 7th layer for following deposition step until reaching total number of 9 or 10 layers, where either PCHI or CS was the final layer of PCHI−PEM, respectively. The CHI−PEM system only composed of CHI and CS was referred as comparisons. PEMs with different compositions were named as B-[X/CS]$_{1.5}$ (X-terminated layer) and B-[X/CS]$_2$ (CS-terminated layer). 'B' refers to basal layers from 1–6 layers and 'X' is CHI or PCHI.

After PEM formation, the crosslinking was performed with 50 mg

mL^{-1} EDC and 11 mg mL^{-1} NHS in 150 mM NaCl solution at pH 5 (Fig. 1c) according to the protocol described previously [4,22]. PEMs were immersed in the crosslinking solutions and incubated at 4 °C for 18 h with gentle shaking. Afterwards, the crosslinking reaction was stopped by washing the samples 3 times with 0.15 M NaCl, pH 8 for each 1h to remove unreacted EDC/NHS.

2.5. Measurement of multilayer growth

The layer growth and PEM formation were studied at 25 °C using surface plasmon resonance (SPR, IBIS Technologies B.V., Enschede, The Netherlands) and quartz crystal microbalance with dissipation monitoring (QCM-*D*, qCell T, 3t Analytik, Tuttlingen, Germany). In SPR measurement, a shift in the angle (m°) is observed upon the binding of molecules at the gold–liquid interface of the gold coating sensor due to the change of refractive index [34]. The cleaned gold senor was fixed in the flow chamber and mounted in the SPR device. To begin the measurement, PEI was first introduced to the flow cell and followed by a rinsing step with alternating injection of CS, CHI and PCHI to achieve 10 layers. Each adsorption step of 1 mg mL^{-1} polyelectrolyte solution at pH 4 was 15 min and the rinsing steps using 150 mM NaCl, pH 4 to remove unbound polyelectrolyte was 3 × 4 min. The mean angle shift (m°) was calculated from 10 values after rinsing obtained from IBIS SPR software 2.1.21 for plotting the graph of layer growth.

QCM-*D* technique was performed to quantify the adsorbed 'acoustic' mass including solvent that is associated with the PEM as well as the damping shift caused by the PEM on the sensor. A piezoelectric AT-cut gold-coated quartz sensor can be excited to resonance by applying an

alternative voltage. The resonance frequency of an oscillating quartz crystal is correlated to the mass of the crystal and thus any mass change from adsorbed or desorbed mass leads to a frequency shift. The Sauerbrey model states a linear relationship between the changes in frequency and mass estimated for a thin, rigid and evenly distributed film when there is no change in dissipation [35]. However, when a polysaccharide-based film with high water content is deposited on the surface, the oscillation of resonator is damped by the adsorbed layer. The Kelvin−Voigt model explains the frequency and energy dissipation changes (ΔF and ΔD) related to film viscoelastic properties and thickness [36]:

$$\frac{\Delta f}{f} = -\frac{d_f \rho_f}{d_q \rho_q}\left(1 - \eta_0 \eta_0 \times \frac{\left(\frac{\eta_f}{\rho_f}\right)\omega^2}{\mu_f^2 + \omega^2 \eta_f^2}\right) \tag{1}$$

$$\Delta D = -\frac{d_f}{d_q \rho_q}\left(\eta_0 \rho_0 \times \frac{\mu_f \omega^2}{\mu_f^2 + \omega^2 \eta_f^2}\right) \tag{2}$$

where $\omega = 2\pi f$ is the angular frequency of oscillation, d_q and ρ_q are the thickness and density of the quartz crystal resonator. η_0 and ρ_0 are bulk viscosity and density. While d_q and ρ_q are known parameters in the QCM-D device and used in the software, d_f, ρ_f, η_f, and μ_f are the thickness, density, viscosity, and shear modulus of absorbed film. The viscoelastic thickness of the film can be calculated by fitting the changes of Δf and ΔD in the software. (qGraph Viewer 1.8). The liquid viscosity and density were assumed to be close to water with parameter values of 0.89 Pa s and 0.997 g cm^{-3}. The film density was fixed at 1.05 g cm^{-3} based on previous QCM studies on PEM made of polysaccharides [37].

To perform the LbL film build-up, the cleaned quartz gold sensor was placed in the QCM measuring device. A continuous flow at 60 μL min^{-1} was used for all polyelectrolyte deposition with a concentration of 1 mg mL^{-1} in 150 mM NaCl, pH 4 to reach equilibrium state for 15 min. Rinsing steps using 150 mM NaCl solution at pH 4 were done for 12 min after each layer deposition. The Voigt thickness was automatically calculated from qGraph Viewer 1.8 software based on F and D shifts.

2.6. Effect of temperature on multilayer mass measured by QCM-D

Frequency shifts of the sensor coated with PEM dependent on temperature were monitored using the QCM-*D* device equipped with a heating chamber. The PEM-coated sensor was mounted in the device and equilibrated with 150 Mm NaCl solution at pH 4 or 7.4 at 20 °C with a flow rate = 60 μL min^{-1} for 10 min. Subsequently, the heating process was started in the device for 1 h. After the temperature reached 40 °C, the cooling process ran for another 1 h to reach 20 °C. The heating-cooling cycle was carried out with 0.33 °C min^{-1} steps.

2.7. Multilayer thickness and hydration degree

The dry thickness of uncrosslinked and crosslinked multilayers was measured by spectroscopic ellipsometry (M − 2000V, J.A. Woollam Co., Lincoln, NE, USA) in the wavelength range of 375–1000 nm at 25 °C. The spectroscopic scan was at the range of angles from 51° to 60°. A cleaned Si wafer coated with SiO$_2$ layer was used as the reference. In addition, the layer thickness was used to examine the stability of PEMs by rinsing with phosphate buffered saline (PBS, pH 7.4, Biochrom AG, Germany) followed by Dulbecco's modified Eagle's medium (DMEM, pH 7.4, HiMedia Laboratories Pvt. Ltd., Germany) and dried with a nitrogen stream. The measurements were done two times on different locations of each PEM surface with duplicate measurements. The thickness was obtained using the WVASE32 software applying Cauchy model [38]. In addition, the hydration degree was calculated by dry thickness and viscoelastic thickness from ellipsometry and Voigt model using equation (3):

$$Hydration\ \% = \frac{Thickness\ (Voigt - Ellipsometry)}{Thickness\ (Voigt)} \tag{3}$$

2.8. Surface wettability of multilayers

Static water contact angle measurement for studying surface wettability of the terminal layers was carried out by OCA 15+ system (Dataphysics GmbH, Filderstadt, Germany) with a heating element. The sessile drop method was performed on the multilayer surfaces first at 20 °C and then at 37 °C. The volume of 1 μL Milli-Q water was dispensed on the surface with a flow rate of 0.5 μL s^{-1}. Ellipse fitting was chosen as the preferred fitting method to calculate the water contact angles (WCA). Each sample was measured at least 10 times at different positions to calculate average value and standard deviation.

2.9. Biological investigations

2.9.1. Protein adsorption and desorption

Fluorometry (FLUOstar Optima, BMG LabTech., Offenburg, Germany) was used to quantify protein adsorption and desorption. FITC-labeled VN (FITC-VN) was prepared according to the protocol for protein labelling (Sigma-Aldrich) as shown in supporting information. Crosslinked PEMs were prepared in black 96-well tissue culture plates (Greiner). The PEM were coated with 70 μL of 5 μg mL^{-1} FITC-VN and incubated at either 25 °C or 37 °C for 1 h. Thereafter, the supernatant of each well was transferred to a new black 96-well plate. The fluorescence intensity of the supernatant was measured to determine the concentration of remaining FITC-VN at an excitation wavelength of 488 nm and an emission wavelength of 530 nm. The fluorescence intensities of known concentrations (0.005, 0.05, 0.1, 0.5 and 5 μg mL^{-1}) of FITC-VN were measured to generate a calibration curve for calculation of the amount of adsorbed VN on the surface (indirect estimation).

After removal of FITC-VN supernatants, the PEMs were rinsed with 70 μL PBS (at 4 or 37 °C, pH 7.4) 3 times to remove excess of protein solution. Desorption of VN was conducted by applying 70 μL PBS to the samples which were incubated at 4 °C or 37 °C for 24 h, followed by incubation with 70 μL of 200 mM NaOH at 37 °C for another 2 h. The PBS and NaOH supernatants were collected and the fluorescence intensity measured to determine the amount of desorbed FITC-VN.

2.9.2. Cell culture

C3H10T1/2 embryonic fibroblasts (Clone 8) were purchased from ATCC (CCL-226, LGC Standards GmbH Wesel, Germany) and cultured in DMEM supplemented with 10% (v/v) fetal bovine serum (FBS, Biochrom AG, Berlin, Germany) and 1% (v/v) antibiotic solution (penicillin/streptomycin, Biochrom AG, Berlin, Germany) at 37 °C in a humidified 5% CO$_2$/95% air atmosphere using a NUAIRE DH Autoflow incubator (Plymouth, Minnesota, USA). Prior to confluence, cells were harvested from the flask using 0.25% trypsin/0.02% EDTA (Biochrom AG, Berlin, Germany) solution for 5 min at 37 °C. The trypsin was neutralized with DMEM containing 10% FBS +1% Pen/strep. After centrifugation of the cell suspension for 5 min at 500 g, the supernatant was aspirated, and the cell pellet was resuspended in DMEM with 10% FBS +1% Pen/strep. Cells were counted manually using a Neubauer chamber.

2.9.3. Cell viability, adhesion, and growth

The crosslinked PEMs prepared in 24 well tissue culture polystyrenes (TCPS, Greiner, Frickenhausen, Germany) were sterilized by ultraviolet light at 254 nm for 30 min and rinsed twice with sterile PBS. Afterwards, the modified substrates were pre-incubated with DMEM containing 1% Pen/strep at 37 °C for 1 h to deactivate any unreacted EDC/NHS after PEM crosslinking. Then, C3H10T1/2 cells were seeded on PEMs at a cell density of 10^4 cells per well in serum-containing DMEM (10% FBS+1% Pen/strep) and incubated at 37 °C/5% CO$_2$/95% air atmosphere.

Cell viability was determined after 24h cultivation by using a

Table 1
Zeta potentials of PEL and degree of substitution (DS) of PNIPAM-*grafted*-CHI.

Sample	Chitosan: PNIPAM [a]	DS$_{PNIPAM}$	Zeta potential (mV) [b]
PNIPAM-*grafted*-chitosan (PCHI)	1:3	0.03	30.7 ± 0.5
Chitosan (CHI)			33.8 ± 0.6
Chondroitin sulfate (CS)			−20.1 ± 1.8

[a] Weight ratio of chitosan and PNIPAM during synthesis.
[b] Measured at 0.5 mg mL^{-1} of PEL, at pH 4 in 20 mM NaCl.

fluorescence-based Live/Dead assay with calcein AM and EthD-III (Bio-tium, Hayward, CA). The cells were rinsed once briefly in Dulbecco's phosphate-buffered saline (DPBS) containing 1 g L^{-1} glucose. The staining solution containing 2 μM calcein AM (green) and 4 μM EthD-III (red) was added into each well and incubated in the dark for 30 min at 37 °C. Subsequently, the PEM samples were washed with DPBS (Lonza Group Ltd, Bornem, Belgium) containing 1 g L^{-1} glucose twice and analyzed through a set of an Ar 488 nm laser and He–Ne 543 nm laser using confocal laser scanning microscopy (Carl Zeiss Micro-Imaging GmbH, Jena, Germany) at 37 °C and 5% CO$_2$. Cell photographs were taken with 10× objectives. Images were processed with the ZEN software (Carl Zeiss). The quantification of cell number, area and aspect ratio were calculated from five images per sample using software Image J.

2.10. Statistical analysis

All statistical analysis was performed with Origin 2019 software. Mean, standard deviation, and analysis of significance were calculated through a one-way ANOVA followed by posthoc Tukey's test (indicated as *). A value of p < 0.05 was considered as significantly different. Furthermore, box-whisker diagrams are shown where appropriate. The

box indicates the 25th and 75th percentiles, the median (dash), and the mean value (black square), respectively.

3. Results and discussion

3.1. Synthesis and thermoresponsive properties of PNIPAM-grafted-chitosan (PCHI)

To obtain thermoresponsive PCHI, PNIPAM-COOH was conjugated to chitosan as presented in Fig. S1a PCHI with the degree of substitution (DS) of 0.03 obtained when a ratio of CHI/PNIPAM-COOH of 1:3 (w/w) was applied as listed in Table 1. Based on ^{1}H NMR spectrum, the calcu-lation of DS of PCHI is described in the supplementary data (Fig. S1b). A further increase of DS of CHI was not possible by increasing PNIPAM concentration, reaction time and temperature despite some findings of other groups. We assume that steric hindrance by the bulky PNIPAM molecule and CHI conformation reduces the number of amino groups along the CHI polymer accessible for *grafting-to*. Because the PEM for-mation depends on ion pairing between the oppositely charged PELs, the charge density of PELs affects the multilayer formation, as well as the structure and physiochemical characteristics of PEMs [14]. Zeta potential reflects the types of ionic species and the number of charges [39]. As shown in Table 1, CHI has a positive zeta potential value of 33.8 ± 0.6 mV, while the zeta potential of PCHI is slightly lower with 30.7 ± 0.5 mV. The decrease in potential for PCHI is due to the modification of a part of the primary amino groups of CHI with uncharged PNIPAM. In contrast, the zeta potential of the strong polyanion CS is −20.1 ± 1.8 mV (Table 1). Overall, even though the zeta potential is slightly reduced for PCHI, it may be possible to be used as a polycation for PEM formation with CS.

DLS technique is a representative method to analyze the hydrody-namic diameter and polydispersity index (PDI) of thermoresponsive polymers [40–43], here the temperature effect on PCHI was investigated
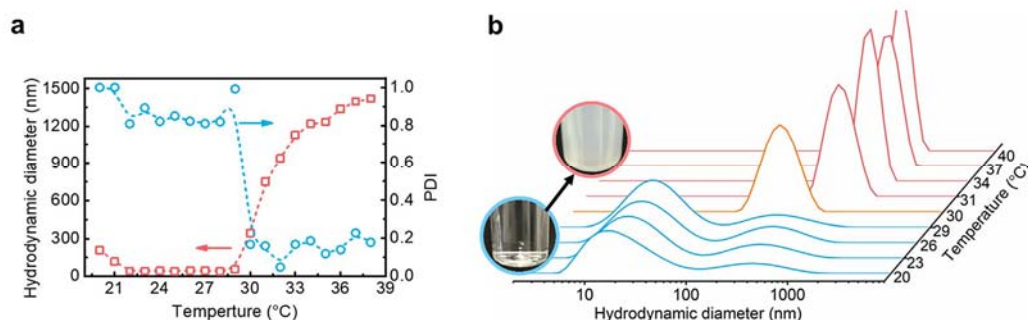

Fig. 2. Dynamic light scattering analysis of PNIPAM-*grafted*-CHI at a concentration of 1 mg mL^{-1}, pH 4 in 150 mM NaCl aqueous solution in the temperature range from 20 to 39 °C. (a) Hydrodynamic diameter (red line) and PDI (blue line). (b) Size distribution and status of solution below (transparent) and above (opaque) T$_{CP}$.
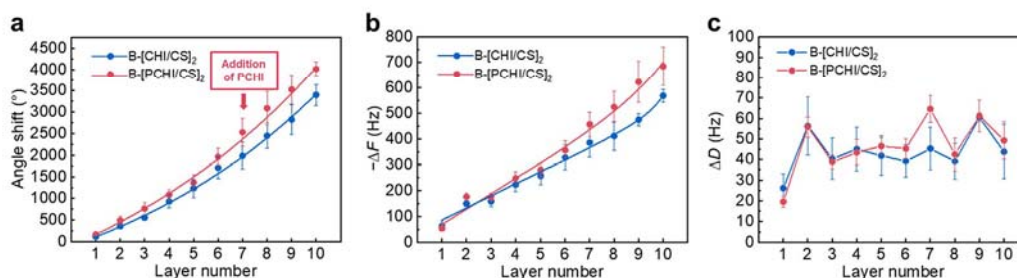

Fig. 3. Layer growth of B-[CHI/CS]$_2$ and B-[PCHI/CS]$_2$ PEMs measured from (a) angle shifts by surface plasmon resonance, and (b) frequency shift −ΔF and (c) damping shift ΔD by QCM-D measurements as a function of layer number. B-[CHI/CS]$_2$ composed of CS and CHI as a reference. [1–10; 1 = PEI, all even numbers = CS. For odd numbers, the 3rd and 5th = CHI while 7th and 9th = PCHI.] n = 20, means ± SD.

Table 2
Comparison of dry thickness (from ellipsometry) and hydrodynamic thickness (from Voigt model) of PEMs. The hydration degree was obtained according to equation (3).

Thickness (nm)	CHI/PCHI−terminated			CS−terminated		
	Ellipsometry	Voigt	Hydration	Ellipsometry	Voigt	Hydration
B-[CHI/CS]	14.8 ± 0.6	17.8 ± 0.3	16.9%	18.8 ± 1.2	19.8 ± 0.8	10.1%
B-[PCHI/CS]	16.4 ± 1.1	22.9 ± 3.9	28.4%	17.9 ± 0.4	24.0 ± 1.3	25.4%

as shown in Fig. 2a. According to recent studies [44], the cloud point temperature (T_{CP}) stands for the phase transition temperature at a specific concentration, whereas the LCST is the lowest temperature in the phase diagram with the full composition range. Therefore, the T_{CP} of PCHI prepared at a concentration of 1 mg mL^{-1}, pH 4 in 150 mM NaCl can be determined by the midpoint of the increasing hydrodynamic diameter [20].

Starting from 20 °C, the size of PCHI dramatically changed from the average 40–1200 nm when heating across T_{CP}, which was confirmed at 31 °C. In addition, PDI of PCHI was close to 1.0 at lower temperature, while the value decreased to below 0.2 above T_{CP}. PDI measured by DLS represents the size distribution corresponding to Fig. 1b [45]. At low

temperature, the hydrogen bonds between the hydrophilic group and water make PCHI soluble in the aqueous solution (transparent in Fig. 2b) [40]. The random coil-like conformation of PNIPAM chains leads to a broad size distribution and high PDI below T_{CP} [46]. It should be noted that PCHI is more extended at acidic condition because the protonation of amino groups causes intrachain charge repulsion. When heating over the T_{CP}, PNIPAM chain collapses from water-swollen coils to uniform aggregates, which consists of the hydrophobic core of PNIPAM and hydrophilic corona of CHI [40,43]. As a result, the distribution of the size became narrow with low value of PDI. Moreover, the inter-chain interaction of hydrophobic groups turns PCHI to aggregate in solution, which causes the light scattering effect (opaque appearance in Fig. 2b).
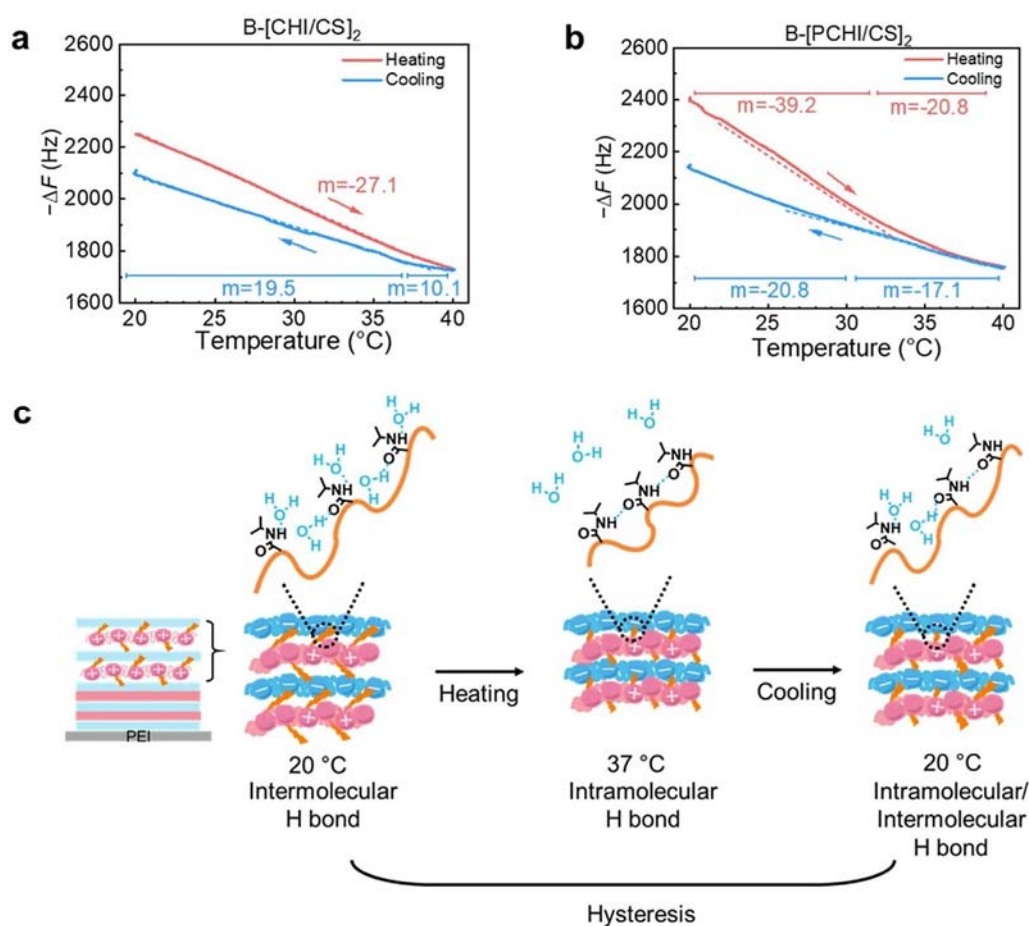

Fig. 4. Temperature dependence of frequency shift in the range of 20–40 °C for (a) B-[CHI/CS]$_2$ and (b) B-[PCHI/CS]$_2$ PEM rinsing with 150 mM NaCl buffer at pH 7.4. The term m refers to the slope of frequency shift during the temperature swap process. The red and blue lines indicate heating and cooling process, respectively. (c) Illustration represents the conformational change of the outmost layer at pH 7.4 related to hydrogen bond binding to PNIPAM from 7th to 10th layers during temperature cycle.
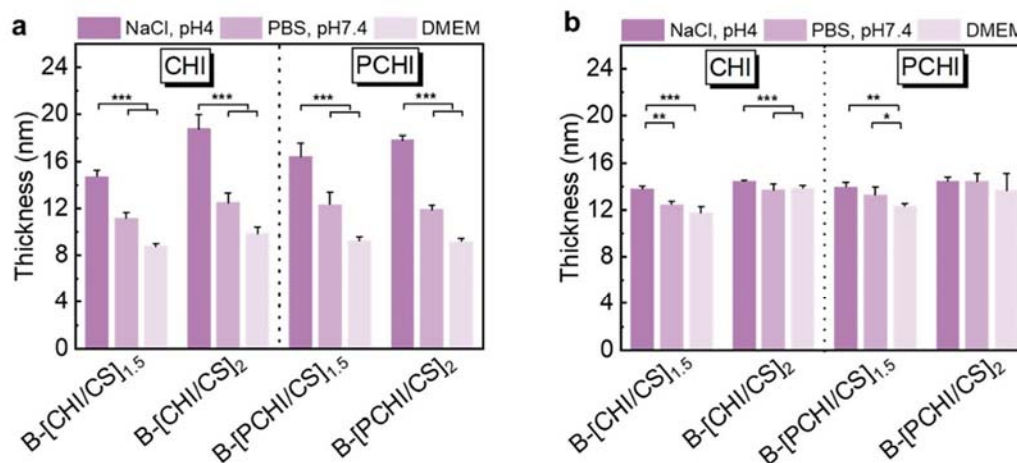
Fig. 5. Dry thickness of (a) uncrosslinked and (b) crosslinked of PEMs measured by ellipsometry after layer formation (deep pink), rinsing with PBS (pink) and with DMEM (light pink). B-[X/CS]$_{1.5}$ represented PEM with terminal layer X = CHI or PCHI, while B-[X/CS]$_2$ referred to PEM with terminal layer CS. Data represent mean ± SD, n = 4; *p ≤ 0.05, **p ≤ 0.01 and ***p ≤ 0.001.

3.2. Multilayer formation

The layer growth of B-[CHI/CS]$_2$ and B-[PCHI/CS]$_2$ was monitored by the optical SPR method. Every layer deposition increased the angle shift corresponding to an increase in the adsorbed mass [47]. Fig. 3a shows an exponential growth behavior for both PEMs, which exhibited similar trends for the initial 6 basal layers based on the same type of PELs corresponding also to findings of other groups studying PEM formation from polysaccharides [48]. Starting from the 7th layer, the angle shift for B-[PCHI/CS] increased stronger for the following layers leading to 500° more than for B-[CHI/CS] at the end of complete PEM formation. Fig. S2a elaborates the normalized angle shift where the PCHI functional layer was added to compare the differences in both multilayers. A larger angle shift was detected after deposition of PCHI on the 7th layer, which caused an approximately doubled increased value compared to deposition of CHI owing to the higher molecular weight of PCHI similar to findings in other studies [30,49].

Different to SPR excluding solvent mass, QCM-D measurement was employed to determine the whole PEM including the 'wet mass' with the coupled water. According to Voigt equation (eqation1), the mass change is proportional to the negative frequency shift −ΔF, reflecting the matter adsorbed on the surface of gold sensor. QCM-D provided similar results to SPR in terms of the adsorbed layer after the addition of PCHI as shown in Fig. 3b and Fig. S2b. More frequency change was detected for B-[PCHI/CS]$_2$ PEM, implicating larger quantity of adsorbed PELs plus intrinsic water than for B-[CHI/CS]$_2$ PEM, which is comparable to findings of SPR studies when water is not involved.

The damping shift measured by QCM-D was monitored to evaluate the mechanical properties of PEMs on the sensor surface after each adsorption step (Fig. 3c). The presence of damping shift ΔD indicated that the absorbed PEM has viscoelastic properties with higher values associated to a softer film, whereas a dissipation is not seen in rigid films [48]. There was an increase in ΔD upon addition of the CS and CHI for the basal layer due to the existence of amino groups, sulfate groups, carboxyl groups, and hydroxyl groups to couple with more water and remained stable to the 6th layers, which seems to form intermingling layers. Strikingly, the measured ΔD increased sharply after PCHI adsorption from the 7th layer compared to CHI adsorption but decreased for the next CS deposition followed by similar trends for both PEMs until the process was completed. Our recent study on PCHI-containing multilayers using heparin as polyanion demonstrated that PNIPAM chains extended at 25 °C coupled more water molecules leading to the remarked swelling of the

PEM and increased ΔD [30]. It has been suggested in previous studies that the added PEL with smaller molecular weight displace small counter ions and water molecules to ionically pair with the prior adsorbed PEL, resulting in denser and more rigid multilayers [18,50]. The hydrogen bonds between PCHI and water were interrupted by following CS deposition bringing out a drop in dissipation values and de-swelling of the film [30]. Overall, despite potential steric hindrance effect of bulky PNIPAM as side chains on and the slightly reduced charge density of CHI, PCHI permits formation of PEM with CS.

Dry thickness could not be calculated with the results of SPR measurement due to unknown changes of refractive index during layer deposition. Hence, in order to know the effect of PNIPAM on water content of PEM, the hydration degree of the terminal CHI/PCHI and CS layers was calculated by comparison of the dry and hydrodynamic thickness obtained from ellipsometry and QCM-D, respectively (Table 2). In general, multilayers composed of polysaccharides or GAGs are soft and hydrated attributed to the presence of hydrophilic functional groups [51, 52]. Here Voigt model was applied to estimate the viscoelastic thickness of the PEMs. Indeed, the hydrodynamic thickness is larger than the dry thickness particularly around 7 nm more in B-[PCHI/CS] PEM, which shows the remarkable hydration degree of 25–28% compared to less than 20% in B-[CHI/CS] PEM. When applying the following CS layer, it caused dehydration in both PEM that is in line with the decreasing dampening shifts. Although the stretched conformation of PNIPAM with more water below LCST seems to reduce the extent of dehydration in CS-terminated PEM, lesser ion pairing due to occupation of a part of amino groups in CHI should also be considered as a reason.

3.3. Temperature-dependent change of PEM mass

To study if conformational changes of PNIPAM bound to CHI during changes of temperature are related to swelling and shrinking of PEM, studies with QCM-D were carried out. Because the PEMs will be further studied in cell experiments, the measurements were carried out with NaCl solution at physiological pH 7.4 in the temperature range of 20–40 °C. Fig. 4a and b depict the temperature effect on the B-[CHI/CS]$_2$ and B-[PCHI/CS]$_2$ PEMs at pH 7.4. During the heating process, −ΔF decreased with the increasing temperature in both cases, indicating that the mass of the multilayer decreased on the resonator surface. Oppositely, −ΔF increased upon cooling process. It should be noted that the changes in viscosity and density of the running buffer with rising temperature contribute to the decrease in −ΔF [53]. Thus, NaCl buffer at 7.4 were
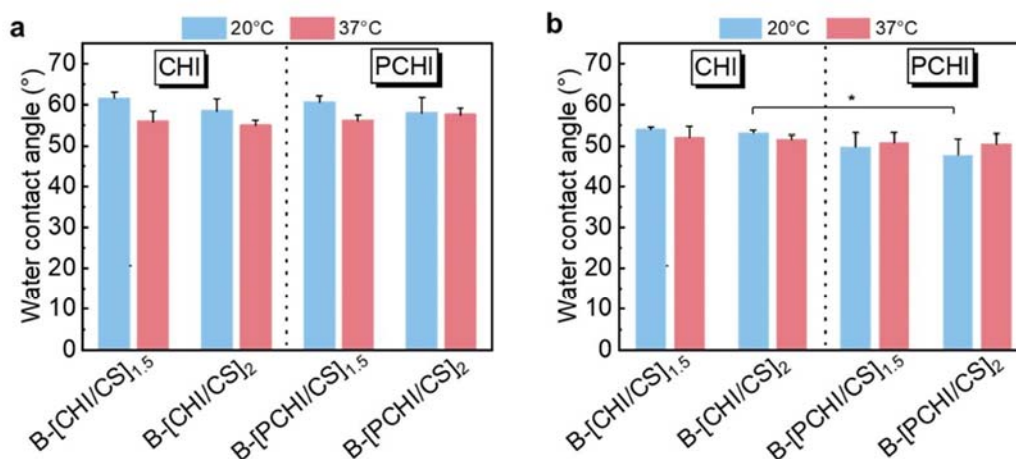
Fig. 6. Static water contact angle measurements of (a) uncrosslinked and (b) crosslinked PEMs with CHI/PCHI or CS terminal layer at 20 °C (blue bar) and 37 °C (red bar). Data represent mean ± SD, n = 5; *p ≤ 0.05.

applied to the bare gold sensor and ensured no substantial differences in $-\Delta F$ during temperature swaps in supporting information Fig. S3. It can be also assumed that no change in PEM mass adsorbed on the surface occurred during the experiment. Hence, the variation in the amount of water molecules present in the PEM must account for the change in ΔF [54]. Interestingly, when NaCl solution was flushed into the dry sensors to achieve a wet state at 20 °C in the beginning, higher $-\Delta F$ in B-[PCHI/CS]$_2$ PEM (200 Hz more) than B-[CHI/CS]$_2$ indicates higher water uptake due to the presence of PNIPAM. Another important observation is that the slope (m) of $-\Delta F$ was −39.2 below 31 °C and decreased to −20.8 above this temperature for B-[PCHI/CS]$_2$ PEM during heating cycle, while B-[CHI/CS]$_2$ PEM showed a constant slope of −27.1 in $-\Delta F$. The reason for the significantly steeper slope of B-[PCHI/CS]$_2$ PEM is that the water could be released during the heating process as PNIPAM gradually collapsed and underwent the coil-globular transition at 31 °C leading to the dehydration of the film. The slope became flatter above 31 °C because low quantity of water diffused out from PNIPAM film [54].

It was observed that both PEM systems showed two different paths during the cooling and heating cycles meaning a hysteresis effect. Upon heating, interdigitation between adjacent layers becomes stronger restricting the mobility of the polymer chains [33]. In other words, polymer layers undergo a rearrangement leading to the irreversible swelling after cooling [27,53]. In addition, hysteresis behavior is more obvious in B-[PCHI/CS]$_2$ PEM. The reason could be the additional hydrogen bonds formed between the collapsed PNIPAM chains upon heating across the coil-to-globular transition, consequently hindering the rehydration of the chains when cooling back to 20 °C (Fig. 4c) [55]. The behavior at pH 4 in Fig. S4 shows less pronounced temperature-induced change of PNIPAM in multilayer due to stronger ion pairing. Overall, despite less mobility of PNIPAM in the multilayer, the findings demonstrates that PEM with PCI as polycation respond to temperature.

3.4. Stability of PEMs

Since the integrity and poor cell adhesive surface of PEMs composed of polysaccharide PELs have been often a main issue under physiological conditions, covalent cross-linking was introduced between carboxylic groups of CS and amino groups of CHI or PCHI [22,30,56]. Fig. 5 depicts the measured dry thicknesses of PEMs by ellipsometry after PEM formation at pH 4 followed by rinsing with PBS and cell culture medium DMEM under physiological conditions. The overall average thickness of uncrosslinked PEMs was around 14.7–18.8 nm depending on the

terminal layer (Fig. 5a). After rinsing the PEMs with the two media at pH 7.4, the overall thickness was reduced to half probably due to the deprotonation of the amino groups of CHI (pK$_a$ ≈ 6.5) at pH 7.4 and the different ion content of medium (phosphate and other anions) resulted in a partial decomposition of PEMs [22]. On the other hand, crosslinked PEMs show a lower thickness about 13.9–14.5 nm (Fig. 5b). The thickness reductions after crosslinking indicates the formation of more compact PEM which have been also observed in other PEMs based on polysaccharides [22,57]. The difference of final average thickness between the crosslinked B-[CHI/CS] PEMs and B-[PCHI/CS] PEMs was not significant. In general, the PEM thickness increased as the molecular weight of the PEL increased due to more coiled conformation [15,57]. Nonetheless, the inclusion of the PCHI functional layer had no discernible effect on the thickness of our systems probably because the measurements were done under dehydrated states resulting in identical values to B-[CHI/CS] PEMs. Moreover, only a decrease of less than 2 nm of crosslinked PEMs after medium rinsing revealed that the formation of amide bonds strengthened the stability of PEMs despite the lower charge density of PCHI.

3.5. Temperature effect on surface wettability

Surface wettability is dependent on the surface composition and represents a prominent factor for the interaction of materials with proteins and cells [3,58]. Therefore, the wettability of the terminal layers with and without crosslinking was investigated by static water contact angle (WCA) measurement after rinsing PEM with PBS and DMEM (Fig. 6a and b). In general, CS coating (WCA ~ 25° − 30°) is supposed to increase the wettability of PEM different to the less wettable chitosan (WCA ~ 90°) [59,60]. Here only slight differences in WCA between the alternating layers indicate the intermingling of PEL corresponding to QCM results and previous studies [17,61]. The average WCA in uncrosslinked PEMs was about 55–61° compared to the noticeable 5° decrease of WCA after crosslinking. This is in line with previous studies using carbodiimide chemistry for crosslinking multilayers composed of polysaccharides and related to the introduction of hydrophilic amides and increasing roughness [62,63].

On the other hand, regarding the surface wettability which could be affected by coil-to-globular transition of PNIPAM [64], the WCA of PEMs was studied at 20 °C and 37 °C. At 20 °C, the values of WCA were slightly lower for PCHI−PEMs than CHI-PEMs, owing to hydrophilic groups of PNIPAM in extended state coupling water molecules below the T$_{CP}$. At 37 °C, the values of WCA for uncrosslinked CHI−PEMs were found 5°
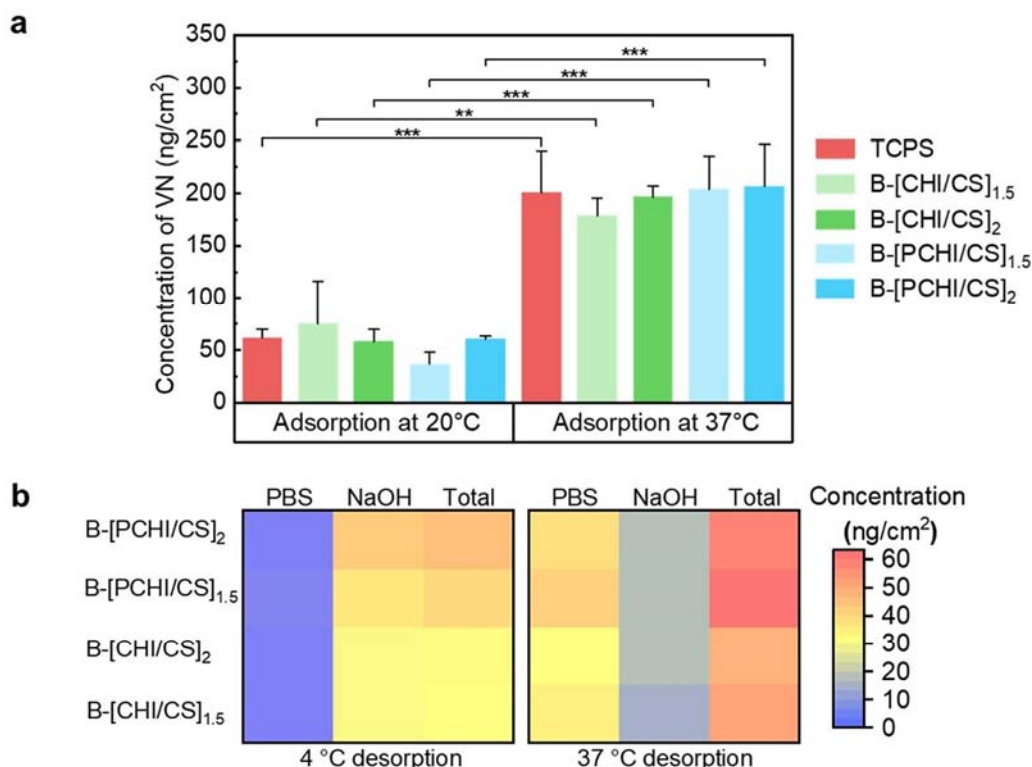
Fig. 7. (a) Temperature effect on vitronectin adsorption onto TCPS, and crosslinked PEMs with CHI/PCHI or CS terminal layer at 20 °C and 37 °C. n = 4, mean ± SD, **p ≤ 0.01 and ***p ≤ 0.001. (b) Temperature effect on vitronectin desorption at 4 °C and 37 °C from PEMs pre-adsorbed with vitronectin at 37 °C in PBS, followed by extraction in 200 mM NaOH for calculation of the cumulative amount of vitronectin.

lower than 20 °C. Although the same trend was also observed for uncrosslinked PCHI−PEMs, the change was rather limited (<5°). In comparison, the WCA for crosslinked CHI−PEMs were lower at 37 °C than 20 °C but less than 5° difference. Specially, the WCA for crosslinked PCHI−PEMs were 1–3° higher at 37 °C than 20 °C, showing an opposite trend to uncrosslinked ones. The results reveal that the temperature has the impact on the surface wettability PCHI-PEM. The reason for lower WCA of uncrosslinked PEMs at higher temperature is probably attributed to thermally-induced rearrangement of PEMs and the decreased surface tension of water upon heating [27,65]. Even though the transition temperature of the uncrosslinked PCHI-PEM was found at 31 °C from QCM results, partial decomposition of uncrosslinked PEMs after rinsing at pH 7.4 did not show visible thermal sensibility related to PNIPAM in WCA. By contrast, the crosslinking seems to restrict some extent of rearrangement and decomposition of the polymers, which is correlated to lower WCA difference in crosslinked CHI-PEMs. Hence, with the enhanced stability, lower wettability in crosslinked PCHI−PEMs at high temperature is mainly contributed by domination of hydrophobic groups and collapse of PNIPAM [49].

3.6. FITC-labeled VN adsorption and desorption

Protein adsorption is dependent on surface properties of materials and related to adhesion of cells [10,66]. Vitronectin (VN) as a major cell adhesive protein secreted by cells or present in serum promotes cell adhesion and spreading even at very low concentrations [67]. Here FITC-VN adsorption was studied on TCPS as tissue culture related control and crosslinked PEMs at different temperatures at 20 (below T_{CP}) and 37 °C (above T_{CP}) shown in Fig. 7a. The values of adsorbed quantities of VN

are based on the calibration curve shown in Fig. S5a. Significantly higher amounts of adsorbed VN with more than 178 ng/cm^2 on all PEM were detected at 37 °C in comparison to only around 36–75 ng/cm^2 adsorbed at 20 °C. A similar trend of the temperature effect was also reported in other study but using ovalbumin on different PNIPAM-modified multilayers [26,64]. According to the change of Gibbs free energy (ΔG), which is defined as

$$\Delta G = \Delta H - T \Delta S \qquad (4)$$

(H: enthalpy; T: temperature; S: entropy), protein adsorption can occur if ΔG < 0 [68]. When temperature is increased, entropy is gained by the release of adsorbed water molecules from the surface and structural rearrangements within the protein [68]. Thus, this thermodynamically driven process causes G of the system to decrease and promotes protein adsorption through hydrophobic interaction between the surface and protein. When integrating PNIPAM in PEMs, the amounts of VN were even greater at 37 °C than B-[CHI/CS] PEMs that seem to corroborate the findings of increased WCA for B-[PCHI/CS] PEM at 37 °C. Although the change in WCA is not significant, several reports claimed that the protein adsorption is mainly dependent on the hydrophobic interaction of dehydrated PNIPAM segments [27,64,69]. On the other hand, CS as GAG with sulfate groups has high affinity to the heparin-binding domain of VN [16]. As a result, higher amounts of VN adsorption were observed on the CS-terminated surfaces as shown in Fig. 7a as well.

Regarding the temperature effect on PNIPAM conformation, VN preadsorbed on PEM films at 37 °C was chosen to study the release/desorption of the protein at either 4 °C (below T_{CP}) or 37 °C (above T_{CP}), as shown in Fig. 7b. In the case of protein desorption in PBS during the first 24 h, obviously higher amounts of VN were released at 37 °C (>30
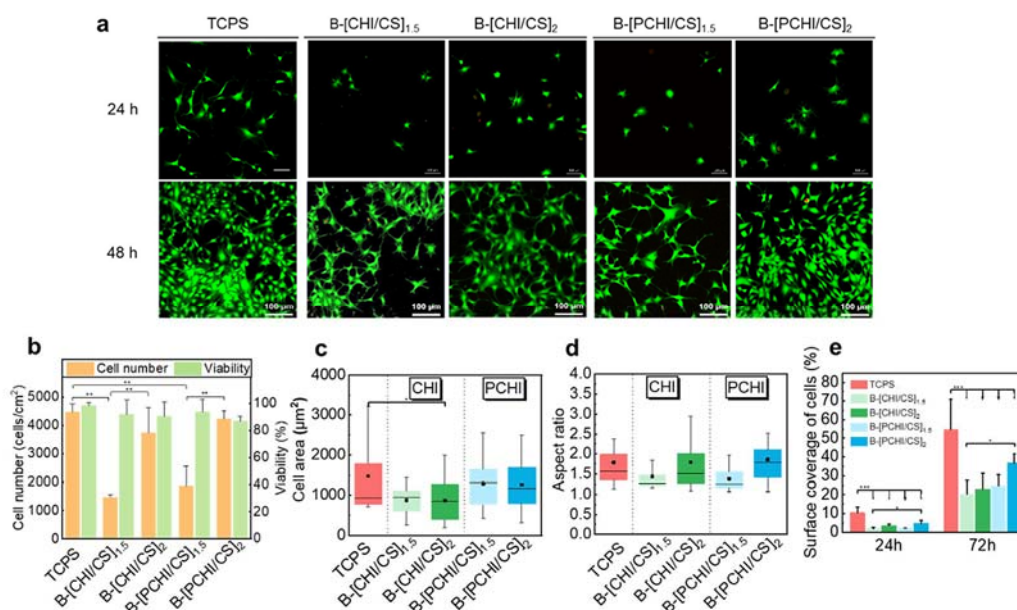
Fig. 8. Viability test and quantification of C3H10T1/2 cells on crosslinked multilayers with PCHI/CHI or CS terminal layers. (a) Confocal images of live (green) and dead (red) cells after 24 h and 72 h culture. Scale bar: 100 μm. Measurements of (b) cell number and viability and (c) cell area and aspect ratio after 24 h. Box plot with whisper represents the first and third quartiles, medians and means. Cell proliferation analyzed by surface coverage after 24 h and 72 h. Cell seeded on tissue culture polystyrene (TCPS) as a control; mean value ± SD with significance level of *p ≤ 0.05 and ***p ≤ 0.001.

ng/cm²) than 4 °C (<10 ng/cm²) from all PEMs. It has been already known that the enhanced protein mobility is kinetically driven by higher temperature [68]. To mobilize any remaining irreversibly adsorbed FITC-VN after the desorption step in PBS, a further extraction was done by NaOH hydrolysis as described in a previous work [70]. Here it was found that the extracted amount was 10 ng/cm² higher in samples processed at 4 °C compared to 37 °C. This is related to the higher amount of VN already released at 37 °C during incubation in PBS. Concerning the cell environment at 37 °C, it is essential to investigate the retention of VN on PEMs at this temperature. Slightly larger amount of VN with 10 ng/cm² was released from B-[PCHI/CS] PEMs, which might be linked to higher adsorption at 37 °C. Importantly, PEMs with CS terminal layers retained more VN on the surface owing to the specific interaction between CS and heparin-binding domain of VN [16]. Compared to almost 100% amount of VN desorbed from TCPS in Fig. S5b, the results suggest the PEM containing PNIPAM with CS terminal layer represents a promising bioactive surface.

3.7. Cytocompatibility studies

Cytocompatibility studies were done with the multipotent embryonic mouse fibroblast cell line that can differentiate into adipocytes, chondrocytes and osteocytes [71]. Since the crosslinking with EDC/NHS can exert some detrimental effects on cells, the cytotoxicity of both crosslinked B-[CHI/CS] and B-[PCHI/CS] PEMs was studied by quantification of the live (green fluorescence)/dead (red fluorescence) C3H10T1/2 cell staining after 24 h and 72 h cultivation (Fig. 8). TCPS as a cell-adhesive and biocompatible material was used as a reference. After 24 h, the CLSM images (Fig. 8a, upper row) show a slightly denser population of viable cells with only few dead cells on CS terminal layers particularly in the presence of PNIPAM. Cell viability is quantified in Fig. 8b showing more than 85% viable cells on PEMs with different terminal layers, while around 98% cells are alive on TCPS. The cell number and area of living cells were also quantified from the images. Notably, twice more cells adhered on CS terminal layers than on the CHI or PCHI terminal layers

(Fig. 8b). Likewise, cell spreading in terms of cell area and aspect ratio indicates that cells were larger and adopted a more elongated shape on the CS terminal layers (Fig. 8c and d). In particular, when cell were plated on PEMs with PCHI, higher cell number and spreading are observed, which are similar to cells cultured on TCPS. Further observations on cell proliferation after 72 h in Fig. 8a (lower row) shows that cells grow on all surfaces. The surface coverage of viable cells after 24 h and 72 h was evaluated from the images. Fig. 8e shows obviously the greatest cell expansion on the crosslinked B-[PCHI/CS]₂ PEM among the other PEMs after 72 h culture. The observation that a lower number of cells adhered on CHI or PCHI terminal layers during the first 24 h, was in line with little growth after 72 h.

Cell adhesion and subsequent spreading on biomaterials surfaces are crucial to govern further cell fates like survival, growth and differentiation [1]. Controlling surface properties like wettability of biocompatible materials is important for cell adhesion on the surfaces [2]. Here we confirmed by QCM and WCA studies that B-[PCHI/CS] PEM exhibiting a more dehydrated and less hydrophilic surfaces at 37 °C (above T_{CP}) promotes cell adhesion and growth due to hydrophobic interaction [10]. This is also related to higher protein adsorption on B-[PCHI/CS] PEM because VN is present in the serum of the culture medium and can support cell adhesion. Cell adhesion on the biomaterial surface is strongly dependent on the specific integrin-binding with adhesive proteins like VN, which could be attributed to ligation to $\alpha_v\beta_3$ integrin [9]. Other studies also found that the number of adhered cells and the rates of cell proliferation can be enhanced on surfaces modified with PNIPAM [72, 73]. Our previous study suggested that chemical crosslinking efficiently improves the stability of PEM and cell adhesion at physiological condition [30]. One of the reasons for increased cell adhesion and spreading on crosslinked PEM is their increased stiffness [74]. This enhances cell mechanosensing through integrins crucial for the contractile activity of actin-myosin cytoskeleton through RhoA/ROCK signaling pathway that promotes focal adhesion formation and spreading of the cells [75]. On the other hand, crosslinking stabilized the integrity of PEMs since CS remained tightly fixed in the terminal layer. CS with sulfate groups

provides the advantage of binding more adhesive proteins secreted by cells (e.g., fibronectin) and from serum (e.g., vitronectin) on the surface due to the specific interaction of protein heparin-binding domains promoting cell adhesion and growth through integrin ligation related to B-[X/CS]$_2$ [76]. On the other hand, B-[X/CS]$_{1.5}$ with either CHI or PCHI as terminal layer does not possess such specific interaction with adhesive proteins like fibronectin and vitronectin which is related to lower cell adhesion. Thus, the results of cytocompatibility studies and cell adhesion/growth underline that the use of CS as biogenic polyanion is crucial for improvement of bioactivity of PCHI−PEMs.

4. Conclusion

A new kind of bioactive and thermoresponsive PEMs for cell culture substrates based on LbL sequential assembly of PCHI and CS is explored here. PCHI with low grafting density of PNIPAM can exhibit thermoresponsive properties and forms intermingling multilayer with CS at pH 4 despite its bulky structure at 25 °C (below T$_{CP}$). Covalent cross-linking is beneficial to effectively strengthen the stability of PEMs under physiological condition by the amide bond formation between amino groups of CHI and carboxylic groups of CS. Most importantly, not only less hydrophilicity of PNIPAM but also the terminal layer using CS for the cross-linked PCHI/CS−PEM play vital roles in promoting VN adsorption and stem cell adhesion at 37 °C. Overall, PEMs combined with PNIPAM and bioactive polysaccharides like CS suggest greater bioactivity, non-toxicity, and stimuli-responsivity for surface coatings. Hence, they are interesting for the application as culture substrata for stem and other cells during their in vitro culture.

CRediT authorship contribution statement

Yi-Tung Lu: Methodology, Validation, Investigation, Data curation, Writing – original draft. **Pei-Tzu Hung:** Investigation, Formal analysis, Data curation, Visualization, Writing – original draft. **Kui Zeng:** Methodology, Writing – review & editing. **Christian Woelk:** Methodology, Resources. **Bodo Fuhrmann:** Methodology, Resources. **Kai Zhang:** Conceptualization, Funding acquisition, Writing – review & editing. **Thomas Groth:** Supervision, Funding acquisition, Project administration, Conceptualization, Writing – review & editing.

Declaration of competing interest

The authors declare that they have no conflict of interest.

Acknowledgement

Appendix A. Supplementary data

Supplementary data to this article can be found online at https://doi.org/10.1016/j.smaim.2022.11.008.

References

[1] O. Guillame-Gentil, O. Semenov, A.S. Roca, T. Groth, R. Zahn, J. Vörös, M. Zenobi-Wong, Engineering the extracellular environment: strategies for building 2D and 3D cellular structures, Adv. Mater. 22 (2010) 5443–5462.

[2] M. Rahmati, E.A. Silva, J.E. Reseland, C.A. Heyward, H.J. Haugen, Biological responses to physicochemical properties of biomaterial surface, Chem. Soc. Rev. 49 (2020) 5178–5224.

[3] G. Altankov, F. Grinnell, T. Groth, Studies on the biocompatibility of materials: fibroblast reorganization of substratum-bound fibronectin on surfaces varying in wettability, J. Biomed. Mater. Res. 30 (1996) 385–391.

[4] M.S. Niepel, F. Almouhanna, B.K. Ekambaram, M. Menzel, A. Heilmann, T. Groth, Cross-linking multilayers of poly-l-lysine and hyaluronic acid: effect on mesenchymal stem cell behavior, Int. J. Artif. Organs 41 (2018) 223–235.

[5] G. Altankov, K. Richau, T. Groth, The role of surface zeta potential and substratum chemistry for regulation of dermal fibroblasts interaction, Mat.-wiss. u. Werkstofftech. 34 (2003) 1120–1128.

[6] M.S. Niepel, B. Fuhrmann, H.S. Leipner, T. Groth, Nanoscaled surface patterns influence adhesion and growth of human dermal fibroblasts, Langmuir 29 (2013) 13278–13290.

[7] P. Esmaeilzadeh, T. Groth, Switchable and obedient interfacial properties that grant new biomedical applications, ACS Appl. Mater. Interfaces 11 (2019) 25637–25653.

[8] K. Nagase, M. Yamato, H. Kanazawa, T. Okano, Poly(N-isopropylacrylamide)-based thermoresponsive surfaces provide new types of biomedical applications, Biomaterials 153 (2018) 27–48.

[9] F. Doberenz, K. Zeng, C. Willems, K. Zhang, T. Groth, Thermoresponsive polymers and their biomedical application in tissue engineering - a review, J. Mater. Chem. B 8 (2020) 607–628.

[10] M. Prawatborisut, S. Jiang, J. Oberländer, V. Mailänder, D. Crespy, K. Landfester, Modulating protein corona and materials–cell interactions with temperature-responsive materials, Adv. Funct. Mater. 32 (2022), 2106353.

[11] X. Fan, M.E. Nash, A.V. Gorelov, F.P. Barry, G. Shaw, Y.A. Rochev, Thermoresponsive substrates used for the growth and controlled differentiation of human mesenchymal stem cells, Macromol. Rapid Commun. 36 (2015) 1897–1901.

[12] I.-C. Peng, C.-C. Yeh, Y.-T. Lu, S. Muduli, Q.-D. Ling, A.A. Alarfaj, M.A. Munusamy, S.S. Kumar, K. Murugan, H. Lee, Y. Chang, A. Higuchi, Continuous harvest of stem cells via partial detachment from thermoresponsive nanobrush surfaces, Biomaterials 76 (2016) 76–86.

[13] T.-C. Sung, H.C. Su, Q.-D. Ling, S.S. Kumar, Y. Chang, S.-T. Hsu, A. Higuchi, Efficient differentiation of human pluripotent stem cells into cardiomyocytes on cell sorting thermoresponsive surface, Biomaterials 253 (2020), 120060.

[14] J. Borges, J.F. Mano, Molecular interactions driving the layer-by-layer assembly of multilayers, Chem. Rev. 114 (2014) 8883–8942.

[15] J.M. Silva, R.L. Reis, J.F. Mano, Biomimetic extracellular environment based on natural Origin polyelectrolyte multilayers, Small 12 (2016) 4308–4342.

[16] Y. Yang, Y.-T. Lu, K. Zeng, T. Heinze, T. Groth, K. Zhang, Recent progress on cellulose-based ionic compounds for biomaterials, Adv. Mater. 33 (2021), e2000717.

[17] R. Anouz, A. Repanas, E. Schwarz, T. Groth, Novel surface coatings using oxidized glycosaminoglycans as delivery systems of bone morphogenetic protein 2 (BMP-2) for bone regeneration, Macromol. Biosci. 18 (2018), e1800283.

[18] J.M. Silva, N. Georgi, R. Costa, P. Sher, R.L. Reis, C.A. van Blitterswijk, M. Karperien, J.F. Mano, Nanostructured 3D constructs based on chitosan and chondroitin sulphate multilayers for cartilage tissue engineering, PLoS One 8 (2013), e55451.

[19] Y.A. Brito Barrera, G. Hause, M. Menzel, C.E.H. Schmelzer, E. Lehner, K. Mäder, C. Wölk, T. Groth, Engineering osteogenic microenvironments by combination of multilayers from collagen type I and chondroitin sulfate with novel cationic liposomes, Mater, Today Bio 7 (2020), 100071.

[20] I. Marsili, M. Dal Bo, F. Berti, G. Toffoli, Chitosan-based biocompatible copolymers for thermoresponsive drug delivery systems: on the development of a standardization system, Pharmaceutics 13 (2021).

[21] L. Richert, F. Boulmedais, P. Lavalle, J. Mutterer, E. Ferreux, G. Decher, P. Schaaf, J.-C. Voegel, C. Picart, Improvement of stability and cell adhesion properties of polyelectrolyte multilayer films by chemical cross-linking, Biomacromolecules 5 (2004) 284–294.

[22] G. Apte, A. Repanas, C. Willems, A. Mujtaba, C.E.H. Schmelzer, A. Raichur, F. Syrowatka, T. Groth, Effect of different crosslinking strategies on physical properties and biocompatibility of freestanding multilayer films made of alginate and chitosan, Macromol. Biosci. 19 (2019), e1900181.

[23] L. Xu, H. Wang, Z. Chu, L. Cai, H. Shi, C. Zhu, D. Pan, J. Pan, X. Fei, Y. Lei, Temperature-responsive multilayer films of micelle-based composites for controlled release of a third-generation EGFR inhibitor, ACS Appl. Polym. Mater. 2 (2020) 741–750.

[24] L. Xu, X. Zhang, Z. Chu, H. Wang, Y. Li, X. Shen, L. Cai, H. Shi, C. Zhu, J. Pan, D. Pan, Temperature-responsive multilayer films based on block copolymer-coated silica nanoparticles for long-term release of Favipiravir, ACS Appl. Nano Mater. 4 (2021) 14014–14025.

[25] T. Liao, M.D. Moussallem, J. Kim, J.B. Schlenoff, T. Ma, N-isopropylacrylamide-based thermoresponsive polyelectrolyte multilayer films for human mesenchymal stem cell expansion, Biotechnol. Prog. 26 (2010) 1705–1713.

[26] A. Osypova, D. Magnin, P. Sibret, A. Aqil, C. Jérôme, C. Dupont-Gillain, C.-M. Pradier, S. Demoustier-Champagne, J. Landoulsi, Dual stimuli-responsive coating designed through layer-by-layer assembly of PAA-b-PNIPAM block copolymers for the control of protein adsorption, Soft Matter 11 (2015) 8154–8164.

[27] A. Osypova, C.-A. Fustin, C.-M. Pradier, J. Landoulsi, S. Demoustier-Champagne, Factors impacting protein adsorption on layer-by-layer assembled stimuli-responsive thin films, Eur. Polym. J. 95 (2017) 195–206.

[28] J.-P. Chen, T.-H. Cheng, Thermo-responsive chitosan-graft-poly(N-isopropylacrylamide) injectable hydrogel for cultivation of chondrocytes and meniscus cells, Macromol. Biosci. 6 (2006) 1026–1039.

[29] S.B. Lee, D. in Ha, S.K. Cho, S.J. Kim, Y.M. Lee, Temperature/pH-sensitive comb-type graft hydrogels composed of chitosan and poly(N-isopropylacrylamide), J. Appl. Polym. Sci. 92 (2004) 2612–2620.

[30] Y.-T. Lu, K. Zeng, B. Fuhrmann, C. Woelk, K. Zhang, T. Groth, Engineering of stable cross-linked multilayers based on thermo-responsive PNIPAM-grafted-chitosan/

heparin to tailor their physiochemical properties and biocompatibility, ACS Appl. Mater. Interfaces 14 (2022) 29550–29562.

[31] J. Giselbrecht, C. Janich, S.R. Pinnapireddy, G. Hause, U. Bakowsky, C. Wölk, A. Langner, Overcoming the polycation dilemma - explorative studies to characterise the efficiency and biocompatibility of newly designed lipofection reagents, Int. J. Pharm. 541 (2018) 81–92.

[32] J.A. Jaber, J.B. Schlenoff, Polyelectrolyte multilayers with reversible thermal responsivity, Macromolecules 38 (2005) 1300–1306.

[33] K. Glinel, C. Déjugnat, M. Prevot, B. Schöler, M. Schönhoff, R.v. Klitzing, Responsive polyelectrolyte multilayers, Colloids Surf. A Physicochem. Eng. Asp. 303 (2007) 3–13.

[34] R.B.M. Schasfoort, Chapter 1. Introduction to surface plasmon resonance, in: R.B.M. Schasfoort (Ed.), Handbook of Surface Plasmon Resonance, Royal Society of Chemistry, Cambridge, 2017, pp. 1–26.

[35] G. Sauerbrey, Verwendung von Schwingquarzen zur Wgung dnner Schichten und zur Mikrowgung, Z. Phys. 155 (1959) 206–222.

[36] M.V. Voinova, M. Rodahl, M. Jonson, B. Kasemo, Viscoelastic acoustic response of layered polymer films at fluid-solid interfaces: continuum mechanics approach, Phys. Scripta 59 (1999) 391–396.

[37] J.M. Silva, J.R. García, A.J. García, J.F. Mano, Tuning cell adhesive properties via layer-by-layer assembly of chitosan and alginate, Acta Biomater. 51 (2017) 279–293.

[38] J. Almodóvar, L.W. Place, J. Gogolski, K. Erickson, M.J. Kipper, Layer-by-layer assembly of polysaccharide-based polyelectrolyte multilayers: a spectroscopic study of hydrophilicity, composition, and ion pairing, Biomacromolecules 12 (2011) 2755–2765.

[39] J.D. Clogston, A.K. Patri, Zeta potential measurement, Methods Mol. Biol. 697 (2011) 63–70.

[40] H. Bao, L. Li, W.C. Leong, L.H. Gan, Thermo-responsive association of chitosan-graft-poly(N-isopropylacrylamide) in aqueous solutions, J. Phys. Chem. B 114 (2010) 10666–10673.

[41] L. Hou, P. Wu, LCST transition of PNIPAM-b-PVCL in water: cooperative aggregation of two distinct thermally responsive segments, Soft Matter 10 (2014) 3578–3586.

[42] K. Zeng, F. Doberenz, Y.-T. Lu, J.P. Nong, S. Fischer, T. Groth, K. Zhang, Synthesis of thermoresponsive PNIPAM-grafted cellulose sulfates for bioactive multilayers via layer-by-layer technique, ACS Appl. Mater. Interfaces 14 (2022) 48384–48396.

[43] C. Chen, M. Liu, C. Gao, S. Lü, J. Chen, X. Yu, E. Ding, C. Yu, J. Guo, G. Cui, A convenient way to synthesize comb-shaped chitosan-graft-poly (N-isopropylacrylamide) copolymer, Carbohydr. Polym. 92 (2013) 621–628.

[44] Q. Zhang, C. Weber, U.S. Schubert, R. Hoogenboom, Thermoresponsive polymers with lower critical solution temperature: from fundamental aspects and measuring techniques to recommended turbidimetry conditions, Mater. Horiz. 4 (2017) 109–116.

[45] M. Danaei, M. Dehghankhold, S. Ataei, F. Hasanzadeh Davarani, R. Javanmard, A. Dokhani, S. Khorasani, M.R. Mozafari, Impact of particle size and polydispersity index on the clinical applications of lipidic nanocarrier systems, Pharmaceutics 10 (2018).

[46] X. Wang, X. Qiu, C. Wu, Comparison of the coil-to-globule and the globule-to-coil transitions of a single poly(N -isopropylacrylamide) homopolymer chain in water, Macromolecules 31 (1998) 2972–2976.

[47] N. Aggarwal, N. Altgärde, S. Svedhem, K. Zhang, S. Fischer, T. Groth, Effect of molecular composition of heparin and cellulose sulfate on multilayer formation and cell response, Langmuir 29 (2013) 13853–13864.

[48] C. Picart, Polyelectrolyte multilayer films: from physico-chemical properties to the control of cellular processes, Curr. Med. Chem. 15 (2008) 685–697.

[49] G.V. Martins, J.F. Mano, N.M. Alves, Dual responsive nanostructured surfaces for biomedical applications, Langmuir 27 (2011) 8415–8423.

[50] S.T. Dubas, J.B. Schlenoff, Factors controlling the growth of polyelectrolyte multilayers, Macromolecules 32 (1999) 8153–8160.

[51] N. Aggarwal, N. Altgärde, S. Svedhem, G. Michanetzis, Y. Missirlis, T. Groth, Tuning cell adhesion and growth on biomimetic polyelectrolyte multilayers by variation of pH during layer-by-layer assembly, Macromol. Biosci. 13 (2013) 1327–1338.

[52] M.P. Sousa, F. Cleymand, J.F. Mano, Elastic chitosan/chondroitin sulfate multilayer membranes, Biomed. Mater. 11 (2016), 35008.

[53] M.A. Plunkett, Z. Wang, M.W. Rutland, D. Johannsmann, Adsorption of pNIPAM layers on hydrophobic gold surfaces, measured in situ by QCM and SPR, Langmuir 19 (2003) 6837–6844.

[54] G. Zhang, Study on conformation change of thermally sensitive linear grafted poly(N-isopropylacrylamide) chains by quartz crystal microbalance, Macromolecules 37 (2004) 6553–6557.

[55] M.H. Futscher, M. Philipp, P. Müller-Buschbaum, A. Schulte, The role of backbone hydration of poly(N-isopropyl acrylamide) across the volume phase transition compared to its monomer, Sci. Rep. 7 (2017), 17012.

[56] G. Cavallaro, S. Micciulla, L. Chiappisi, G. Lazzara, Chitosan-based smart hybrid materials: a physico-chemical perspective, J. Mater. Chem. B 9 (2021) 594–611.

[57] S. Amorim, I. Pashkuleva, C.A. Reis, R.L. Reis, R.A. Pires, Tunable layer-by-layer films containing hyaluronic acid and their interactions with CD44, J. Mater. Chem. B 8 (2020) 3880–3885.

[58] Y. Arima, H. Iwata, Effect of wettability and surface functional groups on protein adsorption and cell adhesion using well-defined mixed self-assembled monolayers, Biomaterials 28 (2007) 3074–3082.

[59] G. Zhou, H. Al-Khoury, T. Groth, Covalent immobilization of glycosaminoglycans to reduce the inflammatory effects of biomaterials, Int. J. Artif. Organs 39 (2016) 37–44.

[60] S. Farris, L. Introzzi, P. Biagioni, T. Holz, A. Schiraldi, L. Piergiovanni, Wetting of biopolymer coatings: contact angle kinetics and image analysis investigation, Langmuir 27 (2011) 7563–7574.

[61] N. Faucheux, R. Schweiss, K. Lützow, C. Werner, T. Groth, Self-assembled monolayers with different terminating groups as model substrates for cell adhesion studies, Biomaterials 25 (2004) 2721–2730.

[62] K. Ren, T. Crouzier, C. Roy, C. Picart, Polyelectrolyte multilayer films of controlled stiffness modulate myoblast cells differentiation, Adv. Funct. Mater. 18 (2008) 1378–1389.

[63] G. Imbir, A. Mzyk, K. Trembecka-Wójciga, E. Jasek-Gajda, H. Plutecka, R. Schirhagl, R. Major, Polyelectrolyte multilayer films modification with Ag and rGO influences platelets activation and aggregate formation under in vitro blood flow, Nanomaterials (Basel) 10 (2020).

[64] Y. Zhou, Y. Zheng, T. Wei, Y. Qu, Y. Wang, W. Zhan, Y. Zhang, G. Pan, D. Li, Q. Yu, H. Chen, Multistimulus responsive biointerfaces with switchable bioadhesion and surface functions, ACS Appl. Mater. Interfaces 12 (2020) 5447–5455.

[65] H. Grünewald, VonR.C. Weast, Handbook of Chemistry and Physics, vol. 52, The Chemical Rubber Co., Cleveland, Ohio/USA, 1972, pp. 445–446. Aufl., XXVII, 2313 S., geb. DM 99.80, Angew. Chem. 84 (1972).

[66] T. Groth, G. Altankov, A. Kostadinova, N. Krasteva, W. Albrecht, D. Paul, Altered vitronectin receptor (?v integrin) function in fibroblasts adhering on hydrophobic glass, J. Biomed. Mater. Res. 44 (1999) 341–351.

[67] N.M. Toromanov, D. Gugutkov, J. Gustavsson, J. Planell, M. Salmerón-Sánchez, G. Altankov, Dynamic behavior of vitronectin at the cell-material interface, ACS Biomater. Sci. Eng. 1 (2015) 927–934.

[68] I. Kiesel, M. Paulus, J. Nase, S. Tiemeyer, C. Sternemann, K. Rüster, F.J. Wirkert, K. Mende, T. Büning, M. Tolan, Temperature-driven adsorption and desorption of proteins at solid-liquid interfaces, Langmuir 30 (2014) 2077–2083.

[69] J. Kobayashi, Y. Arisaka, N. Yui, Y. Akiyama, M. Yamato, T. Okano, Effect of temperature changes on serum protein adsorption on thermoresponsive cell-culture surfaces monitored by A quartz crystal microbalance with dissipation, Int. J. Mol. Sci. 19 (2018).

[70] N.M. Coelho, C. González-García, J.A. Planell, M. Salmerón-Sánchez, G. Altankov, Different assembly of type IV collagen on hydrophilic and hydrophobic substrata alters endothelial cells interaction, Eur. Cell. Mater. 19 (2010) 262–272.

[71] H. Kindi, M. Menzel, A. Heilmann, C.E.H. Schmelzer, M. Herzberg, B. Fuhrmann, G. Gallego-Ferrer, T. Groth, Effect of metal ions on the physical properties of multilayers from hyaluronan and chitosan, and the adhesion, growth and adipogenic differentiation of multipotent mouse fibroblasts, Soft Matter 17 (2021) 8394–8410.

[72] V. Capella, R.E. Rivero, A.C. Liaudat, L.E. Ibarra, D.A. Roma, F. Alustiza, F. Mañas, C.A. Barbero, P. Bosch, C.R. Rivarola, N. Rodríguez, Cytotoxicity and bioadhesive properties of poly-N-isopropylacrylamide hydrogel, Heliyon 5 (2019), e01474.

[73] E. Psarra, U. König, Y. Ueda, C. Bellmann, A. Janke, E. Bittrich, K.-J. Eichhorn, P. Uhlmann, Nanostructured biointerfaces: nanoarchitectonics of thermoresponsive polymer brushes impact protein adsorption and cell adhesion, ACS Appl. Mater. Interfaces 7 (2015) 12516–12529.

[74] M.S. Niepel, B.K. Ekambaram, C.E.H. Schmelzer, T. Groth, Polyelectrolyte multilayers of poly (l-lysine) and hyaluronic acid on nanostructured surfaces affect stem cell response, Nanoscale 11 (2019) 2878–2891.

[75] L. Yu, Y. Hou, W. Xie, J.L.C. Camacho, C. Cheng, A. Holle, J. Young, B. Trappmann, W. Zhao, M.F. Melzig, E.A. Cavalcanti-Adam, C. Zhao, J.P. Spatz, Q. Wei, R. Haag, Ligand diffusion enables force-independent cell adhesion via activating α5β1 integrin and initiating rac and RhoA signaling, Adv. Mater. 32 (2020), 2002566.

[76] A. Köwitsch, G. Zhou, T. Groth, Medical application of glycosaminoglycans: a review, J. Tissue Eng. Regen. Med. 12 (2018) e23–e41.

Chapter 4

Summary – Sustained growth factor delivery from bioactive PNIPAM-*grafted*-chitosan/heparin multilayers as a tool to promote growth and migration of cells

The previous studies have confirmed the enhanced stability, wettability, and biocompatibility of PEMs based on PChi and GAGs. Regarding the PEMs formed at 20 °C, this work further investigated the mechanical properties of PChi-containing PEMs at 37 °C that may be associated with protein adsorption and cell behaviors. In addition, the bioactivity of PEMs was also studied by the interaction with GFs towards cell responses like adhesion, proliferation and migration. Here the surface topography and stiffness of covalently crosslinked PEMs with the terminal layer of either Hep or Chi/PChi (LMW* or HMW) in response to temperature were examined by atomic force microscopy (AFM). PEMs containing PChi were more inhomogeneous and softer due to the bulky structure of PChi at 20 °C. Upon incubation at 37 °C, PEMs with Hep terminal layer became smoother due to interdiffusion of H and aggregation of PChi. The overall surface became softer at 37 °C regarding higher mobility of PELs. Interesting, the dehydration of PNIPAM chains contributed a minor effect and made the surface stiffer than Chi-containing PEMs. However, such behaviors were restricted in PEMs containing LMW*. Higher hydration of PChi inhibited vitronectin (VN) adsorption at 20 °C, while decreased hydration of PChi at 37 °C favored VN adsorption. Abundant sulfate groups in Hep played a dominant role in retaining VN through the specific interaction with VN. As confirmed in Chapter 2 by the PEM stability, higher amount of Hep seemed to remain on HMW-containing PEMs which retained more VN on the PEMs in comparison to LMW*-containing PEMs. Therefore, PEMs containing Chi or HMW with Hep terminal layer was further studied for FGF-2 delivery and cell behaviors.

Based on higher adsorption of VN at 37 °C, loading of FGF-2 was conducted at 37 °C. It is known that VN integrin and FGFR-2 could act synergistically on stimulation of the same signal transductions like MAPK/ERK (extracellular signal-regulated kinase)

pathway that is responsible for cell migration and proliferation. However, higher concentration of VN may compete with FGF-2 to interact with H or inhibit cell activities. Therefore, the concentration of VN was lower to 2 µg mL^{-1} that showed a promoting effect on FGF-2 activity for proliferation of 3T3 mouse embryonic fibroblasts. The delivery of FGF-2 was found to depend on covalent crosslinking degree and PNIPAM effect. Lower crosslinked HMW-containing PEM showed higher uptake and sustained release of FGF-2 compared to lower uptake and burst release of FGF-2 for higher crosslinked Chi-containing PEM. Taking all the factors into account, cell activities were affected by surface and mechanical properties, as well as biological properties. The results demonstrated a less wettable and stiffer surface of HMW-containing PEM promoted better cell adhesion. FGF-2 in a matrix-bond manner, cooperated with VN integrin further induced cell proliferation and migration in HMW-containing PEM after 4-day cultivation. In contrast, FGF-2 in a soluble form was inactivated and unable to support cell activities.

Hence, PEM comprised of bioactive H and HMW could efficiently promote cell proliferation and migration incorporated with the sustain release of matrix-bound FGF-2 in a long-term culture, which can be potentially served as cell culture substrate for production of (stem) cells and bioactive wound dressing for tissue regeneration.

Sustained growth factor delivery from bioactive PNIPAM-*grafted*-chitosan/heparin multilayers as a tool to promote growth and migration of cells

Yi-Tung Lu [a], Pei-Tzu Hung [a], Kui Zeng [b], Matthias Menzel [c], Christian E.H. Schmelzer [d], Kai Zhang [b], Thomas Groth [a,d,*]

[a] *Department of Biomedical Materials, Institute of Pharmacy, Martin Luther University Halle-Wittenberg, Heinrich-Damerow-Strasse 4, 06120 Halle, Saale, Germany*
[b] *Sustainable Materials and Chemistry, Dept. Wood Technology and Wood-based Composites, University of Göttingen, Büsgenweg 4, D-37077 Göttingen, Germany*
[c] *Department of Biological and Macromolecular Materials, Fraunhofer Institute for Microstructure of Materials and Systems (IMWS), Walter-Hülse-Str. 1, 06120 Halle, Saale, Germany*
[d] *Interdisciplinary Center of Material Research, Martin Luther University Halle-Wittenberg, Heinrich-Damerow-Strasse, 06120 Halle, Saale, Germany*

A B S T R A C T

Delivery of growth factors (GFs) is challenging for regulation of cell proliferation and differentiation due to their rapid inactivation under physiological conditions. Here, a bioactive polyelectrolyte multilayer (PEM) is engineered by the combination of thermoresponsive poly(*N*-isopropylacrylamide) (PNIPAM) and glycosaminoglycans to be used as reservoir for GF storage. PNIPAM-*grafted*-chitosan (PChi) with two degrees of substitution (DS) are synthesized, namely LMW* (DS 0.14) and HMW (DS 0.03), by grafting low (2 kDa) and high (10 kDa) molecular weight of PNIPAM on the backbone of chitosan (Chi) to be employed as polycations to form PEM with the polyanion heparin (Hep) at pH 4. Subsequently, PEMs are chemically crosslinked to improve their stability at physiological pH 7.4. Resulting surface and mechanical properties indicate that PEM containing HMW is responsive to temperature at 20 °C and 37 °C, while LMW is not. More importantly, Hep as terminal layer combined with HMW allows not only a better retention of the adhesive protein vitronectin but also a sustained release of FGF-2 at 37 °C. With the synergistic effect of vitronectin and matrix-bound FGF-2, significant promotion on adhesion, proliferation, and migration of 3T3 mouse embryonic fibroblasts is achieved on HMW-containing PEM compared to Chi-containing PEM and exogenously added FGF-2. Thus, PEM containing PNIPAM in combination with bioactive glycosaminoglycans like Hep represents a versatile approach to fabricate a GF delivery system for efficient cell culture, which can be potentially served as cell culture substrate for production of (stem) cells and bioactive wound dressing for tissue regeneration.

1. Introduction

Cell behaviors during medical application of implants is triggered by the interaction with the biomaterial surface and related protein adsorption, cell-cell contacts and soluble bioactive molecules [1]. The latter are represented for example by fibroblast growth factor-2 (FGF-2) that acts as stimulator to promote proliferation and migration of fibroblasts and endothelial cells important for wound healing, and neovascularization, but also related to the maintenance of self-renewal and proliferation of human pluripotent stem cells (hPSC) [2–4]. By binding to transmembrane FGF receptors (FGFR), FGF-2 activates intracellular signaling cascades including Rho family of small GTPases, and mitogen-

activated protein kinase/extracellular signal-regulated kinase (MAPK/ERK) [5]. Specially, these signal transductions can be activated by cooperation of FGFR and cell adhesion molecule integrins (e.g. $\alpha_V\beta_3$) to regulate cell adhesion and spreading [6,7]. FGF-2 is generally supplemented to the culture medium to support cell growth [8]. However, the issues about its short half-life (22–29 h) under physiological environments must be addressed and the local concentration must be well controlled to avoid inhibition of proliferation or differentiation of stem and other cells [9,10]. Sulfated glycosaminoglycans (GAGs) have high affinity to proteins with GAG-binding domains such as extracellular matrix (ECM) proteins (e.g. fibronectin, vitronectin) and GFs (e.g. FGF-2, TGF-β), but also act as a storage reservoir to protect GFs from proteolytic digestion [11,12]. GAGs like heparin (Hep) added to culture media have shown to improve the stability and prolong the half-life of FGF-2 [13]. Therefore, engineering an appropriate delivery system involving GAGs is attractive to prolong the activity of GF like FGF-2 to achieve the desired cell and tissue response.

Layer-by-layer (LbL) assembly has emerged as a facile and cost-effective technique to fabricate biocompatible and bioactive surfaces using negatively charged GAGs for making GFs delivery systems [2,14,15]. By alternating deposition of materials, it is mainly depending on ion pairing between oppositely charged polyelectrolytes (PEs) to form a polyelectrolyte multilayer (PEM) [16]. The physical and mechanical properties of the PEM are based on the nature of selected PE and environmental conditions (e.g., pH, ionic strength, and temperature) [16]. Chitosan (Chi) is widely used as polycation regarding its biocompatibility, abundancy and anti-bacterial properties [17,18]. Multiple studies have reported the use of PEMs as reservoirs for protecting GFs from degradation and prolonging their long-term presentation. For example, loading FGF-2 on PEMs composed of Hep and Chi enhanced the mitogenic activity of mesenchymal stem cells [19]. Another advantage of PEM is that the locally released concentration of GFs can be controlled by chemical crosslinking of the PEM that also improves their stability and modulates their physiochemical properties. In this regard, it was shown previously that delivery of bone morphogenetic protein-2 and FGF-2 from crosslinked PEMs exhibited the ability to induce osteogenic differentiation of myoblasts and promote migration and growth of fibroblasts for wound healing and culture of adipose derived stem cells [2,14,20].

Utilizing LbL technique facilitates engineering of PEMs containing poly(*N*-isopropylacrylamide) (PNIPAM) and has been demonstrated the ability to thermally control protein adsorption or drug delivery such as anti-COVID-19 drug Favipiravir [21–23]. PNIPAM is thermoresponsive and widely applied for drug delivery and cell sheet engineering owing to its lower critical solution temperature (LCST) $\approx$ 32 °C close to the physiological temperature [24]. Below 32 °C, the hydrophilic amide groups are dominant making the polymer highly hydrated, soluble in aqueous solution and repellent to proteins and cells. Its hydrophobic isopropyl groups govern when temperature rises above 32 °C, and lead to the dehydration of the polymer due to the hydrophobic interaction that aids protein adsorption and supports cell adhesion [25,26]. The collapsed PNIPAM becomes a gel to entrap drugs inside the matrix and allow their slow release through the hydrophobic interaction between drugs and PNIPAM [27,28]. PNIPAM has shown a great ability to retain GF activity and sustain their release to promote cell proliferation and differentiation [28–30]. However, the application of PNIPAM-containing PEM for GF delivery in tissue engineering is rarely found due to the lacking anchoring sites of PNIPAM for cells causing inferior cell adhesion [21,23,31]. Thus, a novel approach for enhancing the bioactivity of PNIPAM-containing PEM is desired to regulate cell behaviors.

Our previous study has investigated the ability of a combination of bioactive Hep and PNIPAM-*grafted*-chitosan (PChi) to form a stable PEM upon crosslinking under physiological pH 7.4, and modulate the physical properties in response to temperature (i.e. wettability) related to the biocompatibility and adhesion of stem cells [32]. In this current study,

the effect of temperature on the mechanical properties of PChi-containing PEMs is further studied which may affect protein adsorption and cell behaviors. Vitronectin (VN) as an adhesive protein can promote cell adhesion via the specific binding of cell integrin $\alpha_V\beta_3$ and $\alpha_V\beta_5$ [33]. The bioactivity of PChi or Hep terminated PEMs is interesting for the interaction with VN in response to temperature. FGF-2 and VN have been reported to regulate particularly hPSC responses cooperatively [4,6,34]. The synergistic bioactivity of VN and FGF-2 was assessed here using 3T3 mouse embryonic fibroblasts regarding cell adhesion, migration, and growth. The final goal is to achieve a sustained bioactivity of FGF-2 loaded on these PEMs towards cells, important for future applications in effective culture and large-scale expansion of stem cells that may be superior to use of soluble FGF-2 supplemented in culture medium.

2. Materials and methods

2.1. Materials

Chitosan (deacetylation degree $\geq$92.6 %, 40–150 kDa) was purchased from HMC Heppe Medical Chitosan GmbH (Halle, Germany). Heparin sodium salt (sulfation degree = 1.06, 8–25 kDa) and 1-ethyl-3-(3-dimethylaminopropyl) carbodiimide (EDC) was obtained from Thermo Fisher (Kandel) GmbH (Karlsruhe, Germany). Poly-ethyleneimine (PEI, 750 kDa), *N*-hydroxysuccinimide (NHS), carboxylic acid−terminated PNIPAM (PNIPAM-COOH, 2 and 10 kDa) and fluorescein isothiocyanate (FITC) were provided by Sigma-Aldrich Chemie GmbH (Steinheim, Germany). *n*-Hexane and tetrahydrofuran (THF) were derived from Th. Geyer GmbH & Co. KG (Renningen, Germany). Recombinant human vitronectin (VN) was purchased from PeproTech, Inc. (Hamburg, Germany). FGF-2 (recombinant human FGF-basic FGF) and ELISA kit were obtained from PeproTech, Inc. (New Jersey, USA).

2.2. Synthesis and characterization of PNIPAM-grafted-chitosan

PNIPAM-*grafted*-chitosan (PChi) was synthesized as described previously [32]. Briefly, at 25 °C, the carboxylic groups of PNIPAM-COOH was activated by EDC/NHS to form amide bond with the amino groups located at C2 − position of Chi. Initially, Chi and PNIPAM-COOH (2 or 10 kDa) were separately dissolved in 2 % acetic acid solution. The PNIPAM-COOH solution was reacted for 1 h by adding EDC and NHS followed by mixing with Chi solution to steadily stir overnight at 25 °C. Afterwards, the mixed solution was precipitated in a THF/*n*-hexane solution (4:1) and purified with dialysis membrane (MWCO: 12,000 − 14,000) against Milli-Q water for one week. Finally, the pure PChi was lyophilized by freeze dryer (ALPHA 1–2 LDplus, Christ, Osterode am Harz, Germany). Using weight ratio of Chi/PNIPAM = 1:3 and the molar ratio of repeating unit of Chi/EDC/NHS = 1:3:1.5, the degrees of substitution (DS) of PNIPAM grafted to Chi were characterized by ^{1}H NMR in our previous study [32]. PChi with DS of 0.14 and 0.03 achieved from 2 kDa and 10 kDa of PNIPAM-COOH were named as LMW* and HMW, respectively.

2.3. Multilayer formation by layer-by-layer technique

Glass cover slips (∅ 12 mm, Menzel, Braunschweig, Germany) were cleaned with 25 % NH$_4$OH, 35 % H$_2$O$_2$, and micropure water (1:1:5, v/v/v) at 80 °C for 15 min. Afterwards, the samples were washed with micropure water for 6 × 5 min and dried with nitrogen stream.

The PEM were assembled manually by pipetting solutions of PE applying the same procedure as in previous studies of our and other groups [35,36], for cleaned glass cover slips and tissue culture poly-styrene (TCPS) as substrates used for atomic force microscopy and biological investigations, respectively. PEI as the first anchoring layer was coated to achieve a positive charge on the substrate. The following layers were deposited with two bilayers of polyanion Hep and

2

polycation Chi to achieve a basal multilayer without PNIPAM. Subsequently, PChi replaced Chi from the 7th layer for additional deposition of layers with Hep to form 9 or 10 layers, where PChi or Hep were the final layer of PChi-containing PEM, respectively. PE solution was added on the substrate to prepare every layer and was discarded after 15 min incubation. Subsequently, 0.15 M NaCl solution was used to rinse the surface for 3×4 min to remove unbound PE for 3×4 min. All PE were prepared at 1 mg mL^{-1} in 0.15 M NaCl solution and adjusted their final pH to 4. Chi was dissolved in 0.05 mol L^{-1} acetic acid solution at 50 °C for 3 h and stirred overnight. Chi-containing PEMs as comparison were based on the assembly of Chi and Hep. The PEMs with X terminal layer were referred as B-[X/H]$_{1.5}$ and with Hep terminal layer were defined as B-[X/H]$_2$, where the term 'B' referred to basal layers comprised of 1−6 layers and LMW*, HMW, or Chi were represented as 'X'.

EDC and NHS were used to covalently crosslink the multilayer based on the protocol established earlier in our group [18,37]. The crosslinked solution was prepared by 50 mg mL^{-1} EDC and 11 mg mL^{-1} NHS in 0.15 M, pH 5 NaCl solution and subsequently added to PEMs to react at 4 °C for 18 h under gentle shaking. The solution was discarded from the crosslinked PEM followed by 3 time rinsing of samples with 0.15 M, pH 8 NaCl solution for 1 h to remove unreacted cross-linker.

2.4. Atomic force microscopy measurement

The investigation of roughness and stiffness of PEMs was carried out by atomic force microscope (AFM, Nanowizard IV, JPK-Instruments, Berlin, Germany) in Quantitative Imaging Mode (QI). Samples were first measured in 0.15 M, pH 7.4 NaCl solution at 20 °C using silicon cantilever (qp-BioT, Nanosensors) in a standard liquid cell (JPK-Instruments). Further topographic and spectroscopic measurements were performed in the liquid cell with temperature stabilization at 37 °C. The analysis of roughness and stiffness were calculated by the software JKP Data Processing V5.0.85 and Gwyddion (Gwyddion V2.49, 64-bit).

2.5. Protein adsorption and release studies

2.5.1. Vitronectin adsorption and desorption
VN was labelled with FITC (referred to as FITC-VN) based on the protocol (Sigma-Aldrich) shown in supporting information. The crosslinked PEMs were fabricated in black 96-well tissue culture plates (TCPS, Greiner). FITC-VN at a concentration of 5 μg mL^{-1} dissolved in phosphate-buffered saline (PBS, pH 7.4) was used for incubating samples at either 25 °C or 37 °C for 1 h. Subsequently, the supernatant was aspirated and transferred to a new black 96-well TCPS. The fluorescence intensity (FI) of the supernatants was measured by fluorometry (FLUOstar Optima, BMG LabTech., Offenburg, Germany) at an excitation wavelength of 488 nm and an emission wavelength of 530 nm to determine the concentration of remaining VN after exposure to PEMs.

After transferring FITC-VN supernatants, PBS (at 4 or 37 °C, pH 7.4) with an amount of 70 μL was used to rinse the PEMs 3 times for removal of excessive VN solution. VN desorption was performed by adding 70 μL PBS to the samples for incubation at 4 °C or 37 °C for 24 h and then transferred to a new black 96 well plate. Then 70 μL 0.2 M NaOH was added and incubated for another 2 h. The amount of desorbed VN from PEMs was determined by collecting supernatants of PBS and NaOH for the measurement of FI. A calibration curve was made from the FI of known concentrations (0.005, 0.05, 0.1, 0.5 and 5 μg mL^{-1}) of FITC-VN for calculation of the amount of adsorbed and desorbed VN.

2.5.2. Release of fibroblast growth factor 2 (FGF-2)
The crosslinked PEMs were prepared in the 96-well plate followed by washing with sterile PBS once. All the surfaces were pre-treated with Dulbecco's modified Eagle's medium (DMEM, Lonza, Walkersville, USA) containing 1 % pen/strep/amphotericin B at 37 °C for 1 h to deactivate unreacted EDC/NHS ester that might be reactive during the following VN adsorption and FGF-2 loading. After DMEM was aspirated,

PEMs were incubated in solutions of 5 μg mL^{-1} FGF-2 mixed with 2 μg mL^{-1} VN in 0.15 M, pH 7.4 NaCl at 37 °C for 1 h to allow the loading of FGF-2. Thereafter, the supernatants of FGF-2/VN solutions were collected, and the samples were rinsed once with PBS. Thereafter, 70 μL PBS corresponding to physiological fluids regarding ionic strength and pH value was immediately added to study the release of FGF-2. Half of the supernatant was collected and replaced by fresh PBS after incubation for 2, 4, 6, 8 h at the first day and the following 1–7 days. All the supernatants were stored at −80 °C for further quantification of FGF-2 using a human FGF-basic standard ABTS enzyme-linked immunosorbent assay (ELISA, Peprotech, New Jersey, USA) development kit and ABTS ELISA buffer kit (Peprotech, New Jersey, USA). The use of PBS for release and quantification of FGF-2 was favored for the ELISA assay to avoid any cross-reactivity of antibodies with proteins contained in serum (e.g. growth factors). It was assumed that the PEMs structure is not affected by changing the medium due to the covalent crosslinking and similar ionic strength and same pH of DMEM and PBS to NaCl [32].

2.6. Studies with cells

2.6.1. Cell culture
3T3 mouse embryonic fibroblasts was provided by DSMZ (Deutsche Sammlung von Mikroorganismen und Zellkulturen GmbH, Braunschweig, Germany) and cultured in DMEM supplemented with 10 % fetal bovine serum (FBS, Biochrom AG, Berlin, Germany) and 1 % pen/strep/amphotericin B (BioWhittaker, Lonza, Walkserville, USA) at 37 °C in a humidified 5 % CO$_2$/95 % air atmosphere using a NuAiire DH Autoflow incubator (NuAire Corp., Plymouth, Minnesota, USA). At 80 % confluence, cells were trypsinized by 0.25 % trypsin/0.02 % EDTA (Biochrom AG, Berlin, Germany) solution for 5 min at 37 °C followed by inactivation of trypsin with DMEM containing serum. After the cell suspension was obtained by centrifugation at $500g$ for 5 min, the supernatant was aspirated. The cell pellet was resuspended in DMEM containing 10 % FBS and 1 % pen/strep/amphotericin B. Cell number was manually counted using a Neubauer chamber.

2.6.2. Optimization of VN concentration
The crosslinked PEMs were prepared in the 48-well plate followed by washing with sterile PBS once. All the surfaces were pre-treated with DMEM containing 1 % pen/strep/amphotericin B at 37 °C for 1 h to deactivate unreacted EDC/NHS ester. After aspirating DMEM, 250 μL of VN (at a concentration of 2 or 5 μg mL^{-1} mixed with or without 5 μg mL^{-1} FGF-2 in 0.15 M, pH 7.4 NaCl solution) were coated on PEMs to incubate at 37 °C for 1 h. Thereafter, the FGF-2/VN solutions were discarded, and the surfaces were rinsed with PBS once. 3T3 cells were seeded on the substrates coated with crosslinked PEMs loaded with VN/FGF-2 at a density of 5000 cells per well in 300 μL of DMEM supplemented with low serum (2.5 % FBS). Cells cultured on TCPS in DMEM containing 10 % FBS were used as positive control. On the other hand, soluble FGF-2 at a concentration of 10 ng mL^{-1} in low-serum DMEM (2.5 % FBS) was applied for cells seeded on TCPS coated with VN to compare with PEMs loaded with FGF-2. After 2 days culture, the cell metabolic activity and growth were quantified using Qblue assay (Bio-Chain, Newark, CA, USA). The 10 % of Qblue reagent was added to the medium for reaction at 37 °C for 2 h. After incubation, the 100 μL of supernatant with duplicate were transferred from each sample to the black 96-well plate. The FI of supernatants was measured by fluorometry at a wavelength of 544 nm for excitation and 590 nm for emission.

2.6.3. Cell adhesion studies
After determination of VN concentration, a density of 20,000 cells mL^{-1} of 3 T3 cells were seed on the PEM-coated Nunc Thermanox™ slides (13 mm, Thermo Fisher, NY, USA) pre-adsorbed with VN/FGF-2 that were placed in the 24-well plate in DMEM supplemented with 2.5 % FBS. Cells were incubated for 1 day and fixed with 4 % para-formaldehyde (RotiHistofix, Carl Roth GmbH, Karlsruhe, Germany)

3

solution for 15 min followed by rinsing PBS twice. Afterwards, cell permeabilization was done using 0.1 % Triton X-100 (Sigma-Aldrich Chemie GmbH, Taufkirchen, Germany) in PBS (v/v) for 10 min. The samples were washed with PBS and blocked the non-specific sites by incubation with 1 % (w/v) bovine serum albumin (BSA, Merck, Darmstadt, Germany)/ 1 % (w/v) glycine (ROTH, Carl Roth GmbH, Karlsruhe, Germany) in PBS at room temperature for 1 h. Focal adhesion was stained with the primary mouse antibody (1:100, Sigma) against vinculin and the secondary Cy2-conjugated goat anti-mouse antibody (1:100, Dianova). Phalloidin CruzFluor 555 (1:1000, Santa Cruz Biotechnology, Heidelberg, Germany) was used to visualize actin cytoskeleton. Cell nuclei were stained with TO-PRO3 (1:500, Invitrogen, Darmstadt, Germany). All the staining on the samples were incubated at room temperature for 30 min followed by 3 times PBS washing. Finally, the samples were mounted on the object slides with Roti-Mount FluorCare (Carl Roth GmbH, Karlsruhe, Germany). Confocal laser scanning microscopy (CLSM 701, Carl Zeiss Micro-Imaging GmbH, Jena, Germany) were used for the measurement of cell number with the $10\times$ objective, cell area with $20\times$ objective, and visualization of focal adhesions, actin and nuclei with $63\times$ oil immersion objective. The images were processed by the ZEN2012 software (Carl Zeiss) and analyzed the cell number and area by ImageJ.

2.6.4. Cell growth

Cell growth was performed by Qblue assay. 3T3 cells were seed on 48-well plated coated with VN/FGF-2-loaded PEMs at a density of 5000 cells per well in DMEM supplemented with 2.5 % FBS and incubated at 37 °C in a 5 % CO_2/95 % air atmosphere. The 10 % of Qblue reagent was added to the medium on day 2 and 4 for reaction at 37 °C for 2 h. After incubation, the 100 μL of supernatant with duplicate were transferred from each sample to the black 96-well plate. The FI of supernatants was measured by fluorometry at a wavelength of 544 nm for excitation and 590 nm for emission.

2.6.5. Cell migration

The sterilized cell migration fences (Aix Scientifics CRO, Aachen, Germany) were inserted into the 24-well plate coated with pre-adsorbed VN/FGF-2 PEMs at 37 °C for 30 min to ensure the attachment of the silicone ring on the surface. 150 μL of 3T3 cell suspension in DMEM supplemented with 2.5 % FBS were seeded in the internal channel of the fence at a density of 20,000 cells per well. The external channel was filled with only DMDM. After 24 h incubation at 37 °C, 5 % CO_2/95 % air atmosphere, the fences were removed. The old medium was removed, and cells were rinsed once with DPBS. Additional 5 μg mL^{-1} of mitomycin C (abcr GmbH, Karlsruhe, Germany) was included in DMEM supplemented with 2.5 % FBS and add to each condition to inhibit cell proliferation for migration study. Cells were incubated for another 24 h and 72 h and washed once with DPBS for fixation using methanol (Carl Roth GmbH, Karlsruhe, Germany). The samples were stained with 10 % (v/v) Giemsa (Merck KgaA, Darmstadt, Germany) solution in Milli-Q water for 10 min and subsequently washed with PBS and Milli-Q water. A series of image were photographed along the diameter of the stained area of a cell layer using transmitted light microscope (Nikon ECLIPSE Ti2, Tokyo, Japan). The images were processed using stitching plugin from ImageJ to measure the length of the diameter of the cell layer [38].

2.7. Statistical analysis

All data were performed by Origin Pro 2019 software to obtain a mean value ± standard deviations (SD). The statistical calculation was carried out using a one-way ANOVA with posthoc Turkey's test. The significant difference is indicated as the asterisk when the *p* value ≤0.05. Additionally, the box-whisker plots are presented where applicable. The 25th and 75th percentile, the median (dash) and mean value (empty circle) are illustrated by the box.

3. Results and discussion

3.1. Surface and mechanical properties of multilayers

Since all the PEMs were fabricated and chemically crosslinked at 20 °C, it is important to investigate the effect of size and DS of PNIPAM grafting on Chi during the temperature change from 20 °C to 37 °C on surface properties, like topography and mechanical properties, which are related to protein adsorption, cell adhesion and spreading [39]. Fig. 1A and B represent the wet topography of B-[Chi/H], B-[LMW*/H], and B-[HMW/H] PEMs with either Chi-/LMW*-/HMW- or Hep terminal layers studied by AFM depending on the temperature, respectively. All the PEMs showed an island-like morphology with a roughness (root mean square, Rq) of 1.24–2.46 nm as evaluated in Fig. 1C and Table 1. At 20 °C, the native B-[Chi/H]$_{1.5}$ exhibited the roughest surface while other surfaces were smoother and less granular, which can be explained by the compaction upon addition of smaller molecule of Hep for PEMs with Hep terminal layers and the grafting of PNIPAM for B-[LMW*/H] and B-[HMW/H] PEMs [40,41]. In comparison to the more homogeneous surface of B-[Chi/H], B-[LMW*/H] and B-[HMW/H] PEMs were more inhomogeneous probably due to the bulky structure of LMW* and HMW, which is evident by the rougher and more granular surfaces of their Hep terminal layer also corresponding to their higher dry thickness (Table 1). When PEMs were incubated at 37 °C, surfaces of B-[Chi/H]$_2$ and B-[HMW/H]$_2$ were smoother than at 20 °C. It has been reported that increasing temperature promotes the interdiffusion of polymers and rearrangement of PEMs by breaking the intermolecular interaction (e.g., ionic bonds) between polymers that become more mobile. As a result, a favorable conformation of PEM is reached with a more compact and smoother surface [23,42]. It should be noted that these PEMs were chemically crosslinked with around 40–60 % crosslinking degree that should still permit a certain degree of polymer diffusion (Table 1). In addition, PNIPAM undergoes conformational changes with rising temperature and aggregates resulting in tighter packing and a smoother surface, which is also observed in other PNIPAM-containing PEMs [23,43]. However, B-[LMW*/H] PEMs did not show an alteration of their surface topography during temperature change, probably due to steric hindrance caused by the higher crosslinking degree (54 %) in B-[LMW*/H] PEMs that limits the mobility of PNIPAM chains and other components [44].

To investigate the temperature effect on the mechanical properties of PEM, Young's modulus was measured for different terminal layers as shown in Fig. 1D and Table 1. At 20 °C, the Young's modulus shows a peak of 23 MPa and 24 MPa for B-[Chi/H]$_{1.5}$ and B-[Chi/H]$_2$, respectively, which indicates the stiffest surfaces. The peaks shifted to around 17 MPa for PEMs with LMW* and HMW terminal layers, suggesting PEM involving PNIPAM makes the surface softer because of its higher hydration below LCST [45,46]. The addition of Hep to PEMs indeed stiffened the surfaces, which is correlated to their compact morphology due to diffusion of H inside the PEM increasing ion pairing [41]. Noteworthy, the stiffness is significantly lower for B-[LMW*/H]$_2$ compared to B-[Chi/H]$_2$ and B-[HMW/H]$_2$ ($p \leq 0.05$). This is consistent to the finding that B-[LMW*/H]$_2$ has the most hydrophilic surface as found by WCA indicating a higher water content of this system. As temperature increased to 37 °C, the stiffness decreased and the peaks of all the surfaces shifted to <10 MPa, indicating overall softer surfaces. Such softening effect on PEMs with elevated temperature was also reported in previous studies [42,47]. Köhler and co-workers suggested a "melting" behavior of the more mobile polymers leading to a softer surface investigating the PSS/PDADMAC multilayer capsules [48,49]. On the other hand, since PNIPAM chains dehydrate and collapse above LCST, the hydrophobic interaction and formation of intramolecular hydrogen bonds of PNIPAM should lead to a stiffer surface [46,50]. Here the LMW* and HMW layers only existed in the terminal bilayers, causing probably only minor effects indicated by relatively stiffer surfaces for B-[LMW*/H] and B-[HMW/H] PEMs compared to B-[Chi/H] PEMs at
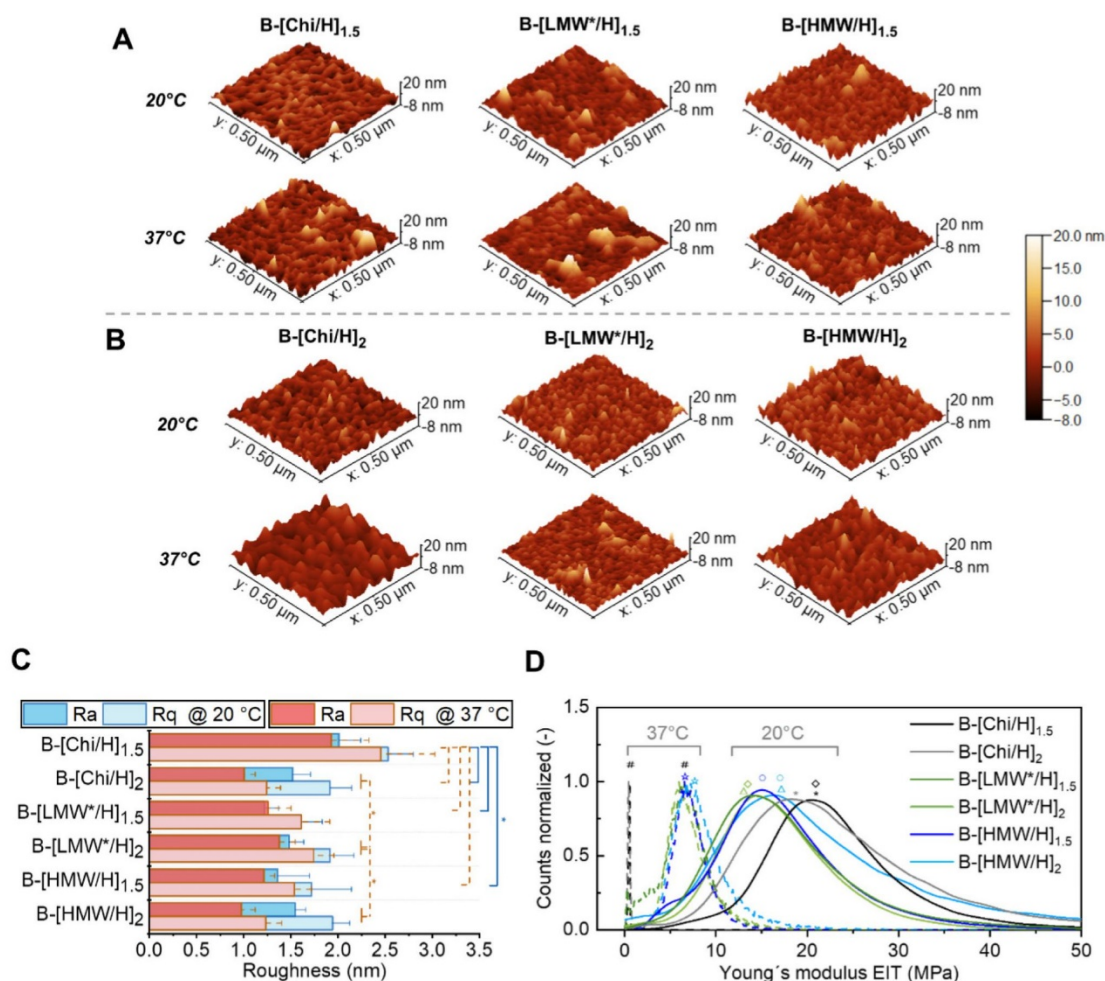
4

Fig. 1. Surface topography of PEMs with (A) Chi/LMW*/HMW terminal layers and (B) Hep terminal layers at 20 °C (upper row) and 37 °C (bottom row) by atomic force microscopy with 0.5×0.5 μm² of scan size. (C) Roughness (Ra: average, deep color, Rq: root mean square, light color) of PEMs at 20 °C (blue bar) and 37 °C (red bar). Data represent means ± SD from ten separated lines, *$p \leq 0.05$. (D) Distribution curves of Young's modulus for different PEMs at 20 °C (solid line) and 37 °C (dot line) with 1×1 μm² of scan size. All the measurements were done under exposure to 0.15 M, pH 7.4 NaCl solution. Data represent means ± SD across the whole scan size, $p \leq 0.05$ (the symbols of *, ○, △, ◇ indicate the significant difference at 20 °C and ☆, # at 37 °C.).

Table 1
Surface properties and mechanical properties for PEMs exposed to 0.15 M, pH 7.4 NaCl at 20 °C and 37 °C. Data of chemical crosslinking degree, thickness, water contact angle (WCA, data from previous study [32]) and AFM data such as stiffness and root mean square (Rq) after rinsing with PBS and DMEM at pH 7.4. (means ± SD).

Surface property	Crosslinking degree (%)	Thickness (nm)	WCA (°)		Rq (nm)		Stiffness (MPa)	
			20 °C	37 °C	20 °C	37 °C	20 °C	37 °C
B-[Chi/H]$_{1.5}$		8.76 ± 1.38	37.84 ± 4.35	37.55 ± 2.32	2.54 ± 0.27	2.46 ± 0.58	23.25 ± 8.66	0.49 ± 0.08
B-[Chi/H]$_2$	59	10.53 ± 0.79	29.98 ± 7.81	30.76 ± 8.13	1.92 ± 0.23	1.25 ± 0.15	24.23 ± 12.39	0.46 ± 0.15
B-[LMW*/H]$_{1.5}$		8.40 ± 0.39	27.78 ± 1.96	32.77 ± 3.63	1.61 ± 0.22	1.62 ± 0.30	17.82 ± 8.48	6.61 ± 2.98
B-[LMW*/H]$_2$	54	11.66 ± 0.96	10.51	14.48 ± 4.10	1.92 ± 0.25	1.74 ± 0.22	19.96 ± 6.67	7.23 ± 2.73
B-[HMW/H]$_{1.5}$		9.67 ± 0.25	33.60 ± 1.18	37.48 ± 1.65	1.72 ± 0.42	1.54 ± 0.18	17.50 ± 7.57	7.35 ± 2.30
B-[HMW/H]$_2$	39	11.38 ± 0.50	27.12 ± 1.45	29.56 ± 1.90	1.95 ± 0.18	1.24 ± 0.17	24.83 ± 20.64	8.61 ± 4.00

37 °C. These observations are related to results of wetting studies in Table S1 showing that PEMs containing PNIPAM have higher water contact angles at 37 °C than at 20 °C. Combining these results, it confirms that HMW is more mobile and able to change its conformation within the B-[HMW/H] PEMs resulting in stiffer surfaces compared to slightly softer surfaces for B-[LMW*/H] PEMs at 37 °C.

3.2. Effect of temperature on vitronectin adsorption and desorption

VN is a plasma protein important for blood coagulation after injury, cell adhesion and tissue remodeling [51]. VN has been used for coating substrata playing a dominant role in maintaining self-renewal and promoting adhesion and proliferation of hPSC in vitro via the specific ligation of $\alpha_v\beta_3$ and $\alpha_v\beta_5$ integrins [33]. The conformational change of PNIPAM with temperature leading to changes of wettability may promote protein adsorption and subsequent cell adhesion [26,52]. Here FITC-labelled VN (named as FITC-VN) was used to study its adsorption on PEMs with different terminal layers and compared to the control surface TCPS at 20 °C and 37 °C as shown in Fig. 2A and B. The amount of adsorbed VN was calculated based on the calibration curve shown in Fig. S1. It was observed that substantially higher quantities of VN adsorbed on all PEMs with about 275–300 ng cm^{-2} at 37 °C in comparison to <100 ng cm^{-2} at 20 °C. At 20 °C, the lowest amount of VN was found on B-[LMW*/H]$_2$, corresponding to the most hydrophilic surface (WCA ≈ 10°, see Table 1) due to prominent hydration effect of LMW* and H. As the temperature increased to 37 °C, the amount of adsorbed VN on B-[LMW*/H] and B-[HMW/H] PEMs was similar to B-[Chi/H] PEMs, which is related to the dehydrated state of PNIPAM leading to less hydrophilic surfaces (Table 1), and thus promoting protein adsorption [53]. Here the temperature plays a key role in protein adsorption as an external factor. Hydrophobic interaction is likely to promote protein adsorption due to the release of water from the interface at higher temperature causing an entropy gain [54]. Jackler et al. observed not only higher adsorption but also more penetration of protein on/into the PEM of Si-PEI-PSS-[PAH-PSS]$_5$ at 42 °C than at 22 °C using staphylococcal nuclease with a MW of 17 kDa [55]. They attributed higher protein adsorption at higher temperature to the entropy gain by the release of counterions and the complexation between proteins and polymer chains. In our case, large Chi or PChi might allow the interpenetration of VN with a MW of about 52 kDa accompanied by the complexation with the polymers in the PEMs regarding higher mobility of molecules at higher temperature. In addition, the amount of around 300 ng cm^{-2} of VN adsorbed on TCPS was found in another study [56].

According to the higher amount of adsorbed VN at 37 °C, VN preadsorbed on PEMs at 37 °C was selected to determine the protein desorption at 4 °C and 37 °C as shown in Fig. 2C. After 24 h desorption in

PBS, a higher amount of 6–12 ng cm^{-2} of VN was released from PEMs at 37 °C compared to negligible release at 4 °C correlated to the mobility of protein at different temperatures, which means that lower temperature stabilizes adsorption of VN. Following the extraction by NaOH at 37 °C to hydrolyze FITC-VN remained on the surfaces, higher cumulative amount of desorbed VN was found at 37 °C than at 4 °C. Considering physiological condition at 37 °C, it is important to know how much VN can be retained on the surfaces at 37 °C to support cell adhesion. B-[LMW*/H]$_{1.5}$ and B-[HMW/H]$_{1.5}$ released the highest amount of VN around 30 ng cm^{-2}. By contrast, only 10–15 ng cm^{-2} was desorbed from their Hep terminal layers. Although protein adsorption and desorption can also be thermally controlled by PNIPAM surface, it seems that Hep plays a dominant role in the association with VN through the specific Hep-binding domain of VN [57]. It should be noted that not all the amount of protein could be depleted from the surface by NaOH regarding the specific binding affinity to Hep that also explains almost 95 % desorbed quantity of VN from TCPS having no specific interaction with VN (Fig. S1B) [58]. B-[HMW/H]$_2$ retained more VN on the surface compared to B-[LMW*/H]$_2$ possibly due to higher amount of Hep remained in B-[HMW/H]$_2$ to binding with VN as confirmed in the previous study by washing step with physiological buffers at pH 7.4 [32]. As mentioned in our previous study, the binding of Hep and protein with Hep-binding domains requires their steric interaction [59]. However, a higher density of PNIPAM in B-[LMW*/H]$_2$ PEM may cause a steric hindrance against change of its conformation as indicated by the AFM studies. This could block some binding sites of Hep that hinder its interaction with VN. As 250 ng cm^{-2} of VN has shown to be the minimal surface density required for hPSC adhesion and growth, B-[HMW/H]$_2$ is preferable for long-term cell culture as a bioactive surface [60].

3.3. Optimization of VN concentration for FGF-2 loading regarding cell reactions

Both VN and FGF-2 possess a high affinity to Hep due to the presence of Hep-binding domains [6]. Thus, the amount of VN should be controlled to avoid the competition between them to bind to heparin that may affect the activity of immobilized FGF-2 and thus cell adhesion, migration, and growth. Fig. 3A illustrates simultaneous incubation of PEM in VN and FGF-2 solutions to immobilize FGF-2 named as iFGF-2. Low serum medium containing 2.5 % FBS was used for iFGF-2-loaded PEMs during cell culture [19]. Here incubation of 2 or 5 µg mL^{-1} VN on B-[Chi/H]$_2$ was studied using 3T3 cells for mitogenic activity that can be promoted by FGF-2. For comparison as a control, the soluble form of FGF-2 (sFGF-2) was added exogenously in low-serum medium to VN-adsorbed TCPS. The growth of 3T3 cells on the surfaces after 2 days of cultivation was detected with Qblue assay that measures FI for the metabolic activity of viable cells as shown in Fig. 3B. Stronger FI was observed for all VN-adsorbed surfaces compared to weaker FI for plain TCPS using 10 % FBS in the medium. Increasing concentration of VN from 2 to 5 µg mL^{-1} slightly decreased FI on B-[Chi/H]$_2$. When B-[Chi/H]$_2$ was loaded with iFGF-2, the FI was visibly higher than non-loaded B-[Chi/H]$_2$, corresponding to a denser population of cells observed from the phase contrast images in Fig. 3C, indicating promoting effect of iFGF-2 on cell growth. The concentration of VN did not significantly affect FI of cells on TCPS cultured with sFGF-2. However, slightly higher FI is observed for iFGF-2-loaded B-[Chi/H]$_2$ when adsorbed with 2 µg mL^{-1} VN than with 5 µg mL^{-1} VN, implicating some competition between VN and iFGF-2 binding to H.

This study is the first report to explore the potential of VN involved in PEM for cell culture. Our study confirmed that the amount of VN adsorbed on the PEMs was around 250–275 ng cm^{-2} from 5 µg mL^{-1} of VN, similar to a study that demonstrates VN could also increase the expression of FGF2 receptor [34]. Although the activation of integrin is thought to be necessary for sustained activity of FGFR-2, an early study has argued that high concentration (> 5 µg mL^{-1}) of VN might inhibit cell adhesion and growth when FGF-2 was immobilized on the surface
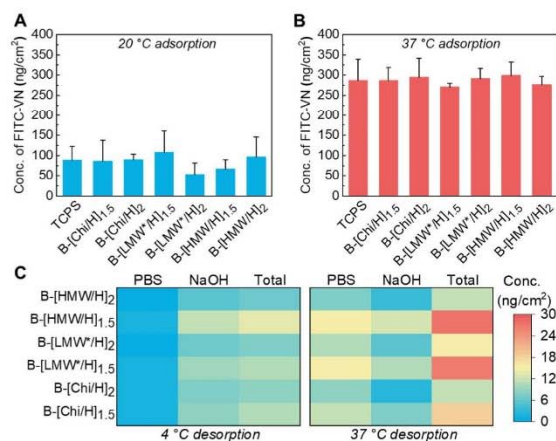

Fig. 2. Amount of FITC-VN adsorbed on Chi/LMW*/HMW or Hep terminated PEMs at (A) 20 °C and (B) 37 °C. (C) Desorption of FITC-VN pre-adsorbed on PEMs at 37 °C in PBS for 24 h at 4 °C (left) and 37 °C (right), succeeded by 2 h extraction in 0.2 M NaOH solution for obtaining cumulative amount of desorbed VN. The unit of VN concentration was transferred from µg mL^{-1} to ng cm^{-2} (= 1000 × 70/0.34) using the volume (70 µL) of the solution added in the 96 well plate with the surface area of 0.34 cm^{-2}.
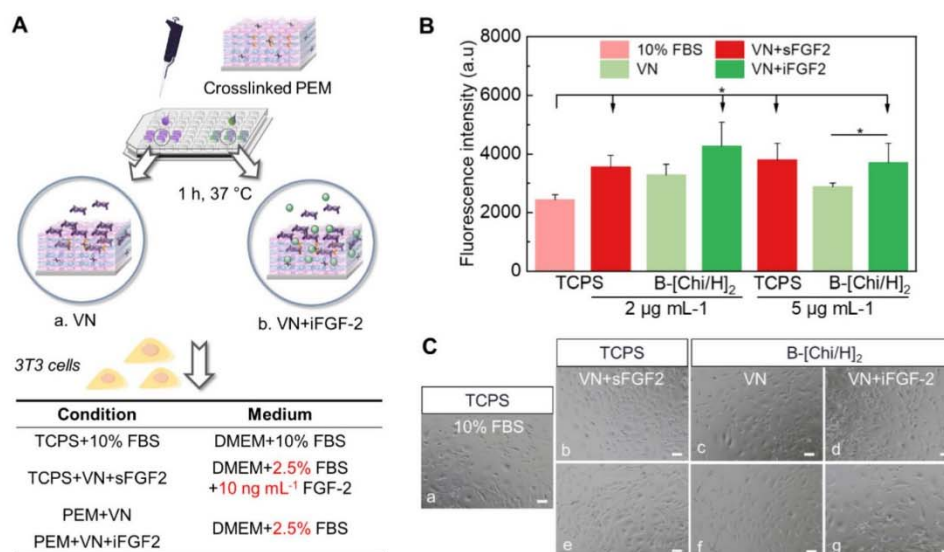
6

Fig. 3. (A) Illustration of adsorption process of VN on PEMs accompanying (a) with or (b) without immobilization of FGF-2 (iFGF-2) for 1 h at 37 °C. 3T3 cells were seeded on the surfaces after removing FGF-2/VN solution in culture medium DMEM supplemented with 2.5 % FBS. Cells seeded on TCPS in DMEM containing 10 % FBS or on TCPS pre-adsorbed with VN in DMEM containing 2.5 % FBS and 10 ng mL^{-1} of soluble FGF-2 (sFGF2) were compared as control. (B) The intensity of cell growth detected using Qblue assay and (C) the cell morphology for PEMs pre-adsorbed with 2 (b − d) or 5 (e − g) µg mL^{-1} of VN and loaded with or without FGF-2 after 2-day culture. Data represent means ± SD, $n = 4$, *$p \leq 0.05$.

[6]. This study also shows 5 µg mL^{-1} VN seemed to compete with iFGF-2 to bind Hep in some but not substantial extent. Therefore, a concentration of 2 µg mL^{-1} VN adsorbed on PEMs is more suitable for this study to promotes iFGF-2 activity in a matrix-bound manner that even surpasses the effect of sFGF-2 on cell growth.

3.4. Release of FGF-2

After optimization of the VN concentration, the ability of FGF-2 uptake and release in B-[Chi/H]$_2$ and B-[HMW/H]$_2$ was studied by ELISA. The calibration curve of the FGF-2 concentration at 10–1000 pg mL^{-1} presents a logarithmic relationship to the absorbance at the wavelength of 405 nm in Fig. 4A. The percentage of cumulative release of FGF-2 from both PEMs at 37 °C was calculated over 7 days as shown in Fig. 4B. For both of PEMs, a high-level release of nearly 20 % was observed for the first 16 h, followed by a slower release at different rates. Notably, the release was faster from B-[Chi/H]$_2$ and reached 40 % of the initial loaded FGF-2 (609 ng mL^{-1}) at day 4 compared to about 30 %

release of initial loaded amount (707 ng mL^{-1}) from B-[HMW/H]$_2$. From day 5 to 7, <5 % of FGF-2 was released from both the PEMs.

It was found previously that thicker, more swollen and less crosslinked PEM can take up more FGF-2 [2,61]. Our previous study has shown that B-[HMW/H]$_2$ is slightly thicker and more hydrated than B-[Chi/H]$_2$ at 20 °C. Nevertheless, the thickness and hydration of B-[HMW/H]$_2$ is supposed to be decreased based on the collapsed PNIPAM chains at 37 °C. The hydrophobic interaction between PNIPAM and FGF-2 might account for the higher uptake of FGF-2 in B-[HMW/H]$_2$ [26]. Additionally, Hep has high affinity to FGF-2 mainly mediated by iduronate-2-sulfates and *N*-sulfate groups while marginally by carboxylic groups and hydroxyl groups in H through ionic interaction and hydrogen bonding [11]. Since the chemical crosslinking is higher for B-[Chi/H]$_2$ (60 %) than B-[HMW/H]$_2$ (40 %) according to our previous study [32], less free carboxylic groups and a more restricted mobility are reducing the capability to bind FGF-2 for B-[Chi/H]$_2$. In contrast, a lower crosslinked B-[HMW/H]$_2$ allows FGF-2 to access Hep and penetrate inside the PEM [2]. On the other hand, Table S1 estimates that the
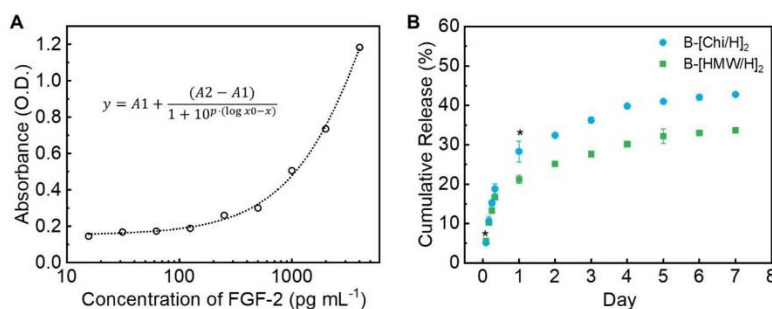

Fig. 4. (A) Calibration curve for FGF-2 at the concentration of 10–4000 pg mL^{-1} with a logarithmic relationship to the absorbance at the wavelength of 405 nm. (A1 = −53.64, A2 = 2.20, R^2 = 0.99) (B) Percentage of cumulative release of FGF-2 from PEMs of B-[Chi/H]$_2$ and B-[HMW/H]$_2$ over the 7 days. Data represent means ± SD, $n = 4$, *$p \leq 0.05$.

release profiles were fit the most accordingly to Higuchi model with the highest correlation coefficient (R^2), suggesting the release mechanism was governed by the diffusion of entrapped FGF-2 out of these PEM that is in well agreement with other studies [2,19]. The release rate of FGF-2 is slower from B-[HMW/H]$_2$ (2.43 ng/day) and faster from B-[Chi/H]$_2$ (3.27 ng/day). Principally, a higher crosslinking degree of the polymer network should delay the release [61]. Our findings show opposite results that could be explained by the hydrophobic effect of PNIPAM at 37 °C to bind FGF-2 in B-[HMW/H]$_2$. Thus, the release of FGF-2 can be sustained by presence of PNIPAM in PEM.

3.5. Cell adhesion studies

The cell adhesion process involves focal adhesion formation where the networks of actin cytoskeleton is connected to ECM proteins through integrins that results in biochemical and mechanical signal transduction into the cell and consequently regulating cell spreading, migration, growth and differentiation [62]. In addition, FGF-2 also promotes these processes through the crosstalk between FGFR and integrins since they co-localize in the focal adhesion contacts [63]. Here, the impact of iFGF-2 loading on VN-adsorbed PEMs for adhesion and spreading of 3T3 cells after 1 day culture was studied by staining nuclei for quantification of

cell number, vinculin for formation of focal adhesion and actin cyto-skeleton for cell spreading. Thermanox as cell culture-treated plastic slides was used as a positive control for cell culture in medium supplemented with 10 % FBS. The low-serum medium containing sFGF2 for VN-adsorbed Thermanox was used for another comparison. In the absence of iFGF-2, Fig. 5A shows the lowest cell number on VN-adsorbed B-[Chi/H]$_2$, while cell number was higher on B-[HMW/H]$_2$ and both Thermanox surfaces. The average cell area was similar on both PEMs as presented in Fig. 5B. CLSM images shown in Fig. 5C visualize that the formation of actin cytoskeleton is observed in cells, indicating good attachments of cells to all the surfaces. For PEMs, a rich formation of focal adhesions was observed at the cell periphery where vinculin is located at the end of actin fibers, however, lesser actin fiber formation was present in cells on B-[Chi/H]$_2$ than on B-[HMW/H]$_2$.

The presence of vinculin-positive focal adhesions and actin stress fiber formation on all VN-adsorbed surfaces indicate the ligation between VN and integrins like $\alpha_V\beta_3$, which activates the intracellular signaling pathway and thereby regulating cell adhesion and spreading [52]. Confirmed by the results of VN adsorption/desorption, both B-[Chi/H]$_2$ and B-[HMW/H]$_2$ have high binding affinity to VN at 37 °C resulting in similar cell spreading. In addition, the higher cell number on B-[HMW/H]$_2$ might be attributed to less wettable surface and increased
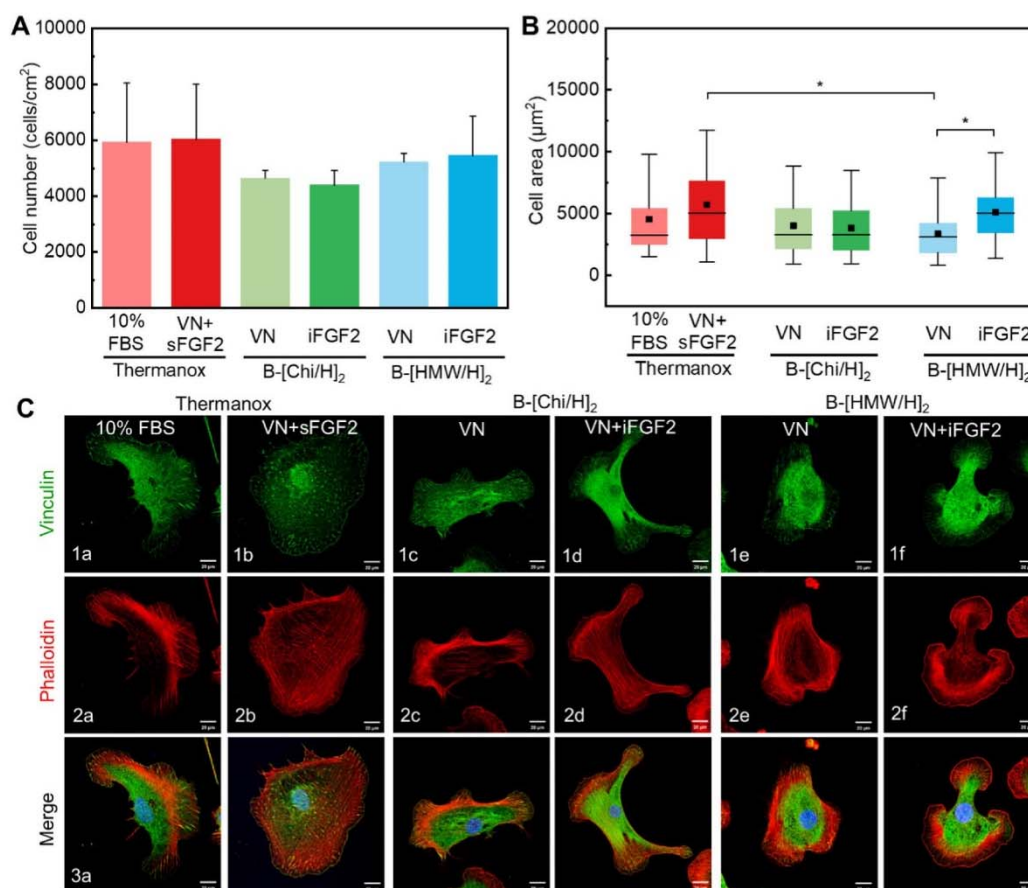

Fig. 5. Quantification of 3T3 cell (A) number and (B) area on different VN-adsorbed PEMs loaded with or without iFGF-2 after 1-day incubation. (C) Confocal laser scanning microscopy images of staining of vinculin (green, 1a–1f), phalloidin (red, 2a–2f) and nuclei (blue, 3a–3f) of cells. Cells seeded on Thermanox in DMEM containing 10 % FBS or on Thermanox pre-adsorbed with VN in DMEM containing 2.5 % FBS and 10 ng mL^{-1} sFGF2 were compared as control. Scale bar: 20 μm. Data represent means ± SD, $n = 4$, *$p \leq 0.05$.

stiffness at 37 °C compared to B-[Chi/H]$_2$. Mechanical properties of biomaterials such as stiffness play an important role in cell adhesion and spreading through mechano-sensing by integrins that regulate RhoA/ROCK signaling pathway for cell adhesion and spreading [64]. Stiffer surfaces induce assembly of actin fiber and formation of focal adhesion, which is displayed by more cell adhesion and spreading on B-[HMW/H]$_2$ than on the softer surface of B-[Chi/H]$_2$ [65].

Loading iFGF-2 on PEMs did not result in any significant difference in quantity of cell adhesion. Notably, cells became larger on B-[HMW/H]$_2$ comparable to fibroblasts on VN-adsorbed Thermanox in the presence of sFGF2, which is indicated by more pronounced actin networks at the leading edge of cells and reveals the formation of well-defined lamellipodium also as a sign of cell migration [66]. This is attributed to more active iFGF-2 within the B-[HMW/H]$_2$ than B-[Chi/H]$_2$ at day 1, where reorganization of actin cytoskeleton can be induced by FGF-2 through the activation of Rho GTPases family like Rac and Cdc42 [67]. In addition, FGFR-2 and VN integrins $\alpha_v\beta_3$ and $\alpha_v\beta_5$ have been reported to regulate cooperatively through many convergent signaling pathways such as MAPK/ERK pathway for cell spreading [6,68]. In comparison, more actin fibers and vinculin distributed across the ventral cell side on VN-adsorbed Thermanox that links to firmly attached and less mobile cells even in the presence of sFGF-2, probably due to stiffer surface than PEMs and lower efficacy of soluble compared to immobilized FGF-2.

3.6. Cell proliferation and migration

The mitogenic activity of iFGF-2 loaded PEMs for the proliferation of 3T3 cells was visualized in Fig. 6A and investigated by FI of Qblue assay for evaluation of metabolic activity after 2- and 4-day cultivation as shown in Fig. 6B. The trend of cell proliferation on day 2 roughly corresponded to cell number counted at day 1. Likewise, B-[Chi/H]$_2$ PEMs

showed the lowest cell number and FI while no significant difference was observed between B-[HMW/H]$_2$ PEMs and TCPS. On day 4, more cells were observed on all the surfaces. Remarkably, loading iFGF-2 on B-[HMW/H]$_2$ exhibited the most pronounced cell proliferation compared to non-loaded B-[HMW/H]$_2$ and both B-[Chi/H]$_2$ PEMs. It was surprising to observe that cell growth is slightly better on non-loaded B-[Chi/H]$_2$ than iFGF-2-loaded one. Cell growth did not take advantage of the sFGF-2 supplemented in low-serum medium for VN-adsorbed TCPS in contrast to significantly more cell growth on plain TCPS supplemented with 10 % FBS.

Our results show the surfaces coated with VN alone enhances cell proliferation due to integrin ligation, the activation of focal adhesion kinase and subsequent MAPK pathway [69]. In addition, the specific interaction of iFGF-2 with Hep in PEMs is supposed to be in a matrix-bound manner to stabilize and prolong the half-life of FGF-2 by formation of a complex with FGFR-2 and integrin that induces intracellular signaling [12,19]. However, a burst release of about 35 % and 40 % of FGF-2 from B-[Chi/H]$_2$ on day 2 and day 4 is related to lower amount of iFGF-2 bound on the PEM matrix and corresponds well to lower FI and hence proliferative effect on cells. By contrast, more iFGF-2 preserved on B-[HMW/H]$_2$ exhibited an exceptional bioactivity promoting cell proliferation. On the other hand, due to degradation of sFGF-2, cell proliferation was inhibited by insufficient amount of sFGF-2 and unavailable crosstalk between FGFR-2 and integrin [15].

The migratory effect of FGF-2 on cells by activation of Rho GTPases family including Rac and Cdc42 is crucial for embryonic development, tissue regeneration and wound healing [19,67]. Here, migration of 3T3 cells was further studied on PEMs by addition of mitomycin C to inhibit cell outgrowth that interferes the estimation on position of migration of a cell layer. Fig. 6C presents the overall large expansion of cell layers about 10.5–11.5 mm on all substrates compared to TCPS with migration
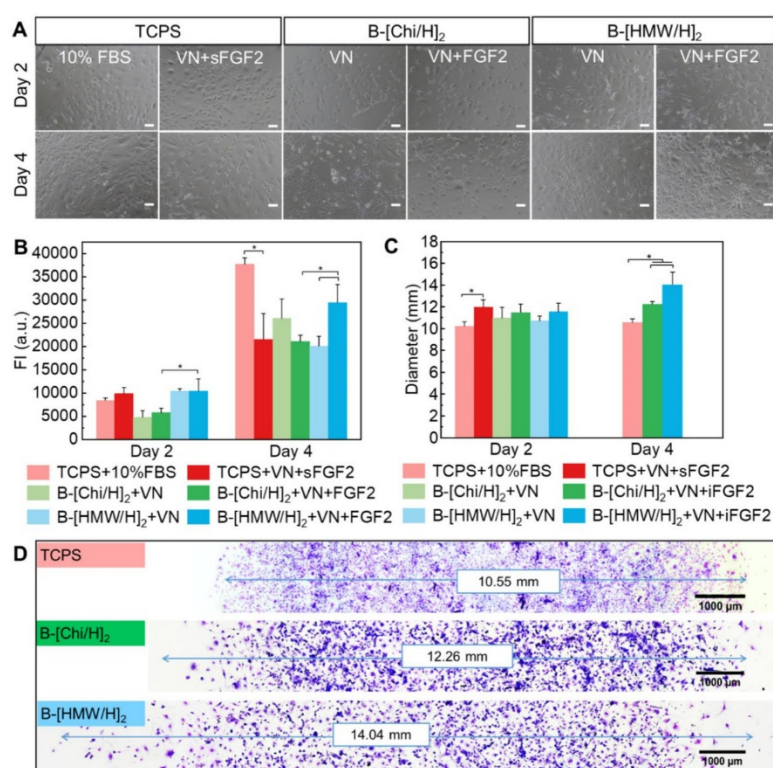

Fig. 6. (A) Phase contrast images of cell morphology and (B) metabolic activity evaluated by Qblue assay to determine the proliferation of 3T3 cells on the different surfaces after 2- and 4- day cultivation. Data represent means ± SD, $n = 6$, *$p \leq 0.05$. Scale bar: 100 μm. Length of 3T3 cell migration on (C) VN-adsorbed PEMs loaded with or without iFGF-2 on day 2 and loaded with FGF-2 on day 4 in 2.5 % FBS medium containing 5 μg mL^{-1} mitomycin C. Migration fence was inserted for TCPS over the culture period to be used as control in 10 % FBS medium. (D) Photographs of cells stained with 10 % Giemsa on VN-adsorbed PEMs loaded with iFGF-2 on day 4. Scale bar: 1000 μm. Data represents means ± SD, $n = 4$, *$p \leq 0.05$.

fence at day 2. A slightly larger cell expansion can be observed on iFGF-2-loaded PEMs with 1 mm more diameter compared to unloaded PEMs. Considering the presentation of FGF-2 activity, cells were continuing cultured on iFGF-2-loaded PEMs until day 4. The migration of the cell layer was significantly promoted to about a diameter of 14 mm on B-[HMW/H]$_2$ as shown in Fig. 6C and D. However, iFGF-2 did not show obvious effect on B-[Chi/H]$_2$ where diameter of the cell layer was only around 12 mm.

The synergistic effect of FGFR-2 and ligation of integrins to VN regulates cell migration via activation of MAPK/ERK activity [6]. The sign of migratory activity of iFGF-2 in the cell adhesion study after 1 day culture has been observed for B-[HMW/H]$_2$. Cell migration stood out on B-[HMW/H]$_2$ regarding the formation of lamellipodium at the leading edge and disassembly of focal adhesion at cell rear (Fig. 5C). Myosin-generated forces transmitted by focal adhesions from actin cytoskeleton to ECM induce a tracking force to pull cell forward [70]. The disassembly of focal adhesion regulated by the inactivation of vinculin and depolymerization of actin filament are evident by weak signal of vinculin and actin at the cell rear [70,71]. During cell migration, proteolysis and remodeling of ECM is required mainly by proteinases like urokinase-type plasminogen activator that can be activated by stimulation of FGF-2 and regulated by VN [3,56]. The presentation of iFGF-2 was better sustained on the surface of B-[HMW/H]$_2$ leading to superior cell migration over the course of 4 days. It seems that the migration was limited on B-[Chi/H]$_2$ probably due to fast release of iFGF-2. Taking all the results together, PEM comprised of bioactive H and HMW efficiently promotes not only cell proliferation but also cell migration in the presence of matrix-bound FGF-2. Both processes are important in wound healing, but also neovascularization and show the versatility of the combination of these PEs with FGF-2 and VN.

4. Conclusion

This study demonstrates a cost-effective and facile LbL technique for coating biomaterials and tissue culture ware allowing the establishment of synergistic bioactive effects of adhesive proteins like VN and growth factors such as FGF-2 to direct cell behaviors when bound to multilayers made of thermoresponsive PNIPAM-*grafted*-chitosan and bioactive heparin. In particular, using high molecular weight of PNIPAM grafted on chitosan as polycation combined with polyanion heparin allows PEM formation and modification with thermoresponsiveness. Heparin plays an important role in retention of adsorbed VN layer and binding of FGF-2 while dehydrated PNIPAM chains at 37 °C enhances the stabilization of VN and FGF-2 in the PEM to promote cell adhesion, proliferation, and migration in a long-term culture of fibroblasts in this study but also potentially for other type of cells like hPSC. Such surface coatings might be interesting for application in culture and programming stem cells in vitro but also in applications related to wound healing when growth and migration of cells like endothelial cells, fibroblasts and keratinocytes is required for tissue regeneration.

CRediT authorship contribution statement

Yi-Tung Lu: Methodology, Validation, Investigation, Data curation, Writing – original draft. **Pei-Tzu Hung:** Investigation, Formal analysis. **Kui Zeng:** Methodology, Writing – review & editing. **Matthias Menzel:** Methodology, Resources, Writing – review & editing. **Christian E.H. Schmelzer:** Methodology, Resources, Writing – review & editing. **Kai Zhang:** Funding acquisition, Writing – review & editing. **Thomas Groth:** Supervision, Funding acquisition, Project administration, Conceptualization, Writing – review & editing.

Declaration of competing interest

The authors declare that they have no known competing financial interests or personal relationships that could have appeared to influence the work reported in this paper.

Data availability

Data will be made available on request.

Acknowledgement

Appendix A. Supplementary data

Supplementary data to this article can be found online at https://doi.org/10.1016/j.bioadv.2023.213589.

References

[1] M. Qu, X. Jiang, X. Zhou, C. Wang, Q. Wu, L. Ren, J. Zhu, S. Zhu, P. Tebon, W. Sun, A. Khademhosseini, Stimuli-responsive delivery of growth factors for tissue engineering, Adv. Healthc. Mater. 9 (2020), e1901714, https://doi.org/10.1002/adhm.201901714.

[2] A. Hautmann, D. Kedilaya, S. Stojanović, M. Radenković, C.K. Marx, S. Najman, M. Pietzsch, J.F. Mano, T. Groth, Free-standing multilayer films as growth factor reservoirs for future wound dressing applications, Biomater. Adv. 142 (2022), 213166, https://doi.org/10.1016/j.bioadv.2022.213166.

[3] B. Boilly, A.S. Vercoutter-Edouart, H. Hondermarck, V. Nurcombe, X. Le Bourhis, FGF signals for cell proliferation and migration through different pathways, Cytokine Growth Factor Rev. 11 (2000) 295–302, https://doi.org/10.1016/s1359-6101(00)00014-9.

[4] A.N. Sohi, H. Naderi-Manesh, M. Soleimani, E.R. Yasaghi, H.K. Manjili, S. Tavaddod, S. Nojehdehi, Synergistic effect of co-immobilized FGF-2 and vitronectin-derived peptide on feeder-free expansion of induced pluripotent stem cells, Mater. Sci. Eng. C Mater. Biol. Appl. 93 (2018) 157–169, https://doi.org/10.1016/j.msec.2018.07.072.

[5] A. Novais, E. Chatzopoulou, C. Chaussain, C. Gorin, The potential of FGF-2 in craniofacial bone tissue engineering: a review, Cells 10 (2021), https://doi.org/10.3390/cells10040932.

[6] M. Rusnati, E. Tanghetti, P. Dell'Era, A. Gualandris, M. Presta, alphavbeta3 integrin mediates the cell-adhesive capacity and biological activity of basic fibroblast growth factor (FGF-2) in cultured endothelial cells, Mol. Biol. Cell 8 (1997) 2449–2461, https://doi.org/10.1091/mbc.8.12.2449.

[7] S. Mori, Y. Takada, Crosstalk between Fibroblast Growth Factor (FGF) receptor and integrin through direct integrin binding to FGF and resulting integrin-FGF-FGFR ternary complex formation, Med. Sci. 1 (2013) 20–36, https://doi.org/10.3390/medsci1010020.

[8] I. Ding, A.M. Peterson, Half-life modeling of basic fibroblast growth factor released from growth factor-eluting polyelectrolyte multilayers, Sci. Rep. 11 (2021) 9808, https://doi.org/10.1038/s41598-021-89229-w.

[9] M. Garcia-Maya, A.A. Anderson, C.E. Kendal, A.V. Kenny, L.C. Edwards-Ingram, A. Holladay, J.L. Saffell, Ligand concentration is a driver of divergent signaling and pleiotropic cellular responses to FGF, J. Cell. Physiol. 206 (2006) 386–393, https://doi.org/10.1002/jcp.20483.

[10] Á. Apáti, T. Berecz, B. Sarkadi, Calcium signaling in human pluripotent stem cells, Cell Calcium 59 (2016) 117–123, https://doi.org/10.1016/j.ceca.2016.01.005.

[11] Y. Yang, Y.-T. Lu, K. Zeng, T. Heinze, T. Groth, K. Zhang, Recent progress on cellulose-based ionic compounds for biomaterials, Adv. Mater. (2020), e2000717, https://doi.org/10.1002/adma.202000717.

[12] A. Weltrowski, M.-L. Da Silva Almeida, D. Peschel, K. Zhang, S. Fischer, T. Groth, Mitogenic activity of sulfated chitosan and cellulose derivatives is related to protection of FGF-2 from proteolytic cleavage, Macromol. Biosci. 12 (2012) 740–750, https://doi.org/10.1002/mabi.201100518.

[13] D. Peschel, K. Zhang, N. Aggarwal, E. Brendler, S. Fischer, T. Groth, Synthesis of novel celluloses derivatives and investigation of their mitogenic activity in the presence and absence of FGF2, Acta Biomater. 6 (2010) 2116–2125, https://doi.org/10.1016/j.actbio.2009.12.032.

[14] R. Anouz, A. Repanas, E. Schwarz, T. Groth, Novel surface coatings using oxidized glycosaminoglycans as delivery systems of Bone Morphogenetic Protein 2 (BMP-2) for bone regeneration, Macromol. Biosci. 18 (2018), e1800283, https://doi.org/10.1002/mabi.201800283.

[15] J.M. Silva, R.L. Reis, J.F. Mano, Biomimetic extracellular environment based on natural origin polyelectrolyte multilayers, Small 12 (2016) 4308–4342, https://doi.org/10.1002/smll.201601355.

[16] J. Borges, J.F. Mano, Molecular interactions driving the layer-by-layer assembly of multilayers, Chem. Rev. 114 (2014) 8883–8942, https://doi.org/10.1021/cr400531v.

[17] L. Richert, F. Boulmedais, P. Lavalle, J. Mutterer, E. Ferreux, G. Decher, J.-C. Voegel, C. Picart, Improvement of stability and cell adhesion properties of polyelectrolyte multilayer films by chemical cross-linkin, Biomacromolecules 5 (2004) 284–294, https://doi.org/10.1021/bm0342281.

[18] G. Apte, A. Repanas, C. Willems, A. Mujtaba, C.E.H. Schmelzer, A. Raichur, F. Syrowatka, T. Groth, Effect of different crosslinking strategies on physical properties and biocompatibility of freestanding multilayer films made of alginate and chitosan, Macromol. Biosci. 19 (2019) e1900181, https://doi.org/10.1002/mabi.201900181.

[19] J. Almodóvar, S. Bacon, J. Gogolski, J.D. Kisiday, M.J. Kipper, Polysaccharide-based polyelectrolyte multilayer surface coatings can enhance mesenchymal stem cell response to adsorbed growth factors, Biomacromolecules 11 (2010) 2629–2639, https://doi.org/10.1021/bm1005799.

[20] R. Mhanna, J. Becher, M. Schnabelrauch, R.L. Reis, I. Pashkuleva, Sulfated alginate as a mimic of sulfated glycosaminoglycans: binding of growth factors and effect on stem cell behavior, Adv. Biosyst. 1 (2017) e1700043, https://doi.org/10.1002/adbi.201700043.

[21] L. Xu, X. Zhang, Z. Chu, H. Wang, Y. Li, X. Shen, L. Cai, H. Shi, C. Zhu, J. Pan, D. Pan, Temperature-responsive multilayer films based on block copolymer-coated silica nanoparticles for long-term release of Favipiravir, ACS Appl. Nano Mater. 4 (2021) 14014–14025, https://doi.org/10.1021/acsanm.1c03334.

[22] Y.-T. Lu, P.-T. Hung, K. Zeng, C. Woelk, B. Fuhrmann, K. Zhang, T. Groth, Surface properties and bioactivity of PNIPAM-grafted-chitosan/chondroitin multilayers, Smart Mater. Med. 4 (2023) 356–367, https://doi.org/10.1016/j.smaim.2022.11.008.

[23] A. Osypova, C.-A. Fustin, C.-M. Pradier, J. Landoulsi, S. Demoustier-Champagne, Factors impacting protein adsorption on layer-by-layer assembled stimuli-responsive thin films, Eur. Polym. J. 95 (2017) 195–206, https://doi.org/10.1016/j.eurpolymj.2017.08.019.

[24] F. Doberenz, K. Zeng, C. Willems, K. Zhang, T. Groth, Thermoresponsive polymers and their biomedical application in tissue engineering - a review, J. Mater. Chem. B 8 (2020) 607–628, https://doi.org/10.1039/c9tb02052g.

[25] M. Prawatborisut, S. Jiang, J. Oberländer, V. Mailänder, D. Crespy, K. Landfester, Modulating protein corona and materials–cell interactions with temperature-responsive materials, Adv. Funct. Mater. 32 (2022) 2106353, https://doi.org/10.1002/adfm.202106353.

[26] J. Kobayashi, Y. Arisaka, N. Yui, Y. Akiyama, M. Yamato, T. Okano, Effect of temperature changes on serum protein adsorption on thermoresponsive cell-culture surfaces monitored by a quartz crystal microbalance with dissipation, Int. J. Mol. Sci. 19 (2018), https://doi.org/10.3390/ijms19051516.

[27] M. Cao, Y. Wang, X. Hu, H. Gong, R. Li, H. Cox, J. Zhang, T.A. Waigh, H. Xu, J. R. Lu, Reversible thermoresponsive peptide-PNIPAM hydrogels for controlled drug delivery, Biomacromolecules 20 (2019) 3601–3610, https://doi.org/10.1021/acs.biomac.9b01009.

[28] C.A. Kavanagh, T.A. Gorelova, I.I. Selezneva, Y.A. Rochev, K.A. Dawson, W. M. Gallagher, A.V. Gorelov, A.K. Keenan, Poly(N-isopropylacrylamide) copolymer films as vehicles for the sustained delivery of proteins to vascular endothelial cells, J. Biomed. Mater. Res. A 72 (2005) 25–35, https://doi.org/10.1002/jbm.a.30192.

[29] J.C. Garbern, E. Minami, P.S. Stayton, C.E. Murry, Delivery of basic fibroblast growth factor with a pH-responsive, injectable hydrogel to improve angiogenesis in infarcted myocardium, Biomaterials 32 (2011) 2407–2416, https://doi.org/10.1016/j.biomaterials.2010.11.075.

[30] E. Smith, J. Yang, L. McGann, W. Sebald, H. Uludag, RGD-grafted thermoreversible polymers to facilitate attachment of BMP-2 responsive C2C12 cells, Biomaterials 26 (2005) 7329–7338, https://doi.org/10.1016/j.biomaterials.2005.05.060.

[31] K. Zeng, F. Doberenz, T.-T. Lu, J.P. Nong, S. Fischer, T. Groth, K. Zhang, Synthesis of thermoresponsive PNIPAM-grafted cellulose sulfates for bioactive multilayers via layer-by-layer technique, ACS Appl. Mater. Interfaces 14 (2022) 48384–48396, https://doi.org/10.1021/acsami.2c12803.

[32] Y.-T. Lu, K. Zeng, B. Fuhrmann, C. Woelk, K. Zhang, T. Groth, Engineering of stable cross-linked multilayers based on thermo-responsive PNIPAM-grafted-chitosan/heparin to tailor their physiochemical properties and biocompatibility, ACS Appl. Mater. Interfaces 14 (2022) 29550–29562, https://doi.org/10.1021/acsami.2c05297.

[33] T.J. Rowland, L.M. Miller, A.J. Blaschke, E.L. Doss, A.J. Bonham, S.T. Hikita, L. V. Johnson, D.O. Clegg, Roles of integrins in human induced pluripotent stem cell growth on Matrigel and vitronectin, Stem Cells Dev. 19 (2010) 1231–1240, https://doi.org/10.1089/scd.2009.0328.

[34] R. Tsou, F.F. Isik, Integrin activation is required for VEGF and FGF receptor protein presence on human microvascular endothelial cells, Mol. Cell. Biochem. 224 (2001) 81–89, https://doi.org/10.1023/a:1011947301849.

[35] T. Crouzier, L. Fourel, T. Boudou, C. Albigès-Rizo, C. Picart, Presentation of BMP-2 from a soft biopolymeric film unveils its activity on cell adhesion and migration, Adv. Mater. 23 (2011) H111–H118, https://doi.org/10.1002/adma.201004637.

[36] R. Anouz, T. Selekere, A. Hautmann, C. Husteden, M. Menzel, C. Woelk, C.E. H. Schmelzer, T. Groth, Intrinsically cross-linked ECM-like multilayers for BMP-2 delivery promote osteogenic differentiation of cells, Adv. Mater. Interfaces 10 (2023) 2201596, https://doi.org/10.1002/admi.202201596.

[37] M.S. Niepel, F. Almouhanna, B.K. Ekambaram, M. Menzel, A. Heilmann, T. Groth, Cross-linking multilayers of poly-l-lysine and hyaluronic acid: effect on mesenchymal stem cell behavior, Int. J. Artif. Organs 41 (2018) 223–235, https://doi.org/10.1177/0391398817752598.

[38] S. Preibisch, S. Saalfeld, P. Tomancak, Globally optimal stitching of tiled 3D microscopic image acquisitions, Bioinformatics 25 (2009) 1463–1465, https://doi.org/10.1093/bioinformatics/btp184.

[39] M. Rahmati, E.A. Silva, J.E. Reseland, C.A. Heyward, H.J. Haugen, Biological responses to physicochemical properties of biomaterial surface, Chem. Soc. Rev. 49 (2020) 5178–5224, https://doi.org/10.1039/d0cs00103a.

[40] M. Lundin, F. Solaqa, E. Thormann, L. Macakova, E. Blomberg, Layer-by-layer assemblies of chitosan and heparin: effect of solution ionic strength and pH, Langmuir 27 (2011) 7537–7548, https://doi.org/10.1021/la200441u.

[41] N. Aggarwal, Modulating cell behaviour through biomimetic multilayers of natural and semi-synthetic glycosaminoglycans, in: Universitäts- und Landesbibliothek Sachsen-Anhalt, 2014, https://doi.org/10.25673/1129.

[42] P. Nazaran, V. Bosio, W. Jaeger, D.F. Anghel, R.V. Klitzing, Lateral mobility of polyelectrolyte chains in multilayers, J. Phys. Chem. B 111 (2007) 8572–8581, https://doi.org/10.1021/jp068768e.

[43] T. Fujie, J.Y. Park, A. Murata, N.C. Estillore, M.C.R. Tria, S. Takeoka, R. C. Advincula, Hydrodynamic transformation of a freestanding polymer nanosheet induced by a thermoresponsive surface, ACS Appl. Mater. Interfaces 1 (2009) 1404–1413, https://doi.org/10.1021/am900111r.

[44] J.A. Jaber, J.B. Schlenoff, Polyelectrolyte multilayers with reversible thermal responsivity, Macromolecules 38 (2005) 1300–1306, https://doi.org/10.1021/ma0485235.

[45] G. Liu, G. Zhang, Collapse and swelling of thermally sensitive poly(N-isopropylacrylamide) brushes monitored with a quartz crystal microbalance, J. Phys. Chem. B 109 (2005) 743–747, https://doi.org/10.1021/jp046903m.

[46] E. Maza, C. von Bilderling, M.L. Cortez, G. Díaz, M. Bianchi, L.I. Pietrasanta, J. M. Giussi, O. Azzaroni, Layer-by-layer assembled microgels can combine conflicting properties: switchable stiffness and wettability without affecting permeability, Langmuir 34 (2018) 3711–3719, https://doi.org/10.1021/acs.langmuir.8b00047.

[47] A.S. Vikulina, Y.G. Anissimov, P. Singh, V.Z. Prokopović, K. Uhlig, M.S. Jaeger, R. von Klitzing, C. Duschl, D. Volodkin, Temperature effect on the build-up of exponentially growing polyelectrolyte multilayers. An exponential-to-linear transition point, Phys. Chem. Chem. Phys. 18 (2016) 7866–7874, https://doi.org/10.1039/c6cp00345a.

[48] K. Köhler, H. Möhwald, G.B. Sukhorukov, Thermal behavior of polyelectrolyte multilayer microcapsules: 2. Insight into molecular mechanisms for the PDADMAC/PSS system, J. Phys. Chem. B 110 (2006) 24002–24010, https://doi.org/10.1021/jp062907a.

[49] R. Mueller, K. Köhler, R. Weinkamer, G. Sukhorukov, A. Fery, Melting of PDADMAC/PSS capsules investigated with AFM force spectroscopy, Macromolecules 38 (2005) 9766–9771, https://doi.org/10.1021/ma0513057.

[50] M.H. Futscher, M. Philipp, P. Müller-Buschbaum, A. Schulte, The role of backbone hydration of poly(N-isopropyl acrylamide) across the volume phase transition compared to its monomer, Sci. Rep. 7 (2017) 17012, https://doi.org/10.1038/s41598-017-17272-7.

[51] D.I. Leavesley, A.S. Kashyap, T. Croll, M. Sivaramakrishnan, A. Shokoohmand, B. G. Hollier, Z. Upton, Vitronectin–master controller or micromanager? IUBMB Life 65 (2013) 807–818, https://doi.org/10.1002/iub.1203.

[52] T. Groth, A. Kostadinova, N. Krasteva, W. Albrecht, D. Paul, Altered Vitronectin receptor (αv integrin) function in fibroblasts adhering on hydrophobic glass, J. Biomed. Mater. Res. 44 (1999) 341–351, https://doi.org/10.1002/(SICI)1097-4636(19990305)44:3<341:AID-JBM13>3.0.CO;2-H.

[53] A. Osypova, D. Magnin, P. Sibret, A. Aqil, C. Jérôme, C. Dupont-Gillain, C.-M. Pradier, S. Demoustier-Champagne, J. Landoulsi, Dual stimuli-responsive coating designed through layer-by-layer assembly of PAA-b-PNIPAM block copolymers for the control of protein adsorption, Soft Matter 11 (2015) 8154–8164, https://doi.org/10.1039/c5sm01545f.

[54] J. Kiesel, M. Paulus, J. Nase, S. Tiemeyer, C. Sternemann, K. Rüster, F.J. Wirkert, K. Mende, T. Büning, M. Tolan, Temperature-driven adsorption and desorption of proteins at solid-liquid interfaces, Langmuir 30 (2014) 2077–2083, https://doi.org/10.1021/la404884a.

[55] G. Jackler, C. Czeslik, R. Steitz, C.A. Royer, Spatial distribution of protein molecules adsorbed at a polyelectrolyte multilayer, Phys. Rev. E Stat. Nonlinear Soft Matter Phys. 71 (2005) 41912, https://doi.org/10.1103/PhysRevE.71.041912.

[56] G. Toromanov, D. Gugutkov, J. Gustavsson, J. Planell, M. Salmerón-Sánchez, G. Altankov, Dynamic behavior of Vitronectin at the cell-material Interface, ACS Biomater. Sci. Eng. 1 (2015) 927–934, https://doi.org/10.1021/acsbiomaterials.5b00147.

[57] I. Capila, R.J. Linhardt, Heparin-protein interactions, Angew. Chem. Int. Ed. 41 (2002) 390–412, https://doi.org/10.1002/1521-3773(20020201)41:3<390:AID-ANIE390>3.0.CO;2-B.

[58] J.L. Bohnert, T.A. Horbett, Changes in adsorbed fibrinogen and albumin interactions with polymers indicated by decreases in detergent elutability, J. Colloid Interface Sci. 111 (1986) 363–377, https://doi.org/10.1016/0021-9797(86)90040-8.

[59] N. Aggarwal, N. Altgärde, S. Svedhem, G. Michanetzis, Y. Missirlis, T. Groth, Tuning cell adhesion and growth on biomimetic polyelectrolyte multilayers by variation of pH during layer-by-layer assembly, Macromol. Biosci. 13 (2013) 1327–1338, https://doi.org/10.1002/mabi.201300153.

[60] L.Y.W. Yap, J. Li, I.Y. Phang, L.T. Ong, J.Z.-E. Ow, J.C.H. Goh, V. Nurcombe, J. Hobley, A.B.H. Choo, S.K.W. Oh, S.M. Cool, W.R. Birch, Defining a threshold surface density of vitronectin for the stable expansion of human embryonic stem cells, Tissue Eng. C Methods 17 (2011) 193–207, https://doi.org/10.1089/ten.tec.2010.0328.

[61] M. Kumorek, O. Janoušková, A. Höcherl, M. Houska, E. Mázl-Chánová, N. Kasoju, L. Cuchalová, R. Matějka, D. Kubies, Effect of crosslinking chemistry of albumin/heparin multilayers on FGF-2 adsorption and endothelial cell behavior, Appl. Surf. Sci. 411 (2017) 240–250, https://doi.org/10.1016/j.apsusc.2017.03.193.

[62] W.H. Goldmann, Role of vinculin in cellular mechanotransduction, Cell Biol. Int. 40 (2016) 241–256, https://doi.org/10.1002/cbin.10563.

[63] G.E. Plopper, H.P. McNamee, L.E. Dike, K. Bojanowski, D.E. Ingber, Convergence of integrin and growth factor receptor signaling pathways within the focal adhesion complex, Mol. Biol. Cell 6 (1995) 1349–1365, https://doi.org/10.1091/mbc.6.10.1349.

[64] R.G. Wells, The role of matrix stiffness in regulating cell behavior, Hepatology 47 (2008) 1394–1400, https://doi.org/10.1002/hep.22193.

[65] J. Blacklock, A. Vetter, A. Lankenau, D. Oupický, H. Möhwald, Tuning the mechanical properties of bioreducible multilayer films for improved cell adhesion and transfection activity, Biomaterials 31 (2010) 7167–7174, https://doi.org/10.1016/j.biomaterials.2010.06.002.

[66] S. Tojkander, G. Gateva, P. Lappalainen, Actin stress fibers–assembly, dynamics and biological roles, J. Cell Sci. 125 (2012) 1855–1864, https://doi.org/10.1242/jcs.098087.

[67] J.G. Lee, E.P. Kay, Cross-talk among Rho GTPases acting downstream of PI 3-kinase induces mesenchymal transformation of corneal endothelial cells mediated by FGF-2, Invest. Ophthalmol. Vis. Sci. 47 (2006) 2358–2368, https://doi.org/10.1167/iovs.05-1490.

[68] S. Klein, F.G. Giancotti, M. Presta, S.M. Albelda, C.A. Buck, D.B. Rifkin, Basic fibroblast growth factor modulates integrin expression in microvascular endothelial cells, Mol. Biol. Cell 4 (1993) 973–982, https://doi.org/10.1091/mbc.4.10.973.

[69] Y.-J. Jin, I. Park, I.-K. Hong, H.-J. Byun, J. Choi, Y.-M. Kim, H. Lee, Fibronectin and vitronectin induce AP-1-mediated matrix metalloproteinase-9 expression through integrin $\alpha(5)\beta(1)/\alpha(v)\beta(3)$-dependent Akt, ERK and JNK signaling pathways in human umbilical vein endothelial cells, Cell. Signal. 23 (2011) 125–134, https://doi.org/10.1016/j.cellsig.2010.08.012.

[70] J.L. Bays, K.A. DeMali, Vinculin in cell-cell and cell-matrix adhesions, Cell. Mol. Life Sci. 74 (2017) 2999–3009, https://doi.org/10.1007/s00018-017-2511-3.

[71] J. Lehtimäki, M. Hakala, P. Lappalainen, Actin filament structures in migrating cells, Handb. Exp. Pharmacol. 235 (2017) 123–152, https://doi.org/10.1007/164_2016_28.

Chapter 5

Summary − Synthesis of thermoresponsive PNIPAM-grafted cellulose sulfates for bioactive multilayers via layer-by-layer technique

GAG-mimetic cellulose sulfate (CS) with the introduced sulfate groups has attractive advantages for biomedical application owing to similar biological activities to native GAGs such as binding of ECM proteins (e.g., FN) and GFs. Based on the exciting outcomes from previous chapters, this paper designed the synthesized routes for PNIPAM-grafted CS (PCS) and focused on the effects of degree of substitution (DS) of sulfate groups and PNIPAM on PCS as polyanions on the formation of PEMs with polycation poly-L-lysine (PLL) or quaternized chitosan (QCHI). Lower sulfated PCS 1 (DSs = 0.41) was synthesized using click chemistry but failed to obtain PCS with higher DSs, while higher sulfated PCS 2 (DSs = 0.93) could be achieved through carbodiimide chemistry. To mimic the condition during PEM formation and physiological environment, the size temperature of cloud point (T_{CP}) of both PCSs were analyzed by DLS in the aqueous solution in the presence or absence of NaCl at pH 4 or 7. Higher sulfation increased the T_{CP} while the presence of kosmotropic Cl⁻ reduced T_{CP}. Both PCSs exhibited the coil-to-globular transition across T_{CP} around 30 – 34 °C and became lager aggregates at 37 °C. The growth, internal structure, stability, and surface properties of a total 10 layers of PEMs from PCSs or their precursors CSs as polyanions combined with PLL or QCHI were studied by SPR, WCA measurements and surface zeta potential. It was confirmed that both PCS2 and QChi had the highest negative and positive charge densities and thus promoted the greatest PEM growth, overcoming the steric hindrance of bulky PNIPAM. These PEMs tended to form intermingled layers since oppositely charged PELs contributed to the surface potential where polycations dominated the surface zeta potential in the acidic region, while polyanions played a role in the basic region. CSs and PCSs were also dominant as terminal layers since all the PEMs presented negatively charged and highly wettable surfaces. Furthermore, type of polycations also came into effect on the composition of surface region of PEM, which was evident by the slightly lower hydrophilicity of PEMs composed of PLL due

to the fact that smaller PLL was more diffusible and might be more present on the surface region compared to QChi-containing PEMs.

The used polycations, sulfation degree and the presence of PNIPAM played crucial roles for the stability and surface properties of PEMs and further determined the cell fate of 3T3 mouse fibroblasts regarding the cytotoxicity, cell adhesion, spreading, and growth. PCS1 with a lower DSs, as the polyanion for PEMs was the most cytotoxic associated with the lower structural stability arising from the decreased ion pairing with polycations. Thereby, cell adhesion and growth over 7 days were inhibited by polycations particularly PLL present on the surface region and released from PEM that could destroy cell membranes. In contrast, higher sulfated PCS2 enhanced the structural stability not only reducing cytotoxicity but also enhancing cell behaviors. This demonstrated a certain sulfation degree was necessary to form a stable PEM and endowed with the important bioactivity binding to the adhesive proteins from the serum and secreted by cells. Moreover, the presence of PNIPAM promoted even better cell adhesion and growth probably due to hydrophobic interactions with serum proteins and hence supported the adhesion and growth of cells.

Overall, PEM using PCS2 particularly in combination with QCHI with an excellent biocompatibility is promising for bioactive and thermoresponsive coatings as cell culture substrates that could replace the use of native GAGs.

Synthesis of Thermoresponsive PNIPAM-Grafted Cellulose Sulfates for Bioactive Multilayers via Layer-by-Layer Technique

Kui Zeng,[†] Falko Doberenz,[†] Yi-Tung Lu,[†] Johanna Phuong Nong, Steffen Fischer, Thomas Groth, and Kai Zhang*
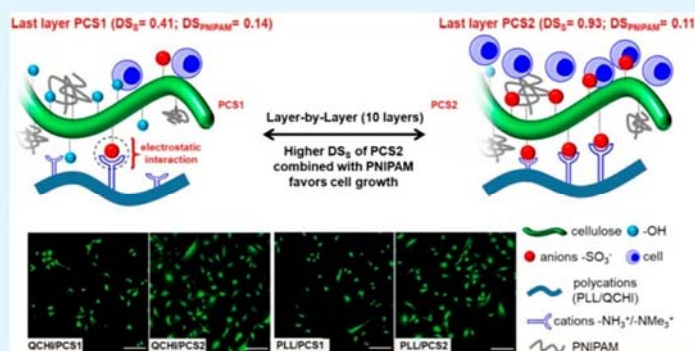
Read Online

ACCESS | 📊 Metrics & More | 📖 Article Recommendations | 🔵 Supporting Information

ABSTRACT: The robust thermoresponsive and bioactive surfaces for tissue engineering by combining poly-*N*-isopropylacrylamide (PNIPAM) and cellulose sulfate (CS) remain highly in demand but not yet realized. Herein, PNIPAM-grafted cellulose sulfates (PCSs) with diverse degrees of substitution ascribed to sulfate groups (DS_S) are synthesized for the first time. Higher sulfated PCS2 generally forms larger aggregates than lower sulfated PCS1 at their cloud point temperatures (T_{CP}) of around 33 °C, whereas PCS1 leads to larger aggregates at body temperature (37 °C). Via the layer-by-layer (LbL) technique, biocompatible polyelectrolyte multilayers (PEMs) composed of PCSs as polyanions in combination with poly-L-lysine (PLL) or quaternized chitosan (QCHI) as polycations were fabricated. The resulting surfaces contained a more intermingled structure of polyanions with both polycations, while higher sulfated cellulose derivatives (CS2 and PCS2) displayed greater stability. Studies on toxicity and biocompatibility of PEM using 3T3 mouse fibroblasts showed a lower cytotoxicity of PEM with PCS2 and CS2 than PCS1 and CS1. Furthermore, the PEM using PCS2 particularly in combination with QCHI demonstrated excellent biocompatibility that is promising for new bioactive, thermoresponsive coatings on biomaterials and substrata for culturing adhesion-dependent cells.

KEYWORDS: *multistep synthesis, PNIPAM cellulose sulfates, thermoresponsive properties, polyelectrolyte multilayers, bioactive properties, layer-by-layer technique*

1. INTRODUCTION

Smart polymers that are responsive to diverse stimuli, e.g., temperature, pH, ionic strength, are of particular interest for biomedical applications, such as controlled release and tissue engineering.[1−4] Among others, stimuli-responsive surfaces constructed from thermoresponsive polymers can be used for the production of cell sheets for simple detachment by changing the environmental temperature below the specific lower critical solution temperature (LCST).[5−7] This can overcome the drawbacks of conventional methods via the application of enzymes or physical cell scrapers that could damage cells and the integrity of confluent cell monolayers.[8,9] One widely used thermoresponsive polymer is poly-*N*-isopropylacrylamide (PNIPAM).[10] The main advantages of its use in biomedical applications include (i) a sharp phase transition cloud point temperature (T_{CP}) at an LCST of 32 °C that is close to the body temperature,[11] (ii) a good water solubility, (iii) low toxicity and excellent biocompatibility, and (iv) its readily commercial availability.[12] The first studies on thermoresponsive surfaces using PNIPAM were carried out in the early 1990s.[13] It established a method of grafting PNIPAM onto tissue-culture polystyrene (TCPS) dishes using electron beam irradiation. However, this method presents some

drawbacks, e.g., the requirement of expensive equipment for the fabrication, the requirement of a certain thickness of PNIPAM coating to control cell adhesion, and detachment on an uncoated TCPS surface.[14] Thus, a combination of PNIPAM with bioactive molecules may help address these issues for its further use in tissue engineering or other biomedical applications.

A broad and important group of bioactive polysaccharides are glycosaminoglycans (GAGs), such as heparin.[15,16] The sulfate group in GAGs plays a crucial role in their bioactivity for interaction with a plethora of proteins with regulatory function in humans, which allows their use as building blocks for implant materials and tissue engineering scaffolds.[17,18] However, GAGs from different sources have variable biological activities, which can result in unpredictable side effects and dilute the target effects during the application.[19,20] In comparison to GAGs, the semisynthetic cellulose sulfate (CS) with introduced sulfate groups in the anhydroglucose units is endowed with biological activities analogous to those of GAGs.[21] Specifically, sulfation in the 2-*O*-position and 6-*O*-position on CS showed similar properties to heparin, such as an anticoagulant effect[22] and binding of extracellular matrix proteins (e.g., fibronectin) and growth factors,[23] which is promising for application in tissue engineering.[24,25]

The layer-by-layer technique (LbL) through electrostatic interactions and ion-pairing of oppositely charged polyelectrolytes has been often used in the broad fields of tissue engineering and drug delivery to fabricate biocompatible and bioactive surface coatings on materials.[26−29] An obvious advantage of the LbL technique is that multilayer thickness can be controlled by the number of deposited layers, type of polyelectrolytes, and the environmental conditions such as pH value and ionic strength.[26] The multilayer containing PNIPAM combined with heparin was used previously to achieve a desired thickness (~12 nm) of surface coatings and showed the promoting effect on biocompatibility and cell adhesion.[14,27] Further important benefits of the multilayer based on bioactive polysaccharides can be used as a reservoir for the controlled release/presentation of growth factors or the uptake of metal ions to promote both growth and differentiation of cells.[30,31]

To date, no report exists about using PNIPAM-grafted CS for the formation of polyelectrolyte multilayers (PEMs) by LbL for application in tissue engineering. The coexistence of bulky PNIPAM chains and sulfation groups in PNIPAM-CS (PCS) would affect its feasibility as polyanion to form PEMs with polycation poly-L-lysine (PLL)[32,33] or quaternized chitosan (QCHI).[34] Herein, we designed a variety of synthetic routes for grafting PNIPAM on CS with distinct sulfation degrees. Thereafter, the investigation was carried out to evaluate their effects on the growth behavior, stability, and surface properties of PEMs, such as the wettability and surface potential, which are important and relevant for the interaction with proteins and cells. Further studies were also carried out to learn about the biocompatibility, cell adhesion, and growth of these multilayers using 3T3 mouse fibroblasts.

2. MATERIALS AND METHODS

2.1. Materials. Commercial microcrystalline cellulose Avicel PH-101 (MCC), potassium *t*-butoxide, cysteamine·HCl, poly(*N*-isopropylacrylamide) carboxylic acid terminated (PNIPAM-COOH) (molecular weight (MW): 2.0 kDa), chlorosulfonic acid, 1,1′-carbonyldiimidazole (CDI), 4-(dimethylamino)pyridine, and poly-(ethylenimine) (PEI, average MW: 750 kDa) were purchased from Sigma-Aldrich. Acetic anhydride and *N*-hydroxysuccinimide (NHS) and glass coverslips were purchased from VWR. Dialysis membrane (molecular weight cutoff (MWCO) = 3.5 kDa and MWCO = 0.5−1.0 kDa) and hydrogen peroxide (H$_2$O$_2$) were purchased from Carl Roth. *N*-(3-(Dimethylamino)propyl)-*N*′-ethylcarbodiimide·hydrochloride (EDC), 2-(*N*-morpholino) ethanesulfonic acid (MES) buffer (0.2 M buffer soln., pH 5.5), and ammonium hydroxide (NH$_4$OH) were purchased from Th. Geyer. Chitosan (CHI, 95/500, degree of deacetylation: 95% and MW: 200−400 kDa) was purchased from Heppe Medical Chitosan GmbH. Glycidyltrimethylammonium chloride (GTMAC, 80% in water) was bought from Tokyo Chemical Industry Co., Ltd. Poly-L-lysine (PLL, MW: 52 kDa) was purchased from Alamanda Polymers. Dimethylformamide, dimethyl sulfoxide, tetrahydrofuran, acetonitrile, and *n*-hexane were dried and stored over 4 Å molecular sieves. Milli-Q water (Milli-Q-plus system, Millipore) was used in the experiment. Gold-coated glass sensors were purchased from Ssens E.V., Netherlands.

2.2. Synthesis of PNIPAM Cellulose Sulfate (PCS). *PCS1.* Cellulose sulfate acrylate from CS1 (DS$_S$ = 0.67) (CSA, the details of preparation and characterization are provided in the Supporting Information.) (1.1 mmol, 253 mg) was dissolved in DI-water (5 mL). PNIPAM-cysteamine (1.1 mmol, 506 mg) was dissolved in DMF (5 mL). The CSA solution and PNIPAM-cysteamine solution were combined in one-neck glass bottle. 4-(dimethylamino)pyridine (2.2 mmol, 61.8 mg) was added into the mixture solution of CSA and PNIPAM-cysteamine, and stirred under 320−400 nm UV irradiation in argon gas at room temperature for 12 h. After the reaction, the solution was basified to pH 8 with NaOH aqueous solution (0.5 M). The solution was then filtered. The liquid phase was dialyzed (in dialysis membrane with a MWCO = 3.5 kDa) against ultrapure water for 1 week and then lyophilized into dry product (yield in wt %: 43.61%). Based on the ^{13}C NMR spectrum, the DS$_S$ of PCS1 was calculated to be 0.41 via comparing the signal integration of the "substituted" (C6s) and "non-substituted" (C6) carbon atoms. In combination with the elemental analysis with ^{13}C NMR analysis, the DS$_{PNIPAM}$ of PCS1 is 0.14. ^{1}H NMR (500 MHz, D$_2$O) in ppm: δ 4.65−4.21 (m, H of CSA), δ 4.14−4.10 (m, H of PNIPAM), δ 4.01−3.56 (m, H of CSA), δ 3.38−3.36 (m, H of PNIPAM), δ 3.34 (s, H of CSA), δ= 2.26−0.98 (m, H of PNIPAM). ^{13}C NMR (125 MHz, D$_2$O) in ppm: 182.36, 175.31, 175.02, 102.26, 78.83, 78.12, 77.96, 77.18, 74.69, 73.76, 72.69, 72.45, 66.08, 59.78, 41.74, 38.65, 21.51. Elemental analysis (found) in wt %: (C = 47.70, H = 7.96, S = 7.71, N = 3.11). Molecular weight: Mn = 10 377; Mw = 38 306; PDI = 3.69.

PCS2. PCS2 was synthesized by the reaction of PNIPAM-COOH with highly sulfated cellulose sulfate (CS2, DS$_S$ = 1.17) via the condition of EDC and NHS in MES buffer solution with a few modifications.[35−37] EDC (0.42 g, 1 equiv.) and NHS (0.13 g, 0.5 equiv.) were dissolved in MES buffer (50 mL) together. PNIPAM-COOH (1.1 g, 0.25 equiv.) was added into the mixture solvent of EDC and NHS. CS2 (0.6 g, 2.2 mmol) was dissolved in MES buffer (30 mL). Then, CS2 and PNIPAM-COOH solutions were combined and stirred at room temperature overnight. The solution was cooled to 4 °C and the product was precipitated after washing with THF/*n*-hexane (200/50 mL) twice.[36] The organic phase was removed and the product in aqueous phase was basified to pH 8 with NaOH aqueous solution (0.5 M), before it was filtered with filter paper. The liquid phase was dialyzed (in dialysis membrane with a MWCO = 3.5 kDa) against ultrapure water for 1 week. Finally, the pure product solution was lyophilized into dry product (yield in wt %: 61.18%). After the determination of PNIPAM-CS2 from ^{13}C NMR and elemental analysis, the DS of PNIPAM-CS2 ascribed to sulfate group and PNIPAM group are 0.93 and 0.11, respectively. ^{1}H NMR (500 MHz, D$_2$O) in ppm: δ 4.62−4.09 (m, H of CS), δ 4.00−3.97 (m, H of PNIPAM), δ 3.95−3.29 (m, H of CS), δ 3.69−3.60 (m, H of PNIPAM) was overlapped in δ 3.95−3.29 (m, H of CS), δ 3.34 (s, H of CSA) δ 2.16−0.99 (m, H of PNIPAM). ^{13}C NMR (125 MHz, D$_2$O) in ppm: 175.32, 174.12, 102.26, 100.16, 79.83−72.25, 66.08, 59.80, 41.73, 34.91, 21.50. Elemental analysis (found) in wt %: (C = 43.50, H = 7.92, S = 6.83, N = 8.14). Molecular weight: Mn = 30335; Mw = 45221; PDI = 1.49.

2.3. Characterization of PNIPAM Cellulose Sulfate (PCS). *Fourier Transform Infrared (FT-IR) Spectroscopy.* The FT-IR spectra were recorded on an Alpha FT-IR Spectrometer (Bruker, Germany) at room temperature. All samples were measured between 4000 and 500 cm^{-1} with a resolution of 4 cm^{-1} and accumulated 24 scans.

Nuclear Magnetic Resonance (NMR) Spectroscopy. The liquid-state ^{13}C NMR and ^{1}H NMR spectra of all polymeric samples were obtained at 25 °C on Bruker Avance III 500 spectrometers in D$_2$O or CDCl$_3$. Up to 150 scans were accumulated for ^{1}H NMR spectra and scans of up to 15 000 were accumulated for the ^{13}C NMR spectra. Chemical shifts are reported relative to the solvent peak.

Elemental Analysis. The elemental analysis was performed with an Elemental Analyzer Vario EL III CHN from Elementar (Hanau, Germany).

Size Exclusion Chromatography (SEC). The molecular weight distribution of the products was determined by SEC on Azura (Company: KNAUER Wissenschaftliche Geräte GmbH; Column: Suprema 3000A and Suprema 100A). Before the measurement, sample (1 mg) was dissolved in 1 mL of aqueous solution with NaNO$_3$ (0.1 M) and NaN$_3$ (0.05%). The solution was filtered with a 0.45 µm CA -filter and the sample solution (30 µL) was injected. The following measurement parameters were used: temperature of the column 30 °C; flow speed 1 mL/min; measurement time 30 min; UV detector 254 nm; calibration with pullulan.

Dynamic Light Scattering. The dynamic light scattering (DLS) measurements were performed on a Zetasizer Nano ZS (Malvern Instruments Ltd., UK) using a 5 mW laser with an incident beam of 633 nm (He−Ne laser). For the particle size measurement, the suspensions were diluted with water to a concentration of 1.5 mg/mL, 1 mg/mL in H$_2$O at pH 4 or 1 mg/mL in 0.15 M NaCl at pH 4 in a disposable cuvette (IDL GmbH, Gießen, Germany). The sizes were measured three times with 15 runs for each measurement and the average sizes from three measurements were used as results. The analysis of the data was done with *OriginPro 8.5* (OriginLab Corporation, MA, US).

Zeta Potential Measurements of Polyelectrolyte Solutions. The zeta potentials of polyelectrolytes (PEL) were studied by electrophoretic light scattering with a Zetasizer ZS (Malvern Panalytical, Malvern, UK). Polyelectrolytes were prepared at 2 mg/mL in a 0.02 M NaCl solution at pH 4. Samples were diluted to 0.5 mg/mL with a 20 mM NaCl buffer before measurement and measured at 25 °C with an applied voltage of 60 V. The measured electrophoretic mobilities were transformed into zeta potentials using Smoluchowski's formula.[38,39]

2.4. Substrate Cleaning. Glass coverslips were cleaned following the RCA-1 protocol for the removal of organic residues on the surface.[40] Milli-Q water and NH$_4$OH were heated to 80 °C and then H$_2$O$_2$ was added to the mixture (NH$_4$OH:H$_2$O$_2$:Milli-Q water = 1:1:5) and incubated for 15 min. Subsequently, substrates were extensively washed in Milli-Q water and dried in a stream of compressed nitrogen gas. Gold-coated glass sensors for SPR measurements were rinsed with 99.8% ethanol and Milli-Q water and immediately used for the SPR measurements.

2.5. Polyelectrolyte Multilayer Assembly. Diverse substrates were used with Si-Wafer for ellipsometry, gold sensors for SPR, glass for streaming potential measurements, and tissue culture polystyrene (TCPS) wells for cell experiments. TCPS without PEM was used for control experiment. Polycations (QCHI and PLL) and polyanions (CS derivatives) were prepared at a concentration of 1 mg/mL in 0.15 M NaCl buffer. PEI used as an anchoring layer on the substrate was prepared at a concentration of 5 mg/mL and the pH of PEI was adjusted to 4. All the PEL solutions were filtered with a 0.22 µm filter. PEM assembly is based on the alternating adsorption of polycations and polyanions (CS1, CS2, PCS1 and PCS2) on substrates with intermediate washing steps with NaCl solution (150 mM, pH 4, 3 × 1 min). The layer sequence was CS derivatives and altered with polycation (QCHI, PLL) until the fifth layer to achieve basal layers. PCS derivatives were used for the outer layers to form another five functional layers with polycations. Odd layers utilized PLL or QCHI, while CS or PCS was used for even layers.

2.6. Measurement of Multilayer Growth. The multilayer growth was studied by surface plasmon resonance (SPR) measurements using an IBIS-iSPR device (IBIS Technologies B.V., Hengelo, The Netherlands). SPR is based on the excitation of surface plasmons at the gold/liquid interface. The adsorption of macromolecules onto a gold-coated sensor surface results in the change of the refractive index, which is measured as shift in the resonance angle. This angle shift (m°) proportionally corresponds to mass adsorption on the gold sensor. Hence, the multilayer growth can be monitored during LbL layer formation. The cleaned gold sensor was placed in the measurement chamber and equilibrated with degassed 0.15 M NaCl buffer solution at pH 4 to record a stable baseline upon which the angle shift is based. Thereafter, PEM formation was performed via LbL assembly. Degassed PEL solutions were injected and run over the gold sensor for 10 min. After the PEL deposition, the measurement chamber was rinsed with 0.15 M NaCl solution for three times 5 min each to remove unbound compounds. Adsorption and rising times were chosen regarding the angle shift reaching an equilibrium. The angle shift was measured in 10 different regions of interest in the sensor, which were predefined by the software for plotting the graphs.

2.7. Streaming Potential Measurements. The zeta potential of PEM was determined using the SurPASS electrokinetic analyzer (Anton Paar, Graz, Austria). Therefore, PEM systems were prepared on special glass slides (10 × 20 mm^2, Paul Marienfeld GmbH & Co. KG, Lauda-Königshofen, Germany) for streaming potential measurements. Two glass slides modified with the identical PEM were inserted into the measuring cell, creating a small gap through which the electrolyte (0.01 M KCl in water) was pumped. A flow rate of 100−150 mL/min was adjusted at a maximum pressure of 300 mbar. Before starting the measurement, hydrochloric acid (HCl) was used to adjust the pH value to 2.5. During the measurement, automated titration with sodium hydroxide (NaOH) adjusted the pH in the range of 2.5 to 9.5. The zeta potential was calculated by the provided software. Each PEM was measured twice with the device.

2.8. Water Contact Angle Measurements. The surface wettability of the various polyelectrolyte multilayer compositions on Si wafers was determined by static contact angle measurements using an OCA 15+ device (Dataphysics GmbH, Filderstadt, Germany). The measurements were performed after washing the samples in pH 7.4 phosphate buffered saline and subsequently dried using nitrogen gas. The droplets of fresh Milli-Q water (3 µL) dispersed through a 0.52 µm outer diameter needle at a rate of 0.5 µL/s. Measurements were performed in duplicates at room temperature by placing three droplets per sample using the sessile drop method. Automated baseline and drop shape analysis provided by the software (SCA 20, Dataphysics) was performed. The contact angle for each drop was calculated using ellipse fitting.

2.9. Cell Culture. The 3T3 mouse fibroblast cell line was obtained from DSMZ (Deutsche Sammlung von Mikroorganismen and Zellkulturen GmbH, Braunschweig). 3T3 cells were cultured in T75 flasks, seeded at a density between 5000 and 6000 cells/cm^2 in Dulbecco's modified Eagle's medium (DMEM, Lonza, Walkersville, USA) containing 4.5 g/L glucose and 4 mM glutamine, supplemented with 10% fetal bovine serum (FBS Superior, Biochrom GmbH, Berlin, Germany) and 1% penicillin, streptomycin, and amphotericin B (BioWhittaker, Lonza, Walkserville, USA). Cultured cells are grown at 37 °C in a humidified incubator (5% CO$_2$/95% air atmosphere). At 70−90% confluency of the cells, trypsinization was performed by washing the cells with sterile PBS once and adding 0.25% trypsin/0.02% ethylenediaminetetraacetic acid (EDTA) (Biochrom GmbH, Berlin, Germany) solution for 5 min incubation at 37 °C, followed by adding serum-containing DMEM to inactivate trypsin. The cell suspension was centrifuged for 5 min at 500 rpm, resulting in a cell pellet. The supernatant was removed, and the cells were resuspended in fresh DMEM. Cells were counted using a Neubauer chamber and seeded in new culture flask or at certain cell densities in well plates.

2.10. Cell Viability Assay. Viability of 3T3 mouse fibroblasts cells and subsequent biocompatibility of PEM films was assessed using a live/dead assay. A cell viability/cytotoxicity assay kit (Biotium, Fremont, USA) consisting of dyes calcein AM (green staining) and

Scheme 1. (A) Schematic Illustration for the General Synthesis of PCS; (B) Two Synthesis Routes: (1) Strategy 1 As a Multistep Reaction Including Steps 1−3; (2) Strategy 2 As the Direct Esterification
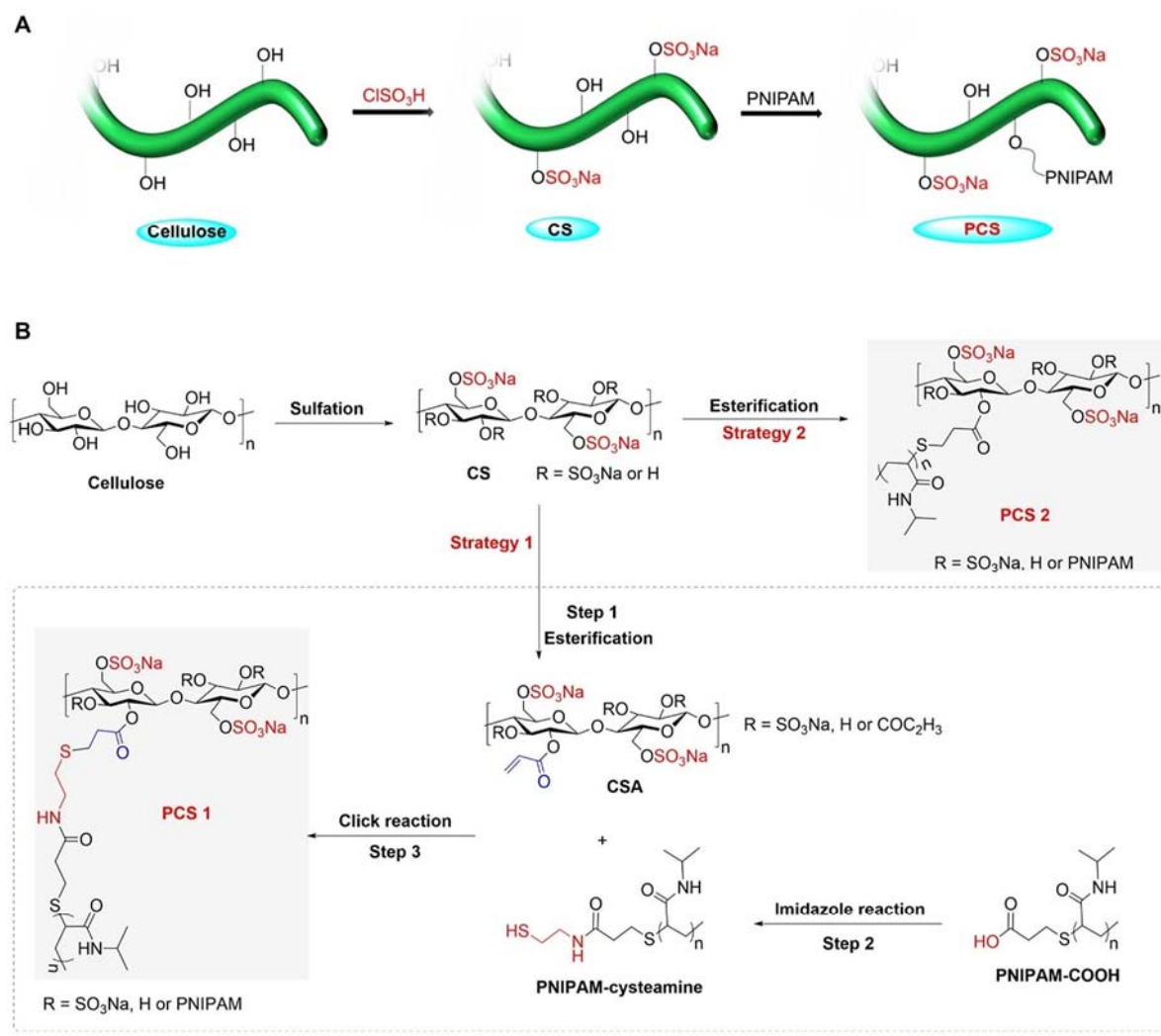
ethidium homodimer III (red (DNA) staining) was used to detect living and dead cells, respectively. Cells were seeded on different PEM-coated wells of a 24-well plate at a density of 5000 cells/cm² and cultivated for 24 h before staining according to the manufacturer's protocol. Cells were seeded in uncoated tissue culture polystyrene wells as control. Images were taken using a confocal laser scanning microscope (CLSM, LSM 710, Carl Zeiss, Oberkochen, Germany). Images were analyzed using Fiji software[41] using at least 10 images per condition to quantify the cell density and cell area.

2.11. Cell Growth Assay. Cell metabolic activity was quantified using a QBlue assay. PEM-coated 48-well plates were sterilized using a UV chamber for 60 min at 2.5 kJ at a wavelength of 254 nm. 3T3 cells were seeded into the wells at a density of 13 500 cells/cm². After 1, 4, and 7 days of cell culture, cells were washed with colorless DMEM. Subsequently, 300 μL of a 10% Qblue solution (in colorless DMEM, w/o FBS) was added to the well, followed by 2 h incubation at 37 °C. After incubation, 100 μL of the supernatant has been transferred to a black 96-well plate for excitation at 540 nm wavelength in a fluorescence plate reader (Fluostar Optima, BMG Labtech, Ortenberg, Germany).

2.12. Statistical Analysis. All the data were statistically calculated as the means ± standard deviations using *Origin* software. Analysis of significance is performed with the one-way ANOVA. A value of $p \leq 0.05$ was considered significantly different and is indicated by *.

3. RESULTS AND DISCUSSION

3.1. Synthesis and Characterization of PCS. To obtain the PCS containing both sulfate groups and PNIPAM grafting, we designed multistep synthetic methods (Scheme 1). Starting with cellulose, CS was synthesized at first and PNIPAM chains were introduced thereafter into the CS backbone, leading to PCS (Scheme 1A). According to the protocol established by Zhang et al.,[42] CS1 with a low DS_S ascribed to sulfate groups of (0.67) and CS2 with a higher DS_S of 1.17 were obtained via a quasi-homogeneous nucleophilic substitution reaction (Scheme 1B and Table S1).

In strategy 1, cellulose sulfate acrylate (CSA) was synthesized from CS1 with acryloyl chloride via a nucleophilic substitution reaction (Scheme 1B, step 1).[43] In parallel,
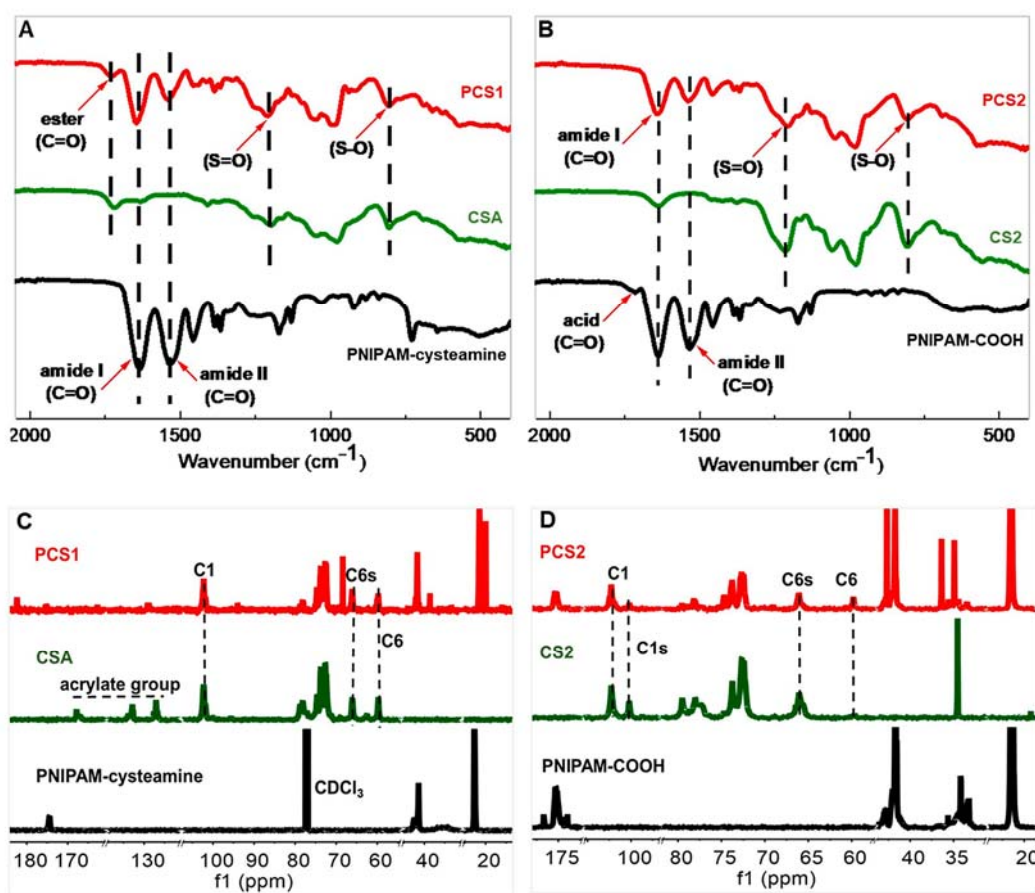
Figure 1. (A) FT-IR spectra of PCS1, CSA and PNIPAM-cysteamine. (B) FT-IR spectra of PCS2, CS2, and PNIPAM-COOH. (C) ^{13}C NMR spectra of PCS1, CSA, and PNIPAM-cysteamine. (D) ^{13}C NMR spectra of PCS2, CS2, and PNIPAM-COOH.

PNIPAM-cysteamine was prepared with the imidazole reaction of cysteamine hydrochloride and commercial PNIPAM-COOH (Scheme 1B, step 2).[44] After that, lower sulfated PCS1 (DS_S of 0.41) was synthesized via the click reaction of PNIPAM-cysteamine with CSA under UV light at ambient conditions (Scheme 1B, step 3). Due to the desulfation during step 1 of strategy 1,[45] there was a failure to obtain higher sulfated PCS with strategy 1. Alternatively, by strategy 2, PCS2 with a higher DS_S (0.93) was successfully synthesized after the esterification of CS2 with PNIPAM-COOH through the EDC/NHS-catalyzed reaction (Scheme 1B).[35−37]

Spectroscopic characterization was carried out after the synthesis of the products. Characteristic signals at 1726 cm^{-1} (C=O), 1209 cm^{-1} (S=O), and 809 cm^{-1} (S−O) are visible within the FT-IR spectrum of PCS1, while the signals attributed to amide I (1640 cm^{-1}) and amide II (1535 cm^{-1}) are also present (Figure 1A). The presence of important moieties of PCS1 was further verified by ^{13}C NMR spectra (Figure 1C). The ^{13}C NMR signal of acrylate groups in CSA disappeared after the click reaction, which revealed the addition reaction between the thiol group and acrylate group. Furthermore, the signals derived from PNIPAM-cysteamine and CSA emerged in the ^{13}C NMR spectrum of

PCS1. Therefore, PCS1 was successfully prepared as demonstrated by the ^{13}C NMR and FT-IR spectra.

In the FT-IR spectrum of PCS2 (Figure 1B), signals of amide I (1636 cm^{-1}), amide II (1537 cm^{-1}) of PNIPAM, and signals at 1212 cm^{-1} (S=O) and 808 cm^{-1} (S−O) of CS2 were found. Notably, the characteristic signal of carboxyl acids (1719 cm^{-1}) derived from PNIPAM-COOH disappeared in the FT-IR spectrum of PCS2, which indicates the successful esterification of CS2 with PNIAPM-COOH. Furthermore, the chemical structure of PCS2 was further verified by its ^{13}C NMR spectrum, compared with the spectra of CS2 and PNIPAM-COOH (Figure 1D).

With the final materials PCS1 and PCS2 in hand, we next probed the coil-to-globular transition of PCS by measuring the hydrodynamic radius (R_h) and polydisperse index (PDI) using DLS. The T_{CP} refers to the cloud point temperature of a polymer solution at a specific concentration.[46] For instance, heating PCS1 aqueous solutions from 25 °C to 32 °C did not show any macroscopic thermoresponsive phenomenon (Figure 2A, left side glass vial). The clouding first appeared at 33 °C and the reversible T_{CP} matched well with the DLS analysis during heating−cooling cycles (Figure 2A, curves on the right side). The DLS curves exhibited multiple peaks below 32 °C, while a single peak was visible above 33 °C, indicating a total
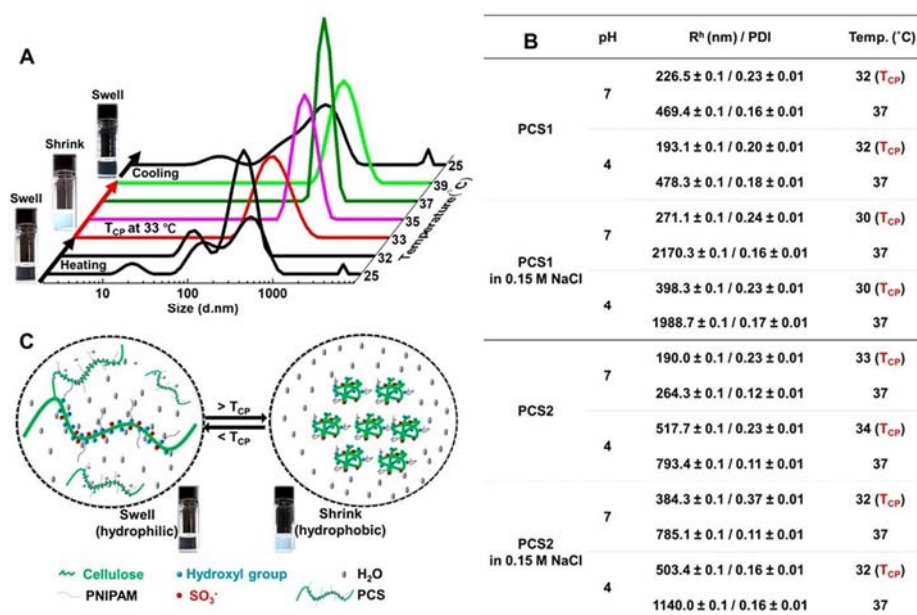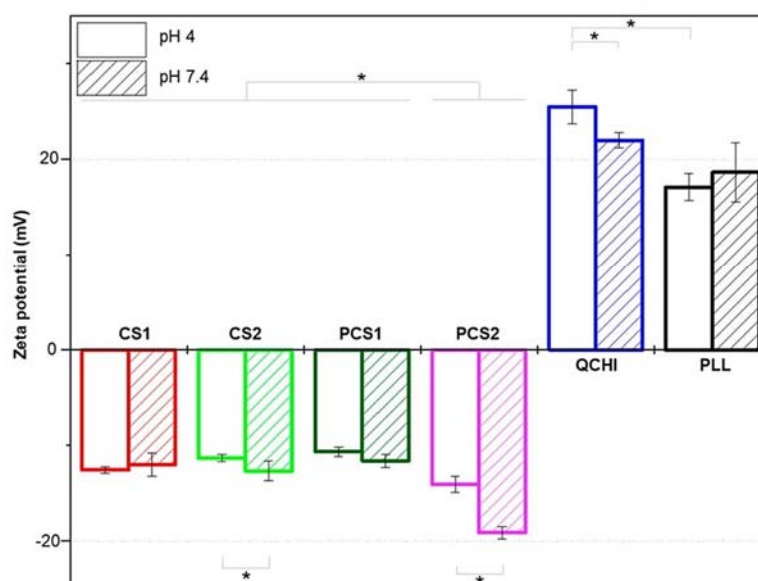
B	pH	R^h (nm) / PDI	Temp. (°C)
PCS1	7	226.5 ± 0.1 / 0.23 ± 0.01	32 (T$_{CP}$)
		469.4 ± 0.1 / 0.16 ± 0.01	37
	4	193.1 ± 0.1 / 0.20 ± 0.01	32 (T$_{CP}$)
		478.3 ± 0.1 / 0.18 ± 0.01	37
PCS1 in 0.15 M NaCl	7	271.1 ± 0.1 / 0.24 ± 0.01	30 (T$_{CP}$)
		2170.3 ± 0.1 / 0.16 ± 0.01	37
	4	398.3 ± 0.1 / 0.23 ± 0.01	30 (T$_{CP}$)
		1988.7 ± 0.1 / 0.17 ± 0.01	37
PCS2	7	190.0 ± 0.1 / 0.23 ± 0.01	33 (T$_{CP}$)
		264.3 ± 0.1 / 0.12 ± 0.01	37
	4	517.7 ± 0.1 / 0.23 ± 0.01	34 (T$_{CP}$)
		793.4 ± 0.1 / 0.11 ± 0.01	37
PCS2 in 0.15 M NaCl	7	384.3 ± 0.1 / 0.37 ± 0.01	32 (T$_{CP}$)
		785.1 ± 0.1 / 0.11 ± 0.01	37
	4	503.4 ± 0.1 / 0.16 ± 0.01	32 (T$_{CP}$)
		1140.0 ± 0.1 / 0.16 ± 0.01	37

Figure 2. (A) Dynamic light scattering analysis of T_{CP} and curves of PCS1 at a concentration of 1.2 mg/mL in aqueous solutions at pH 7. (B) Dynamic light scattering analysis of hydrodynamic radius (R_h) and polydisperse index (PDI) of PCS (concentration 1.0 mg/mL in aqueous solutions with/without NaCl) at T_{CP} and 37 °C. (C) Schematic illustration for the thermoresponsive behavior of PCS in aqueous solutions.

Figure 3. Zeta potential measurements of polyelectrolytes used for multilayer formation measured at pH 4 and pH 7.4. Bar graphs show mean values with standard deviations. Significance is indicated by * ($p \leq 0.05$) and was determined by Kruskal−Wallis test. QCHI, quaternized chitosan; PLL, poly-L-lysine.

coil-to-globular transition of PCS1.[47] Similar phenomenon was also observed for aqueous PCS2 solutions at pH 7.

To mimic the physiological conditions for real biomedical applications, we studied thermoresponsive properties of PCS1 and PCS2 in the presence of NaCl (0.15 M) under different pH values (Figure 2B). In the presence of NaCl at T_{CP}, PCS1 and PCS2 showed a slightly lower T_{CP} and formed larger

aggregates compared to their solutions without NaCl. The reason could be the presence of kosmotropic anions such as Cl⁻ ions that are more hydrophilic and thus more hydrated ions will be involved in the aggregates formed around T_{CP}. Moreover, in the presence of NaCl, PCS2 formed larger aggregates than PCS1 at T_{CP}, whereas PCS1 generated larger aggregates at body temperature (37 °C).
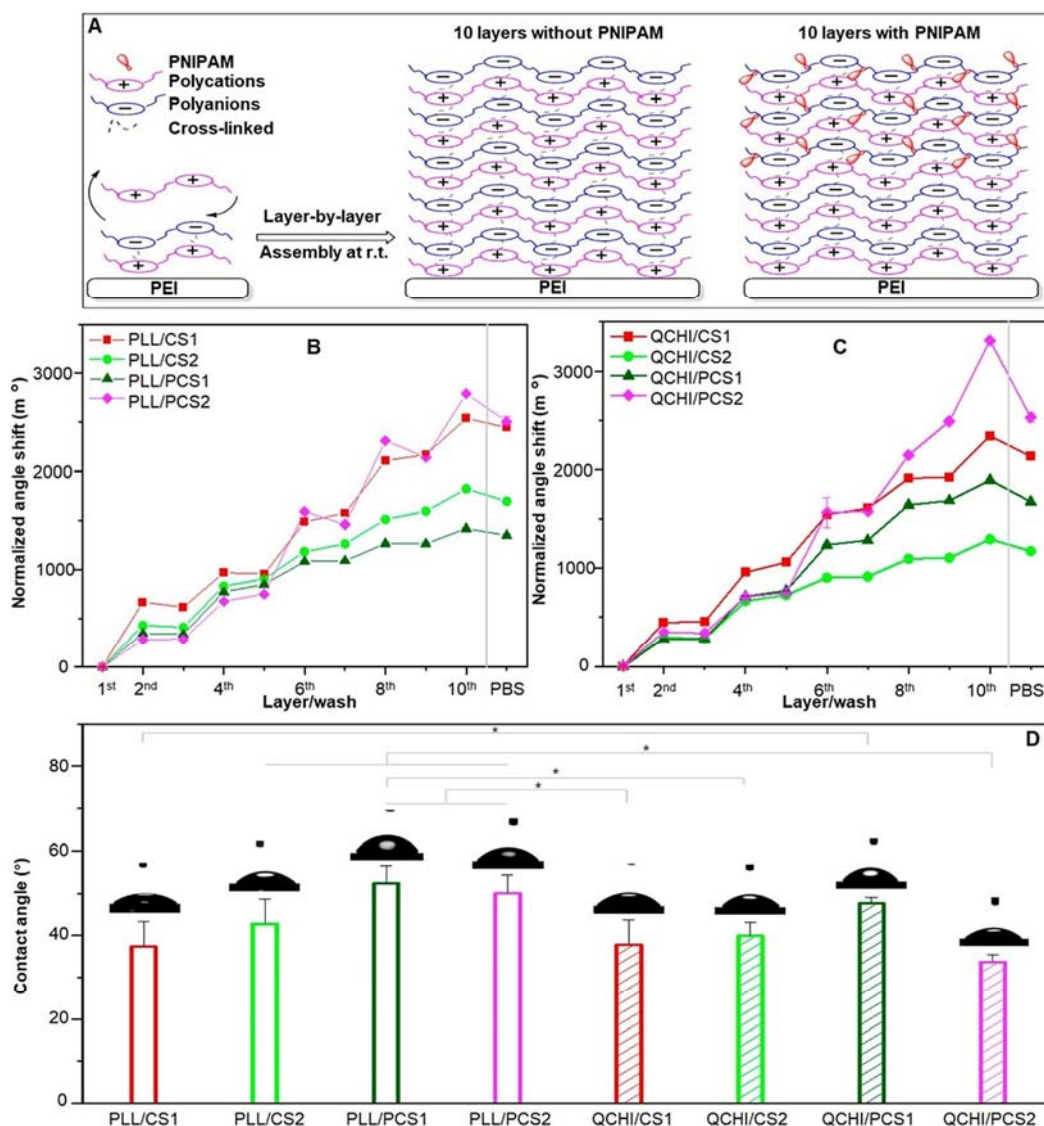
Figure 4. (A) Schematic illustration of the preparation of PEM via the layer-by-layer technique. Surface plasmon resonance measurements of the layer growth of PEM showing the normalized angle shift after each layer deposition. (B) PLL as polycation. (C) QCHI as polycation. (Even layers represent polyanions (polycations/CS, CS1 or 2 from 2nd to 10th layer; polycations/PCS, CS2 for basal layer from 2nd to 5th layer and PCS1 or PCS2 for functional layer from 6th to 10th layer) and odd layers represent polycations (1st, PEI; 3rd to 9th, PLL or QCHI)). (D) Static water contact angles of terminal polyanion layers measured with sessile drop method. Measurements were done in triplicates. Bars represent average values with standard deviations. Significance testing was done by one-way ANOVA with significance level $p \leq 0.05$, indicated by *.

It was observed on chitosan-*graft*-PNIPAM in aqueous solutions that micelles were formed at low pH (<4) and >32 °C, while higher pH value led to larger aggregates.[48] At 37 °C, PCS1 showed a similar trend with the formation of larger aggregates at pH 7 than pH 4. In comparison, PCS2 showed even a different trend and the aggregates became smaller at pH 7. Therefore, the hydrophilic sulfate groups in PCS backbones should have strongly affected the formation of aggregates and their sizes. The stronger electrostatic repulsion provided by higher charges from more sulfate groups on PCS2 chains could have hampered the aggregation at 37 °C.[49] In addition, the

PDI values became generally slightly lower at pH 4 (Figure 2B), which indicates more uniform PCS aggregates at 37 °C than at T_{CP}.[50] Based on these results, a schematic illustration can be proposed for the thermoresponsive behaviors (Figure 2C). First, the PCS chains at lower temperatures swell via intermolecular hydrogen bonding between hydrophilic PCS chains with water molecules.[11] When the solution temperature is elevated above T_{CP}, hydrophobic PNIPAM chains are formed and drag the PCS chains into formation of aggregates, disrupting the intermolecular hydrogen bonding.[51] Consequently, the aqueous solutions of PCS became cloudy, while
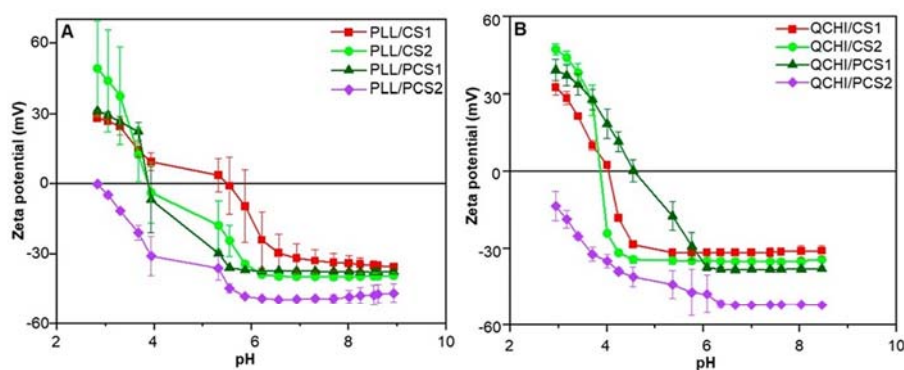
Figure 5. pH-dependent surface zeta potentials of multilayer films after the assembly at different pH values (acid-to-base pH titration). Use of different CS and PCS as polyanion with (A) PLL and (B) QCHI as polycation with CS and PCS as terminal layers.

the aggregation process is totally reversible. Due to the presence of anionic sulfate groups, the aggregation behaviors of PCS chains are also affected by pH and different ionic strength of the aqueous solutions in addition to temperature, as shown in Figure 2.

For the fabrication of PEM films via the LbL technique, oppositely charged PELs are necessary. The zeta potentials of PELs including negatively charged CSs and PCSs as well as positively charged polycations applied for multilayer formation were measured with electrophoretic light scattering and are shown in Figure 3. At pH 4, PCSs and their precursors CSs show negative potentials between −11 and −14 mV with PCS2 having the most negative charge. Both polycations possess positive zeta potentials with about 26 mV for QCHI and 17 mV for PLL. At pH 7.4, PCS1, CS1, and CS2 showed similar or slightly lower zeta potentials, whereas only PCS2 exhibited a stronger decrease of zeta potential of −5 mV. The negative zeta potentials of CS derivatives are based on the presence of sulfate groups. As to the polycations, the zeta potential of PLL slightly increased with 1.6 mV at the higher pH value 7.4. In comparison, the zeta potential of QCHI significantly decreased by 3.5 mV, which should be because of the deprotonation of QCHI chains at higher pH values. Nevertheless, both of the polycations, namely, QCHI and PLL, show sufficiently high positive charges at both pH values for PEM formation.[52] Overall, the zeta potential measurements suggest that the oppositely charged CSs/PCSs and PLL/QCHI can be used for the fabrication of multilayers.

3.2. Fabrication of Polyelectrolyte Multilayers (PEM) with LbL Technique. PLL and QCHI have been often used previously as polycations for multilayer formation,[53,54] but not in combination with CS that has been applied as the polyanion previously to make bioactive PEMs.[25,55] In particular, the macromolecular architecture due to the grafting of bulky noncharged PNIPAM along the polyanionic PCS chains would further affect the formation of PEMs by the LbL technique.

SPR measurements were performed to assess PEM formation/growth and their stability after washing with PBS (Figure 4A−C). The angle shift for PEI as the first layer was set at zero to make comparison of layer growth between the different PEMs easier. For PLL-containing PEMs (Figure 4B), PCS1 and CS2 showed angle shifts for the 10th layer of ~1500 m° and 1900 m°, respectively. Distinctly 100 m° higher angle shifts were observed with CS1 or PCS2 as polyanions. Using QCHI as polycation (Figure 4C), PCS1 showed higher angle

shifts than CS2, but still had lower angle shifts than CS1 and PCS2. Notably, the angle shift of the PEM of QCHI/CS1 was almost the same as that of the PEM of PLL/CS1, while the PEM of QCHI/PCS2 exceeded all other values and reached the highest angle shift of about 3400 m°.

It was reported that a higher sulfation degree of CS led to more compact PEMs that were characterized by lower angle shifts in SPR studies and lower hydration found by quartz microbalance measurements.[55] PEMs with CS1 as the polyanion show higher angle shifts than CS2, which is also probably related to the slightly higher charge density of CS1 compared to CS2.[56−58] Furthermore, the higher charge density of PCS2 as also seen in the zeta potential measurements seems to play a dominating role to overcome the steric repulsive effect of PNIPAM allowing stronger adsorption to both polycations during the PEM formation.[55] Moreover, it is notable that the polycations also affected the PEM formation and growth, as QCHI-containing PEMs showed higher angle shifts when combined with either PCS1 or PCS2 than PLL. This could be attributed to the higher absolute zeta potential of QCHI in comparison to PLL, which enhances the formation of PEMs by overcoming steric repulsive effects of PNIPAM side chains. Another important observation was that a change of rinsing solution from 0.15 M NaCl at pH 4 to PBS with pH 7.4 caused a decrease in angle shifts for all PEMs, which indicates some loss of polyelectrolytes due to the decrease in charge density by the partial deprotonation of primary amino groups of PLL and QCHI.

The surface properties of biomaterials, such as wettability and surface potential, are related to protein adsorption and cell adhesion affecting the biocompatibility.[59−61] Moreover, the wetting properties and surface potential of PEM may also provide hints about the composition of the outermost layer.[59] The wettability of the terminal polyanion layer of PEM was determined by static water contact angle (WCA) measurements (Figure 4D). Overall, it was observed that all surfaces were hydrophilic, with WCAs in a narrow range of about 30−50°, which indicates the dominant role of CSs/PCSs in the terminal layer of these PEMs. Such hydrophilic surface properties of all PEMs are probably related to the presence of sulfate and hydroxyl groups in the terminal layer.[61] Compared to CSs, PCSs led to slightly larger WCA, particularly in combination with PLL (55−58°). This effect is probably related to the slightly lower hydrophilicity of PLL and/or the fact that PLL is more diffusible due to its lower
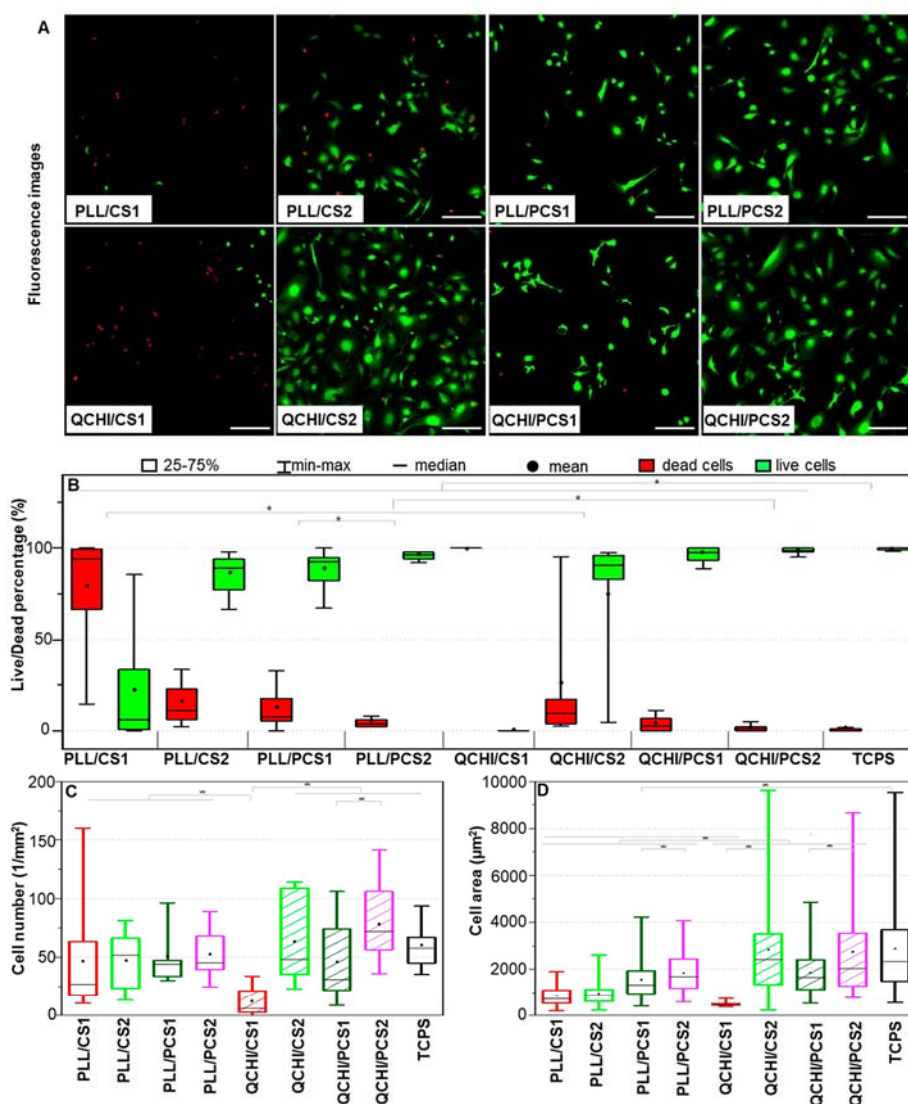
Figure 6. (A) Fluorescence images of 3T3 cells on different PEM surfaces. Live cells were stained visibly green of the cell cytoskeleton and dead cells were red of the nuclei. Scale bar = 200 μm. (B) Live/dead ratios of 3T3 mouse fibroblasts seeded on PEM and TCPS as positive control. Quantification of (C) cell density and (D) cell area of 3T3 cells cultured for 24 h in different PEM-coated wells. The box plot corresponds to upper and lower quartile, the band corresponds to the median and the square/point corresponds to the mean value. Whiskers represent maximum and minimum of data. The significance level $p \leq 0.05$ is indicated by *.

MW and may be also more present in the surface region of the PEM.[62] No significant difference was observed for CS1 and CS2 in combination with either of the polycations.

The surface zeta potentials of all PEM decreased to negative values with increasing pH values (Figure 5A). This is due to the intermingled character of PEM and the existence of a swollen surface layer in which both polyelectrolytes contribute to the surface potential.[63] Hence, polycations dominate the surface zeta potential in the acidic region, while polyanions play a role in the basic region as found in previous studies on multilayers.[55,64] Most strikingly, PEM with PCS2 as the polyanion possessed a high negative surface zeta potential throughout the whole pH titration range, indicating the

formation of a stable and more uniform terminal layer with PCS2 in comparison to CSs and PCS1. This result is also consistent with the lowest WCA values of PCS2/QCHI.

Furthermore, it is also visible that CS2 resulted in lower surface zeta potentials at both pH 4 and pH 7.4, which is related to their higher sulfation degree regardless of the use of PLL or QCHI as the polycation. The similar surface zeta potentials during pH titration of PLL/CS2 and PLL/PCS1 also indicate a certain intermingled composition of the surface region of both PEMs. Only the PEM of CS1/PLL showed a point of zero charge (PZC) of pH ~5.5, which should be primarily due to the lower amount of sulfate groups and potential interpenetration of PLL in the surface layer. The
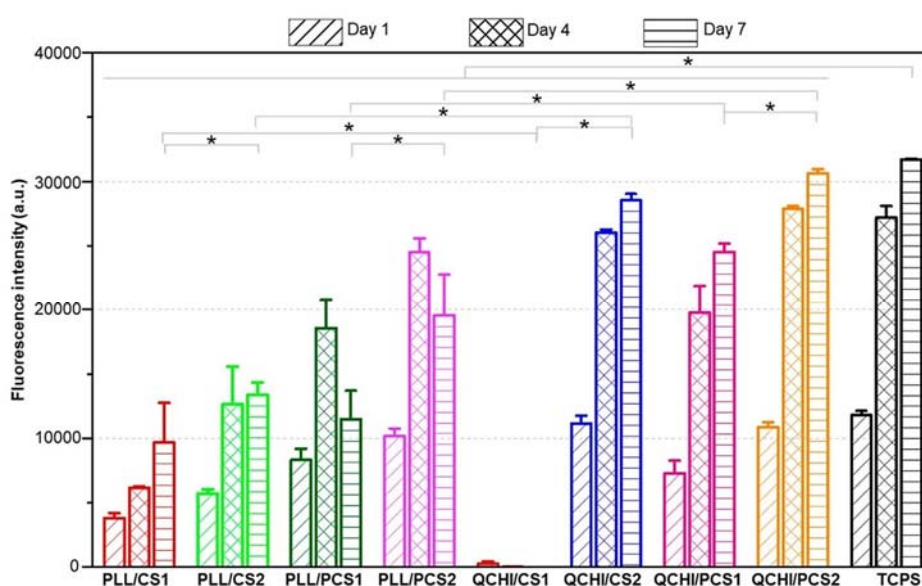
Figure 7. Study of fibroblast growth using a Deep Blue Cell Viability test over the course of 7 days. Bar graphs shows the fluorescence intensities (FI) after cell culture for 1, 4, or 7 days. Higher FI values correspond to higher metabolic activity, meaning that cells have grown and are viable over the course of time. The significance level $p \leq 0.05$ is indicated by *.

combination of CSs or PCS1 as the polyanion with QCHI as the polycation resulted in similar surface zeta potentials as those of PEMs with PLL as the polycation. Only the PZC values of PEMs of QCHI/CS1 and QCHI/PCS1 were shifted to more acidic pH values of pH 4.1 and 4.6, respectively.

3.3. Biocompatibility Studies. The use of polycations PLL and QCHI can be relevant to cytotoxic effects as known from previous studies.[65,34] In addition, physical properties including wettability and zeta potential have effects on cell adhesion and growth as well.[60,61] In our PEM layers, cytotoxicity was studied using 3T3 mouse fibroblasts recommended by the ISO 10993−5 with a live/dead assay using CLSM images (Figure 6A).

After 24 h of culturing time, a live/dead cell ratio (LDCR) of 100% was observed for TCPS, which was used as the positive control substrate (Figure 6B). The PEMs using CS1 combined with QCHI or PLL as polycation were the most cytotoxic, with an LDCR of 0% and 20%, respectively. PEMs with CS2 combining QCHI or PLL were less cytotoxic with LDCR of ~80%, respectively. On the other hand, using PEMs containing PCS1 or PCS2, the LDCR was even higher for PLL/PCS1 and 95% for PLL/PCS2. The use of QCHI as the polycation reduced cytotoxicity further, with an LDCR of around 98% for PEMs of QCHI/PCS1 and QCHI/PCS2, which is comparative to the viability for TCPS.

The findings of cytotoxicity studies were also associated with quantifying adhering cells and their spreading from the live cell staining. Cell density and area were the lowest for QCHI/CS1 and PLL/CS1, as shown in Figure 6C, D. Further cytotoxicity study on PEM containing QCHI showed that cell densities on QCHI/CS2 and QCHI/PCS2 were higher than on TCPS (60 cells/mm²). For PLL-containing PEMs, cell numbers were very similar to all PEMs containing CSs and PCSs and less than TCPS. Among them, the cell density was the highest for PLL/PCS2. Concerning the cell spreading quantification, the

measurements revealed substantially larger cell areas for PEMs containing QCHI compared to PLL-containing PEMs (Figure 6D). Cell areas on PEMs of QCHI/CS2 and QCHI/PCS2 were similar, with TCPS having an area of around 2800 μm^2, while cells on QCHI/PCS1 showed less spreading morphology. Especially, the cell areas were significantly lower for PLL-containing PEMs compared to TCPS. Cells seeded on PEMs of PLL/CS1 and PLL/CS2 were the smallest, with areas below 1000 μm^2, whereas only the cell areas were nearly two times higher on PEMs of PLL/PCS1 at 1600 μm^2 and PLL/PCS2 at 1800 μm^2.

The growth of 3T3 mouse fibroblasts was studied over the course of 7 days by performing a Deep Blue assay. On day 1 and day 4, the fluorescence intensity for all films was detected, indicating the presence of viable cells, except for the PEM of QCHI/CS1, which did not permit any growth of cells during the whole period of 7 days (Figure 7). A close relationship to cytotoxicity and cell adhesion studies was seen for PEMs containing PLL as the polycation, which was lower for all PEMs (except CS1) in comparison to the use of QCHI. Particularly, PEMs containing CS1 or PCS1 were characterized by slower cell growth compared to the PEMs containing CS2 or PCS2. After 7 days, the differences regarding cell growth between QCHI-containing PEMs and PLL-containing PEMs were significant (except for QCHI/CS1, which was lower than PLL/CS1).

The results of cell culture studies indicate that the type of polycation, DS_S, and grafting of PNIPAM play crucial roles for the stability and surface properties of PEMs and further determine the cell fate regarding the cytotoxicity, cell adhesion, spreading, and growth. It is obvious that the PEM with CS1 as the polyanion showed a lower structural stability regardless of combining PLL or QCHI. This is probably due to the low DS_S value, which decreases the ion pairing with the polycations,[66] further allowing the release of PLL and QCHI, which are both

---

highly cytotoxic.[65] These released polycations with high positive charge density could destroy cell membranes. In particular, cell growth was further inhibited on PEMs containing PLL after 7 days due to its more intermingling layers than PEMs containing QCHI. In comparison, the presence of PNIPAM in PCS1 for the formation of PEM seems to reduce the cytotoxicity and increase the adhesion, spreading, and growth of fibroblasts. The reason is because the hydrophobic interactions of PNIPAM within PCS1 above LCST during culture of cells at 37 °C should have contributed to higher stability and WCA of PEM, which favored more adsorption of proteins from serum and secreted by cells.[27,60] It is also important to note that the higher structural stability of PEMs was derived from the higher DS_S of CS2 and PCS2 due to the improved ion pairing with polycations. It helps to reduce the cytotoxicity and at the same time enhance the adhesion and spreading of cells as signs of intracellular processes affecting mitogenic signaling, which is followed by increased cell growth.[67] This can be considered as representation of the bioactivity of CS that was reported previously to increase with higher DS_S and underlines the necessity to have a certain sulfation degree for forming stable PEMs and providing them with the desired bioactivity.[55,68,69] In addition, grafting of PNIPAM to the PCS2 backbone further improved these behaviors, which may also be interpreted by additional hydrophobic interactions with serum protein supporting the adhesion and growth of cells.[70]

4. CONCLUSIONS

PNIPAM-grafted cellulose sulfates PCS1 (DS_S 0.41) and PCS2 (DS_S 0.93) as GAG-mimetic compounds with thermoresponsive properties were successfully synthesized via two synthetic strategies. Their thermoresponsive properties were found to be affected by parameters such as DS_S, pH, and ionic strength. Higher sulfated PCS2 generally shows a higher T_{CP} than PCS1 and the presence of NaCl slightly decreases the T_{CP}. PCS2 generally forms larger aggregates than PCS1 at T_{CP}, whereas lower sulfated PCS1 leads to larger aggregates at body temperature (37 °C). PCSs and precursor CSs were used as polyanions for constructing PEMs and for cell cultures. It can be concluded from zeta surface potential and SPR measurements of PEMs that PCS2 with a higher DS_S is related to the fabrication of stable, bioactive multilayer systems that promote the adhesion and growth of cells, particularly if QCHI is used as the polycation during multilayer formation. In contrast, PCS1 with low DS_S is not sufficient to form stable multilayers. Hence, PEMs of QCH/PCS2 are promising for future studies to investigate the potential of these coatings to be used as reservoirs for growth factors and their thermosensitive properties for the generation of cell sheets for tissue engineering.

ASSOCIATED CONTENT

ⓈI Supporting Information

The Supporting Information is available free of charge at https://pubs.acs.org/doi/10.1021/acsami.2c12803.

> Data that support the findings of this study, including materials, experimental procedures, characterization data, and spectra (PDF)

■ AUTHOR INFORMATION

Corresponding Author

Kai Zhang − *Sustainable Materials and Chemistry, Department of Wood Technology and Wood-based Composites, University of Göttingen, Göttingen D-37077, Germany;* ● orcid.org/0000-0002-5783-946X; Email: kai.zhang@uni-goettingen.de

Authors

Kui Zeng − *Sustainable Materials and Chemistry, Department of Wood Technology and Wood-based Composites, University of Göttingen, Göttingen D-37077, Germany*

Falko Doberenz − *Department Biomedical Materials, Institute of Pharmacy, Martin Luther University Halle-Wittenberg, Halle (Saale) 06120, Germany*

Yi-Tung Lu − *Department Biomedical Materials, Institute of Pharmacy, Martin Luther University Halle-Wittenberg, Halle (Saale) 06120, Germany*

Johanna Phuong Nong − *Institute of Plant and Wood Chemistry (IPWC), Technische Universität Dresden, Tharandt 01737, Germany*

Steffen Fischer − *Institute of Plant and Wood Chemistry (IPWC), Technische Universität Dresden, Tharandt 01737, Germany*

Thomas Groth − *Department Biomedical Materials, Institute of Pharmacy, Martin Luther University Halle-Wittenberg, Halle (Saale) 06120, Germany; Interdisciplinary Center of Material Science, Martin Luther University Halle-Wittenberg, Halle (Saale) 06099, Germany;* ● orcid.org/0000-0001-6647-9657

Complete contact information is available at:
https://pubs.acs.org/10.1021/acsami.2c12803

Author Contributions

†K.Z., F.D., and Y.-T.L. contributed equally to this work. The manuscript was written through contributions of all authors. All authors have given approval to the final version of the manuscript.

Notes

The authors declare no competing financial interest.

■ REFERENCES

(1) Hoffman, A. S. Stimuli-Responsive Polymers: Biomedical Applications and Challenges for Clinical Translation. *Adv. Drug Delivery Rev.* **2013**, *65*, 10−16.
(2) Lv, P.; Lu, X.; Wang, L.; Feng, W. Nanocellulose-Based Functional Materials: From Chiral Photonics to Soft Actuator and Energy Storage. *Adv. Funct. Mater.* **2021**, *31*, 2104991.
(3) De las Heras Alarcón, C.; Pennadam, S.; Alexander, C. Stimuli Responsive Polymers for Biomedical Applications. *Chem. Soc. Rev.* **2005**, *34*, 276−285.

(4) Esmaeilzadeh, P.; Groth, T. Switchable and Obedient Interfacial Properties That Grant New Biomedical Applications. *ACS Appl. Mater. Interfaces* **2019**, *11*, 25637−25653.

(5) Cole, M. A.; Voelcker, N. H.; Thissen, H.; Griesser, H. J. Stimuli-Responsive Interfaces and Systems for the Control of Protein−Surface and Cell−Surface Interactions. *Biomaterials* **2009**, *30*, 1827−1850.

(6) Yamada, N.; Okano, T.; Sakai, H.; Karikusa, F.; Sawasaki, Y.; Sakurai, Y. Thermo-Responsive Polymeric Surfaces; Control of Attachment and Detachment of Cultured Cells. *Macromol. Rapid Commun.* **1990**, *11*, 571−576.

(7) Bordat, A.; Boissenot, T.; Nicolas, J.; Tsapis, N. Thermores-ponsive Polymer Nanocarriers for Biomedical Applications. *Adv. Drug Delivery Rev.* **2019**, *138*, 167−192.

(8) Kushida, A.; Yamato, M.; Konno, C.; Kikuchi, A.; Sakurai, Y.; Okano, T. Decrease in Culture Temperature Releases Monolayer Endothelial Cell Sheets Together with Deposited Fibronectin Matrix from Temperature-Responsive Culture Surfaces. *J. Biomed. Mater. Res.: An Official Journal of The Society for Biomaterials, The Japanese Society for Biomaterials, and The Australian Society for Biomaterials* **1999**, *45*, 355−362.

(9) Brun-Graeppi, A. K. A. S.; Richard, C.; Bessodes, M.; Scherman, D.; Merten, O.-W. Thermoresponsive Surfaces for Cell Culture and Enzyme-Free Cell Detachment. *Prog. Polym. Sci.* **2010**, *35*, 1311−1324.

(10) Tang, L.; Wang, L.; Yang, X.; Feng, Y.; Li, Y.; Feng, W. Poly (N-Isopropylacrylamide)-Based Smart Hydrogels: Design, Properties and Applications. *Prog. Mater. Sci.* **2021**, *115*, 100702.

(11) Fujishige, S.; Kubota, K.; Ando, I. Phase Transition of Aqueous Solutions of Poly (N-Isopropylacrylamide) and Poly (N-Isopropyl-methacrylamide). *J. Phys. Chem.* **1989**, *93*, 3311−3313.

(12) Cooperstein, M. A.; Canavan, H. E. Assessment of Cytotoxicity of (N-Isopropyl Acrylamide) and Poly (N-Isopropyl Acrylamide)-Coated Surfaces. *Biointerphases* **2013**, *8*, 19.

(13) Okano, T.; Yamada, N.; Sakai, H.; Sakurai, Y. A Novel Recovery System for Cultured Cells Using Plasma-Treated Poly-styrene Dishes Grafted with Poly (N-Isopropylacrylamide). *J. Biomed. Mater. Res.* **1993**, *27*, 1243−1251.

(14) Doberenz, F.; Zeng, K.; Willems, C.; Zhang, K.; Groth, T. Thermoresponsive Polymers and Their Biomedical Application in Tissue Engineering. *J. Mater. Chem. B* **2020**, *8*, 607−628.

(15) Rapraeger, A. C.; Krufka, A.; Olwin, B. B. Requirement of Heparan Sulfate for Bfgf-Mediated Fibroblast Growth and Myoblast Differentiation. *Science* **1991**, *252*, 1705−1708.

(16) Köwitsch, A.; Zhou, G.; Groth, T. Medical Application of Glycosaminoglycans: A Review. *J. Tissue Eng. Regen. Med.* **2018**, *12*, e23−e41.

(17) Gandhi, N. S.; Mancera, R. L. The Structure of Glycosaminoglycans and Their Interactions with Proteins. *Chem. Biol. Drug Des.* **2008**, *72*, 455−482.

(18) Rabenstein, D. L. Heparin and Heparan Sulfate: Structure and Function. *Nat. Prod. Rep.* **2002**, *19*, 312−331.

(19) Liu, H.; Zhang, Z.; Linhardt, R. J. Lessons Learned from the Contamination of Heparin. *Nat. Prod. Rep.* **2009**, *26*, 313−321.

(20) Guerrini, M.; Beccati, D.; Shriver, Z.; Naggi, A.; Viswanathan, K.; Bisio, A.; Capila, I.; Lansing, J. C.; Guglieri, S.; Fraser, B.; et al. Oversulfated Chondroitin Sulfate Is a Contaminant in Heparin Associated with Adverse Clinical Events. *Nat. Biotechnol.* **2008**, *26*, 669−675.

(21) Zhang, K.; Peschel, D.; Bäucker, E.; Groth, T.; Fischer, S. Synthesis and Characterisation of Cellulose Sulfates Regarding the Degrees of Substitution, Degrees of Polymerisation and Morphology. *Carbohydr. Polym.* **2011**, *83*, 1659−1664.

(22) Groth, T.; Wagenknecht, W. Anticoagulant Potential of Regioselective Derivatized Cellulose. *Biomaterials* **2001**, *22*, 2719−2729.

(23) Aggarwal, N.; Altgärde, N.; Svedhem, S.; Zhang, K.; Fischer, S.; Groth, T. Effect of Molecular Composition of Heparin and Cellulose Sulfate on Multilayer Formation and Cell Response. *Langmuir* **2013**, *29*, 13853−13864.

(24) Zeng, K.; Groth, T.; Zhang, K. Recent Advances in Artificially Sulfated Polysaccharides for Applications in Cell Growth and Differentiation, Drug Delivery, and Tissue Engineering. *ChemBio-Chem.* **2019**, *20*, 737−746.

(25) Yang, Y.; Lu, Y. T.; Zeng, K.; Heinze, T.; Groth, T.; Zhang, K. Recent Progress on Cellulose-Based Ionic Compounds for Bio-materials. *Adv. Mater.* **2021**, *33*, 2000717.

(26) Costa, R. R.; Mano, J. F. Polyelectrolyte Multilayered Assemblies in Biomedical Technologies. *Chem. Soc. Rev.* **2014**, *43*, 3453−3479.

(27) Lu, Y.-T.; Zeng, K.; Fuhrmann, B.; Woelk, C.; Zhang, K.; Groth, T. Engineering of Stable Cross-Linked Multilayers Based on Thermo-Responsive Pnipam-Grafted-Chitosan/Heparin to Tailor Their Physiochemical Properties and Biocompatibility. *ACS Appl. Mater. Interfaces* **2022**, *14*, 29550−29562.

(28) Schlenoff, J. B.; Dubas, S. T. Mechanism of Polyelectrolyte Multilayer Growth: Charge Overcompensation and Distribution. *Macromolecules* **2001**, *34*, 592−598.

(29) AlKhoury, H.; Hautmann, A.; Erdmann, F.; Zhou, G.; Stojanović, S.; Najman, S.; Groth, T. Study on the Potential Mechanism of Anti-Inflammatory Activity of Covalently Immobilized Hyaluronan and Heparin. *J. Biomed. Mater. Res.* **2020**, *108*, 1099−1111.

(30) Anouz, R.; Repanas, A.; Schwarz, E.; Groth, T. Novel Surface Coatings Using Oxidized Glycosaminoglycans as Delivery Systems of Bone Morphogenetic Protein 2 (Bmp-2) for Bone Regeneration. *Macromol. Biosci.* **2018**, *18*, 1800283.

(31) Kindi, H.; Menzel, M.; Heilmann, A.; Schmelzer, C. E.; Herzberg, M.; Fuhrmann, B.; Gallego-Ferrer, G.; Groth, T. Effect of Metal Ions on the Physical Properties of Multilayers from Hyaluronan and Chitosan, and the Adhesion, Growth and Adipogenic Differ-entiation of Multipotent Mouse Fibroblasts. *Soft Matter* **2021**, *17*, 8394−8410.

(32) Picart, C.; Lavalle, P.; Hubert, P.; Cuisinier, F.; Decher, G.; Schaaf, P.; Voegel, J.-C. Buildup Mechanism for Poly (L-Lysine)/ Hyaluronic Acid Films onto a Solid Surface. *Langmuir* **2001**, *17*, 7414−7424.

(33) Teixeira, R.; Reis, R. L.; Pashkuleva, I. Influence of the Sulfation Degree of Glycosaminoglycans on Their Multilayer Assembly with Poly-L-Lysine. *Colloids Surf. B: Biointerfaces* **2016**, *145*, 567−575.

(34) Pathak, K.; Misra, S. K.; Sehgal, A.; Singh, S.; Bungau, S.; Najda, A.; Gruszecki, R.; Behl, T. Biomedical Applications of Quaternized Chitosan. *Polymers* **2021**, *13*, 2514.

(35) Young, J.-J.; Cheng, K.-M.; Tsou, T.-L.; Liu, H.-W.; Wang, H.-J. Preparation of Cross-Linked Hyaluronic Acid Film Using 2-Chloro-1-Methylpyridinium Iodide or Water-Soluble 1-Ethyl-(3, 3-Dimethyla-minopropyl) Carbodiimide. *J. Biomater. Sci. Polym. Ed.* **2004**, *15*, 767−780.

(36) Lee, S. B.; Ha, D. I.; Cho, S. K.; Kim, S. J.; Lee, Y. M. Temperature/Ph-Sensitive Comb-Type Graft Hydrogels Composed of Chitosan and Poly (N-Isopropylacrylamide). *J. Appl. Polym. Sci.* **2004**, *92*, 2612−2620.

(37) Everaerts, F.; Torrianni, M.; Hendriks, M.; Feijen, J. Biomechanical Properties of Carbodiimide Crosslinked Collagen: Influence of the Formation of Ester Crosslinks. *J. Biomed. Mater. Res. A: An Official Journal of The Society for Biomaterials, The Japanese Society for Biomaterials, and The Australian Society for Biomaterials and the Korean Society for Biomaterials* **2008**, *85*, 547−555.

(38) Delgado, A. V.; González-Caballero, F.; Hunter, R.; Koopal, L. K.; Lyklema, J. Measurement and Interpretation of Electrokinetic Phenomena (Iupac Technical Report). *Pure Appl. Chem.* **2005**, *77*, 1753−1805.

(39) Kaszuba, M.; Corbett, J.; Watson, F. M.; Jones, A. High-Concentration Zeta Potential Measurements Using Light-Scattering Techniques. *Philos. Trans. R. Soc. A* **2010**, *368*, 4439−4451.

(40) Reinhardt, K. A.; Kern, W. *Handbook of Silicon Wafer Cleaning Technology*, 2nd ed; Elsevier, 2008.

(41) Schindelin, J.; Arganda-Carreras, I.; Frise, E.; Kaynig, V.; Longair, M.; Pietzsch, T.; Preibisch, S.; Rueden, C.; Saalfeld, S.;

Schmid, B.; et al. Fiji: An Open-Source Platform for Biological-Image Analysis. *Nat. Methods* **2012**, *9*, 676−682.

(42) Zhang, K.; Brendler, E.; Fischer, S.; Raman, F. T. Investigation of Sodium Cellulose Sulfate. *Cellulose* **2010**, *17*, 427−435.

(43) Bojanić, V.; Jovanović, S.; Tabaković, R.; Tabaković, I. Synthesis and Electrochemistry of Grafted Copolymers of Cellulose with 4-Vinylpyridine, 1-Vinylimidazole, 1-Vinyl-2-Pyrrolidinone, and 9-Vinylcarbazole. *J. Appl. Polym. Sci.* **1996**, *60*, 1719−1725.

(44) Shan, J.; Nuopponen, M.; Jiang, H.; Kauppinen, E.; Tenhu, H. Preparation of Poly (N-Isopropylacrylamide)-Monolayer-Protected Gold Clusters: Synthesis Methods, Core Size, and Thickness of Monolayer. *Macromolecules* **2003**, *36*, 4526−4533.

(45) Bedini, E.; Laezza, A.; Parrilli, M.; Iadonisi, A. A Review of Chemical Methods for the Selective Sulfation and Desulfation of Polysaccharides. *Carbohydr. Polym.* **2017**, *174*, 1224−1239.

(46) Zhang, Q.; Weber, C.; Schubert, U. S.; Hoogenboom, R. Thermoresponsive Polymers with Lower Critical Solution Temperature: From Fundamental Aspects and Measuring Techniques to Recommended Turbidimetry Conditions. *Mater. Horiz.* **2017**, *4*, 109−116.

(47) Wang, X.; Qiu, X.; Wu, C. Comparison of the Coil-to-Globule and the Globule-to-Coil Transitions of a Single Poly (N-Isopropylacrylamide) Homopolymer Chain in Water. *Macromolecules* **1998**, *31*, 2972−2976.

(48) Bao, H.; Li, L.; Leong, W. C.; Gan, L. H. Thermo-Responsive Association of Chitosan-Graft-Poly (N-Isopropylacrylamide) in Aqueous Solutions. *J. Phys. Chem. B* **2010**, *114*, 10666−10673.

(49) Bhattacharya, D. S.; Svechkarev, D.; Bapat, A.; Patil, P.; Hollingsworth, M. A.; Mohs, A. M. Sulfation Modulates the Targeting Properties of Hyaluronic Acid to P-Selectin and Cd44. *ACS Biomater. Sci. Eng.* **2020**, *6*, 3585−3598.

(50) Danaei, M.; Dehghankhold, M.; Ataei, S.; Hasanzadeh Davarani, F.; Javanmard, R.; Dokhani, A.; Khorasani, S.; Mozafari, M. Impact of Particle Size and Polydispersity Index on the Clinical Applications of Lipidic Nanocarrier Systems. *Pharmaceutics* **2018**, *10*, 57.

(51) Schild, H. G. Poly (N-Isopropylacrylamide): Experiment, Theory and Application. *Prog. Polym. Sci.* **1992**, *17*, 163−249.

(52) Nilsen-Nygaard, J.; Strand, S. P.; Vårum, K. M.; Draget, K. I.; Nordgård, C. T. Chitosan: Gels and Interfacial Properties. *Polymers* **2015**, *7*, 552−579.

(53) Wang, W.; Meng, Q.; Li, Q.; Liu, J.; Zhou, M.; Jin, Z.; Zhao, K. Chitosan Derivatives and Their Application in Biomedicine. *Int. J. Mol. Sci.* **2020**, *21*, 487.

(54) Zhou, Y.; Yang, H.; Liu, X.; Mao, J.; Gu, S.; Xu, W. Potential of Quaternization-Functionalized Chitosan Fiber for Wound Dressing. *Int. J. Biol. Macromol.* **2013**, *52*, 327−332.

(55) Aggarwal, N.; Altgärde, N.; Svedhem, S.; Zhang, K.; Fischer, S.; Groth, T. Study on Multilayer Structures Prepared from Heparin and Semi-Synthetic Cellulose Sulfates as Polyanions and Their Influence on Cellular Response. *Colloids Surf. B: Biointerfaces* **2014**, *116*, 93−103.

(56) Borges, J.; Mano, J. F. Molecular Interactions Driving the Layer-by-Layer Assembly of Multilayers. *Chem. Rev.* **2014**, *114*, 8883−8942.

(57) Gericke, M.; Doliška, A.; Stana, J.; Liebert, T.; Heinze, T.; Stana-Kleinschek, K. Semi-Synthetic Polysaccharide Sulfates as Anticoagulant Coatings for Pet, 1−Cellulose Sulfate. *Macromol. Biosci.* **2011**, *11*, 549−556.

(58) Stratz, J.; Liedmann, A.; Heinze, T.; Fischer, S.; Groth, T. Effect of Sulfation Route and Subsequent Oxidation on Derivatization Degree and Biocompatibility of Cellulose Sulfates. *Macromol. Biosci* **2020**, *20*, e1900403.

(59) Bongrand, P.; Capo, C.; Depieds, R. Physics of Cell Adhesion. *Prog. Surf. Sci.* **1982**, *12*, 217−285.

(60) Altankov, G.; Richau, K.; Groth, T. The Role of Surface Zeta Potential and Substratum Chemistry for Regulation of Dermal Fibroblasts Interaction. *Materialwissenschaft und Werkstofftechnik:*

Entwicklung, Fertigung, Prüfung, Eigenschaften und Anwendungen technischer Werkstoffe **2003**, *34*, 1120−1128.

(61) Faucheux, N.; Schweiss, R.; Lützow, K.; Werner, C.; Groth, T. Self-Assembled Monolayers with Different Terminating Groups as Model Substrates for Cell Adhesion Studies. *Biomaterials* **2004**, *25*, 2721−2730.

(62) Yamanlar, S.; Sant, S.; Boudou, T.; Picart, C.; Khademhosseini, A. Surface Functionalization of Hyaluronic Acid Hydrogels by Polyelectrolyte Multilayer Films. *Biomaterials* **2011**, *32*, 5590−5599.

(63) Duval, J. F.; Küttner, D.; Werner, C.; Zimmermann, R. Electrohydrodynamics of Soft Polyelectrolyte Multilayers: Point of Zero-Streaming Current. *Langmuir* **2011**, *27*, 10739−10752.

(64) Husteden, C.; Doberenz, F.; Goergen, N.; Pinnapireddy, S. R.; Janich, C.; Langner, A.; Syrowatka, F.; Repanas, A.; Erdmann, F.; Jedelska, J.; et al. Contact-Triggered Lipofection from Multilayer Films Designed as Surfaces for in Situ Transfection Strategies in Tissue Engineering. *ACS Appl. Mater. Interfaces* **2020**, *12*, 8963−8977.

(65) Fischer, D.; Li, Y.; Ahlemeyer, B.; Krieglstein, J.; Kissel, T. In Vitro Cytotoxicity Testing of Polycations: Influence of Polymer Structure on Cell Viability and Hemolysis. *Biomaterials* **2003**, *24*, 1121−1131.

(66) Volodkin, D.; von Klitzing, R. Competing Mechanisms in Polyelectrolyte Multilayer Formation and Swelling: Polycation−Polyanion Pairing Vs. Polyelectrolyte−Ion Pairing. *Curr. Opin. Colloid Interface Sci.* **2014**, *19*, 25−31.

(67) Webb, K.; Hlady, V.; Tresco, P. A. Relationships among Cell Attachment, Spreading, Cytoskeletal Organization, and Migration Rate for Anchorage-Dependent Cells on Model Surfaces. *J. Biomed. Mater. Res.: An Official Journal of The Society for Biomaterials and The Japanese Society for Biomaterials* **2000**, *49*, 362−368.

(68) Peschel, D.; Zhang, K.; Aggarwal, N.; Brendler, E.; Fischer, S.; Groth, T. Synthesis of Novel Celluloses Derivatives and Investigation of Their Mitogenic Activity in the Presence and Absence of Fgf2. *Acta Biomater.* **2010**, *6*, 2116−2125.

(69) Peschel, D.; Zhang, K.; Fischer, S.; Groth, T. Modulation of Osteogenic Activity of Bmp-2 by Cellulose and Chitosan Derivatives. *Acta Biomater.* **2012**, *8*, 183−193.

(70) Altankov, G.; Grinnell, F.; Groth, T. Studies on the Biocompatibility of Materials: Fibroblast Reorganization of Substratum-Bound Fibronectin on Surfaces Varying in Wettability. *J. Biomed. Mater. Res.: An Official Journal of The Society for Biomaterials and The Japanese Society for Biomaterials* **1996**, *30*, 385−391.

Summarizing discussion and future perspectives

The aim of this PhD work was to develop thermoresponsive polyelectrolyte multilayer systems (PEM) with tailored surface properties and enhanced bioactivity to regulate cell activities in terms of adhesion, proliferation, and migration as well as to thermally control cell detachment without the impediment of cell integrity. Using LbL technique, as a facile and straightforward approach, allowed the combination of the thermoresponsive polymer PNIPAM and native or mimetic GAGs (Hep, ChS, CS) on the surfaces via alternating adsorption of oppositely charged PELs. First, two strategies were employed to modify PELs with PNIPAM for PEM formation, by preparation of PChi as a polycation or PCS as a polyanion. Second, either the post covalent crosslinking between Chi and GAGs or the use of stronger polycations (QChi, PLL) could improve the structural stability and integrity of PEMs. Third, native or biomimetic GAGs as terminal layers provided a better bioactivity of the PNIPAM-containing coatings to direct cell responses by interacting with adhesive proteins (VN) and GFs (FGF-2). In addition, the collapsed and dehydrated PNIPAM chains at 37 °C helped to achieve their sustained release and directed the presentation of FGF-2 immobilized in PEMs. The novelty of this work is especially highlighted by the synergistic effect of immobilized VN and FGF-2 on the regulation of cell adhesion, proliferation, and migration.

Studies were first focused on the ability of PChi (LMW*, HMW) to construct PEM with native GAGs (Hep, ChS) at pH 4 and on the stability of PEMs by post covalent crosslinking. LMW* and HMW were selected as polycations regarding their pronounced thermoresponsive behaviors (e.g., conformational change and $T_{CP} \approx$ 31−33 °C) that might facilitate tailoring surface properties for cell adhesion and detachment. Both LMW* and HMW were able to form PEMs with both GAGs, however, a partial disassembly of PEMs occurred after exposure to pH 7.4 due to the deprotonation of Chi. In particular, LMW* with the lowest charge density showed significant disability to maintain the PEM integrity ($\approx$ 50% decrease in thickness) under these conditions. Low stability of PEMs resulted in a decreased adhesion of C3H10T1/2 multipotent embryonic mouse fibroblasts. Indeed, the PEM integrity was maintained after covalent crosslinking by the formation of amide bonds and thus improving cell adhesion.

The temperature effect on the surface properties of crosslinked PEMs based on Hep and PChi provided more insight into their association with proteins (VN, FGF-2), cell activities and detachment. Combining the results from QCM-D, wettability, roughness, and stiffness, all pointed out a certain extent of thermoresponsivity of PEMs containing HMW in the temperature range of 20−37 °C. Although LMW* and HMW showed similar thermoresponsive behaviors in the aqueous solution, such behaviors were significantly restricted for the PEMs containing LMW* probably due to steric hindrance of higher DS. Higher density of PNIPAM grafted on the surface has been reported to limit its temperature response particularly in the PEM that involves many interactions such as ion paring and covalent bonding [63,170]. The presence of collapsed HMW at 37 °C seemed to contribute to dehydration and stiffness, making surfaces stiffer than Chi-containing PEMs. In addition, temperature also played an important role for the surface properties of PEMs. Our findings showed these PEMs became overall smoother, more compact and softer at 37 °C than at 20 °C from AFM measurement. It has been reported that increasing temperature induces higher mobility and interdiffusion of PELs leading to a structural rearrangement of the PEM [198].

Regarding the high affinity of sulfated GAGs to adhesive proteins and GFs, the bioactivity of PEMs was primarily assessed by studies on VN adsorption/desorption in dependence of the temperature effect. The interactions between VN and PEM were mainly attributed to three factors: temperature, hydrophobic interaction with PNIPAM and specific binding to GAGs. Higher temperature (37 °C), the presence of PNIPAM and GAG terminal layers led to higher VN adsorption. In addition, higher temperature could promote interdiffusion of polymers. Thus, VN might penetrate into the PEMs based on the higher mobility of VN at higher temperature, which was in agreement with a study that showed the diffusion of a fluorescent-labelled protein (FGF-2) throughout the PEMs [135]. Importantly, GAGs as terminal layers played dominant roles in retaining VN in the PEMs at 37 °C. Thereby, higher retention of protein (e.g., VN, FN) from the serum of culture medium or secreted by cells promoted better adhesion and spreading of C3H10T1/2 cells on GAG terminal layers. Nevertheless, the ability to retain VN was limited for PEM containing LMW*, possibly due to the lower amount of GAG and steric hindrance due to the higher density of PNIPAM. Thus, further studies were focused on PEM containing HMW or Chi with Hep terminal layer. Based on the higher adsorption of VN at 37 °C, the potential of the PEMs for GF delivery was also

investigated at 37 °C. It was found previously that less crosslinked PEM can take up more FGF-2 [135,213]. The HMW-containing PEM was less crosslinked (40%) than the Chi-containing PEM (60%). Thus, lower crosslinking degree of HMW-containing PEM and an expected hydrophobic interaction of PNIPAM with proteins at 37°C are assumed as the main reasons for superior uptake and sustained release of FGF-2 over 7 days compared to a burst release from Chi-containing PEM.

The effect of the cooperative activity of VN and FGF-2 with PEMs on cell responses was studied here for the first time. They were both adsorbed on the PEMs for the regulation of cell behavior in the low-serum medium. Cell responses should be connected to ligation of integrins and FGF-2 receptor, allowing the regulation of signal transduction pathways. Cell activities and ECM remodeling depend on the activation of RhoA/ROCK signaling through mechanosensing, activation of Rho GTPases family like Rac and Cdc42 by FGF-2, and MAPK/ERK signaling by synergistic activity of VN/FGF-2 [45,182,217]. Since the HMW-containing PEM exhibited a stiffer surface than the Chi-containing PEM at 37 °C, better cell adhesion was found related to the assembly of actin fibers and formation of focal adhesions. It is worth noting that GF loaded on PEMs in a matrix-bound manner allows the crosstalk between integrins and GF receptors that regulate the same intracellular signaling pathways [133,134]. According to the exceptional bioactivity of the HMW-containing PEM that better retained VN and sustained release of FGF-2, the synergistic activity of VN/FGF-2 was more pronounced on cell responses that was confirmed by more spreading, higher proliferation, and migration of 3T3 fibroblasts. In contrast, soluble FGF-2 could not efficiently support such cell behaviors because of the absence of crosstalk between FGFR-2 and VN integrins, as well as its rapid degradation in the medium. Overall, these extensive studies suggest an attractive strategy to fabricate a stimuli-responsive coating combining PNIPAM and GAGs to tailor the surface properties and enhance the bioactivity to effectively promote cell adhesion, proliferation, and migration.

While adjustment of DS and MW of PNIPAM were in the focus to tailor surface properties and bioactivity of PChi-containing PEMs, the effects of sulfation degree and type of polycations were studied for PCS-containing PEMs. In this part, GAG-mimetic CS provided a possibility to replace native GAGs in combination with PNIPAM for PEM formation. Lower sulfated PCS 1 and higher sulfated PCS 2 were prepared as polyanions to construct PEMs with two different polycations (PLL, QChi). Unlike Chi

which deprotonates and becomes uncharged at pH 7.4, PLL and QChi possess positive charges at both pH 4 and 7.4 that reduce their dependency on pH for PEM integrity. The charge density and sulfation degree of PCS were the keys for keeping control on PEM formation and integrity. PCS 2 with higher sulfation degree and negative charge density overcame the steric hindrance caused by PNIPAM to assemble PEMs with both polycations. The information of the internal structure and surface properties of PEMs were obtained from the results of surface wettability and zeta potential related to the type and molecular weight of polycation. The terminal layers of negatively charged PCSs dominated the surface properties for QChi-containing PEMs, evident by more wettable surfaces and decreased point of zero charge (PZC). Interestingly, increased PZC and less wettable surface were observed for PLL-containing PEMs, indicating the presence of PLL in the surface region. PLL smaller than QChi can easier diffuse into PEM resulting in forming more intermingling layers and present at the outmost region of the PEMs.

The structural stability of PEMs, type of polycation, sulfation degree and PNIPAM effect were crucial for cytotoxicity of PEM that was also strongly associated with cell fate in terms of cell adhesion, spreading and growth. Both polycations were highly positive charged that can destroy the cell membrane which is cytotoxic [167]. As lower sulfated PCS 1 with reduced ion paring with polycations resulted in lower stability of PEMs, the released polycations caused high cytotoxicity to 3T3 fibroblasts and low cell adhesion. The intermingling layers of PLL at the surface region further inhibited cell spreading and growth. Since PCS 2 was more present in the surface region of the QChi-containing PEMs, cell behaviors were predominantly attributed to sulfation degree and PNIPAM effect. Higher sulfated PCS 2 not only improved the structural stability of PEM but also enhanced the interaction with proteins from serum or secreted by cells. Noteworthy, the dehydration of PNIPAM at 37 °C should also contribute to the interaction with proteins through hydrophobic interaction, which was supported by higher cell adhesion and growth. Hence, the combination of higher sulfated PCS 2 possessing also more bioactivity and QChi presented another interesting approach to fabricate bioactive PNIPAM-containing PEM.

The initial objective behind the development of PNIPAM-containing PEMs was to enable cell detachment driven by reducing the temperature. The detachment mechanism is based on the hydration and decreased stiffness of surfaces when the

environmental temperature is decreased from 37 °C to below LCST [74,222]. Consequently, the swelling of PNIPAM induces more hydrophilic and softer surface leading to protein desorption and thus cell detachment. Here, the PEMs based on PChi and native GAGs were further explored their potential in cell detachment using C3H10T1/2 cells. Cells were cultured on the PEMs containing Chi or PChi with Hep as terminal layer. After incubation at 37 °C for 48 h, these PEMs were exposed to 20 °C for 1 h, followed by incubation at 4 °C for another 1 h. **Figure S1A** showed no significant change in cell morphology after the incubation at both 20 and 4 °C. The detachment ratio was calculated in **Figure S1C** and less than 2 % of cells detached from all the surfaces. On the other hand, cells cultured on PEMs based on ChS and HMW also showed no obvious difference in cell morphology in **Figure S2**. Our results were different to the findings from Liao et. al., who demonstrated more than 70% detachment of hMSCs from PEMs prepared by PSS-co-PNIPAM/PAH-co-PNIPAM after cooling the surfaces to 4 °C for 1 h [176]. Although the wetting properties, roughness, and stiffness have confirmed that the HMW-containing PEM exhibited better ability to thermally change conformation than the LMW*-containing PEM, it seems that the extent of thermoresponsivity could not suffice the requirements for temperature-induced cell detachment. Therefore, we postulate insufficient thermoresponsive behaviors of PEMs for cell detachment because of several reasons. First, Okano's group reported a high MW (>50 kDa) and grafting density (0.03 chains/nm^2) of PNIPAM on surfaces to favor cell detachment [82]. Second, a high degree of interpenetration in the PEM by ionic and covalent crosslinking could reduce the thermoresponsivity of PNIPAM due to steric hindrance [170,177]. As the PEMs prepared by Liao et. al. using both polycation and polyanion modified with a portion of 50% PNIPAM were strong PELs with higher charge density and higher MWs (90 kDa), lower interpenetration between layers allowed thermoresponsive behavior of PNIPAM to promote cell detachment. In our case, the relatively low MW and grafting density as well as higher interpenetration of the PEMs is probably the reason for the lack of cell detachment. In addition, a higher density of PNIPAM on PChi (less amino groups/fewer positive charges) and the use of polysaccharides could result in a rather unstable and highly hydrated PEM. Another possible reason could be the high affinity of the PEMs to ECM proteins as an anchoring layer for strong cell adhesion, which was evident by less than 10 µg cm^{-2} of VN (< 3% from the adsorbed amount) desorbed form the surfaces by cooling the PEM from 37 °C to 4 °C [223]. Finally, the responding time and

temperature for the detachment can be different for varying phenotype of cells or origins due to their different metabolic requirements [224]. Therefore, these factors should be finetuned in future for such PNIPAM-containing PEMs in the application for cell sheet engineering.

In conclusion, this PhD work provides fundamental insights into the presented PEM constructs based on polysaccharides containing PNIPAM with enhanced bioactivity, paving the way for the future applications like free standing PEM films in wound healing applications since proliferation and migration of cells like endothelial cells, fibroblasts and keratinocytes are important during tissue regeneration. In particular, the immobilization of GFs and adhesive proteins on such PEM may be an interesting approach to prolong the GF activity and improve the efficiency on culture and programming tissue and stem cells like PSC without the need to add soluble GF regularly. Finally, using higher molecular weight of PNIPAM may improve the thermoresponsive behavior of the PEM to better induce the cell detachment below the LCST.

Supporting information
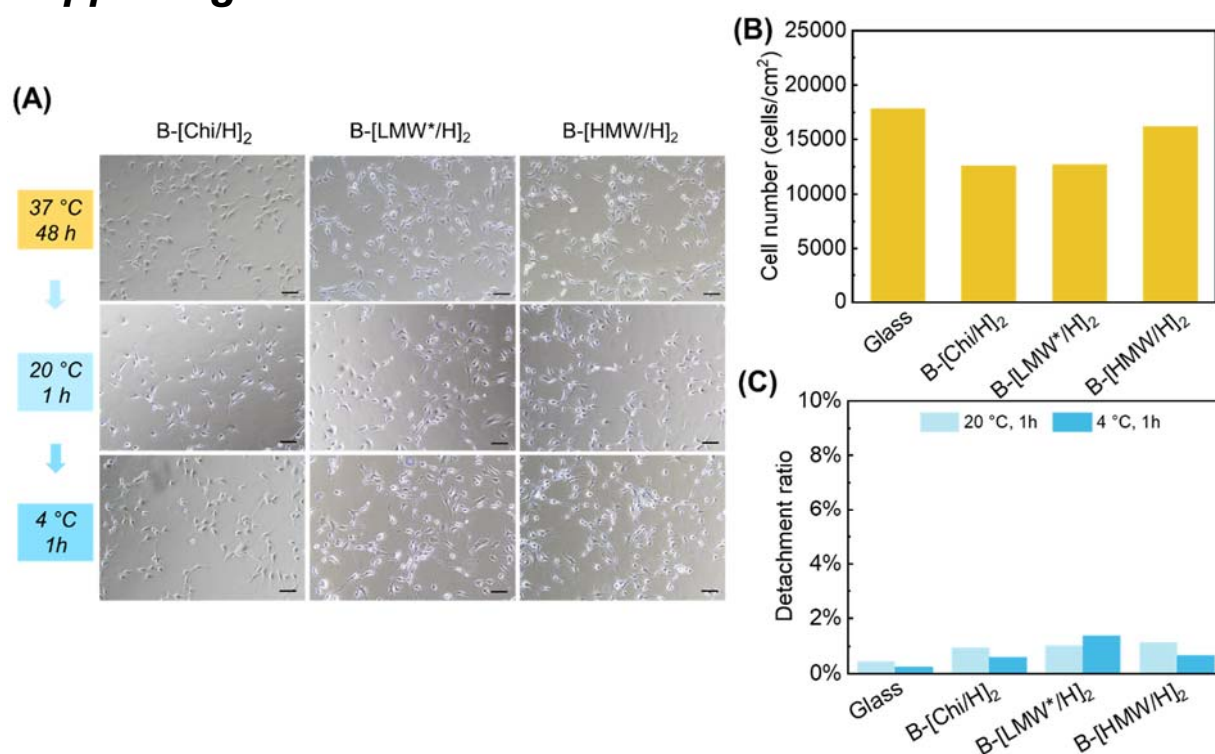
Figure S1. (A) Phase contrast image of C3H10T1/2 cells on crosslinked PEMs with Hep terminal layers after 48 h culture at 37 °C (upper row), cooling at 20 °C for 1 h (middle row), and cooling at 4 °C for another 1 h (lower row) Scale bar: 100 μm. Calculation of (B) cell number at 48 h culture and (C) detachment ratio after cooling at 20 °C for 1 h and 4 °C for another 1 h. (Detachment ratio = number of detached cells / numbers of adhered cells before detachment)
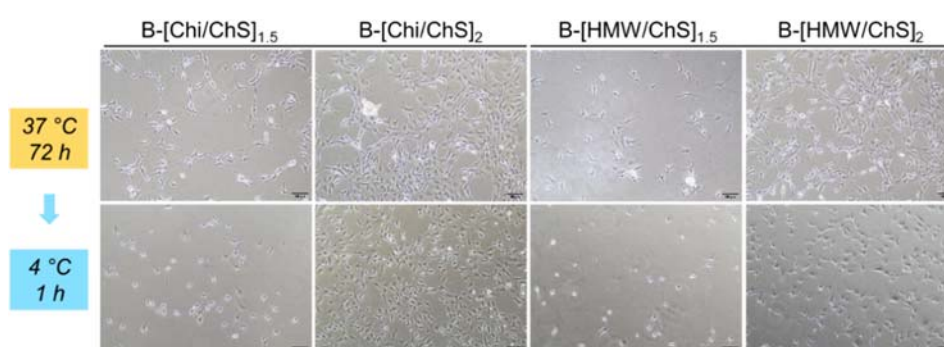
Figure S2. (A) Phase contrast image of C3H10T1/2 cells on crosslinked PEMs with ChS or PChi/Chi terminal layers after 72 h culture at 37 °C (upper row), and cooling at 4 °C for another 1 h (lower row) Scale bar: 100 μm.

Acknowledgement

I would like to express my heartfelt appreciation to my boyfriend for always listening to me. Your constant support, encouragement and patience have been my rock throughout this challenging times especially during the writing of the thesis.

I would like to convey my profound gratitude to a special person, who brings me the countless courage and fortitude in pursuing my goals.

Finally, I would like to extend my sincerest gratitude and genuine appreciation to my beloved family for always standing by my side and being my biggest cheerleaders. Your unwavering love, understanding, and support have been my strength and guiding light. I am deeply grateful for your belief in me, making this journey more meaningful and fulfilling.

Publication list with declaration of self-contribution to research articles

1. **<u>Y.-T. Lu</u>**, K. Zeng, B. Fuhrmann, C. Woelk, K. Zhang, T. Groth, Engineering of Stable Cross-linked Multilayers Based on Thermo-responsive PNIPAM-*Grafted*-Chitosan/Heparin to Tailor Their Physiochemical Properties and Biocompatibility. *ACS Appl. Mater. Interfaces*, 14 (**2022**), 26, 29550–29562.

My contribution was 80%. I performed most of the experiments, analyzed all the experimental data and wrote the full paper. Dr. K. Zeng contributed to the synthesis and characterization of polymers from the group of Prof. Dr. Zhang. The ellipsometry measurement was supported by B. Fuhrmann. The zeta potential measurement was done with the assistance of Dr. C. Woelk. Prof. Dr. T. Groth supported the planning of experiments and also contributed during the revision of the manuscript.

2. **<u>Y.-T. Lu</u>**, P.-T. Hung, K. Zeng, B. Fuhrmann, C. Woelk, K. Zhang, T. Groth, Surface Properties and Bioactivity of PNIPAM-*Grafted*-Chitosan/Chondroitin Multilayers. *Smart Materials in Medicine*, 4 (**2023**), 356-367.

My contribution was 70%. I synthesized and characterized the polymers, evaluated all the data, writing the full paper and planning all the experiments with the support by Prof. Dr. T. Groth. P.-T. Hung was involved in writing the manuscript and assisted me to perform SPR, QCM-D, protein adsorption and biocompatibility test. Dr. K. Zeng contributed to the synthesis and characterization of polymer from the group of Prof. Dr. Zhang. The ellipsometry measurement was supported by B. Fuhrmann. The zeta potential measurement was done with the assistance of Dr. C. Woelk.

3. **<u>Y.-T. Lu</u>**, P.-T. Hung, K. Zeng, M. Menzel, C. E. H. Schmelzer, K. Zhang, T. Groth, Sustained Growth Factor Delivery from Bioactive PNIPAM-*Grafted*-Chitosan/Heparin Multilayers as a Tool to Promote Growth and Migration of Cells. *Submitted*.

My contribution was 85%. I performed most of the experiments, analyzed all the experimental data and wrote the full paper. P.-T. Hung assisted me with the preparation of ELISA assay. AFM was performed by M. Menzel under the supervision of Dr. C. E. H. Schmelzer. K. Zeng contributed to the revision of the manuscript from the group of Prof. Dr. Zhang. Prof. Dr. T. Groth supported the planning of experiments and also contributed during the revision of the manuscript.

4. K. Zeng, F. Doberenz, **Y.-T. Lu**, T. Groth, K. Zhang, Synthesis of Thermoresponsive PNIPAM-Cellulose Sulfates for Fabrication of Bioactive Multilayers Using Layer-by-Layer Technique. *ACS Appl. Mater. Interfaces*, 14 (**2022**), 43, 48384–48396.

My contribution was about 30%. I mainly contributed to writing and revision of the manuscript. I also assist to evaluate results and answered reviewers' comments during the revision of the manuscript.

5. Y. Yang, **Y.-T. Lu**, K. Zeng, T. Heinze, T. Groth, K. Zhang, Recent Progress on Cellulose-Based Ionic Compounds for Biomaterials. *Adv. Mater.*, (**2020**) 2000717.

My contribution was about 35%. I assembled and wrote all the parts in section 2 'Glycoscience and Glycosaminoglycans' and in section 3.2 'Application of Ionic Cellulose Derivatives as Biomaterials'. Prof. Dr. T. Groth helped in planning and revising the manuscript.

Published abstract

1. Y.-T. Lu, K. Zeng, K. Zhang, B. Fuhrmann, T. Groth, Development of stable thermoresponsive multilayers based on cross-linked PNIPAM-*grafted*-chitosan and heparin for application in tissue engineering. *Tissue Engineering Part A*, **2022**, 28, Suppl. 1, S-1-S-694. https://doi.org/10.1089/ten.tea.2022.29025.abstracts

2. Y.-T. Lu, K. Zeng, K. Zhang, T. Groth, Development of biogenic thermoresponsive polyelectrolyte multilayers towards tissue engineering. *The International Journal of Artificial Organs*, **2020**, 43 (8), 506-555. https://doi.org/10.1177/0391398820937567

Oral presentation

1. Y.-T. Lu, K. Zeng, K. Zhang, B. Fuhrmann, T. Groth, Engineering of stable PNIPAM-grafted chitosan/heparin multilayers for biomedical applications. *European Society for Artificial Organs- International Federation for Artificial Organs (ESAO-IFAO) Webinar*, 25th November **2021**, Halle, Germany, Online.

2. Y.-T. Lu, K. Zeng, K. Zhang, B. Fuhrmann, T. Groth, Engineering of stable PNIPAM-grafted chitosan/heparin multilayers for biomedical applications. *European Chitin Society (EUCHIS) Webinar*, 26th October **2021**. Germany, Online.

3. Y.-T. Lu, K. Zeng, K. Zhang, B. Fuhrmann, T. Groth, Engineering of stable thermoresponsive multilayers based on cross-linked chitosan-*grafted*-PNIPAM and heparin for cell sheet generation. *American Society for Internal Artificial Organs (ASIAO) 66th Annual Conference*, 10th − 12th June **2021**, Washington, DC., the U.S, Online.

Poster

1. Y.-T. Lu, K. Zeng, M. Menzel, C. E. H. Schmelzer, K. Zhang, T. Groth, Development of Biogenic Thermoresponsive Polyelectrolyte Multilayers for the Application in Tissue Engineering. *European Society for Artificial Organs (ESAO) Winter School*, 15th – 18th February **2023**, Lutherstadt Wittenberg, Germany.

2. Y.-T. Lu, K. Zeng, M. Menzel, C. E. H. Schmelzer, B. Fuhrmann, K. Zhang, T. Groth, Temperature effect on physiochemical and biological properties of crosslinked PNIPAM-*graft*-chitosan/heparin multilayer. *Tissue Engineering and Regenerative Medicine International Society (TERMIS) European Chapter Conference*, 28th June – 1st July **2022**. Krakow, Poland.

3. Y.-T. Lu, K. Zeng, K. Zhang, B. Fuhrmann, T. Groth, Development of stable thermoresponsive multilayers based on cross-linked PNIPAM-*grafted*-chitosan and heparin for application in tissue engineering. *The 6th world congress of the Tissue Engineering and Regenerative Medicine International Society (TERMIS)*, 15th – 19th November **2021**. Maastricht, the Netherlands, Online.

4. Y.-T. Lu, K. Zeng, K. Zhang, B. Fuhrmann, T. Groth, Engineering of stable thermoresponsive multilayers based on cross-linked chitosan-*grafted*-PNIPAM and heparin for cell sheet generation. *31st Conference of European Society for Biomaterials (ESB),* 5th – 9th September **2021**, Porto, Portugal, Online.

5. Y.-T. Lu, K. Zeng, K. Zhang, B. Fuhrmann, T. Groth, Stable thermoresponsive multilayers based on cross-linked chitosan-*grafted*-PNIPAM and heparin for cell sheet generation. *ESAO/TERMIS-EU Winter School*, 24th – 26th February **2021**, Zaragoza, Spain, Online.

6. Y.-T. Lu, K. Zeng, K. Zhang, T. Groth, Development of biogenic thermoresponsive polyelectrolyte multilayers for the application on tissue engineering. *European Society for Artificial Organs (ESAO) Winter School*, 26th – 29th February **2020**. Lutherstadt Wittenberg, Germany

7. Y.-T. Lu, K. Zeng, K. Zhang, T. Groth, Development of biogenic thermoresponsive polyelectrolyte multilayers for the application on tissue engineering. *2nd International Workshop on Advanced Materials for Healthcare Applications*, 8th – 9th October **2019**, Funchal, Madeira, Portugal.

Curriculum vitae

Personal data

Name:	Yi-Tung Lu
Date of birth:	16. June 1992 in New Taipei City, Taiwan
Acdemic degree:	Master of Science

Education

01/2019 – present	Ph.D. student, Biomedical Materials Group in Institute of Pharmacy, Martin-Luther-University Halle-Wittenberg, Germany (Supervisor: Prof. Dr. rer. nat. habil. Thomas Groth)
	Title of PhD thesis: Development of biogenic thermoresponsive multilayers based on polysaccharides for tissue engineering applications
09/2014 – 06/2016	M.Sc., Biomedical Engineering Group in Department of Chemical & Materials Engineering, National Central University, Taiwan (Supervisor: Chair Prof. Dr. Akon Higuchi)
	Title of Master thesis: Human Embryonic Stem Cell Culture Using Oligopeptides
09/2010–06/2014	B.Sc., Department of Chemical Engineering & Materials Science, Yuan Ze University, Taiwan

Work experience

07/2020–07/2021	Trainee of Master Thesis in Biomedical Materials Group, Institute of Pharmacy, Martin Luther University Halle-Wittenberg, Germany
03/2019–04/2019	Research Exchange in Department of Wood Technology and Wood-based Composites, University of Göttingen, Germany
12/2016–04/2018	Photolithography Engineer in Department of Process Engineering, EPISTAR Corporation, Taiwan

Award / Grant

01/2019−12/2022   Scholarship from International Graduate School AGRIPOLY, European Regional Development Fund and the Federal State Saxony-Anhalt, Germany

Halle (Saale), 11. June 2023

Yi-Tung Lu

Selbstständigkeitserklärung

Hiermit erkläre ich gemäß § 5 der Promotionsordnung der Naturwissenschaftlichen Fakultät I der Martin-Luther-Universität Halle-Wittenberg, dass ich die Ergebnisse der vorliegenden kumulativen Dissertationsarbeit

Development of biogenic thermoresponsive multilayers based on

polysaccharides for tissue engineering applications

am Institut für Pharmazie in der Arbeitsgruppe Biomedizinische Materialien unter Anleitung von Prof. Dr. rer. nat. habil. Thomas Groth selbständig erarbeitet und die Dissertation ohne fremde Hilfe verfasst habe.

Weiterhin erkläre ich, dass ich keine anderen als die von mir angegebenen Quellen und Hilfsmittel zur Erstellung meiner Dissertation verwendet habe. Den benutzen Werken wörtlich oder inhaltlich entnommene Stellen sind als solche gekennzeichnet.

Ferner erkläre ich, dass ich mich mit der vorliegenden Dissertationsarbeit erstmals um die Erlangung eines Doktorgrades bewerbe.

Halle (Saale), den 11. June 2023

M.Sc. Yi-Tung Lu